Far North Prescribed Wells Area Groundwater Model

Volume 4 – Flow dynamics and potentiometric surface development

Department for Environment and Water
September, 2023

DEW Technical report 2023-72

Government of South Australia
Department for Environment and Water

Department for Environment and Water
Government of South Australia
September, 2023

81-95 Waymouth St, ADELAIDE SA 5000
Telephone +61 (8) 8463 6946
Facsimile +61 (8) 8463 6999
ABN 36702093234

www.environment.sa.gov.au

Contributors to this volume: Daniel Wohling, Innovative Groundwater Solutions Pty Ltd and Mark Keppel, Department for Environment and Water

Reviewers of this volume: Lloyd Sampson and Juliette Woods, Department for Environment and Water, and Paul Howe, CDM Smith Pty Ltd, Keith Phillipson, Australasian Groundwater and Environmental Consultants Pty Ltd and Hugh Middlemis, HydroGeoLogic Pty Ltd

ISBN XXX-X-XXXXXX-XX-X

Preferred way to cite this publication

Department for Environment and Water (2023). *Far North Prescribed Wells Area Groundwater Model. Volume 4 – Flow dynamics and Potentiometric Surface Development*, DEW-TR-2023-72, Government of South Australia, Department for Environment and Water, Adelaide.

Download this document at https://www.waterconnect.sa.gov.au

Foreword

The Department for Environment and Water (DEW) is responsible for the management of the State's natural resources, ranging from policy leadership to on-ground delivery in consultation with government, industry and communities.

High-quality science and effective monitoring provide the foundation for the successful management of our environment and natural resources. This is achieved through undertaking appropriate research, investigations, assessments, monitoring and evaluation.

DEW's strong partnerships with educational and research institutions, industries, government agencies, Natural Resources Management Boards and the community ensures that there is continual capacity building across the sector, and that the best skills and expertise are used to inform decision making.

John Schutz
CHIEF EXECUTIVE
DEPARTMENT FOR ENVIRONMENT AND WATER

Acknowledgements

Internal review of the report was provided by:

- project technical lead Mark Keppel, Principal Hydrogeologist, Department for Environment and Water (DEW)
- Principal Hydrogeologist (former) Lloyd Sampson, DEW
- project groundwater modelling technical lead Juliette Woods, Principal Groundwater Modeller, DEW.
- project technical geology lead Tony Hill, Deputy Director, Geoscience and Exploration Branch and Principal Geologist, Department for Energy and Mining (DEM)
- project independent expert technical advisor, Hugh Middlemis, Principal Groundwater Engineer, HydroGeoLogic.

External review of the report was provided by:

- Paul Howe Principal Hydrogeologist, CDM Smith Pty Ltd
- Keith Phillipson, Principal Modeller, Australasian Groundwater and Environmental Consultants Pty Ltd.

DEW would like to thank the following people and organisations for their assistance with this project:

- Andrew Stannard, Principal Environmental Advisor SANTOS, for the provision of water use data from south-west Queensland tenements of SANTOS
- Michael Mayrhofer Senior Specialist Environment – Water, Broken Hill Proprietary (BHP) Olympic Dam, for the provision of pressure, temperature and salinity data from BHPs Wellfield A and Wellfield B
- Scott Delaney, Manager Development Western Flank Oil of Beach Energy, for the provision of water use data from their Western Flank tenements
- Daniel Radulovic Team Leader Mining Compliance and Regulation, DEM: for coordinating a review of unreleased water-related drill-hole data from active and non-active tenements
- Dominic Pepicelli Principal Reservoir Engineer, DEM, for advice on petroleum well test data.

Contents

1 Introduction 1

1.1 The Far North Prescribed Wells Area (FNPWA) 1
1.2 Previous modelling 1
1.3 The study area 4
1.4 Reporting structure 4
1.5 Volume objective 5
1.6 Hydrostratigraphy 6

2 Data sources 9

2.1 Water-well data 9
2.2 Petroleum well data 11
2.2.1 Stratigraphy-based descrimination of petroleum well data 13

3 Development of the uncorrected potentiometric surfaces 15

3.1 Method 15
3.2 Results 15

4 Theory of density and flow 18

4.1 Importance of density variance 18
4.2 Heat flows, thermal conductivity and thermal gradients 18
4.3 Salinity 21
4.4 Viscosity effects on groundwater flow 22
4.5 Correcting for temperature and salinity 22
4.5.1 Reference density 22
4.5.2 Density of groundwater 22
4.5.3 Driving force ratio (DFR) 23

5 Density correction methodology 24

5.1 Applying the correction for temperature and salinity 24
5.2 Assigning temperature 26
5.2.1 Data collation and quality assurance 26
5.2.2 Estimating temperature in the absence of measurement and exploring temperature as a function of depth 27
5.2.3 How the choice of temperature approximation affects density and head 29
5.3 Assigning salinity 32
5.3.1 Water wells 32
5.3.2 Petroleum wells 34
5.4 Development of density-corrected potentiometric surfaces 35
5.4.1 Reference-density determination 35
5.4.2 Density correction of head data and generation of potentiometric surfaces 36
5.4.3 Alternative correction application methodologies and reasons for rejection 36
5.5 Potentiometric surfaces of the Hutton Sandstone and Poolowanna Formation 38

6 The density-corrected potentiometric surfaces 39

6.1 General flow patterns 39

6.2 Key differences between potentiometric surface interpolations 40
6.3 Key differences between uncorrected and density-corrected potentiometric surfaces 43
6.4 Determining the extent of artesian, confined and unsaturated zones in the J-K aquifer 43
6.5 Initial groundwater conditions for numerical modelling, J-K aquifer 46
6.6 Potentiometric surfaces of the Hutton–Poolowanna Aquifer 47

7 Driving force ratio 50
7.1 Mapping the driving force ratio 50
7.2 Implications for modelling and uncertainty 54

8 Review of pressure versus elevation data with respect to groundwater flow 56
8.1 Petroleum well-derived pressure data 57
8.2 Aquifer and confining Units 58
8.3 The wellfields scale 60
8.4 Comparison between the Cooper and Eromanga Basins 64
8.5 Summary of pressure versus elevation data analysis 65

9 Data gaps and limitations 66
9.1 Well distribution 66
9.2 Data quality 66
9.3 Temperature gradients and correcting water levels for density and non-isothermal flow 66
9.4 Sub regional groundwater flow systems 67

10 Closing remarks, model assumptions and conclusions 69

11 Appendices 71
A. Exploration of gridding methodology used to develop the potentiometric surface 71
11.1 Comparison of initial gridding outputs from two software packages 72
11.2 Exploring different gridding algorithms 72
11.2.1 Surfer™ 72
11.2.2 Petrosys™ 76
11.2.3 ArcMap™ 77
11.3 Penultimate sequence of gridding and contouring 78
11.4 Back interpolation results 79
11.5 Final sequence of gridding, contouring and back interpolation 82
11.5.1 Surfer™ 82
11.5.2 Petrosys™ 82
11.6 Selection of acceptable 2019 potentiometric surfaces 83
B. Back Interpolation of potentiometric surfaces against well and spring datasets 85
C. EC to TDS conversion 103
D. Exploration of density corrections applied to the uncorrected potentiometric surface grids 105
E. 2019 Uncorrected Potentiometric Surface Contour Maps 107
F. 2019 Density-corrected Potentiometric Surface Contour Maps 113

12 Units of measurement 119
12.1 Units of measurement commonly used (SI and non-SI Australian legal) 119
12.2 Shortened forms 119

13 Glossary 120

14 References **127**

List of figures

Figure 1: Examples of density-corrected potentiometric surfaces developed for the J-K aquifer from A) Group 3 (primary conceptualisation) B) Group 2 (primary alternative conceptualisation) and C) Potentiometric surface interpretation for the Hutton–Poolowanna aquifer. 2

Figure 1.1: Location map of the Far North Prescribed Wells Area and study area. 2

Figure 1.2: Total licensed volume (176 ML/d) presented by licence purpose description, FNPWA. 3

Figure 1.3: Licensed volume sourced from the GAB hydrogeological super-basin (134 ML/d) presented by licence purpose description, FNPWA. 3

Figure 1.4: A) 3D projection of structure surface used in numerical model. B) Cross section through study area showing model layers and key structures. 8

Figure 2.1: Location and most recent date of water level and pressure observations. A) J-K aquifer B) Hutton–Poolowanna aquifer. 12

Figure 3.1: Example of an uncorrected potentiometric surface that broadly matches study conceptualisation 16

Figure 4.1: Maximum recorded groundwater temperature versus depth of screened interval. 19

Figure 4.2: Temperature data, modelled temperature profile and linear gradient for Big Lake 33). 20

Figure 4.3: Heat flow map of Australia 21

Figure 5.1: Spatial distribution of wells with measured maximum groundwater temperature versus wells requiring an estimated bottom-hole temperature. 28

Figure 5.2: Histogram of screen depth for water wells and petroleum wells. 31

Figure 5.3: A) Depth to the mid-point of the Main Eromanga Aquifer Sequence and B) J-K aquifer salinity represented by Thiessen polygons 37

Figure 6.1: Examples of uncorrected potentiometric surfaces developed for the J-K aquifer from each group 41

Figure 6.2: Examples of density-corrected potentiometric surfaces developed for the J-K aquifer from each group 42

Figure 6.3: Difference between uncorrected and density-corrected potentiometric surfaces developed for the J-K aquifer from each group 44

Figure 6.4: Extent of artesian, confined and unsaturated conditions in the J-K aquifer based on uncorrected potentiometric surface (environmental head) 45

Figure 6.5: A) Density-corrected potentiometric surface for the J-K aquifer (Layer 1 and 3) B)'Primary alternative' density-corrected potentiometric surface 48

Figure 6.6 : A) Uncorrected and B) density-corrected potentiometric surface of the Hutton Sandstone and Poolowanna Formation. C) Density-corrected head contours near Cadenza-1 and Paranta-1 49

Figure 7.1: Slope of the Main Eromanga Aquifer Sequence (mid-point depth) 51

Figure 7.2: Hydraulic gradient of the J-K aquifer (Group 1, Panel A; Group 2, Panel B; Group 3, Panel C; Group 4, Panel D) 52

Figure 7.3: Driving force ratio (Group 1, Panel A; Group 2, Panel B; Group 3, Panel C; Group 4, Panel D) 53

Figure 8.1: Formation pressure vs screen depth for petroleum wells in the Eromanga Basin units of the Cooper Basin region. 57

Figure 8.2: Density-corrected RSWL vs screen depth for petroleum wells in the Eromanga Basin units of the Cooper Basin 58

Figure 8.3: Namur and Adori Sandstone-derived RSWL measurements from Petroleum well derived test-work 59

Figure 8.4: Hutton Sandstone-derived RSWL measurements from Petroleum well derived test work 59

Figure 8.5: Birkhead, Murta, Poolowanna and Westbourne Formation-derived RSWL measurements from petroleum well derived test work 60

Figure 8.6: Location map for Worrior, Snatcher, Moomba, Merrimilia wellfields and Winna 4 61

Figure 8.7: RSWL measurements from Worrior Wellfield 61

Figure 8.8: RSWL measurements from Snatcher Wellfield 62

Figure 8.9: RSWL measurements from Snatcher Wellfield compared to time 62
Figure 8.10: RSWL measurements from Merrimelia and Moomba wellfields 63
Figure 8.11: RSWL measurements from Winna 4 64
Figure 8.12: Comparison of pressure versus depth between Cooper and Eromanga Basin-derived measurements. A) Formation pressure (m head) versus screen depth (m), B) Corrected RSWL versus Screen elevation (m AHD), C) Corrected RSWL versus Time (years), D) Location of data points 65
Figure 11.1: Comparison of typical gridding methods using *Surfer's 'GridData_Comparison'* script (Datum: GDA94 SA Lamberts; Contours at: 20 m AHD intervals) 73
Figure 11.2: Initial *Surfer*™ variograms 75
Figure 11.3: Final *Surfer*™ Variograms 76
Figure 11.4: Example of an acceptable potentiometric surface (A) and those excluded from further analysis (B, C, D) [10 m AHD contour intervals are not shown on Panel B or C due to the large data range] 81
Figure 11.5: A) Groundwater temperature of the J-K aquifer (mid-point) and B) 2019 density-corrected potentiometric surface (grid method) of the J-K aquifer 106
Figure .11.6: 2019 uncorrected potentiometric surfaces of the J-K aquifer (I) 108
Figure 11.7: 2019 uncorrected potentiometric surface of the J-K aquifer (II) 109
Figure 11.8: 2019 uncorrected potentiometric surface of the J-K aquifer (III) 110
Figure 11.9: 2019 uncorrected potentiometric surface of the J-K aquifer (IV) 111
Figure 11.10: 2019 uncorrected potentiometric surface of the J-K aquifer (V) 112
Figure 11.11: 2019 density-corrected potentiometric surface of the J-K aquifer (I) 114
Figure 11.12: 2019 density-corrected potentiometric surface of the J-K aquifer (II) 115
Figure 11.13: 2019 density-corrected potentiometric surface of the J-K aquifer (III) 116
Figure 11.14: 2019 density-corrected potentiometric surface of the J-K aquifer (IV) 117
Figure 11.15: 2019 density-corrected potentiometric surface of the J-K aquifer (V) 118

List of tables

Table 1-1: Summary of hydrostratigraphic unit nomenclature and relationship to model layer design. 7
Table 5-1: Uncertainty analysis of density correction methodology 25
Table 5-2: Difference in estimated BHT (maximum groundwater temperature) for wells with no BHT recorded between linear line of best-fit cases. 30
Table 5-3: Summary of screen depths for water wells and petroleum wells. 31
Table 5-4: Comparison of hydraulic head density corrections for water wells based on variable BHT estimates and production zone depth. The key variable input are the statistical values found in Tables 5-2 and 5-3. Key outputs ae in colour. 33
Table 5-5: Comparison of hydraulic head density corrections for petroleum wells based on variable BHT estimates and production zone depth. The key variable input are the statistical values found in Tables 5-2 and 5-3. Key outputs ae in colour. 33
Table 5-6: Depth to mid-point of the J-K aquifer at GAB springs. 36
Table 7-1: Summary of mapped DFR for each of the representative potentiometric surface 54
Table 11-1: Back interpolation of penultimate potentiometric surfaces against well and spring datasets. (Note: 5 129 total springs (SA Geodata only), cells are square). 85
Table 11-2: Back interpolation of final potentiometric surfaces against well and spring datasets. (Note: 5 163 total springs. Cells are square). 91
Table 11-3: EC to TDS conversion table. 103

Executive summary

The documentation for the Far North Prescribed Wells Area Groundwater Model is presented over several volumes. The purpose of these reports is to provide an overview of the study area, provide scientific evidence for the conceptual hydrogeological model (CHM) used as the basis for the decisions and assumptions used during model construction and history matching. This volume (Volume 4) provides a description of groundwater flow dynamics, through the development of a density-corrected potentiometric surface.

A scientifically-sound and density-corrected potentiometric surface is crucial to understanding and interpreting major regional groundwater flow systems such as the Eromanga Basin where deep aquifers can have high water temperatures. Potentiometric surfaces were developed for the two main hydrostratigraphic unit groupings within the Main Eromanga Aquifer Sequence. The first and most extensive is the Cadna-owie–Algebuckina–Adori–Namur Sandstone aquifer grouping (J-K aquifer), which covers the entire study area and exhibits high hydraulic connectivity between its hydrostratigraphic formations. The second grouping is the deep Hutton –Poolowanna aquifer; although of limited extent, it is laterally continuous on its western side with the J-K aquifer, and yet is conceptually regarded as sufficiently deep and hydraulically isolated by the overlying Birkhead Formation confining unit to warrant separate treatment in the east.

Initially, uncorrected hydraulic head data for the J-K aquifer was generated to describe the environmental head distribution. Preliminary gridding of the uncorrected head data highlighted significant differences between surfaces generated using similar algorithms, but different software packages. This was especially the case in the central and eastern parts of the study area where there is limited data to constrain the interpolation methods. Subsequently, rigorous testing of various gridding algorithms established a range of potentiometric surfaces that are acceptable in terms of consistency with the CHM. These potentiometric surfaces were then used to describe the extent of artesian and non-artesian conditions, saturated and confined aquifer conditions, and to hypothesise an alternative CHM for uncertainty analysis testing.

Multiple versions of density-corrected potentiometric surfaces of the J-K aquifer unit were then generated to determine groundwater flow directions and potential recharge and discharge areas. Available aquifer salinity and temperature data and the temperature gradient were used, along with a relationship for depth-dependent temperature in the well column. An average areal reference density of 997.2 kg/m^3 was applied for correction; this represents the average density found near the springs within the study area.

All interpreted potentiometric surface variations show a generally radial pattern of flow with inflows and recharge from the east, north, west and parts of the south, and with flows toward discharge zones near the springs and towards some of the southern margins (Figure 1). Other features include steep hydraulic gradients along the western and north-western margins of the basin, and a depression near the western edge of the underlying Cooper Basin that reflects discharge from co-produced water extraction on the 'Western Flank' (Figure 1). Pressure data from the Cooper Basin region also suggests a general downward flow direction of groundwater, although the specifics of this are variable across the basin as well as between formations.

However, significant differences between the interpolated potentiometric surfaces are also obvious. The 19 most scientifically plausible potentiometric surfaces can be divided into four groups that display similar features. The largest variations between groupings generally occur where the software employed interpolated surfaces in regions that were data poor. In such regions, interpretive variations include significant differences in groundwater flow direction as well as magnitude of head. For the purposes of choosing an initial condition for modelling, a representative surface from Group 3 was chosen because this group displays a groundwater flow pattern similar to what is conceptually understood to occur, with inflows from the north (Northern Territory), north-east and east (Queensland) (Figure 1A). Group 2 is the 'primary alternative' to Group 3 because it is the group of surfaces that shows the least flow from the east and therefore differs the most from the primary conceptualisation (Figure 1B).

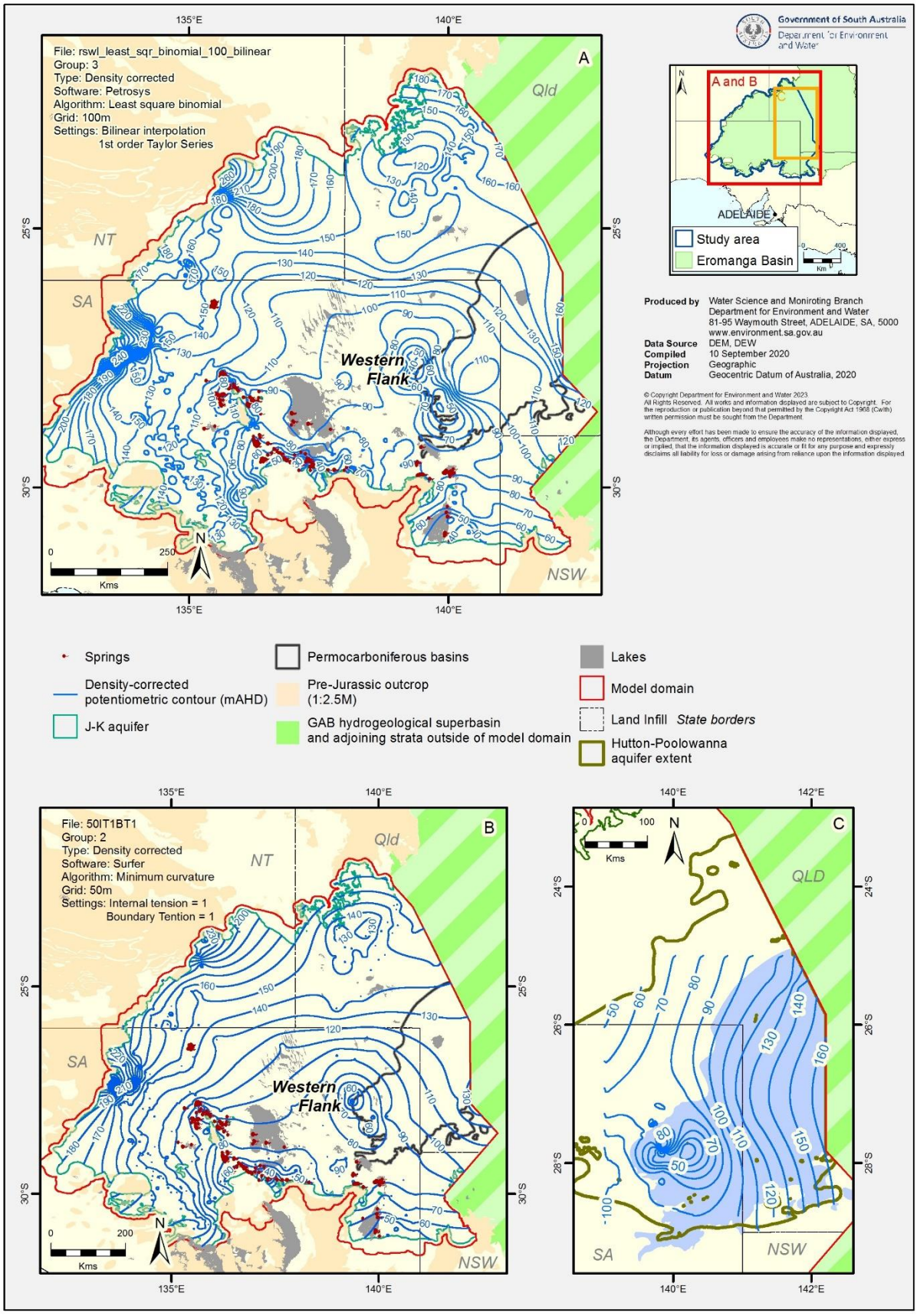

Figure 1: **Examples of density-corrected potentiometric surfaces developed for the J-K aquifer from A) Group 3 (primary conceptualisation) B) Group 2 (primary alternative conceptualisation) and C) Potentiometric surface interpretation for the Hutton–Poolowanna aquifer.**

Separate uncorrected and corrected potentiometric surfaces for the Hutton–Poolowanna aquifer were generated. As this potentiometric surface is not considered as critical with respect to springs and considering the sparse data points when compared to the J-K aquifer, the algorithm assessment was not undertaken. Rather, the minimum curvature was chosen as it was able to produce a few potentiometric surfaces for the J-K aquifer considered plausible during this study. Potentiometric surface contours for the Hutton–Poolowanna aquifer show a general inflow into the study area from the east (Figure 1C).

The potential for vertical flow within the Eromanga and Cooper Basin regions was investigated. Pressure versus depth profiles were generated from petroleum industry data, to determine the distribution of formation pore pressures. Although the same formation-pressure database as compiled for potentiometric surface calculation was used, all pressure data were corrected to a freshwater head and pressure data were described against a common height datum (m AHD). Overall, when pressure measurements are compared to elevation, there is a relatively lower pressure found in deeper strata compared to those above, suggesting a downward pressure gradient. The gradient may be natural but is likely to at least be partly due to petroleum hydrocarbon extraction. Evidence for a potential downward pressure gradient does not suggest groundwater migration is actually occurring, as other evidence is required for this to be established.

The effect of temperature-derived density-driven (non-isothermal) flow cannot be ignored when evaluating the Eromanga Basin groundwater flow system. It can lead to mixed convection processes and possibly free convection. A driving force ratio (DFR) analysis was undertaken to determine the relative importance of free convection in the J-K aquifer and to assess the validity of potentiometric surfaces for use during this study. The DFR depends on the fluid density, the hydraulic gradient and the aquifer slope.

DFR analysis suggests that between 40 and 50% of the study area may be influenced by mixed convection processes (and possibly free convection), predominantly in the deeper parts of the Eromanga Basin and encompassing the Cooper Basin region. Further, groundwater temperatures in these parts of the study area are typically high, making fluid density relatively low. DFR analysis consequently suggests that in these areas, an isothermal assumption and assumed potentiometric surfaces may be inaccurate. However, and most importantly key management zones around artesian springs are not interpreted to be impacted by free convection and therefore the generated potentiometric surfaces are still considered useful for the purposes of this study.

Consequently, while the effects of temperature variations on the hydrodynamics of the Great Artesian Basin (GAB) hydrogeological super-basin are the subject of ongoing research, for the purpose of this model, it is assumed that the Eromanga Basin in South Australia is predominantly a forced convection (horizontal) flow system. Uncertainties related to free convection can be partially addressed within the numerical modelling workflow. Longer term, this assumption will be revisited periodically as new data, scenarios and technology come to hand.

Other data gaps and uncertainties include:

- ***Well distribution*** Although well infrastructure associated with the J-K aquifer is extensive, this infrastructure is not evenly distributed across the basin, and there are large parts of the basin where there are no wells present.
- ***Data quality*** Although a protocol for data validation was applied to limit the use of poor-quality data being used in potentiometric surface generation, there may be unresolved data quality issues that affect interpretation. For example, the use of wells in the Far North Monitoring Network that are also water supply wells may result in an unresolvable inherent error even though reasonable effort is taken to allow wells to recover before measurement.

- ***Temperature gradients and correcting water levels for density*** Correction of aquifer pressure measurements to account for density assumes a linear temperature gradient between the screened interval and the measurement point. Where no temperature has been recorded at the time an aquifer pressure has been measured, the bottom-hole temperature was estimated using an approximate geothermal gradient for the J-K aquifer across the study area. However, significant variations in gradient may occur between Mesozoic and Permo-Carboniferous units, driven by the insulator effects of significant coal measures found in the latter. Such variations are best described when a continuous temperature log for a given well is collected. This identifies a data requirement of continuous temperature data from shut-in monitoring bores to provide data to benchmark the methodology. Consequently, the lack of continuous temperature log data represents a data gap concerning adequately capturing variations in temperature gradient over the study area.
- ***Sub-regional groundwater flow systems*** For this conceptual hydrogeological model, groundwater levels and pressures from the Cadna-owie Formation, Algebuckina Sandstone and lateral equivalents such as the Namur Sandstone and Adori Sandstone have been interpreted together, resulting in a single potentiometric surface to describe groundwater flow for the J-K aquifer. However, at a sub-regional level, there may be lateral discontinuity caused by either structural deformation or lithological heterogeneity and consequently several discrete or semi-discrete or sub-basinal groundwater flow systems may be present.
- For the purposes of groundwater regulation and management, initially conceptualising a single groundwater system is an appropriate simplification as it fosters a 'whole of groundwater system' approach to management. In the absence of concrete evidence, assuming lateral flow continuity across the basin is a conservative approach. Finally, best practice modelling principles (Barnett et al. 2012) encourage the development of an unbiased balance between model simplicity and complexity, as in this case, noting that model predictions that integrate larger areas are often less uncertain because characterisation methods are well-suited to discern bulk properties.

1 Introduction

Groundwater in the Far North Prescribed Wells Area (FNPWA) is vital for the success of the mining, energy, pastoral and tourism industries, and the provision of community water supplies in the Landscape SA South Australian Arid Lands (LSA SAAL) Management Region (Figure 1.1). The continued success and expansion of these industries is dependent on balancing the needs of existing users and the environment. Of particular environmental importance are the spring wetland communities in the discharge areas of the Great Artesian Basin (GAB) hydrogeological super-basin which are listed under the Commonwealth *Environmental Protection and Biodiversity Conservation Act 1999*. Protection of these environments is regulated and managed at a State level through the Far North Water Allocation Plan (FNWAP), through the description and implementation of spring buffer zones, water management zones and drawdown triggers at state borders. Further, the South Australian Government also has regulatory responsibilities over water management under the *Roxby Downs (Indenture Ratification) Act 1982*.

With demand for groundwater expected to grow in the mining and energy industries, a new numerical groundwater flow model is required to evaluate current knowledge and determine key knowledge gaps. This model will also be a tool to inform management of groundwater resources, both ongoing and for future major developments.

1.1 The Far North Prescribed Wells Area (FNPWA)

Groundwater in the FNPWA is managed under the FNWAP; a key principle being to manage groundwater resources by pressure (head) and to allocate by volume. The FNPWA was prescribed on 27 March 2003, and the first WAP was adopted on 16 February 2009. The 2021 FNWAP was adopted on the 27 February 2021.

Currently, the total groundwater allocation is 176 ML/d (2018–19 data) (Figure 1.2), with the majority (approximately 76% or 134 ML/d) sourced from the GAB hydrogeological super-basin aquifers (Figure 1.3). These allocations are made up of mining, industrial and human requirement supplies, co-produced water (water extracted with petroleum hydrocarbons), stock and domestic use, bore-fed wetlands and other amounts. Demand on the groundwater resources is expected to grow, particularly in response to growth in the mineral and energy industries.

1.2 Previous modelling

Although several groundwater models cover part of the western margin of the GAB hydrogeological super-basin, they are subject to one or more of the following limitations in terms of suitability for cumulative impact assessment to inform management of aquifers within South Australia (SA):

- a small or constrained geographical extent
- an over-simplified or limited aquifer system representation
- proprietary ownership by private companies that prohibits use for regulatory water resource assessments
- being based on outdated hydrogeological conceptualisations that do not reflect the current understanding of basin structure and groundwater processes including recharge and discharge
- not taking into account other interconnected basins that form important water resources in the FNPWA
- not being designed to consider the cumulative impacts of multiple groundwater users.

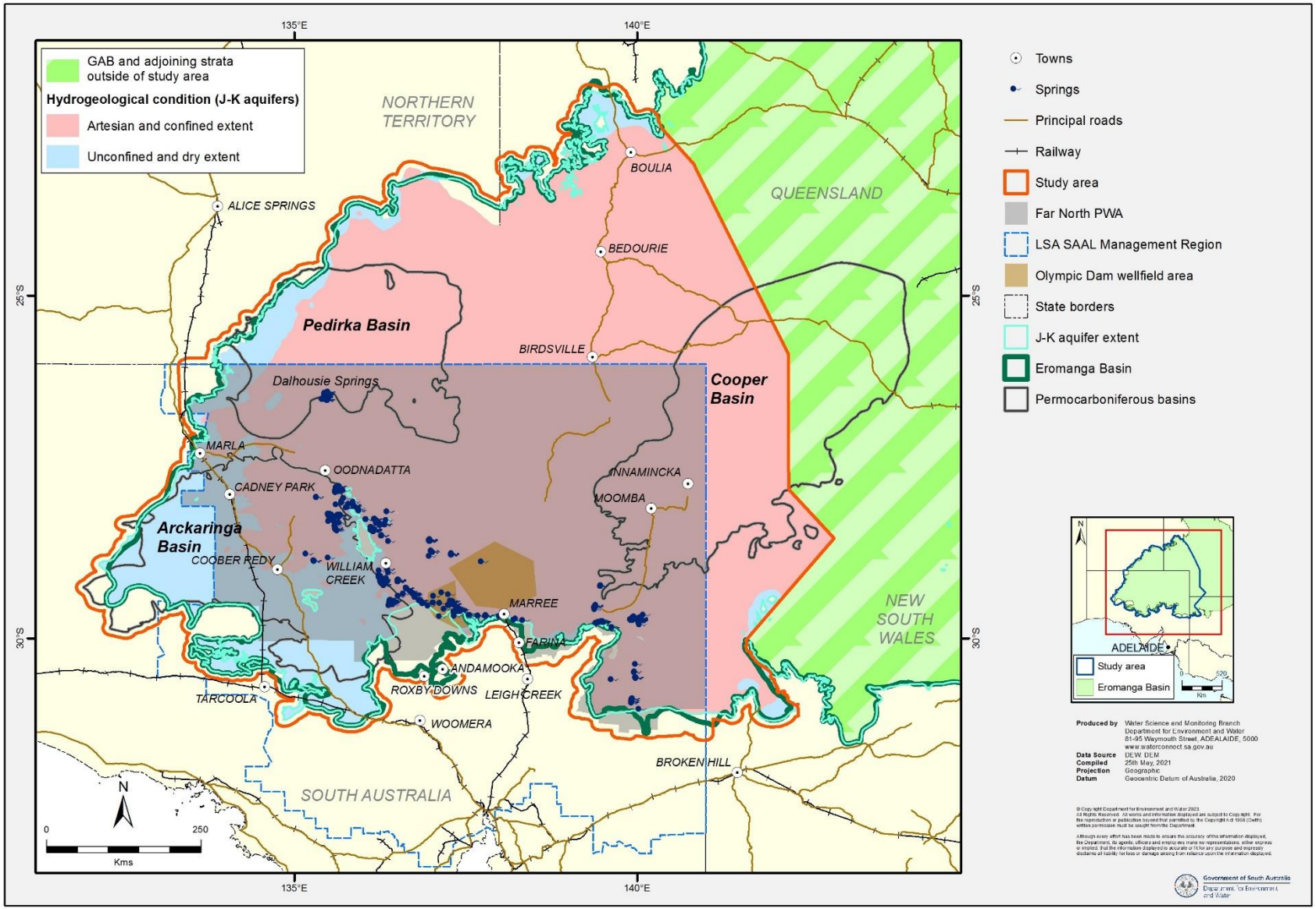

Figure 1.1: Location map of the Far North Prescribed Wells Area and study area.

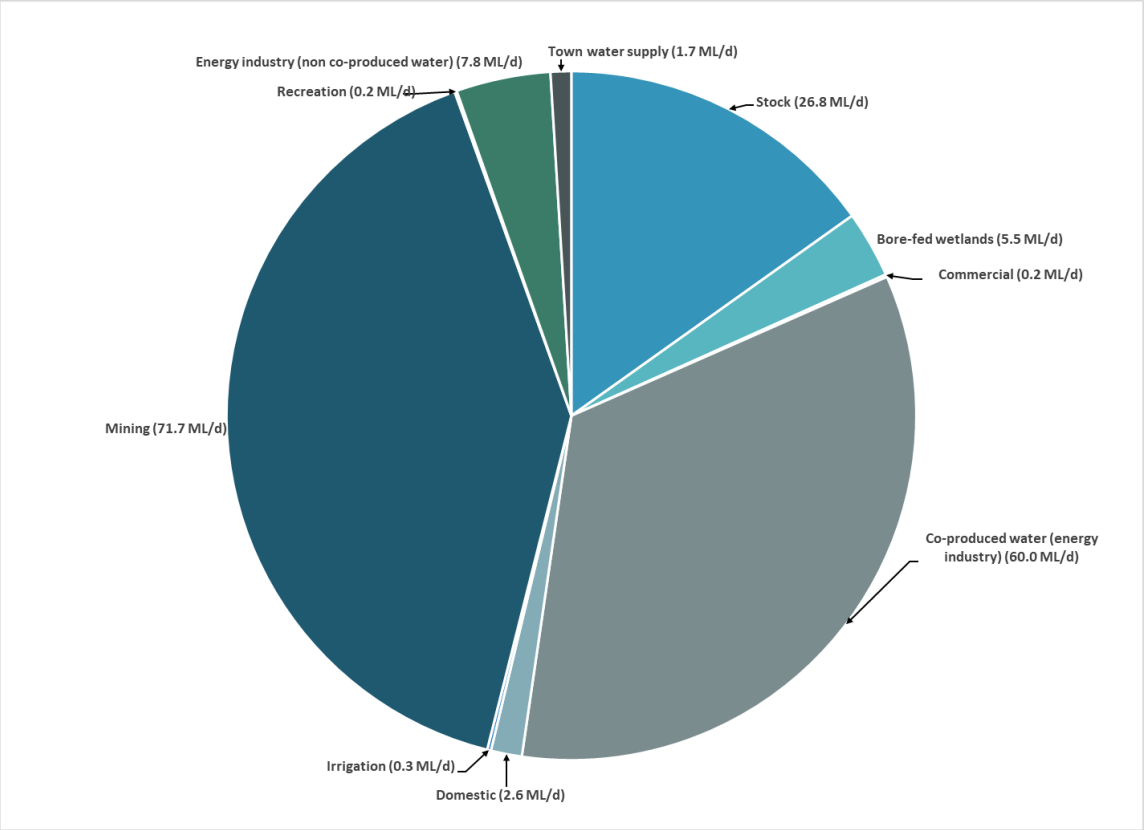

Figure 1.2: Total licensed volume (176 ML/d) presented by licence purpose description, FNPWA.

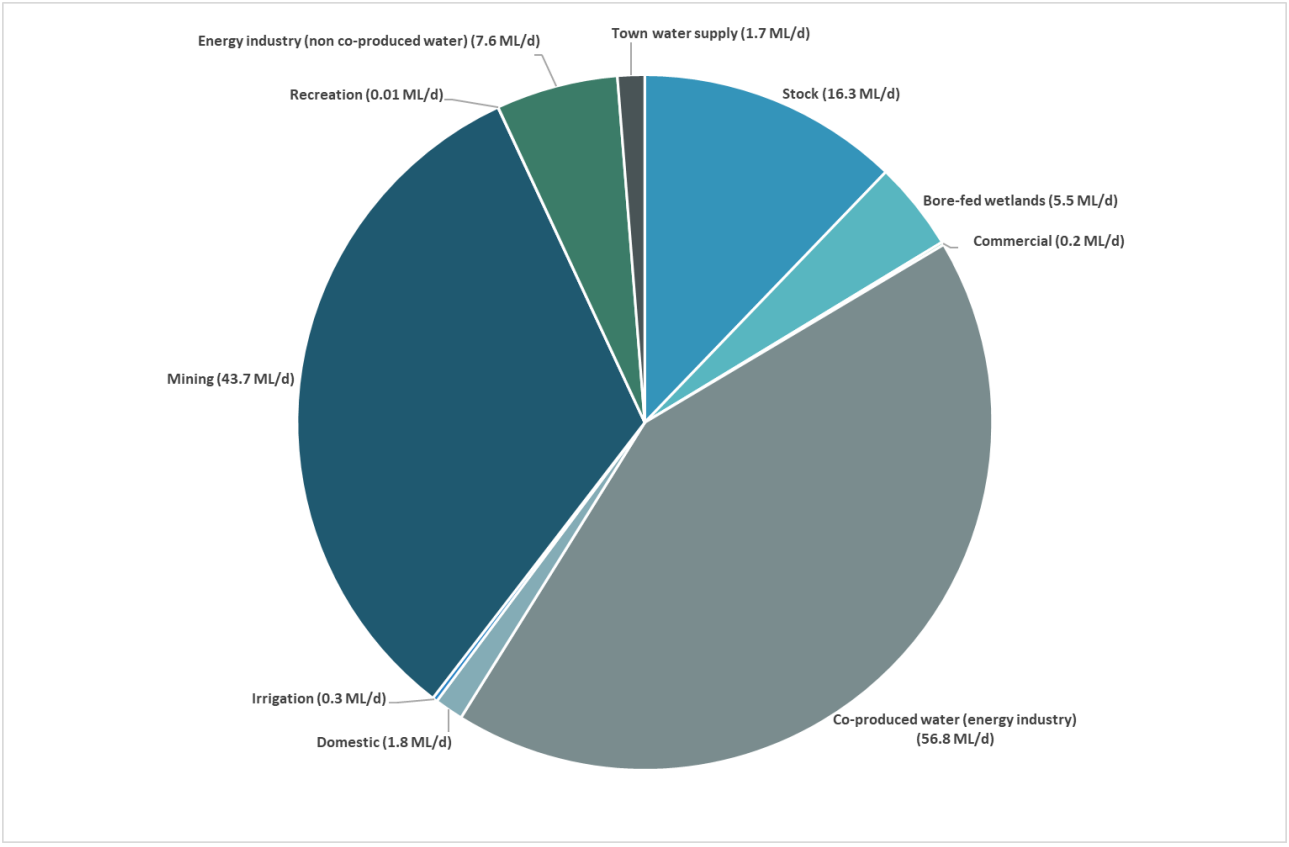

Figure 1.3: Licensed volume sourced from the GAB hydrogeological super-basin (134 ML/d) presented by licence purpose description, FNPWA.

DEW has developed a numerical groundwater flow model to address the gaps identified in the existing models and to provide a tool to inform management of groundwater resources in the FNPWA. This model is consistent with the latest science and knowledge can be updated in the future, providing a quantitative and predictive tool for development assessments and to inform management decisions. Further discussion of previous modelling is provided in Volume 8 of this report.

1.3 The study area

To cover an area of sufficient extent to achieve the model objectives, the study area (Figure 1.1) encompasses portions of the Eromanga Basin in Queensland (Qld) and New South Wales (NSW), part of the Cooper Basin in Queensland, and the entirety of the following administrative areas and features of hydrogeological significance:

- Eromanga Bain in SA and the Norther Territory (NT)
- Cooper Basin in SA
- Pedirka Basin
- Arckaringa Basin
- the Far North Prescribed Wells Area (PWA).

The initial model design is to simulate groundwater flow within the Main Eromanga Aquifer Sequence, with a focus on the Far North PWA in SA. Future modelling programs may involve extensions to other groundwater flow systems, such as the Cooper, Arckaringa and Pedirka Basins.

The study area (Figure 1.1) covers a total area of about 721,370 km^2. A 10 km-wide external buffer encompassing the features described in the above dot points extends beyond the southern, western and northern perimeters of the study area. The eastern boundary extends between 245 km and 420 km from the NT border into Qld; between 125 km and 190 km from the SA border into Queensland; and between 60 km and 140 km into NSW from the SA border. The eastern boundary is designed to allow for lateral inflow of groundwater to the study area in some areas and no flow in others, consistent with the groundwater flow system contours interpreted during this project. The spatial extent of the eastern boundary was selected to provide a sufficient distance away from the areas of interest in SA, so that the hydraulic conditions along the boundary do not materially influence simulation results.

1.4 Reporting structure

Given the size and multi-faceted nature of the investigation supporting model development, reporting occurs over several volumes:

1. Simplified technical summary
2. Hydrogeological framework
3. Hydraulic parametrisation
4. Groundwater flow system dynamics
5. Time series data
6. Recharge and ischarge processes
7. Water use and balance estimations
8. Model construction and history matching

1.5 Volume objective

This volume (Volume 4) provides a description of groundwater flow dynamics within the study area. These dynamics are primarily described through the development of a density-corrected potentiometric surface. The volume is broken into 10 chapters:

- **Chapter 1**: (this chapter): introduction to the project and volume topic
- **Chapter2**: discussion of the two primary data sources (water and petroleum wells) and the data validation process
- **Chapter 3**: development of a scientifically plausible uncorrected potentiometric surface for the study area and investigation of algorithm efficacy in doing so
- **Chapter 4**: an introduction to the salient points of density effects on groundwater flow in groundwater systems pertinent to this study
- **Chapter 5**: an overview of the density correction methodology employed for this study and assessment of reference density choice
- **Chapter 6**: a discussion of the scientifically plausible density-corrected potentiometric surfaces developed for this study and justification for the choice of primary and alternative conceptualisation versions
- **Chapter 7**: Driving force ratio (DFR) analysis as means of assessing the relative importance of free convection on groundwater flow as well as the validity of potentiometric surfaces for use during this study
- **Chapter 8**: a review of pressure versus elevation data from petroleum wells in the Cooper Basin region to explore general trends in groundwater flow
- **Chapter 9**: a discussion of key limitations and data gaps
- **Chapter 10**: concluding remarks.

A scientifically-sound density-corrected potentiometric surface is crucial to understanding and interpreting major regional groundwater flow systems such as the Eromanga Basin where deep aquifer sequences involve high water temperatures. Potentiometric surfaces were developed for the two main hydrostratigraphic unit groupings within the Main Eromanga Aquifer Sequence. The first and most extensive is the Cadna-owie–Algebuckina–Adori/–Namur Sandstone aquifer grouping (J-K aquifer), which covers the entire modelling domain and exhibits high hydraulic connectivity between its hydrostratigraphic formations. The second grouping is the deep Hutton–Poolowanna aquifer; although of limited extent, it is laterally continuous on its western side with the J-K aquifer, and yet it warrants separate treatment as it is deep and hydraulically isolated by the overlying Birkhead Formation

confining unit. The year 2019 was used as the cut-off for data review as this marks the commencement date of the modelling project.

1.6 Hydrostratigraphy

Table 1.1 and Figure 1.4, which have been taken from Volume 2, summarise the key stratigraphic, hydrostratigraphic and model layer nomenclature used during this study. The terms discussed below are used throughout this and other volumes.

As stated previously, the study area covers a sizable portion of the Mesozoic Eromanga Basin, including its entire occurrence in SA and the NT. The Eromanga Basin is the largest volumetric component of the GAB hydrogeological super-basin (Krieg 1995) and can be described as having a bowl shape that is partly defined and modified by faulting (Figure 1.4).

In the SA part of the Eromanga Basin, the most important strata sequence is the Cadna-owie Formation, the Algebuckina Sandstone, and their lateral equivalents (primarily the Namur Sandstone and Adori Sandstone). The collective hydrostratigraphic terminology commonly used in SA for aquifers and partial aquifers within these chronostratigraphically and lithologically connected extensive units is the 'J-K aquifer' (Table 1.1). It should be noted that within this general hydrostratigraphic nomenclature there can exist sub-regional scale lithological variation or structural deformation that may promote the development of sub-basinal groundwater flow systems.

The other important aquifer grouping is found in the deeper parts of the Eromanga Basin near the Cooper Basin and is associated predominantly with the Hutton Sandstone and the Poolowanna Formation. In the Cooper Basin region, these aquifer and partial aquifer units and/or groupings are separated from one another by a series of finer grained confining units such as such as the Birkhead, Murta and Westbourne formations (Table 1.1).

The initial design of the model is to primarily simulate groundwater flow within the sequence of strata defined by the top of the Cadna-owie Formation, called the 'C Horizon', to the base of Mesozoic sediments (base of the Poolowanna Formation), or the top of the pre-Jurassic units, called the '"J-Horizon'. Collectively, this package of aquifers and confining units is called the 'Main Eromanga Aquifer Sequence' (Table 1.1). It is essentially the combination of the extensive J-K aquifer and the sub-basinal Hutton–Poolowanna aquifer, including intervening confining units.

The Main Eromanga Aquifer Sequence is overlain by a confining unit composed of shaly mudstone units of low permeability that are collectively part of the Rolling Downs Group. The main elements of this group are the Bulldog Shale and Oodnadatta Formations which outcrop extensively near the western margin of the GAB hydrogeological super-basin, whereas the Wallumbilla Formation and Allaru Mudstone occur at depth in the central portions of the basin near the borders of SA and Qld.

Of the strata underlying the Main Eromanga Aquifer Sequence, the most important are the sedimentary rocks of the Permo-Carboniferous Arckaringa, Pedirka and Cooper basins. Not only do the sandstones, siltstones, shales, diamictites and coal beds in these basin sediments contain aquifers themselves, but also significant oil, gas and coal resources under varying degrees of development. Outside of the Permo-Carboniferous basins, metasedimentary rocks of the early Paleozoic Warburton Basin, Precambrian rocks of the Adelaide Geosyncline and crystalline Archaean rock may also be found.

For model construction, the Main Eromanga Aquifer Sequence was discretised into 5 model layers based on regional scale hydrostratigraphy (Figure 1.4). These included the Cadna-owie Formation Aquifer/leaky aquitard, the Murta Formation confining layer, the Namur–Algebuckina Sandstone Aquifer, the Birkhead Formation confining layer and the Hutton–Poolowanna aquifer. Underlying these is a layer of nominal thickness representative of the Pre-Jurassic Basement.

Table 1.1: Summary of hydrostratigraphic unit nomenclature and relationship to model layer design.

Collective term	Western study area					Cooper Basin region, study area					Whole of study area	
	Stratigraphic unit	Hydrostratigraphic unit	Model layer name	Hydrogeological characteristic	Qualitative permeability	Stratigraphic unit	Hydrostratigraphic unit	Model layer name	Hydrogeological characteristic	Qualitative permeability	[a]Max. thick. (m)	[a]Ave. thick. (m)
Main confining units	Rolling Downs Group	Main confining unit		Confining unit	Low	Rolling Downs Group	Main confining units		Confining unit	Low	NA	NA
"C' Horizon												
Main Eromanga Aquifer Sequence	Cadna-owie Formation (and lateral equivalents)	J-K aquifer	Cadna-owie Formation (Layer 1)	Partial aquifer/ aquifer	Medium	Cadna-owie Formation	Intra-sequence confining unit	Cadna-owie Formation (Layer 1)	Leaky aquitard	Low	689[b]	42
	Algebuckina Sandstone		Namur–Algebuckina Sandstone aquifer, (Layer 3)	Aquifer	High	Murta Formation and McKinlay Member	Intra-sequence confining unit	Murta Formation confining unit (Layer 2)	Low permeability confining unit. McKinlay Member included initially as conservative option; however, an alternative conceptualisation to include within layer 3 is an option.	Low	122	49
						Adori Sandstone, Westbourne Formation*, Namur Sandstone	J-K aquifer	Namur–Algebuckina Sandstone aquifer (Layer 3)	Aquifer	High	1259	211
						Birkhead Formation	Intra-sequence confining unit	Birkhead Formation confining unit (Layer 4)	Low permeability confining unit	Low	225	72
						Hutton Sandstone and Poolowanna Formation	Hutton–Poolowanna aquifer	Hutton–Poolowanna aquifer (Layer 5)	Aquifer	Medium	855	256
'J' Horizon												
Basement	Pre-Jurassic	Basement	Pre-Jurassic Basement (Layer 6)	Partial aquifer. A designated thickness specified below layer 3 with variable boundary conditions to allow for broad upward or downward leakage. Base of Layer 6 is a no flow boundary	Variable	Pre-Jurassic	Basement	Pre-Jurassic Basement (Layer 6)	A designated thickness specified below Layer 5 with variable boundary conditions to allow for broad upward or downward leakage. Base of layer 6 is a no flow boundary	Variable	NA	User defined

Note: Table shading reflects hydrogeological properties of model layers. [a] Depths based off isopach interpolation. [b] Maximum thickness was interpolated in close vicinity to a mapped fault but cannot be confirmed. Confirmed thickness of 357 m based off intersection found in Well Unit no. 684200195.

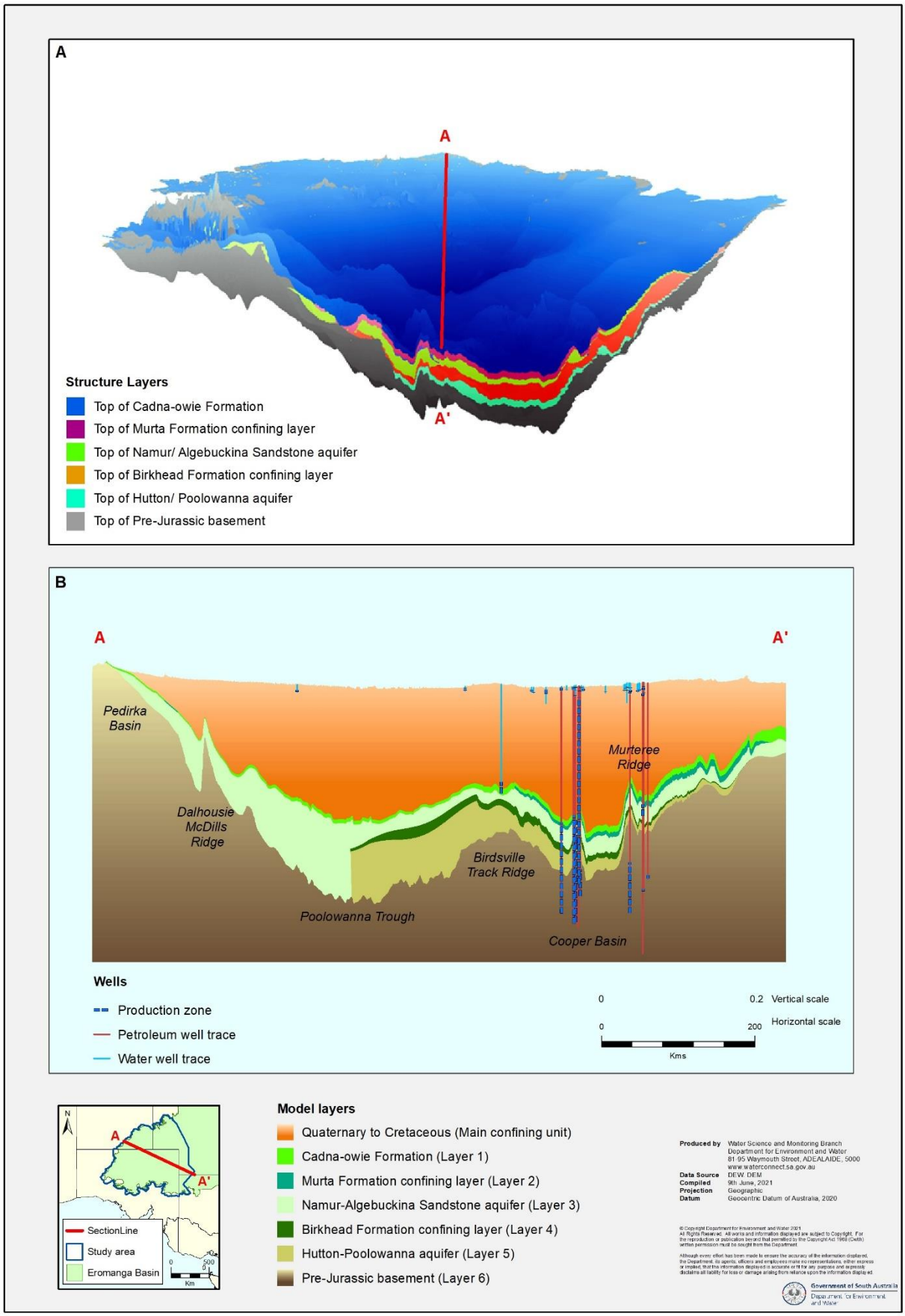

Figure 1.4: A) 3D projection of structure surface used in numerical model. B) Cross section through study area showing model layers and key structures.

2 Data sources

This chapter describes the sources from which water level and pressure (hydraulic head) data were obtained, as well as how data were collated and evaluated. This validated water level data were then used to develop the potentiometric surfaces for use in numerical modelling. The primary sources included water-well and petroleum-well data found in both State Government and industry-maintained databases.

Water-level (potentiometric surface) maps of current conditions are used as initial heads for the groundwater numerical model. The accuracy of a potentiometric surface map depends on the spatial distribution of the bores and the accuracy of bore locations and measured water levels. Given the sparsity of data, the potentiometric surface maps are not strictly constrained temporally. Rather, the surfaces use a combination of ranked data between the present day and the mid-20th Century.

2.1 Water-well data

A systematic process was applied to compile, filter, verify and re-evaluate water level records. This data was used to develop a set of density-corrected potentiometric surfaces that represent current groundwater conditions within the study area. Raw data from the following sources were included:

- Water level records for the Main Eromanga Aquifer Sequence were sourced from SA Geodata. Observations spanning 1886 to the April–May 2019 monitoring round of the State Far North Groundwater Monitoring Network. It comprises approximately 7,000 individual records from over 1,000 wells. Note that data processing of water level records from the Far North Monitoring Network occurred prior to the late October to November 2019 monitoring round. As such, the latest water level observations recorded in October to November 2019 from 43 of 71 monitoring network wells were not incorporated in the 2019 potentiometric surfaces.
- In April 2019, Broken Hill Proprietary (BHP) provided DEW with a database of 11,448 water level records from 108 wells that monitor groundwater responses to extraction at Wellfield A and Wellfield B for the Olympic Dam mine. Therefore, any subsequent monitoring records were not incorporated in the 2019 potentiometric surfaces.
- The Queensland Government, Department of Natural Resources and Mines (DNRM) Groundwater Database was interrogated to source approximately 3,600 water level records from 81 wells with a screen completion across a single Main Eromanga Aquifer Sequence unit within the Queensland portion of the study area (Queensland Government, 2019b).
- Water level records from the J-K aquifer were sourced from the NT Government's online water information portal, NR Maps. These data were cross-referenced against water level records collated as part of previous potentiometric surface mapping (Sampson et al. 2013) and bore audit records provided by the NT Government and comprised records from 160 wells.
- Aquifer pressure observations recorded in mid-2019 from four wells in western NSW were sourced from WaterNSW to improve the accuracy of gridding along the eastern boundary of the study area.

Individual water level observations were then used to develop a data-quality rating categorisation based on the best-available data for each well using the following (in order of reliability):

1. valid time-series shut-in pressures (for artesian wells) and non-pumping water levels (for non-artesian wells)
2. time-series flowing pressures for artesian wells
3. time-series observations recording no pressure but rather a qualitative indication of artesian condition reported. In such cases, a depth to water of zero is typically provided
4. reported depths (or observations recorded at the time of drilling)
5. qualitative comments concerning the presence of groundwater
6. observations requiring further check in the database
7. suspected erroneous pressures (for artesian wells) and water levels (for non-artesian wells).

Observations flagged in SA Geodata as 'pumping', 'dry' or 'anomalous' were excluded from further analysis, while other observations were subsequently checked and re-rated (if required) according to available records in the database.

Valid water level and pressure observations were then classified by the time of observation into seven categories, typically in 10-year blocks: 2010 to 2019, 2000 to 2009, 1990 to 1999, 1980 to 1989, 1970 to 1979, 1960 to 1969, and 1959 and older. For each well, the latest recorded, valid water level and pressure observation in the 2010 to 2019 category was identified; this limited the number of water level and pressure observations from individual wells to a total of 429 observations: comprising 337 in SA, 23 in south-west Qld, 65 in the NT and 4 in NSW (Figure 2.1).

A process similar to that used by Sampson et al. (2013) was implemented to infill the 2010 to 2019 dataset with progressively older water level observations from wells that did not have more recent observations, to develop the potentiometric surface. Although trend analysis in nearby wells was considered, ultimately no attempt was made to incorporate such trends into older well datasets. The reason for this was that such trend data was nearly always associated with larger groundwater developments and therefore trends were not interpreted to be regional.

The logic for using this approach is that there is limited regular water level monitoring across the basin, necessitating the use of older readings to provide adequate coverage. This is particularly true for the non-artesian region of the basin on the western margin in the broad vicinity of Marla (Figure 2.1). Other justifications for this approach include:

- No seasonal variation of water levels is observed in the artesian and sub-artesian portions of the Main Eromanga Aquifer Sequence.
- Obtaining artesian pressure measurements from wellheads of variable condition can be problematic leading to infrequent measurements of high quality.

As illustrated in Figure 2.1, most selected pre-2000 data points occur on the western margin of the basin. This process was iterative to ensure that any older water level observations did not generate obvious errors in the potentiometric surface. Multiple interim gridding runs were undertaken to validate the 'historical' observations. A final set of 800 water well observations were used to develop the uncorrected J-K aquifer potentiometric surface.

Of note, only 3 water wells from the original dataset were found to be completed in the Hutton Sandstone; of these, one contained a water level measurement deemed unreliable and the other 2 had single measurements pre-dating 1970. Consequently, all three data points were excluded. Consequently, the potentiometric surface developed for the Hutton–Poolowanna aquifer is entirely derived from petroleum well data.

2.2 Petroleum well data

Potentiometric surface development also included petroleum well derived formation-water pressure observations (that is, representative groundwater conditions in the J-K and Hutton–Poolowanna aquifers, not representative of oil or gas pressure). Data were sourced from open file records via the Petroleum Exploration and Production System (PEPS)-SA database, SA Government reports and closed file records provided by industry for both SA and south-west Queensland (Queensland government 2019a). SANTOS, Beach Petroleum and Senex Energy provided raw and interpreted data. DEW maintained a database of all formation-pressure records outside the public domain to ensure the confidentiality of closed file data provided for the development of the groundwater model. The database maintains a record of the well ID, data origin, measurement methodology, test date, test depth, stratigraphic unit, pressure, temperature and salinity.

Formation pressures were derived from stabilised shut-in pressures or interpreted pressures from wireline logs. Such data can be derived from several testing or logging methodologies, including:

- Drill Stem Test (DST) – where a well is temporarily completed so the pressure, permeability, and productivity capacity of a sequence of intersected strata can be measured
- Formation Multi-Tester (FMT) – a type of wireline logger used to collect several reservoir rock characteristics, including identification of fluid types, pressures, permeability, and formation productivity
- Modular formation Dynamics Tester (MDT) – a type of wireline logger designed to take real-time flowline resistivity measurements for the evaluation of fluid property, formational permeability, and flow potential.

The filtered data set of DST and FMT data from SANTOS tenements (SA only) from Dubsky and McPhail (2001) provided the preliminary set of representative formation water pressures from tests not containing hydrocarbons, that is, test intervals reporting water with the absence of oil or gas shows. This work identified 312 valid pressures in the Eromanga and Cooper basins from DSTs, while a further 600 valid tests were interpreted from FMTs. These data were merged with industry data obtained for this project. To determine valid formation-water pressures from the petroleum well records, a review of the quality of the DST and MDT data was undertaken. This involved:

- Tests that were reported as mechanically invalid, curtailed or suspect were removed.
- Tests that reported trace hydrocarbons, gas or were supercharged were removed.
- Tests that reported depleted formation pressure in the comments field were removed.
- From raw DST data, the maximum shut-in pressure was adopted from the initial and final flow periods ensuring that samples were filtered to avoid those that were supercharged or reported a water cushion.
- Where interpreted DST data was provided, the absolute formation pressure under stable formation conditions (P*) was selected in preference to maximum shut-in pressure. P* represents the absolute formation pressure under stable formation conditions and is derived from forward-modelling of the shut-in pressure data. Consequently, P* provides the most accurate representation of formation pressure. It is important to note that whilst some oil reservoirs receive ‘pressure support’ from regional aquifers, correcting pressures for hydrocarbon fluid density is not possible without a detailed understanding of fluid composition. Thus, selecting tests that reported water-filled fluid, under natural conditions, was critical to ensure pressures were representative of aquifer formation pressure. Where available, temperature was derived from the outside temperature gauge at the test interval (down-hole).

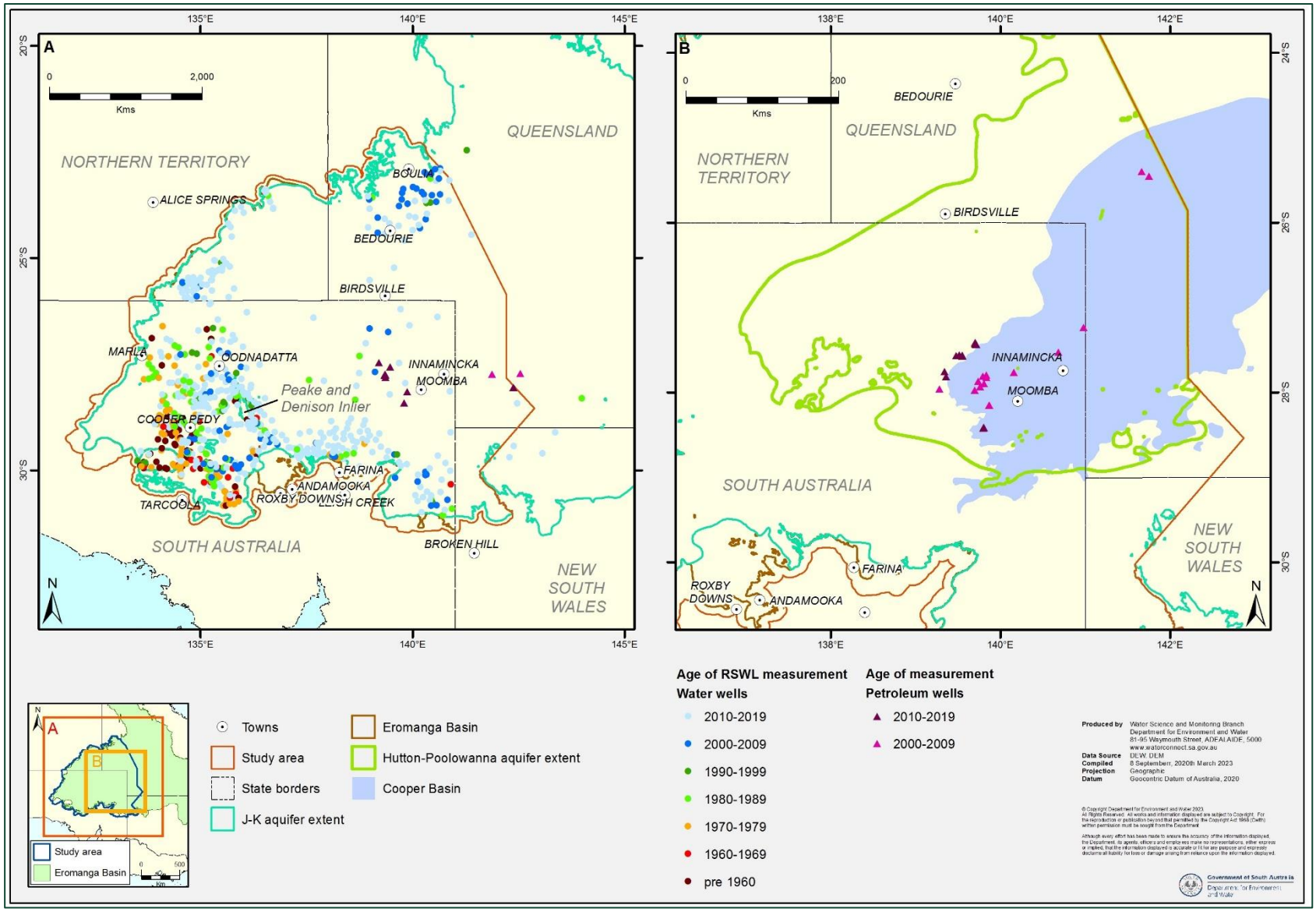

Figure 2.1: Location and most recent date of water level and pressure observations. A) J-K aquifer B) Hutton–Poolowanna aquifer.

- Where P* was not estimated, the maximum stabilised shut-in pressure from the initial and final flow periods was adopted.

The dataset was classified into three categories corresponding to Main Eromanga Aquifer Sequence stratigraphic units representing layers to be used in the numerical model:

1. Cadna-owie Formation, Hooray Sandstone (Queensland) and Murta Formation
2. McKinlay Member, Namur Sandstone, Adori Sandstone and Westbourne Formation (lateral equivalents of the Algebuckina Sandstone found to the west)
3. Birkhead Formation, Hutton Sandstone and Poolowanna Formation.

Often a DST or MDT at an individual well records multiple observations against each layer grouping described above. Where an individual well had multiple records against any of the three stratigraphic categories, a manual process was used to determine the most representative formation pressure for each category. This included review of 'mobility' data provided by the petroleum industry, and hierarchical selection of formation pressures with 'regional' aquifers ranked higher than 'discrete' aquifers, which were ranked higher than 'aquitard' sequences. For example, in the second Main Eromanga Aquifer Sequence stratigraphic unit category, formation pressures from the Namur Sandstone were ranked in preference to formation pressures from the McKinlay Member, which were ranked in preference to formation pressures from the Adori Sandstone, which were ranked in preference to formation pressures from the Westbourne Formation.

The petroleum well formation pressures were then classified by the date of observation into seven categories, typically in 10-year blocks, consistent with the water well data. That is, observations between 2010 to 2019, 2000 to 2009, 1990 to 1999, 1980 to 1989, 1970 to 1979, 1960 to 1969, and 1959 and older. Following preliminary gridding, formation pressures recorded prior to 2000 were deemed to have a high likelihood of not being representative of current pressure conditions in the petroleum fields and were therefore excluded.

2.2.1 Stratigraphy-based descrimination of petroleum well data

Petroleum data was obtained from many formations found within the Main Eromanga Aquifer Sequence (Table 1.1). For the purposes of this study, only data from stratigraphic formations defined as part of the J-K aquifer were included (Table 1.1). Therefore, data from the Murta and Cadna-owie formations were excluded. Contributing to this decision were observations that the Murta Formation is typically a confining, low permeability unit which separates the overlying Cadna-owie Formation from the underlying Namur Sandstone. Further, Kellett et al. (2012) described the Cadna-owie Formation as a leaky aquitard in the central Eromanga Basin. No formation pressures from the Hooray Sandstone were recorded between 2000 and 2019.

Further, the permeability of the McKinlay Member is variable due to its lithological composition ranging from high permeability sand sequences to lower permeability clays/mudstones. Some sand sequences of the McKinlay Member are connected vertically to the Namur Sandstone, while other sand sequences form discrete sand lenses are isolated from the Namur Sandstone by lower permeability units. Co-produced water from discrete McKinlay Member sand sequences typically leads to formation pressures that are much lower than the regional Namur Sandstone. Two formation pressures from the McKinlay Member were recorded between 2000 and 2019; however, one of the 2 was excluded due to a large difference in formation pressure (significantly lower) compared to the formation pressure of the Namur Sandstone recorded at an adjacent petroleum well.

Twenty-four formation pressures from the Namur Sandstone were recorded between 2000 and 2019, 3 of which were later excluded, as they were deemed inconsistent with nearby observations.

Two formation pressures from the Adori Sandstone were recorded between 2000 and 2019; however, one was excluded due to a large discrepancy with nearby observations.

Five formation pressures from the Westbourne Formation were recorded between 2000 and 2019; however, all of these were excluded on a similar basis to the Murta Formation – being typically a low permeability unit with isolated and discontinuous sand lenses.

After filtering and analysis, the petroleum well dataset from the J-K aquifer hydrostratigraphic unit consisted of 23 formation (water) pressures recorded between 2000 and 2019, with all of those coming from the McKinlay Member, Namur Sandstone and Adori Sandstone. Subsequent gridding of the combined water well and petroleum well data highlighted that many of the formation-pressure records older than 2010 were not representative of current pressure conditions. This is particularly true along the Western Flank (for example, Bauer and Callawonga wellfields) where co-produced water extraction from the J-K aquifer has significantly increased since 2010. Therefore, a secondary date filter was applied to identify petroleum well formation pressures from 2010 to 2019. Thirteen petroleum well formation (water) pressures from the Namur Sandstone and McKinlay Member were recorded between 2010 and 2019. This limited the spatial extent of observations in Queensland; therefore, 2 additional Namur Sandstone formation pressures were included in the 2000 to 2010 date category (Figure 2.1). Although the difference in time for these 2 extra Namur Sandstone formation pressures and the rest of the data set represent a potential error in interpretation, the absence of data in this part of the study area to constrain the potentiometric surface interpretation was found to be a potential source of error.

Finally, formation pressures from the deep Hutton Sandstone and Birkhead and Poolowanna formations were assessed separately. A total of 60 formation pressures from this grouping met the date criteria. Of those, 16 from the Birkhead Formation were excluded, with a further 5 excluded from the Hutton Sandstone due to large discrepancies with surrounding observations. Five formation pressures met the date criteria for the Poolowanna Formation, leaving a total of 39 data-points from which the Hutton-Poolowanna aquifer potentiometric surface was developed.

3 Development of the uncorrected potentiometric surfaces

The development of an uncorrected potentiometric surface is a necessary step to develop a density-corrected potentiometric surface. The uncorrected potentiometric surface describes hydraulic head as it may be measured in the field, but without any correction made to account for either the temperature of groundwater within the aquifer or the salinity. Consequently, this uncorrected potentiometric surface has also been described as an 'environmental head'. Although the uncorrected potentiometric surface forms an inaccurate basis for the assessment of vertical and lateral hydraulic gradients because density effects have not been considered, it is still important to the assessment of groundwater flow direction(s), and groundwater volume calculations because it describes the head above land surface or 'excess head'. This excess head is particularly relevant when describing the vulnerability of springs, other GDEs and existing infrastructure to groundwater extraction.

The development of the surface is described in detail in Appendix A. This chapter provides a summary.

3.1 Method

Gridding and contouring of the data occurred in multiple stages interspersed with regular assessment of gridding outputs and further validation of water level data. Notably, inconsistencies were observed between potentiometric surfaces generated using the same gridding methodology but applied in different contouring software packages. This underlined the need to develop a rigorous procedure for generating the 2019 potentiometric surface.

Consequently, several potentiometric surfaces were generated using the full array of gridding and contouring options available in three software packages *Petrosys*, *Surfer* and *ArcMap*. Technical details are provided in Appendix A, which presents a discussion of the various algorithms and software packages investigated during this study, as well as the methodology used to validate and ultimately select conceptually plausible surfaces.

Such comprehensive analysis was warranted to investigate data uncertainties by implementing fundamental scientific methods and principles: observation, measurement, testing and repeatability. The gridding methods evaluated are essentially purely mathematical approaches to interpolating a potentiometric surface and as such do not consider the groundwater flow system dynamics. Ultimately the potentiometric surface outputs provided by an adequately calibrated numerical groundwater model are more representative of the groundwater flow systems.

Note that the influence of faults was not considered during gridding, largely because of insufficient evidence.

3.2 Results

After the potentiometric surface generation and validation procedure as described in Appendix A were completed, 19 potentiometric surfaces were concluded to be 'conceptually plausible' (Figure 3.1 provides one example). Chapter 6 provides a more detailed discussion of these surfaces with respect to groundwater conceptualisation. These results highlight that the validation of well data and inclusion of higher accuracy elevation data markedly improved the fit between well data and interpolated surfaces.

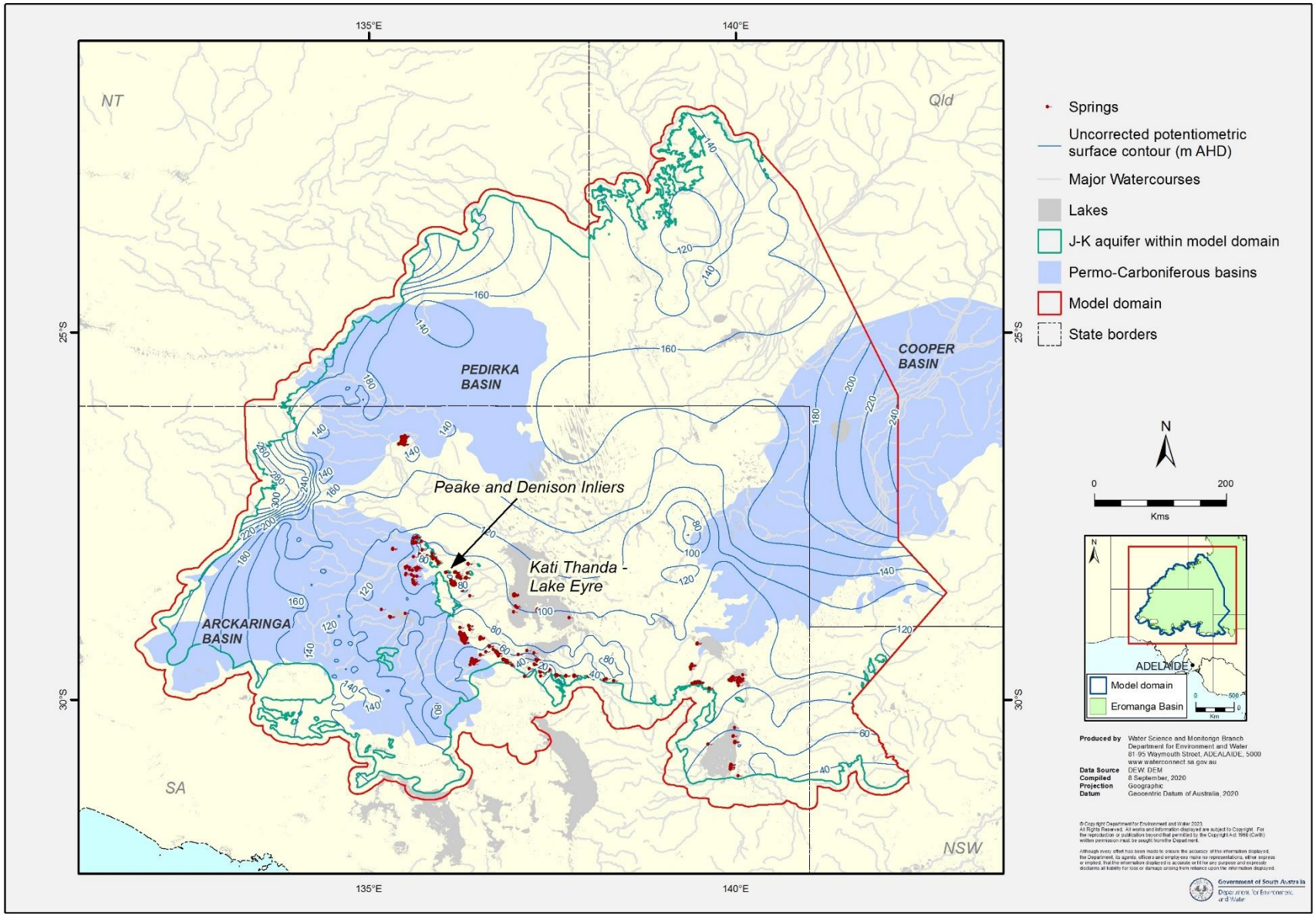

Figure 3.1: Example of an uncorrected potentiometric surface that broadly matches study conceptualisation

Key observations include:

- The smallest range between the minimum and maximum back interpolation values (comparing the original point source data value to the interpolated value at the same point) at well data points occurred with the 100 m x 100 m cell size (*Petrosys*™) and 50 m x 50 m cell size (*Surfer*™) using Minimum Curvature with no internal tension.
- Surfaces generated using Minimum Curvature with no internal tension in *Surfer*™ at 100 m x 100 m cell size, had a smaller range than the *Surfer*™ 50 m x 50 m cell size generated using Minimum Curvature with internal tension applied.
- The range and standard deviation consistently improved with declining cell size for *Petrosys*™ surfaces and those using the 2nd order Taylor series polynomial, compared to 1st order Taylor series polynomial.
- Bicubic interpolation in *Petrosys*™ provided better results (back interpolation) than the bilinear interpolation for all the cell sizes.
- Applying no internal tension in *Surfer*™ provided better results (back interpolation) compared to surfaces where internal tension was applied.
- The secondary gridding extent tested using only variants of the Minimum Curvature algorithm in *Petrosys*™ highlighted near identical results in terms of back interpolating raster values within ±1 m and ±0.5 m of the measured hydraulic head value at each well.
- Other algorithms tested in *Petrosys*™ provided similar results in terms of honouring the data points at the wells compared to the Minimum Curvature method. These included the Distance Weighted Average, Hybrid and Least Square Binomial methods.
- Surfaces generated using Kriging in *Surfer*™ (Linear, Spherical and Exponential) provided a good fit to well data points (> 98.3 % of back interpolated values within ±0.5 m of the hydraulic head value at each data point −50 m x 50 m cell size); however all were excluded from further assessment following review against the conceptual understanding of groundwater flow because the method was found to produce anisotropic groundwater flow characteristics considered unrealistic.

4 Theory of density and flow

4.1 Importance of density variance

The primary driver of groundwater flow in most groundwater systems is gravity (Töth 1963). Groundwater flow hydrodynamics can be affected by a range of interacting forces or processes including advective flow, the interaction of gravity and topography, as well as salinity and temperature that are integral to buoyancy, viscous resistance, density and thermal effects (Ataie-Ashanti et al. 2018). All these processes are potentially significant to the Far North PWA groundwater model, especially the effects of density variations due to temperature gradients, and to a lesser degree due to salinity and viscosity effects.

The aim of this chapter is to introduce the theory and basic concepts of density variation on groundwater flow as it pertains to the study area. This is done to determine the importance of density effects on flow when developing a potentiometric surface, as well as highlighting density variation as a potentially important limitation on modelling assumptions that presume primarily gravity-driven (isothermal) flow.

In simplistic terms, groundwater temperature may be described as having a proportionally linear relationship with depth. GAB spring temperatures (Figure 4 1) typically range from 20°C to 45°C and wellhead temperatures range from 25°C to 100°C (Habermehl and Pestov 2002), while the temperature at the base of the Eromanga Basin in SA can be more than 140˚C (Beardsmore 2004).

However, these higher temperatures at depth may greatly influence the flow system; compared to freshwater at a temperature of 25˚C; the temperature conditions described above may reduce the groundwater density by more than 4%, and the dynamic viscosity by a factor of 4.

Recent studies note that free convection could be possible in many parts of the Eromanga Basin, due to steep temperature gradients and thick and permeable aquifers (see for example, Pestov 2000). Where cooler, denser water sits above warmer, lighter waters, the system is inherently unstable; free convection cells can develop as the cooler, denser fluid sinks and the warmer, lighter fluid moves up (Love et al. 2013; Weatherill et al. 2004). Further, Raffensperger and Vlassopoulos (1999) found that, in large sedimentary basins, free convection is unlikely to happen unless particular conditions are present, such as a thick permeable aquifer with a high basal heat flow.

Studies within the GAB suggest that assuming isothermal flow by ignoring thermal effects on water density may cause errors in calculations of aquifer pressure (Habermehl and Pestov 2002), in some cases up to 6% (Pestov 1998). Thus, there is a requirement to consider the impact that heat may have on groundwater flow within the study area. Consequently, the high temperatures inherent in the deeper sections of the J-K aquifer indicate that the measured potentiometric levels must be corrected for the density and temperature variations to derive density-corrected head potentials for use in mapping and modelling (Love et al. 2013a).

4.2 Heat flows, thermal conductivity and thermal gradients

In simple terms, thermal energy flows at a constant rate to the surface of the earth at any given location (conservation of energy). Heat flow is equal to the product of thermal gradient and thermal conductivity. The thermal gradient is the proportional change in temperature with depth whilst thermal conductivity is the ability of a media to conduct heat. Thermal gradient is important with respect to correcting for density effects in groundwater because it may be used to estimate the temperature for a given groundwater pressure measurement, particularly if a simple linear relationship is inferred (Figure 4.1).

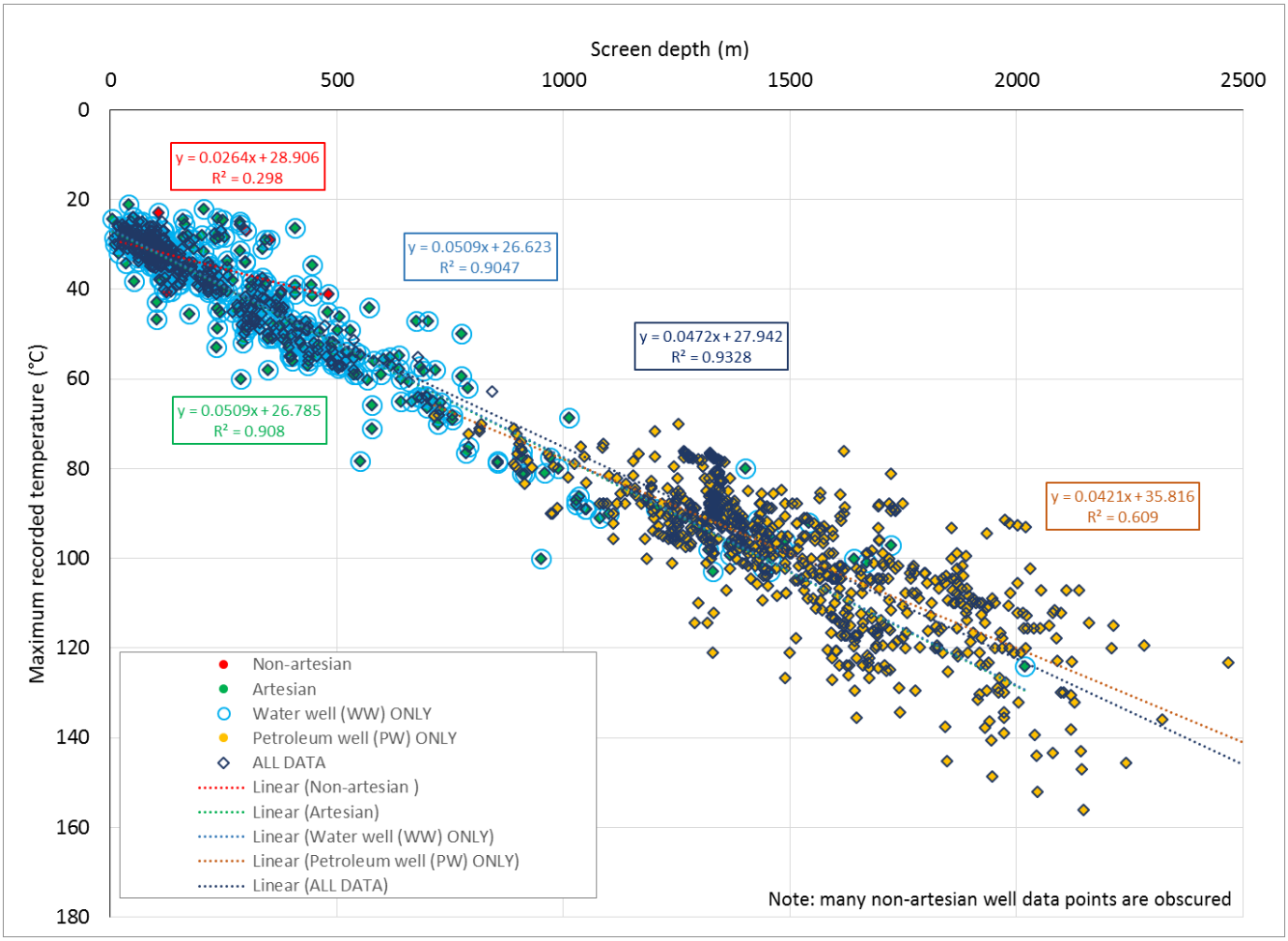

Figure 4.1: Maximum recorded groundwater temperature versus depth of screened interval.

As the thermal conductivity of rock changes with depth, the thermal gradient also changes, because the heat flow remains constant. This change in thermal conductivity with depth occurs because different lithologies conduct heat with different efficiencies. High thermal gradients are observed in low thermal conductivity rocks, such as coal, and low thermal gradients are observed in high thermal conductivity rocks, such as quartzite. Consequently, an important variable concerning the properties of a porous medium are the lithological variations that impact thermal conductivities that may contribute to concomitant variations in thermal gradient.

For example, Beardsmore (2004) found that the abundance of coal in the Cooper Basin has caused the containing formations to have lower-than-average thermal conductivities while the corresponding thermal gradients are correspondingly high. Figure 4 2 (after Beardsmore 2004, using correction from Horner, 1951) illustrates the effect the coal-rich Permian section has on the average thermal gradient down to 3,000 m in the Cooper Basin caused by variation in thermal conductivity. In the given example from petroleum well "Big Lake 33", measured temperatures do not increase linearly with depth as may be expected if thermal conductivity was homogenous. The use of a linear gradient model in this example is observed to overestimate the temperate through the Copper Basin strata, with the error greater than 20°C at the base of the Eromanga Basin sequence.

Variations in heat flow for a continental land mass can be presented in the form of a map. A heat flow map (Figure 4.3) is not a temperature map, nor is it a map of geothermal potential. However, it is a unique way to characterize the thermal state of the crust because it is independent of depth and has a single value at each location. 'Average' continental heat flow (or flux) is about 65 mW/m^2, with heat flow greater than 80 mW/m^2 typically regarded as 'high'. A heat flow map first presented by HDR (2011) (Figure 4.3) shows that large portions of the Tasman Fold Belt, Adelaide Fold Belt and Northern Australia have estimated heat flows ≥ 80 mW/m^2, which is around 25% above 'average'. Notably, a significant portion of central Australia south of the Cooper Basin is estimated to have heat flows exceeding 100 mW/m^2, or more than 50% above 'average'. Such high heat flows more than 100 mW/m^2 were also noted by Beardsmore (2004) in discrete areas.

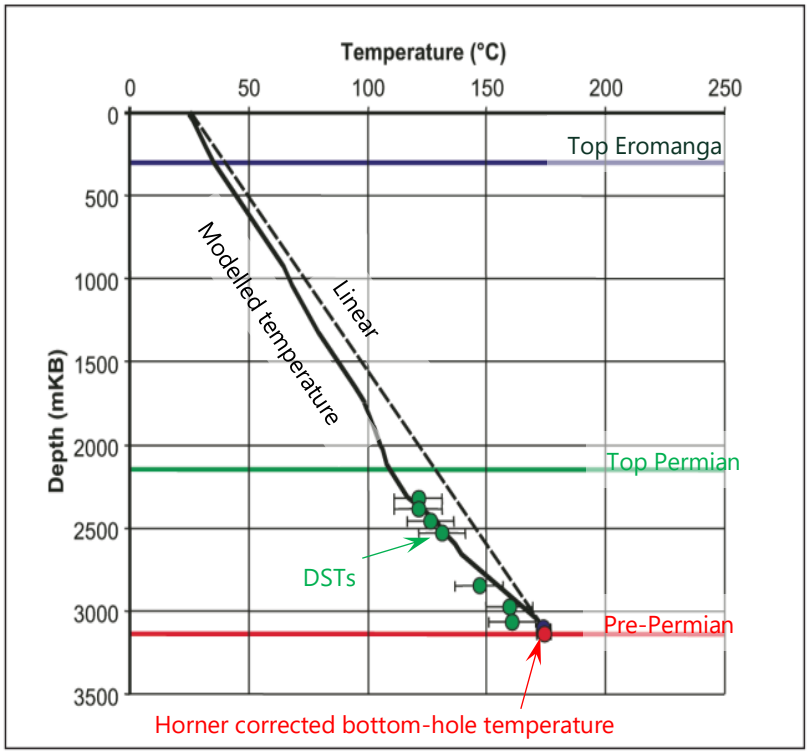

Figure 4.2: Temperature data, modelled temperature profile and linear gradient for Big Lake 33).

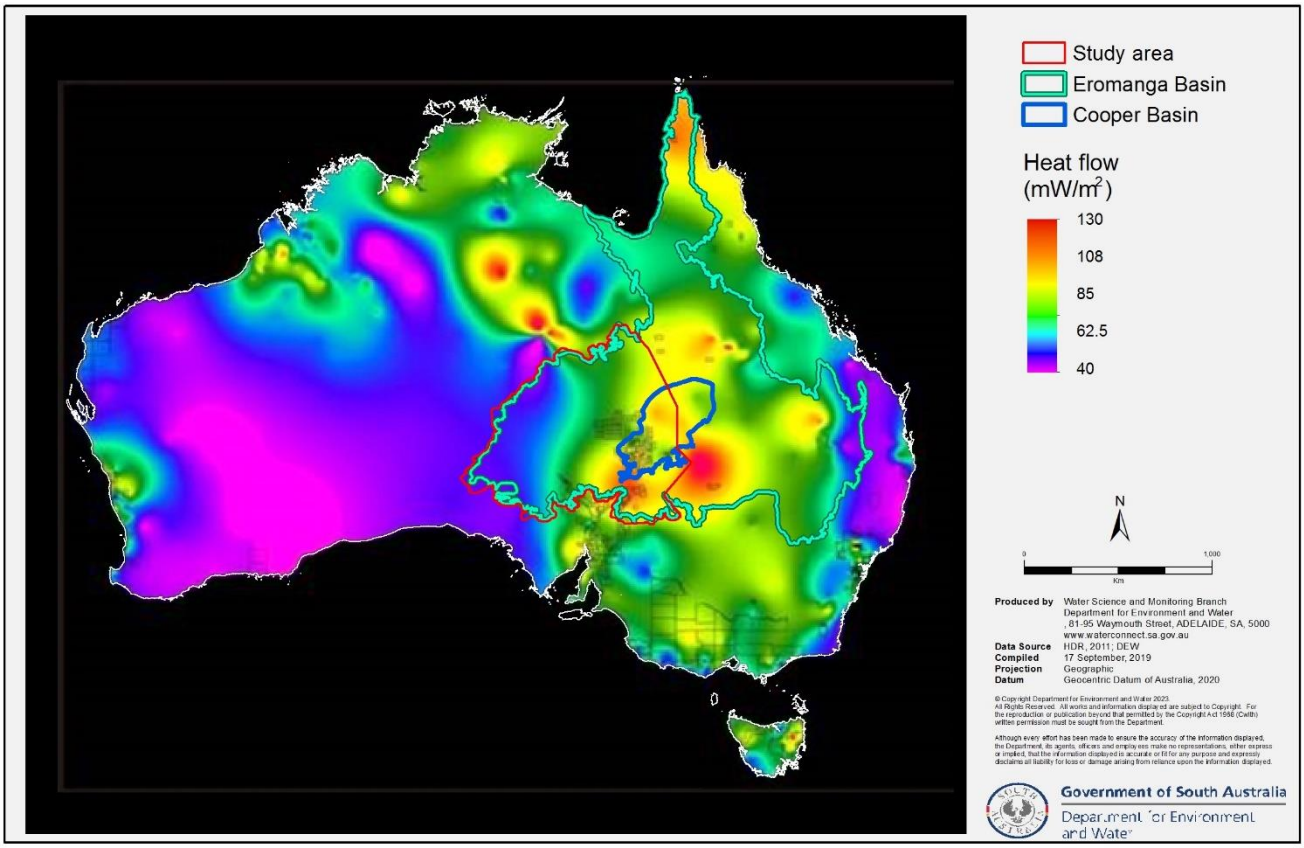

Figure 4.3: Heat flow map of Australia

4.3 Salinity

Salinity variations may also cause instability and therefore free convection. Simmons (2005) describes how a very modest salinity-derived density gradient (for example, 2 g/L, about 5% of seawater) can provide an equivalent 'driving force' in density terms to that of a groundwater head gradient of 1 m per 1000 m. However, the limited salinity gradients in the GAB result in only a low potential for convection in the central-artesian portion of the GAB east of the Peake and Denison Inliers. Priestley et al. (2020) noted that chloride concentrations are typically less than 9 mmol/L in this region, whereas Ransley et al. (2015) noted that low salinity values are found in the 'Cadna-owie–Hooray aquifer' (equivalent to the J-K aquifer) along the eastern margins of the Eromanga, Carpentaria and Surat Basins, as well as the Cape York region in far north Queensland.

Highly saline groundwater in the study area is typically restricted to the south-western margin of the Eromanga Basin where GAB aquifers are typically shallow and thin compared to areas further east. Ransley et al. (2015) noted that this region is near an interpreted recharge zone, where recharge rates are extremely low and salt deposits are present near the surface. Priestley et al (2020) noted that chloride concentrations are between 52 and 930 mmol/L, whereas Keppel et al. (2015) noted that groundwater from Mesozoic, Permo-Carboniferous and Pre-carboniferous basement aquifers from the Lake Phillipson region west of the Stuart Ranges were all partly distinguishable by their hyper-salinity. Consequently, density impacts attributable to salinity are likely to be relatively minor and localised to areas on the south-western margin of the study area.

4.4 Viscosity effects on groundwater flow

Dynamic viscosity variations due to temperature do not affect potentiometric heads as such, but they do influence the flow system, as velocity is inversely proportional to viscosity (Pestov 2000). Dynamic viscosity also influences the Rayleigh number (Ra), which determines the steady state behaviour of a variable density system (Weatherill et al. 2004). As typical horizontal velocities in the Eromanga Basin have been calculated at ≈1 m/yr (Love et al. 2013a) and 1.2 to 2.5 m/yr (Ransley and Smerdon 2012), the potential viscosity effects on regional scale GAB hydrogeological super-basin flow systems for the 100-to-200-year assessment period are small and are not material to the Far North modelling objectives.

4.5 Correcting for temperature and salinity

As the density of groundwater within an aquifer may vary due to temperature, salinity and increasing pressure with depth, the application of Darcy's Law to assess groundwater flow rates and direction may be invalid, unless the environmental (or uncorrected) head is converted to an equivalent reference-density head.

4.5.1 Reference density

Often an equivalent freshwater head is used as the reference density, which assumes a density of ≈ 999 kg/m^3 (that is, a temperature of 20°C and salinity of 1,000 mg/L). However, Rousseau-Gueutin et al. (2013) stated that groundwater flow in a sedimentary aquifer with variable density occurs due to two driving forces:

1. the hydraulic head gradient caused by pressure and/or topographic differences
2. buoyancy due to density differences and the slope of the aquifer.

The reference-density head ($h_{r,i}$) is defined as:

$$\boldsymbol{h_{r,i} = z_i + \frac{P_i}{\rho_r g}} \quad 1$$

Where z_i is the elevation at the measurement point, P_i is the pressure at the measurement point, ρ_r is the reference density and g is the gravitational acceleration constant.

The reference-density head can also be calculated using the measured hydraulic head (h_i):

$$\boldsymbol{h_{r,i} = \left(\frac{\rho_i}{\rho_r}\right) h_i - \frac{(\rho_i - \rho_r)}{\rho_r} . z_i} \quad 2$$

Where ρ_i is the density of the fluid at the measurement point.

To infer horizontal flow rates and direction, all reference-density head measurements need to be referenced against the same elevation. Post et al. (2007) noted that even under hydrostatic conditions the freshwater head varies with depth. For the purposes of this work, a reference elevation reduced to the Australian Height Datum (m AHD) has been used.

4.5.2 Density of groundwater

The density of groundwater can be estimated using analytical expressions such as those of McCutcheon et al. (1993) and Batzle and Wang (1992). Batzle and Wang (1992) was selected for this study as it provides a more accurate estimate of density at atmospheric pressure over the temperature range 20°C to 350°C, with salinities less than 320,000 mg/L and within the pressure range 5 MPa to 100 MPa (Rousseau-Gueutin et al. 2013). Furthermore, Adams and Bachu (2002) concluded that the Batzle and Wang (1992) algorithm is more suitable for sedimentary basins. OGIA (2016) used the method of McCutcheon et al (1993) to undertake density-correction of groundwater head data from the Surat Basin portion of the GAB hydrogeological super-basin, as conditions there differ from those of the present study area.

The Batzle and Wang (1992) equation for the density of groundwater is:

$$\boldsymbol{\rho_w = 1 + 1e^{-6}\left(-80T - 3.3T^2 + 0.00175T^3 + 489P - 2TP + 0.061T^2P - 1.3e^{-5}T^3 - 0.333P^2 - 0.002TP^2\right)} \quad 3$$

and

$$\boldsymbol{\rho_b = \rho_w + S\left[0.668 + 0.44S + 1e^{-6}\{300P - 2400PS + T(80 + 3T + 3300S - S - 13P + 47PS)\}\right]} \quad 4$$

Where ρ_w is the density of water (g/cm^3), ρ_b is the density of brine (g/cm^3), S is the salinity weight fraction (ppm/10^6), P is the pressure (MPa) and T is the water temperature (°C).

4.5.3 Driving force ratio (DFR)

Finally, Rousseau-Gueutin et al. (2013) emphasised that even when hydraulic heads have been corrected for density, an additional density gradient exists. A driving force ratio (DFR) (or mixed convection ratio) defines the significance of hydraulic factors compared to buoyancy along the slope of the aquifer:

$$\boldsymbol{DFR = \frac{\rho_i - \rho_f}{\rho_f}\frac{|\nabla E|}{|\nabla H|}} \quad 5$$

Where ρ_i is the density at the measurement point, ρ_f is the freshwater density, ∇E is the aquifer slope and ∇H is the hydraulic gradient.

DFR analysis can be a useful means of determining whether groundwater may be subject to buoyancy forces and therefore the potential for error when assuming gravity as the primary driving force behind groundwater flow interpretation. Rousseau-Gueutin et al. (2013) stated that when the DFR is less than a threshold value of 0.5 the main driving force for groundwater flow is gravity. Under these conditions, groundwater flow rates and directions can be described accurately by the freshwater potentiometric surface. When the DFR is calculated to be between 0.5 and 1.0 the influence of buoyancy forces on groundwater flow is significant and the freshwater potentiometric surface may not be accurate. In these cases, it is important to use an areal mean density. Finally, if the DFR is greater than a threshold value of 1.0 free convection can occur, and the corrected potentiometric surface should not be used to infer groundwater flow rates and directions.

5 Density correction methodology

Having described the importance of density variation on the interpretation of groundwater flow and consequently the requirement to account for density variation when developing a potentiometric surface in Chapter 4, this chapter describes the development of density-corrected potentiometric surfaces. An outline of the methodology employed is as follows:

- Determine the most appropriate equation for temperature and salinity-related correction.
- Review compiled well data and where no appropriate temperature data is available, estimate a temperature using the general linear relationship between temperature and depth.
- Define the most appropriate reference density with which to undertake density correction.
- Assign a salinity and apply a temperature and salinity corrections to individual hydraulic head data
- Interpolate density-corrected potentiometric surfaces using the 19 algorithms determined as providing the most scientifically plausible solutions as described in Chapter 3.

Further, this chapter highlights the data uncertainty associated with generating regional potentiometric surfaces in deep, high temperature and steeply sloping aquifers.

An alternative method of applying a density correction to the uncorrected potentiometric surface grids was explored but ultimately rejected.

5.1 Applying the correction for temperature and salinity

To obtain accurate groundwater flow rates and directions in variable-density groundwater systems, a correction for temperature and salinity must applied to groundwater head data (Rousseau-Gueutin et al. 2013) (Section 4.5). The datasets examined during this assessment comprised water wells (WW), petroleum wells (PW) and combined water well and petroleum well data (ALL DATA).

Although Section 4 presents evidence for the relationship between thermal conductance and gradient and how this may complicate the relationship between depth and temperature because of lithological heterogeneity, like Rousseau-Gueutin et al. (2013) and Bekesi et al. (2013), this assessment assumes a linear density distribution in the well for reasons of simplicity. The mean density of the well-water column is calculated assuming a constant salinity in the well and the average groundwater temperature between the sampling point (typically at the wellhead) and at the screened interval. This methodology varies slightly from Rousseau-Gueutin et al. (2013) and Bekesi et al. (2013) who estimated the density in the well column based on an incremental summation of density based on i increments.

Table 5.1 presents a comparison of the difference in density-corrected hydraulic head, reported as the reduced standing water level (RSWL, m AHD), calculated using two alternate algorithms that is, as described by a) Batzle and Wang (1992), compared to b) McCutcheon et al. (1993) for two cases; 1) low temperature shallow production zone versus 2) high temperature deep production zone. Inputs for the uncertainty analysis are based on wells located along the unconfined, non-artesian western margin (representing a low temperature, shallow production zone) and confined, artesian north-east portion of the J-K aquifer (representing a high temperature, deep production zone), respectively.

The key findings from this analysis are:

- At low temperatures, occurring where the Main Eromanga Aquifer Sequence is shallow, the difference between the two correction methods is small and within field measurement error (≈ 1 cm).

Table 5.1: Uncertainty analysis of density-correction methodology

Ground-water source	Screen depth [m]	Av. column temp. [°C]	Ground elev. [m AHD]	SWL [m bgs]	Uncorrected RSWL h [m AHD]	Total dissolved solids (TDS) [mg/L]	Screen elevation Zi [m AHD]	Correction method	Corrected RSWL hf, i [m AHD]	Difference [m]
Low temperature, shallow production zone	25	29	100	10	90	1,000	75	Batzle & Wang 1992	89.95	−−0.05
								McCutcheon et al. 1993	89.97	−0.03
High temperature, deep production zone	1,500	101	30	−110	140	1,000	−1470	Batzle & Wang 1992	79.34	−60.66
								McCutcheon et al. 1993	74.33	−65.67

- At high temperatures, occurring where the Main Eromanga Aquifer Sequence is deep, the correction results in a maximum difference of 60 to 65 m from the raw data, and the difference between the two correction methods is significant (approximately 5 m) and could potentially influence the inferred groundwater flow direction.

The density corrections are approximately double those given in OGIA (2016) for the Surat Basin, as the Cooper Basin has much higher observed temperatures, for example, 60°C at 1,500 m bgs. However, as explained in Chapter 4 and Volume 2, depocentres in the Cooper Basin region are characterised as having abnormally high heat flows and steep thermal gradients.

5.2 Assigning temperature

5.2.1 Data collation and quality assurance

Data on pressure and temperature was obtained mainly from the WW and PW discussed in Chapter 2. This was supplemented by data from the OzTemp data base. Notwithstanding the uncertainties highlighted in Section 4.2 concerning the impact heterogeneous thermal conductivity may have on thermal gradients, a linear temperature gradient between the screened interval mid-point and measurement point (typically at ground surface for water wells) was assumed for simplicity. The temperature gradient within the well, at the time of measurement, is influenced by the yield of the well, duration of flow prior to sampling and depth of the well.

The bottom-hole temperature (BHT) in this instance is defined as the groundwater temperature at the screened interval of a water well or the sample interval from a petroleum industry test. Although we acknowledge that true groundwater and water-well temperatures as measured may differ because of the difficulty in collecting in situ groundwater temperatures within the formation, scrutiny of recorded water well temperature records to only accept those considered to represent the most likely true groundwater temperature was undertaken. Therefore, the BHT for WW has been estimated from the maximum-recorded temperature for each well. For low-yielding artesian wells and wells with very deep completion intervals, the maximum-recorded temperature at the surface is unlikely to accurately represent the BHT due to cooling and/or phase separation. Data obviously influenced by the effects of cooling within the well-water column were filtered from the final dataset.

- The groundwater temperatures from water wells were sourced from both non-artesian and artesian wells.
- Groundwater temperatures at non-artesian wells are measured from a pumped water sample from the well; the duration of pumping is not recorded in the database and therefore unknown.
- Water-well temperatures at artesian wells are measured after the well has been allowed to flow and are assumed here to be representative of groundwater temperatures. The period of flow prior to measuring the temperature (and groundwater pressure) varies. As such, several groundwater temperature measurements were deemed to be not representative of the maximum possible flowing temperature from that well and were omitted (as outliers) from the analysis.
- Additional water-well temperature data were sourced from geophysical log records in the SA Geodata database.

Three hundred and eighty-six (386) water-wells out of 1,007 completed in the Main Eromanga Aquifer Sequence in SA have at least one water well temperature recorded. This leaves 62% of water wells with no temperature recorded at any time, for which an estimated (or maximum) BHT is required to correct hydraulic head measurements for variations in density in the well-water column. Estimates were made using a linear regression calculated between the BHT and screen depth interval presented in Figure 4.1. These are typically non-artesian wells located in the Western Recharge Zone and to a lesser degree, the South West Springs Zone (Figure 5.1).

No groundwater temperatures were available for 4 of the 52 water wells completed in the Main Eromanga Aquifer Sequence in south-west Queensland and for all J-K aquifer water wells in the NT.

For the petroleum wells, a total of 573 formation pressures have been recorded in Eromanga Basin units that represent natural formation water pressure in SA and south-west Queensland (that is, not affected by hydrocarbons or the test procedure) (Figure 5.1). Out of the total of 573 representative formation water pressures, 221 have corresponding groundwater (gauge) temperatures from various downhole tests including cement bond log BHT, drill stem tests (DST), formation modular tests (FMT/MDT), repeat formation tests (RFT), wireline log BHT, Formation Pressure Test – Gamma Ray log (XPT-GR) and static temperature surveys. This left 61% of petroleum well formation 'water' pressures that require an estimated BHT to correct formation pressures to equivalent reference-density hydraulic head measurements. Petroleum well formation temperatures were collated from the PEPS-SA database, data provided by industry and the OZTemp database (Holgate and Gerner 2010).

The OZTemp database is a collation of borehole temperature data and heat flow measurements from throughout Australia. The dataset was filtered to include only those wells within the study area and measuring temperature in the Eromanga Basin, Cooper/Eromanga Basins and Eromanga/Pedirka Basins fields. This included 4,237 temperature measurements from 1,258 individual wells. A series of additional filters were applied to ensure only representative temperature data would be retained:

- The *depth of temperature* field was verified against the depth to base Eromanga (Sampson et al. 2013) to filter out temperature data from basins underlying the Eromanga Basin. The surfaces from Sampson et al. (2013) were used in preference to the ones developed for this study as the latter were still under development.
- A filter was applied to remove data that measured formation temperature from a depth of greater than 2,500 m bgs in the Queensland portion of the study area ensuring data from the Cooper Basin was excluded.
- Anomalous readings were filtered according to a comments field in the OZTemp database.
- The *lag time* field was used to identify data measured equal to or more than 24 hours after completion of drilling to account for any influence drilling fluids may have on cooling the formation water.
- The final filtered dataset included 58 temperature measurements from 49 individual wells. Approximately 53% of those temperature measurements were from cement bond logs, 44% from wireline temperature logs and the remaining 3% of measurements were recorded as unknown type.

5.2.2 Estimating temperature in the absence of measurement and exploring temperature as a function of depth

Where there was no recorded temperature accompanying an aquifer pressure measurement, the temperature gradient in the well cannot be ascertained and an alternative method to estimate this temperature was applied.

This method entailed the use of a linear line of best fit through groundwater temperature, calculated with outliers omitted, against screen depth (either the mid-point of a water-well screen or the gauge depth from a petroleum test) and provides an estimate of the temperature gradient through the Main Eromanga Aquifer Sequence and an estimated temperature at the top of the J-K aquifer and Hutton–Poolowanna Aquifer (Figure 4.1). Accordingly, the linear correlation can then be applied to the screen depth for any well that has no BHT record to estimate a groundwater temperature. Specifically, the 'y-intercept' gives an estimated groundwater temperature at the top of each aquifer; and the 'slope of the line' estimates the regional temperature gradient through each aquifer.

Combinations of temperature data from water wells (WW) and petroleum wells (PW) were analysed to establish the 'goodness of fit' or 'coefficient of determination (r^2)' to determine the most suitable linear correlation for estimating groundwater temperature in the Main Eromanga Aquifer Sequence.

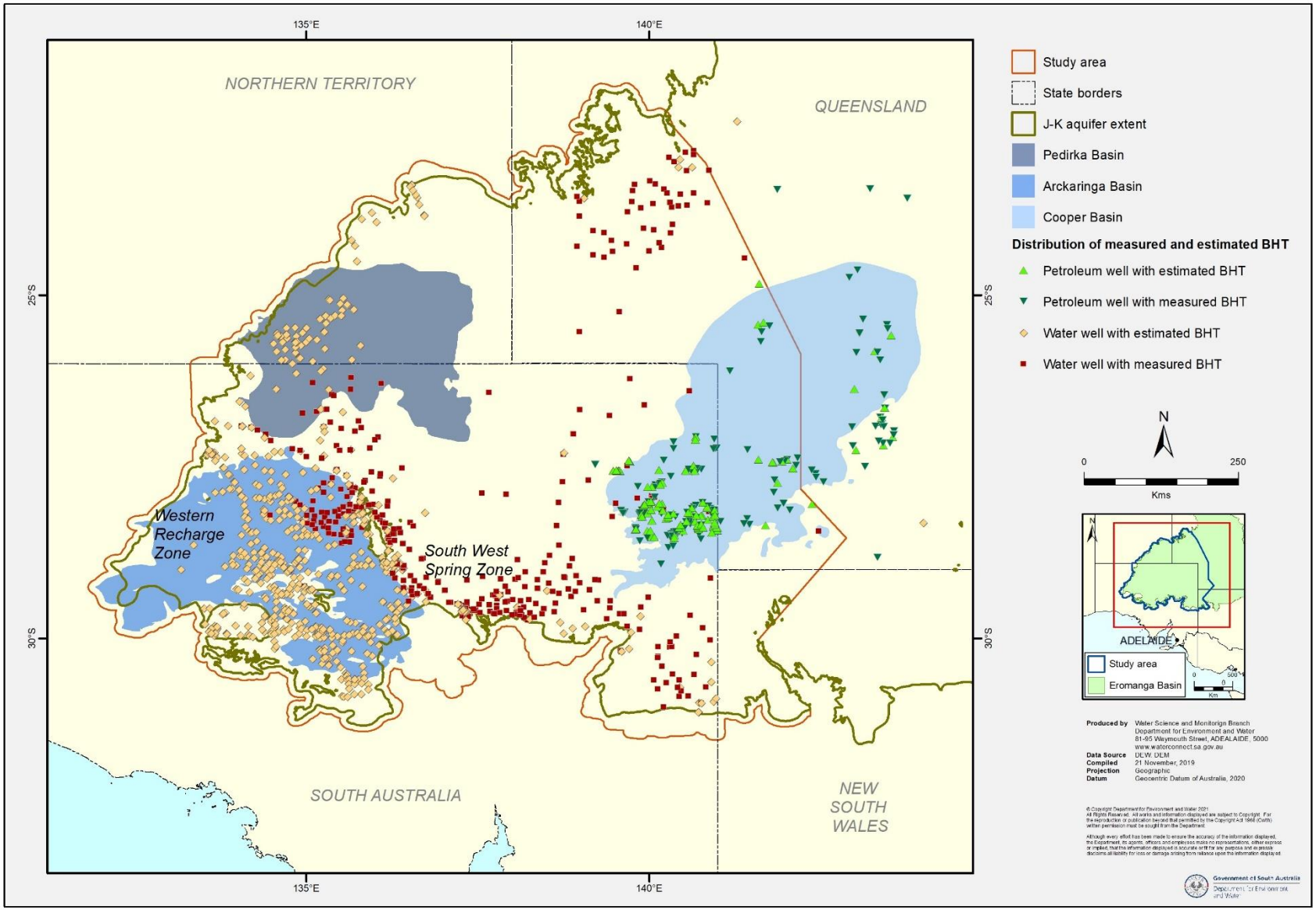

Figure 5.1: Spatial distribution of wells with measured maximum groundwater temperature versus wells requiring an estimated bottom-hole temperature.

Water wells were considered first (WW ONLY). Initially, groundwater temperatures from non-artesian wells were analysed separately from artesian wells with non-artesian wells having a poor data fit (r^2 = 0.3, y = 0.03x + 28.91), and artesian wells having a good data fit (r^2 = 0.91, y = 0.05x + 26.79) (Figure 4.1). This difference between non-artesian (confined and unconfined) may highlight that there is added difficulty in measuring water-well temperature and therefore estimating groundwater temperature from the non-artesian (confined and unconfined) regions. Subsequently, non-artesian and artesian water wells (WW ONLY) were analysed together and resulted in a similar fit of data to artesian wells only (r^2 = 0.91, y = 0.05x + 26.62). The temperature gradient (slope of the line) of 50.9°C/km, with groundwater temperature at the top of the Main Eromanga Aquifer Sequence (y-intercept) for water wells is consistent with the results detailed in Bekesi et al. (2013) for water wells near the Olympic Dam wellfields (y = 0.05x + 28.7). Furthermore, the *P-value* ($5E^{-248}$) and *Significance F* ($2.6E^{-232}$) confirm the relationship between groundwater temperature and depth is significant.

Temperature data from petroleum wells (PW ONLY, Figure 4.1) were then analysed separately from water wells and resulted in an average data fit (r^2=0.61, y = 0.04x + 35.82), although the *P-value* ($1.24E^{-59}$ and *Significance F* ($5E^{-143}$) highlight that the correlation is significant. The temperature gradient of 42.1°C/km is like individual temperature gradients provided by Beach Energy for formations in the Eromanga Basin and Nappamerri Group (Cooper Basin) located in the Nappamerri Trough (28 to 41 °C/km).

Analysis of petroleum groundwater-temperature data split between the various downhole techniques did not provide conclusive results (data not presented). However, data from certain test types clustered below the PW ONLY line of best fit (for example, MDT tests) whereas data from static temperature survey (STS) typically plotted above the PW ONLY line of best fit. These observations likely relate to the spatial location where each test was performed rather than the actual test type, as well as the source formation of the groundwater temperature data. The cluster of data from MDT tests below the PW ONLY line of best fit is sourced exclusively from the Namur Formation on the western flank, while the STS test data are exclusively from the Nappamerri Trough region.

An analysis of groundwater temperature and depth for individual formations also proved inconclusive (data not presented), this may be due to limited data for individual formations.

Finally, all water well and petroleum well temperature data (ALL DATA) were analysed together. This provided the best data fit described by the following formula:

Groundwater temperature = 0.047 x aquifer depth + 27.94 (r^2 = 0.93) 6

Moreover, the *P-value* (0) and *Significance F* (0) indicate a significant correlation between groundwater temperature and depth using both water well and petroleum data. Upper and lower 95th percentiles of the ALL DATA linear correlation are 0.048 and 0.047, respectively for the slope of the line: and 28.83 and 27.05, respectively for the y-intercept.

The groundwater temperature at the top of the artesian and non-artesian components of the J-K aquifer, where they either outcrop or sub-crop is therefore estimated to be 27.9°C (±0.9°C); and the temperature gradient is estimated to be 47.2°C / km (±0.7°C / km).

5.2.3 How the choice of temperature approximation affects density and head

Given that both the WW ONLY and PW ONLY correlations were deemed statistically significant, the linear line of best fit for each case was used to predict BHTs and then compared against the predicted BHT from the ALL DATA linear line of best fit. This was performed on wells that did not have a measured BHT (that is, 62% of water wells and 61% of petroleum wells). Table 5.2 provides a summary of the comparison between predicted BHTs from the ALL DATA case, and WW ONLY and PW ONLY cases, respectively. The 'minimum' category indicates the largest difference between the predicted BHTs where the WW ONLY and PW ONLY cases, respectively, are higher than the ALL DATA case. Conversely, the 'maximum' category indicates the largest difference between the predicted BHTs where the ALL DATA case is higher than the WW ONLY and PW ONLY cases, respectively. The 'mean' (arithmetic) and 'median' categories are positive values in all cases, indicating that the mean and median predicted BHT are higher for the ALL DATA case.

Data from Table 5.2 was then used to investigate potential sensitivity in deriving density-corrected hydraulic heads for both water wells and petroleum wells using linear line of best-fit correlations. The 'minimum' difference in estimated BHT were added to BHTs calculated using the ALL DATA linear correlation; whereas the 'maximum' and 'mean' difference in estimated BHT were deducted from BHTs calculated using the ALL DATA linear correlation. The process of estimating BHTs for sensitivity testing was replicated for shallow, median and deep water well and petroleum well production zones.

Table 5.2: Difference in estimated BHT (maximum groundwater temperature) for wells with no BHT recorded between linear line of best-fit cases.

	Difference in estimated BHT (°C)	
	ALL DATA minus WW ONLY	**ALL DATA minus PW ONLY**
Minimum	−3.81	−4.46
Maximum	1.32	4.45
Mean	1.01	1.20
Median	1.10	1.26

The potential sensitivity in deriving density-corrected hydraulic heads was tested for water wells and petroleum wells using linear line of best-fit correlations. The 'minimum' difference in estimated BHT were added to BHTs calculated using the ALL DATA linear correlation; whereas the 'maximum' and 'mean' difference in estimated BHT were deducted from BHTs calculated using the ALL DATA linear correlation. The process of estimating BHTs for sensitivity testing was replicated for shallow, median and deep-water wells and petroleum production zones using equation 6 in Section 5.2.2.

A histogram of screen depth mid-points shows that more than 50% of water wells have screen depths less 100 m and approximately 95% have screen depths less than 700 m; whereas less than 1% of petroleum wells have screen depth (gauge depth) recorded as less than 700 m (Figure 5.2). Table 5.3 provides a summary of minimum, maximum, mean (arithmetic) and median screen depths for both water wells and petroleum wells.

Water wells (WW), Petroleum wells (PW) and a combined water well and petroleum well (ALL DATA) datasets were examined during this assessment. Parameters for the comparison were selected as follows:

- For the shallow water wells, a production zone of 25 m was selected despite the minimum screen depth of 0.5 m (Table 5.3); the remainder of production zones, both water wells and petroleum wells, were then selected based on the values presented in Table 5.3
- The estimated temperature at the top of the J-K aquifer (surface temperature) was assigned 27.9 °C, consistent with the ALL DATA linear correlation.
- A constant salinity of 2 000 mg/L was selected as it reasonably approximates the average salinity found in most J-K aquifer groundwater and is also a simple constant.
- Ground elevation (m AHD) and standing water level (SWL, m bgs) for each simulation were derived from the well corresponding to the minimum, median and maximum screen depth intervals found in Table 5.3.

The results are provided in Table 5.4 and Table 5.5. For shallow and median depth water wells, the difference between density-corrected hydraulic heads due to the selection of BHTs based on ALL DATA or WW ONLY linear correlations does not fundamentally change the corrected hydraulic head (Table 5.4). The largest difference in the estimated BHT (+3.81 °C) causes a maximum 0.01 m (shallow depth) and 0.09 m (median depth) difference in corrected hydraulic head. The mean BHT difference (-1.01 °C) generates a corrected hydraulic head 0.02 m higher for the WW ONLY correlation but would be considered within measurement error.

For deeper (hotter) water well production zones, at a maximum BHT difference of 3.81 °C, the corrected hydraulic head is estimated to be 2.51 m lower using the WW ONLY correlation. Conversely, using a mean BHT differential of −1.01 °C, the corrected hydraulic head would be 0.66 m higher using the WW ONLY correlation. As shown by Figure 5.2, deeper (hotter) water wells are not common and therefore any uncertainty in the hydraulic head correction due to BHTs estimated using the ALL DATA correlation is considered acceptable.

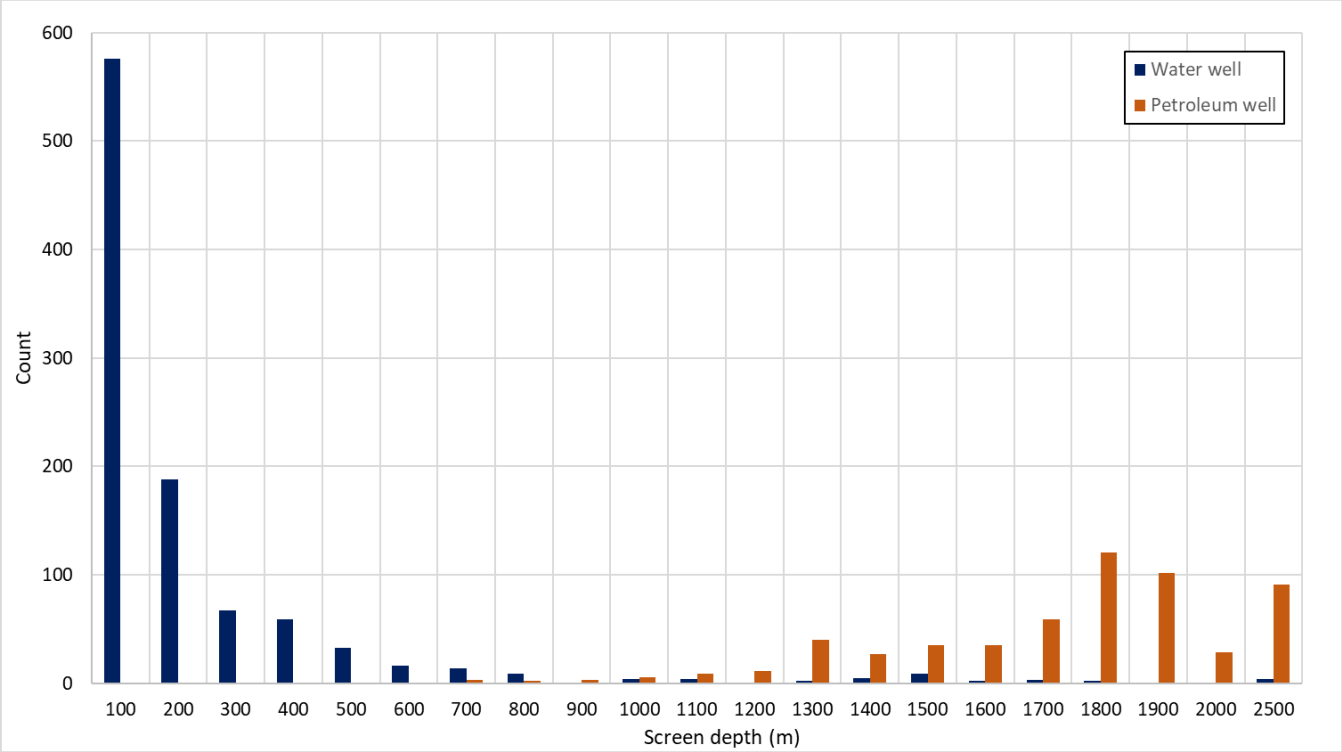

Figure 5.2: Histogram of screen depth for water wells and petroleum wells.

Table 5.3: Summary of screen depths for water wells and petroleum wells.

	Water well screen depth (m)	Petroleum well screen (gauge) depth (m)
Minimum (shallow)	0.5	670
Maximum (deep)	2250	2467
Mean	184	1702
Median	84	1767

After water wells (WW) were examined, the ALL DATA and PW datasets were examined in comparison. The minimum and maximum difference in predicted BHT comparing ALL DATA and PW ONLY linear correlations are of similar magnitude (that is, 4.46°C higher than the ALL DATA estimated BHT and 4.45°C less than the ALL DATA estimated BHT); and result in approximately 1.50 m, 6 m and 10 m differences in correct hydraulic head for shallow, median and deep petroleum well production zones, respectively (Table 5.5). Table 5.5 also illustrates that the mean difference in predicted BHT (that is, 1.2°C less than the ALL DATA estimated BHT) results in corrected hydraulic heads 0.39 m, 1.60 m and 2.75 m lower than the ALL DATA case for shallow, median and deep petroleum well production zones, respectively. This analysis highlights that selection of an appropriate algorithm to estimate BHT for petroleum wells is essential to ensure potentiometric surfaces, as accurately as possibly, can be used to predict groundwater flow fields.

Given that the ALL DATA correlation provides the best data fit (r^2 = 0.93), and *P-value* and *Significance F* indicate the correlation between screen depth and temperature is significant, the ALL DATA correlation is demonstrated as acceptable for estimating BHT for petroleum wells.

5.3 Assigning salinity

Salinity data for water and petroleum wells were processed separately due to their differing sources, collection methodologies and contamination considerations. Salinity from water wells may be collected from either a water quality meter during well development or monitoring phases, or from water chemistry analysis. Petroleum-well data, is sourced from laboratory and field water quality reports obtained from sampling undertaken during DSTs. Where salinity is derived from chemical analysis, data requires processing to account for contamination during drilling and well installation (Dubsky and McPhail 2001). Further details may be found below.

5.3.1 Water wells

For hydraulic head corrections, groundwater salinity is assumed to be constant in each well-water column. For all non-artesian and artesian water wells with production zones completed in the Main Eromanga Aquifer Sequence, the latest recorded salinity at each well has been assigned to that well. Salinity is recorded as either Total Dissolved Solids (TDS, mg/L) or Electrical Conductivity (EC, µS/cm). SA Geodata uses an inbuilt algorithm to convert between TDS and EC (Appendix C). Therefore, for every salinity sample, both TDS and EC are available. Salinity across the study area is discussed further in Volume 6 of this report.

Salinity samples entered as TDS are typically the summation of anions and cations. Salinity samples recorded as EC are a combination of field observations inclusive of a measured well temperature, field observations with no temperature recorded in the database (and assumed to be reported against a standard temperature of 25^{0}C, that is, as specific conductance, *SpEC*), and samples analysed in a laboratory or DEW office and reported against a standard temperature of 25^{0}C (that is, also *SpEC*). Where a field temperature has been recorded that EC value is retained for conversion to TDS. Where the EC was reported, or assumed to be reported against a standard temperature of 25^{0}C, the *SpEC* was converted to EC inclusive of either the measured or estimated groundwater temperature using the following equation (USGS 2019):

$$\boldsymbol{SpEC_{25}} = \frac{\boldsymbol{EC_m}}{\boldsymbol{1+0.0191(t_m-25)}} \quad 7$$

Where EC_{25} is the specific conductance at 25^{0}C, EC_m is the measured electrical conductivity, t_m is the groundwater temperature at the time of EC_m measurement and 0.0191 is the linear temperature compensation factor.

This equation is re-arranged to estimate the measured EC at the temperature of the aquifer if the *SpEC* is known and temperature of the aquifer is known or has been estimated:

$$\boldsymbol{EC_m = SpEC_{25}\left(1 + 0.0191(t_m - 25)\right)} \quad 8$$

Table 5.4: Comparison of hydraulic head density corrections for water wells based on variable BHT estimates and production zone depth. The key variable input are the statistical values found in Tables 5-2 and 5-3. Key outputs ae in colour.

Sensitivity test	Screen depth (Table 5-3) [m]	Calculated BHT difference (Table 5-2) [°C]	Estimated BHT [°C]	Estimated surface temperature [°C]	Average well column temperature [°C]	Ground Elevation [m AHD]	Screen elevation Z_i, [m AHD]	SWL [m bgs]	RSWL [m AHD]	Pressure [MPa]	Salinity TDS [kg/L]	Average density of groundwater ρ_i, [kg/m^3]	Fresh water density ρ_f, [kg/m^3]	Freshwater equivalent RSWL [m AHD]	Density correction [m]	Difference in density correction from ALL DATA BHT [m]
Shallow water well production zone (low temperature)	25	NA	29.12	27.94	28.53	100	75.00	10.00	90	0.882	0.002	996.810	999	89.97	−0.03	0.00
	25	3.81	32.93	27.94	30.44	100	75.00	10.00	90	0.882	0.002	996.295	999	89.96	−0.04	0.01
	25	−1.32	27.80	27.94	27.87	100	75.00	10.00	90	0.882	0.002	996.984	999	89.97	−0.03	0.00
	25	−1.01	28.11	27.94	28.03	100	75.00	10.00	90	0.882	0.002	996.943	999	89.97	−0.03	0.00
Median water well production zone (low temperature)	84	NA	31.91	27.94	29.92	200	−54.08	73.00	127	1.245	0.002	996.596	999	126.56	−0.44	0.00
	84	3.81	35.72	27.94	31.83	200	−52.17	73.00	127	1.245	0.002	996.064	999	126.47	−0.53	0.09
	84	−1.32	30.59	27.94	29.26	200	−54.74	73.00	127	1.245	0.002	996.776	999	126.60	−0.40	−0.03
	84	−1.01	30.90	27.94	29.42	200	−54.58	73.00	127	1.245	0.002	996.734	999	126.59	−0.41	−0.02
Deep water well production zone (hot temperature)	2250	NA	134.14	27.94	81.04	22	−2168.96	−107.00	129	1.265	0.002	974.698	999	73.10	−55.90	0.00
	2250	3.81	137.95	27.94	82.95	22	−2167.05	−107.00	129	1.265	0.002	973.585	999	70.59	−58.41	2.51
	2250	−1.32	132.82	27.94	80.38	22	−2169.62	−107.00	129	1.265	0.002	975.079	999	73.96	−55.04	−0.86
	2250	−1.01	133.13	27.94	80.54	22	−2169.46	−107.00	129	1.265	0.002	974.990	999	73.76	−55.24	−0.66

Table 5.5: Comparison of hydraulic head density corrections for petroleum wells based on variable BHT estimates and production zone depth The key variable input are the statistical values found in Tables 5-2 and 5-3. Key outputs ae in colour.

Sensitivity test	Screen depth (Table 5-3) [m]	Calculated BHT difference (Table 5-2) [°C]	Estimated BHT [°C]	Reference elevation [m AHD]	Screen elevation Z_i, [m AHD]	Formation pressure [m head]	RSWL [m AHD]	Pressure [MPa]	Salinity TDS [kg/L]	Average density of groundwater ρ_i [kg/m^3]	Fresh water density ρ_f, [kg/m^3]	Freshwater equivalent RSWL [m AHD]	Density correction [m]	Difference in density correction from ALL DATA BHT [m]
Shallow petroleum well production zone (moderate temperature)	670	NA	59.57	201	−469	720	251	2.461	0.002	986.302	999	241.85	−9.15	0.00
	670	4.46	64.03	201	−469	720	251	2.461	0.002	984.217	999	240.35	−10.65	1.50
	670	−4.45	55.12	201	−469	720	251	2.461	0.002	988.265	999	243.26	−7.74	−1.41
	670	−1.20	58.37	201	−469	720	251	2.461	0.002	986.843	999	242.24	−8.76	−0.39
Median petroleum well production zone (hot temperature)	1767	NA	111.34	42	−1725	1792	67	0.657	0.002	954.316	999	−13.15	−80.15	0.00
	1767	4.46	115.80	42	−1725	1792	67	0.657	0.002	950.928	999	−19.23	−86.23	6.08
	1767	−4.45	106.89	42	−1725	1792	67	0.657	0.002	957.590	999	−7.28	−74.28	−5.87
	1767	−1.20	110.14	42	−1725	1792	67	0.657	0.002	955.210	999	−11.55	−78.55	−1.60
Deep petroleum well production zone (hot temperature)	2467	NA	144.38	38	−2429	2493	64	0.627	0.002	926.714	999	−116.39	−180.39	0.00
	2467	4.46	148.84	38	−2429	2493	64	0.627	0.002	922.559	999	−126.76	−190.76	10.37
	2467	−4.45	139.93	38	−2429	2493	64	0.627	0.002	930.760	999	−106.29	−170.29	−10.10
	2467	−1.20	143.18	38	−2429	2493	64	0.627	0.002	927.815	999	−113.64	−177.64	−2.75

Finally, all EC data, inclusive of temperature, either measured or estimated were converted to TDS using the EC to TDS conversion factors inbuilt in SA Geodata (Appendix C).

Water wells completed in the Main Eromanga Aquifer Sequence with no historical salinity data were assigned a salinity (TDS) based Thiessen polygon analysis of salinity from 1,061 water and petroleum wells completed in the J K aquifer. The Thiessen polygon salinity raster was sampled for each water well with no historical salinity data using the 'Point Sampling Tool' in Quantum Geographic Information System (QGIS) (Figure 5 3). This method was chosen instead of using grid-derived data because gridding and contouring were found to produce unrealistic local data extremes (bullseyes) that did not resemble the current understanding of groundwater conditions in the Main Eromanga Aquifer Sequence.

5.3.2 Petroleum wells

Laboratory and field water quality reports obtained from sampling undertaken during DSTs and active petroleum production were reviewed to assign salinity values to formation pressures from petroleum tests and for interpretation of groundwater processes. Data included:

- sample date, depth and target formation (that is, aquifer monitored)
- temperature (typically laboratory recorded), pH, alkalinity
- major ions for example, Na^{+}, Ca^{2+}, K^{+}, Mg^{2-}, Cl^{-}, SO_4^{2-}, HCO_3^{-}
- various metal suites incorporating common and trace metals
- hydrocarbons
- TDS based on summation of major ion constituents.

For tests that did not report against a stratigraphic formation, the PEPS-SA database was interrogated. Formations correlating to the sample intervals were matched to the date of the water quality test via careful inspection. This involved reviewing the target formation from production records at the time of the sampling. For tests that reported more than one production interval during a given period, the water quality was assigned to all formations. Subsequently, some salinity or water quality samples were assigned multiple formation intervals for a given sampling event.

In total, 21,735 water-quality sampling events were collated, many of which contained various combinations of field and laboratory data. The data were consolidated into a spreadsheet to enable rapid filtering and validation.

Raw chemistry data was filtered to obtain valid salinity readings for target formations. The filtering process aimed to identify valid water samples and eliminate common contaminants encountered during DST and FMT tests. This method followed similar criteria proposed by Bowyer (1991) as cited in Dubsky and McPhail (2001). The method included the following limitations in providing valid samples:

- an ionic balance of equal to or less than 5%
- wells with a pH range < 8.5 to > 4.5. This accounts for potential influence of alkaline-based muds or unusual acidity not expected in natural groundwater.
- potassium content K^{+} < 1 000 mg/L (Dubsky and McPhail (2001) used 1,000 mg/L). This vetting tenet removes samples likely to be contaminated by potassium chloride (KCl) drilling muds. We noted that Bowyer (1991) recommended a cut off value of 180 mg/L; however, given uncertainty concerning natural concentrations of K^{+} expected in potentially connate waters from deeper portions of the Cooper Basin and a natural tendency for K^{+} and Cl^{-} concentrations to proportionally increase, it was considered that the use of 180 mg/L may be too conservative without further information. Keppel et al (2015) collected several samples from Eromanga, Arckaringa and Precambrian aquifers from the south-eastern corner of the Arckaringa Basin that returned K^{+} concentrations greater than 180 mg/L. The age and usage history of these water wells, as well as the sampling

protocols employed suggest such concentrations may not be related to contamination. Further, wells with elevated concentrations of K^+ were found to have K^+: Cl^- ratios like those found in seawater.

- a ratio of Na^+ to K^+ > 3 in milli-equivalents to screen for KCl mud contamination
- sulphate < 150 mg/L. Sulphate (SO_4^{2-}) is known to be a minor constituent in waters over the central and eastern GAB (Love et al. 2013b). Removing high values accounts for contamination introduced by make-up water or drilling muds.
- resistivity values (Rw) less than 7 ohm/m.
- samples with a Na to Cl ratio (milli-equivalents) between 0.5 and 5.0. This is a primary screen for recognising natural groundwater. It also accounts for samples contaminated by 'gel chem' and gypsum filtrates.

After the vetting process, 4,438 valid salinity samples were obtained. Of these, 633 salinity measurements related to formations within the Eromanga Basin. The remaining valid salinity samples were disregarded if they were from formations within the Cooper Basin (3,362) or could not be assigned to a formation (443). The average salinity for each Eromanga Basin formation was evaluated from the 633 valid petroleum-well salinity samples and appropriately assigned to valid formation pressures that did not have associated recorded salinity.

5.4 Development of density-corrected potentiometric surfaces

As described at the beginning of this chapter, the potentiometric surface requires correction for density variations, related to temperature and salinity changes, as this has a profound impact on groundwater flow gradients. To do this, a reference density is used and so the first step is to select an acceptable reference density to then apply during correction.

5.4.1 Reference-density determination

Normally a freshwater density of 999 kg/m^3 is employed; however, because groundwater within the Eromanga Basin aquifer units is interpreted to be subject to buoyancy effects (Rousseau-Gueutin et al. 2013), a specific reference density is required based on the correlated relationship between the temperature and screened depth of the wells subject to density variation (Figure 4.1).

The chosen reference density was 997.2 kg/m^3, which represents the average groundwater density near the springs. This was calculated using the analytical expression of Batzle and Wang (1992) as described in equations 3 and 4. This was chosen because the principal focus of groundwater management in the GAB, in terms of maintaining artesian pressure, are the iconic GAB springs.

Three key datasets were used to derive an areal mean density at GAB springs:

- A single temperature of the Main Eromanga Aquifer Sequence below the GAB springs was estimated by assuming a linear temperature gradient between the ground surface and mid-point depth of the Main Eromanga Aquifer Sequence (Figure 5.3A), consistent with the assumptions described in Section 5.2 and equation 6 for assigning bottom-hole temperatures. Note that at GAB springs in SA, there are no occurrences of either the Birkhead formation or the Hutton–Poolowanna aquifer.
- Stratigraphic surfaces for the 'C' and 'J' Horizons (Chapter 2 and Appendix A) were used to generate an isopach of the Main Eromanga Aquifer Sequence (or the 'C-J isopach') using the 'Raster Calculator' in QGIS. Similarly, the C horizon and 1-second Shuttle Radar Topography Mission (SRTM) DEM-H (Gallant et al. 2011) were used to generate an isopach of ground surface to the top of the J-K aquifer (or the 'A-C isopach'). The Raster Calculator was then used to divide the C-J isopach by 2 (that is, a half isopach of the Main Eromanga Aquifer Sequence); and the half C-J isopach added to the A-C isopach for a resulting depth to mid-point of the Main Eromanga Aquifer Sequence raster (m) (Figure 5.3A). The depth to the mid-point of the Main Eromanga Aquifer Sequence at 5,129 GAB springs was calculated using the Point Sampling Tool in QGIS.

- Table 5.6 summarizes the minimum, maximum, average and median depth to the mid-point of the Main Eromanga Aquifer Sequence at those spring locations. The depth at approximately 14 springs was not estimated due to the 400 m grid cell size not exactly matching the location of those springs. A cluster of springs in the Lake Eyre and Lake Blanche region were estimated to have a large depth to mid-point of the Main Eromanga Aquifer Sequence and thus may potentially bias the results. Nearer to the basin margin where most springs occur, the median depth provides a more representative aquifer depth. Thus, an aquifer temperature representative of the GAB spring locations was calculated to be 30.6°C (Equation 6).

Table 5.6: Depth to mid-point of the J-K aquifer at GAB springs.

Average depth (m)	Median depth (m)	Minimum depth (m)	Maximum depth (m)
127.9	56.5	0.3	994.3

1. A mean potentiometric surface elevation (60.25 m AHD) was calculated from the back interpolation of the final 19 uncorrected potentiometric surfaces at each of the 5,129 GAB spring locations (Section 11.6).

2. A mean salinity of 3,601 mg/L was estimated for the spring locations based on a Thiessen polygon analysis of J-K aquifer salinity from 1,061 water and petroleum wells (Figure 5.3B) by sampling the Thiessen polygon salinity raster using the Point Sampling Tool in QGIS.

5.4.2 Density correction of head data and generation of potentiometric surfaces

The reference-density head was then calculated for individual measured hydraulic head measurements (h_i) using equation 1.

Consistent with gridding of the uncorrected dataset, 19 density-corrected potentiometric surfaces were generated using the algorithm and process settings described in Section 11.6. Gridding of the density-corrected dataset was completed in *Surfer*™ at the gridding extent used for the uncorrected potentiometric surfaces: X (675,000, 1,905,000) and Y (1,980,000, 3,130,000) using 50 m x 50 m grid cell size. Seven Minimum Curvature surfaces were generated by applying the Internal Tension and Boundary Tension combinations detailed in Appendix A. Since the *Petrosys*™ workflow was already established and automated, the density-corrected dataset was also gridded using cell sizes from 10,000 m x 10,000 m to 100 m x 100 m. No 50 m x 50 m grids were generated using *Petrosys*™ due to the processing requirements and available computing power.

The final density-corrected, as well as uncorrected potentiometric surfaces are presented and discussed in Chapter 6.

5.4.3 Alternative correction application methodologies and reasons for rejection

Using a single correction density for a study area as large and variable as this will result in an unavoidable error because the temperature gradients across the area are expected to vary with differences in aquifer depth, thickness, groundwater salinity and the thermal conductance of the lithology. Whilst alternative methods to undertake correction using different reference densities, with calculations based on well type and sub-region were explored, these were ultimately abandoned for the simpler approach of using a single reference density for the entire study area.

- Correction using reference densities developed for water and petroleum wells, separately based on the screened (measurement) depth, rather than on well type (that is, water well versus petroleum well) (data not shown) was found to be unsuccessful because the generalised form of Darcy's Law for estimating groundwater flow in variable density systems is only valid under the assumption of constant density.

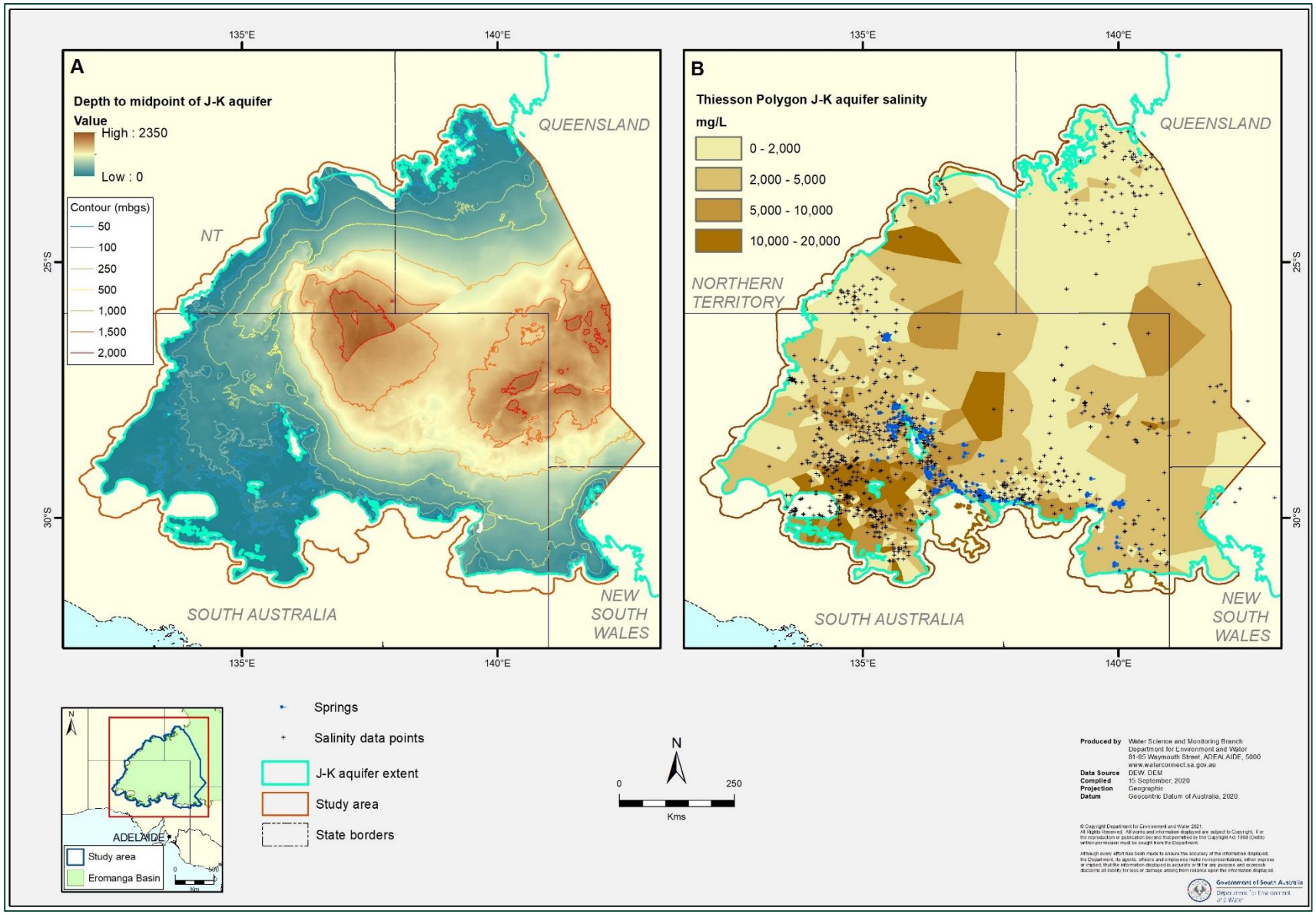

Figure 5.3: A) Depth to the mid-point of the Main Eromanga Aquifer Sequence and B) J-K aquifer salinity represented by Thiessen polygons

- Development of sub-regional density-corrected potentiometric surfaces within the J-K aquifer based on unique reference densities calculated for each sub-region was considered, as this approach in theory, could produce a more accurate understanding of local groundwater flow conditions. However, the development of sub-regional potentiometric surfaces, using sub-regional specific reference densities would not allow direct inference of groundwater interaction and flow across the basin and between sub-regions.

Finally, an alternative density-correction process was tested by applying the density correction to each cell of the uncorrected potentiometric surface grids as opposed to the individual well observations. However, this method was ultimately abandoned. The sharp changes in layer thickness, particularly east of the Cooper Basin and the margins of Thiessen polygons were being reflected in the density-corrected potentiometric surface more obviously than what would be expected to occur in reality. In reality, changes in the potentiometric surface related to density are more likely to transition over a distance rather than form distinct linear change. Further detail of the methodology is provided in Appendix E.

5.5 Potentiometric surfaces of the Hutton Sandstone and Poolowanna Formation

Separate uncorrected and corrected potentiometric surfaces for the Hutton–Poolowanna aquifer were generated as these units were deemed to be isolated from younger J-K aquifer units by the regionally confining Birkhead Formation. As this potentiometric surface is not considered as critical with respect to springs and considering the sparse data points when compared to the J-K aquifer, the algorithm assessment was not undertaken. Instead, a Minimum Curvature algorithm with no internal or Boundary Tension was applied in Surfer™ to generate the potentiometric surface. This algorithm produced several potentiometric surfaces for the J-K aquifer considered plausible during this study. Data sources are described in Section 5.1, and the density correction method described in Section 5 was also applied.

The final density-corrected, as well as uncorrected potentiometric surfaces are presented and discussed in Chapter 6.

6 The density-corrected potentiometric surfaces

The learnings regarding the adequacy of various algorithmic gridding methods to adequately depict an uncorrected potentiometric surface were applied to the density-corrected data. Instead of undertaking the same review process as for uncorrected data, the 7 Minimum Curvature methods generated using *Surfer* at a 50 m x 50 m grid and the 12 methods using *Petrosys* at a 100 m x 100 m grid that were found to produce the most plausible uncorrected potentiometric surfaces were used to interpolate corresponding density-corrected potentiometric surfaces. When viewed collectively, this suite of potentiometric surfaces also captures the likely range of uncertainty. This chapter describes the resultant density-corrected potentiometric surfaces using the 19 algorithmic gridding methodologies deemed in Chapter 3 as most capable of generating a scientifically plausible representation of groundwater flow within the J-K aquifer.

6.1 General flow patterns

Key similarities between all the uncorrected (Appendix E) and density-corrected (Appendix F) potentiometric surfaces for the J-K aquifer include:

- A generally radial pattern occurs, with inflows and recharge from the east, north, west and parts of the south, with flows toward discharge zones near the springs and along some of the southern margins.
- Steep hydraulic gradients along the west and north-western margins of the Eromanga Basin (for example, north and south of Marla) indicate an area of recharge and/or through-flow from adjacent groundwater flow systems to the J-K aquifer. Alternatively, steep gradients in these areas may be reflective of lower hydraulic conductivity.
- Contributions of recharge to the J-K aquifer from fractured rock aquifers is also indicated by mapped contours along the southern area of the Peake and Denison Inliers and from the Northern Flinders Ranges. Such forms of recharge may be related to 'Mountain System Recharge' (Wohling et al. 2013), where Mesozoic aquifers are recharged via through-flow from fractured rock aquifers found in adjacent highland areas. Such flow systems may occur in relatively close proximity to spring discharge zones (for example, see Halihan et al. 2020) and may also partly contribute to spring discharge in addition to more regionally sourced flow.
- A depression in the potentiometric surface occurs along the western flank of the Cooper Basin that is likely to represent drawdown due to co-produced extraction and pastoral water use.
- A depression in the potentiometric surface adjacent to and north of Bedourie (Figure 6.1 and Figure 6.2) is likely to represent drawdown due to pastoral water use
- Areas of discharge occur along the southern edge of the J-K aquifer south of Lake Frome near Maree, and to the south of Stuart Shelf and the Peake and Denison Inliers (Figure 6.1 and Figure 6.2).

6.2 Key differences between potentiometric surface interpolations

However, significant differences between the interpolated potentiometric surfaces are also apparent. The 19 plausible potentiometric surfaces were divided into four groups that displayed similar features.

Figure 6.1 and Figure 6.2 illustrate representative uncorrected and equivalent corrected potentiometric surfaces respectively. For these figures, the representative potentiometric surface has the following algorithm and interpolation settings.

- Panel A represents Group 1 (*Surfer,* Minimum Curvature, Internal Tension = 0, Boundary Tension = 0).
- Panel B represents Group 2 (*Surfer,* Minimum Curvature, Internal Tension =1, Boundary Tension = 1).
- Panel C represents Group 3 (*Petrosys,* Least Square Binomial., Bilinear interpolation, 1st order Taylor series).
- Panel D represents Group 4 (*Petrosys,* Minimum Curvature, Bicubic interpolation, 1st order Taylor series).

Further, Appendix E and Appendix F provide the uncorrected and density-corrected contour maps for all 19 recommended 2019 potentiometric surfaces, as well as the groupings, software and algorithm details.

- **Group 1** consists of two potentiometric surfaces generated in *Surfer* using Minimum Curvature with the internal tension set to zero (50 m grids). Groundwater inflow to SA occurs from the NT, as well as via the northern and eastern border with Qld as shown by the steep hydraulic gradient along the eastern model boundary.
- **Group 2** consists of two potentiometric surfaces generated in *Surfer* using Minimum Curvature with the internal tension set to 1 (50 m grids). Groundwater inflow into SA occurs from the NT and the northern border with QLD. Groundwater inflow into SA along the eastern border with Qld is limited compared to other groupings.
- **Group 3** consists of three potentiometric surfaces generated in *Surfer* using Minimum Curvature with variable internal and boundary tensions (50 m grids), and four generated in *Petrosys* using Least Square Plane, Least Square Binomial and Distance Weighted Average algorithms (100 m grids). Groundwater inflow to SA occurs from the NT, as well as via the northern and eastern border with Qld. Groundwater flow from Qld along the eastern model boundary occurs along a lower hydraulic gradient compared to Group 1. This lower gradient may be suggestive of either lower groundwater volumes or higher transmissivity than suggested by Group 1. Groundwater inflow to SA occurs along the border with NSW.
- **Group 4** consists of four potentiometric surfaces generated in *Petrosys* using Minimum Curvature and Hybrid algorithms (100 m grid). Groundwater inflow to SA occurs from the NT, as well as via the northern and eastern border with Qld as shown by the steep hydraulic gradient along the eastern model boundary.

The largest variations between groupings generally occurs where the software employed interpolated surfaces in regions that were data poor. In such regions, interpretive variations included significant differences in groundwater flow direction as well as magnitude of head. For uncorrected potentiometric surfaces, differences of up to ±40 m can occur in areas with no measured head data. Further, many spring vents have a mismatch between the potentiometric surfaces of greater than 0.2 m of excess head (that is, artesian pressure above the recorded spring elevation), with a maximum difference over a spring vent of ≈7.5m.

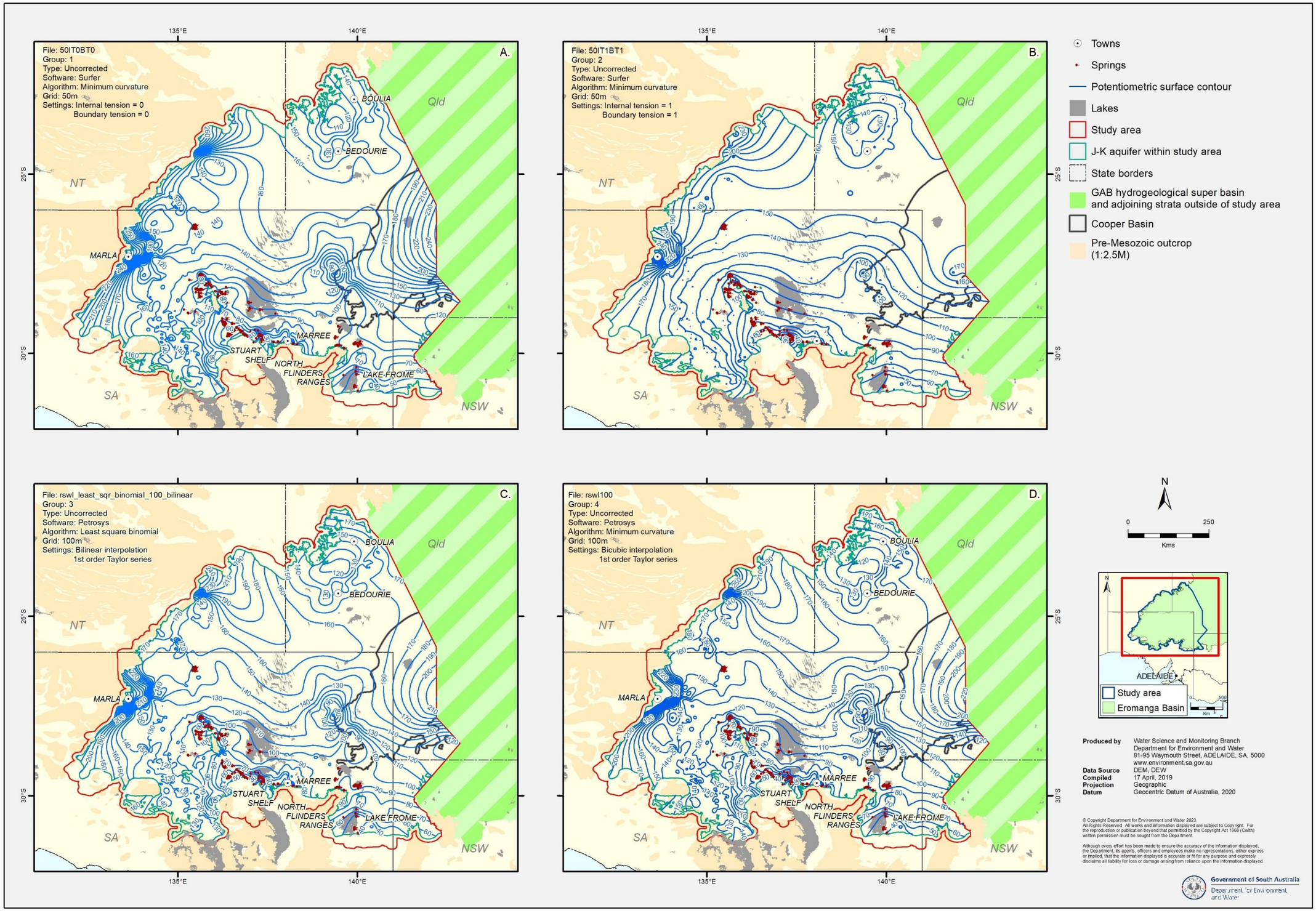

Figure 6.1: Examples of uncorrected potentiometric surfaces developed for the J-K aquifer from each group

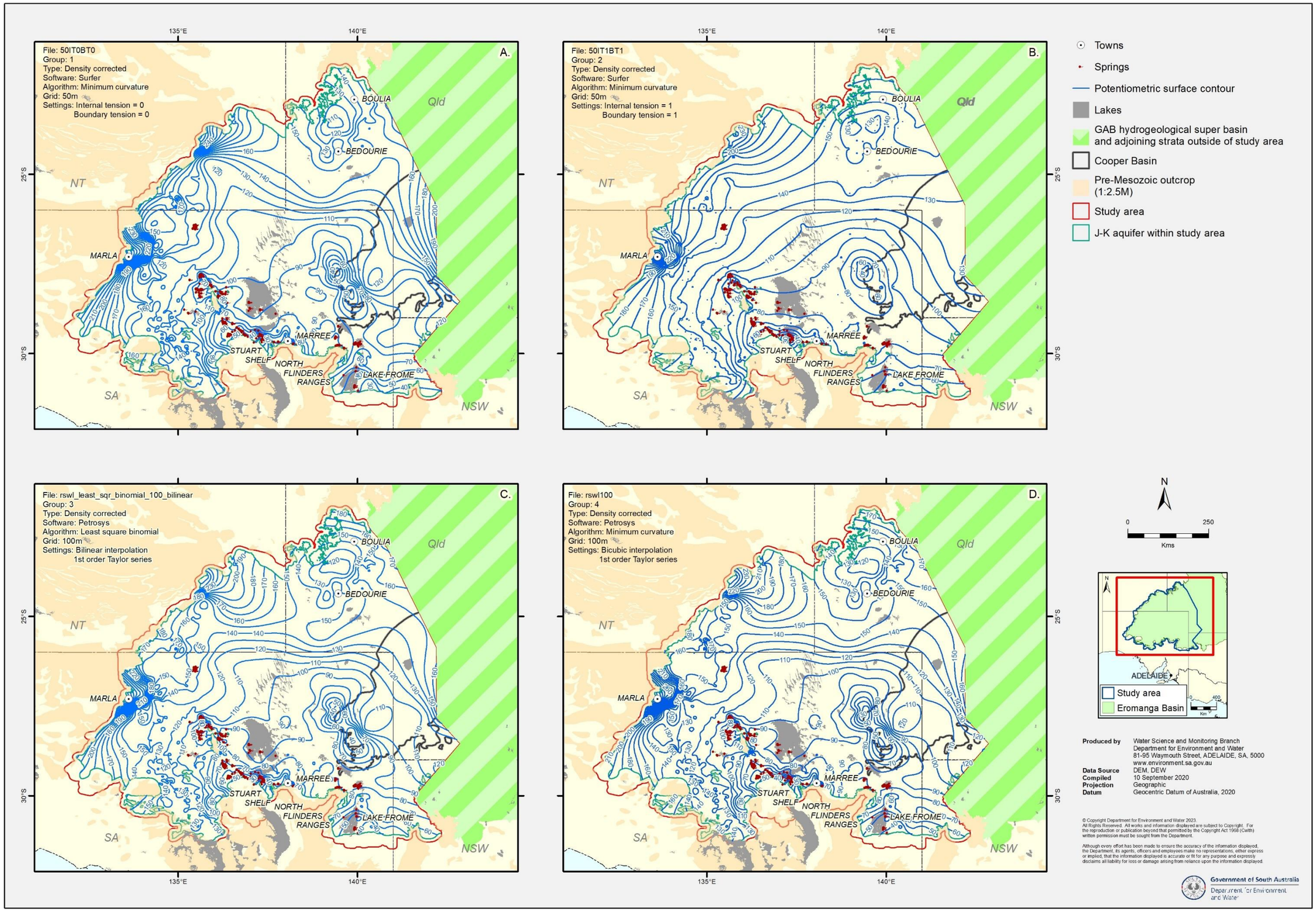

Figure 6.2: Examples of density-corrected potentiometric surfaces developed for the J-K aquifer from each group

6.3 Key differences between uncorrected and density-corrected potentiometric surfaces

The largest corrections occurred from wells located in the central and eastern parts of the study area where hot, deep wells are most common (Figure 6.3). A maximum correction attributable to density of <−84 m. In particular, the western Flank of the Cooper Basin and the Poolowanna Trough located between the Cooper and Pedirka basins in South Australia returned large areas of significant density correction. In contrast, corrections to a maximum of approximately 2.0 m were obtained from shallow, highly saline wells. The most saline groundwater in the study area is found near the south-west margin within the Arckaringa Basin area. The median density correction was 0.01 m (mean was 2.45 m). Fifty-six percent of density-corrected heads are lower than the environmental head (observed at the wellhead), and 56% of density corrections are within ±0.1 m (73% within ±0.5 m).

6.4 Determining the extent of artesian, confined and unsaturated zones in the J-K aquifer

The extent of non-artesian/artesian groundwater conditions, unconfined/confined conditions and saturated/unsaturated conditions, and potential error, has been estimated for the J-K aquifer for each of the representative uncorrected potentiometric surface from each group as described in Chapter 3. These extents are presented in Figure 6.4.

To estimate the extent of non-artesian and artesian conditions, each J-K aquifer potentiometric surface was subtracted from the ground elevation of the 1-second Shuttle Radar Topography Mission, hydrologically enforced digital elevation model (SRTM DEM-H) (Gallant et al. 2011) to estimate a 'depth to potentiometric surface' raster for all the 19 plausible potentiometric surfaces. The zero-metre contour from each 'depth to potentiometric surface' represents the boundary condition of non-artesian and artesian conditions in the J-K aquifer (Figure 6.4). In some areas, there are only subtle differences (<100 m) between the extent of artesian groundwater illustrated by the four potentiometric surface groups. However, there are also significant differences of up to 50 km between the extents of artesian water as highlighted in the NT. The large differences typically occur in areas with limited well data to control the interpolation of the potentiometric surfaces. However, the extent of artesian groundwater conditions generally honours the locations of flowing GAB springs.

The extent of confined aquifer conditions – defined as where the uncorrected potentiometric surface has a higher elevation higher than the top of the C horizon – was estimated by subtracting the J-K aquifer potentiometric surfaces from the C Horizon stratigraphic surface. Where the C Horizon and the potentiometric surface are equal represents the boundary between non-artesian and artesian conditions (Figure 6.4). In areas of higher data density and greater well control, the extents of generally non-artesian groundwater conditions in the J-K aquifer only have minor differences between groups (<100 m). However, in areas of lower data density, the extent of confined groundwater conditions may be up to 10 km different between the four potentiometric surface groups. In all cases the boundary between confined and artesian conditions roughly followed the Torrens Hinge Zone and northern extent of the Adelaide Geosyncline but varied where erosion associated with the surface hydrology had removed confining unit sedimentary rocks. Additional boundaries exist where either aquifer units thinned or were closer to the surface, including within the NSW portion of the study area, near the northern margin of the study area in Qld, or where basement highs occur.

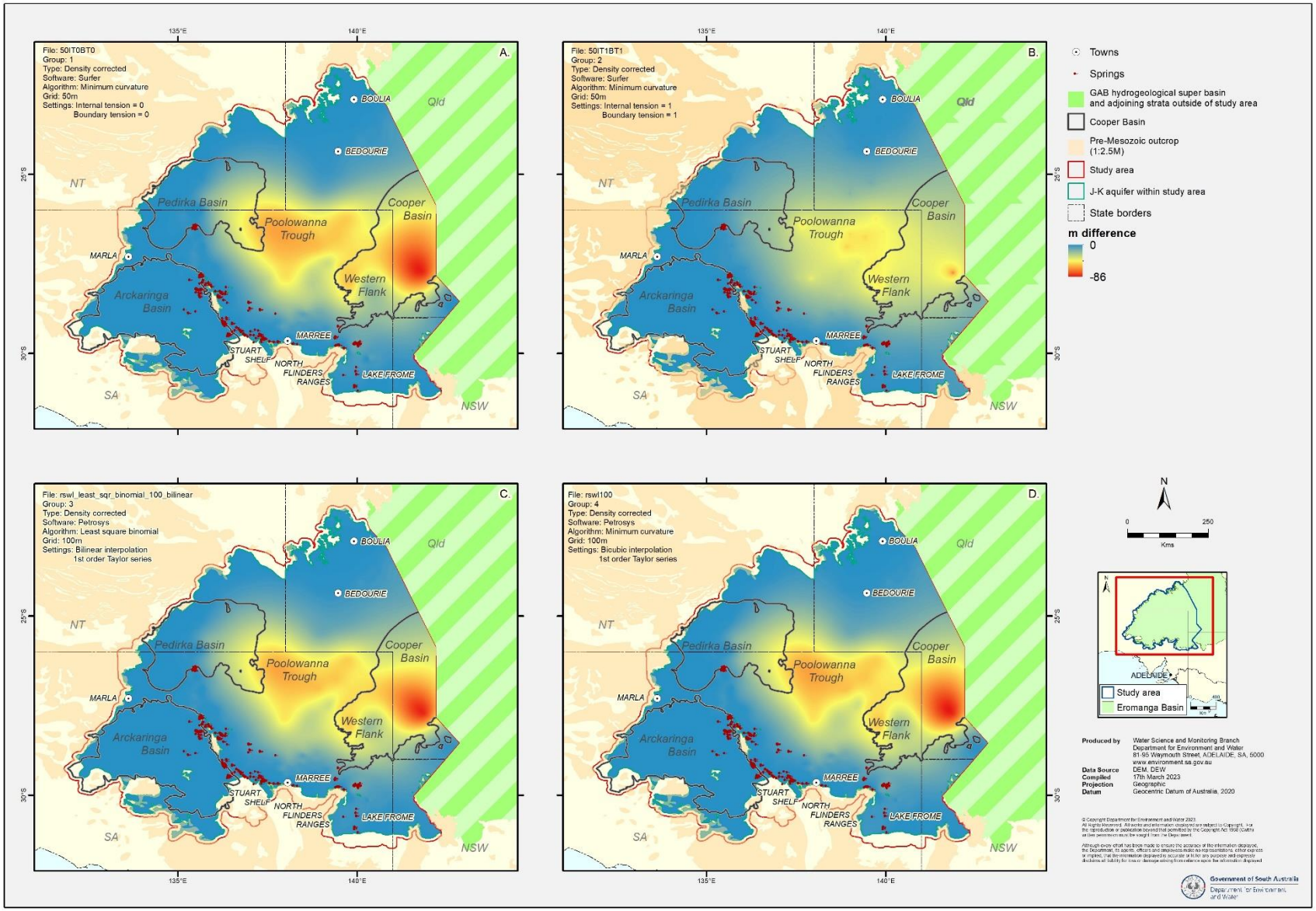

Figure 6.3: Difference between uncorrected and density-corrected potentiometric surfaces developed for the J-K aquifer from each group

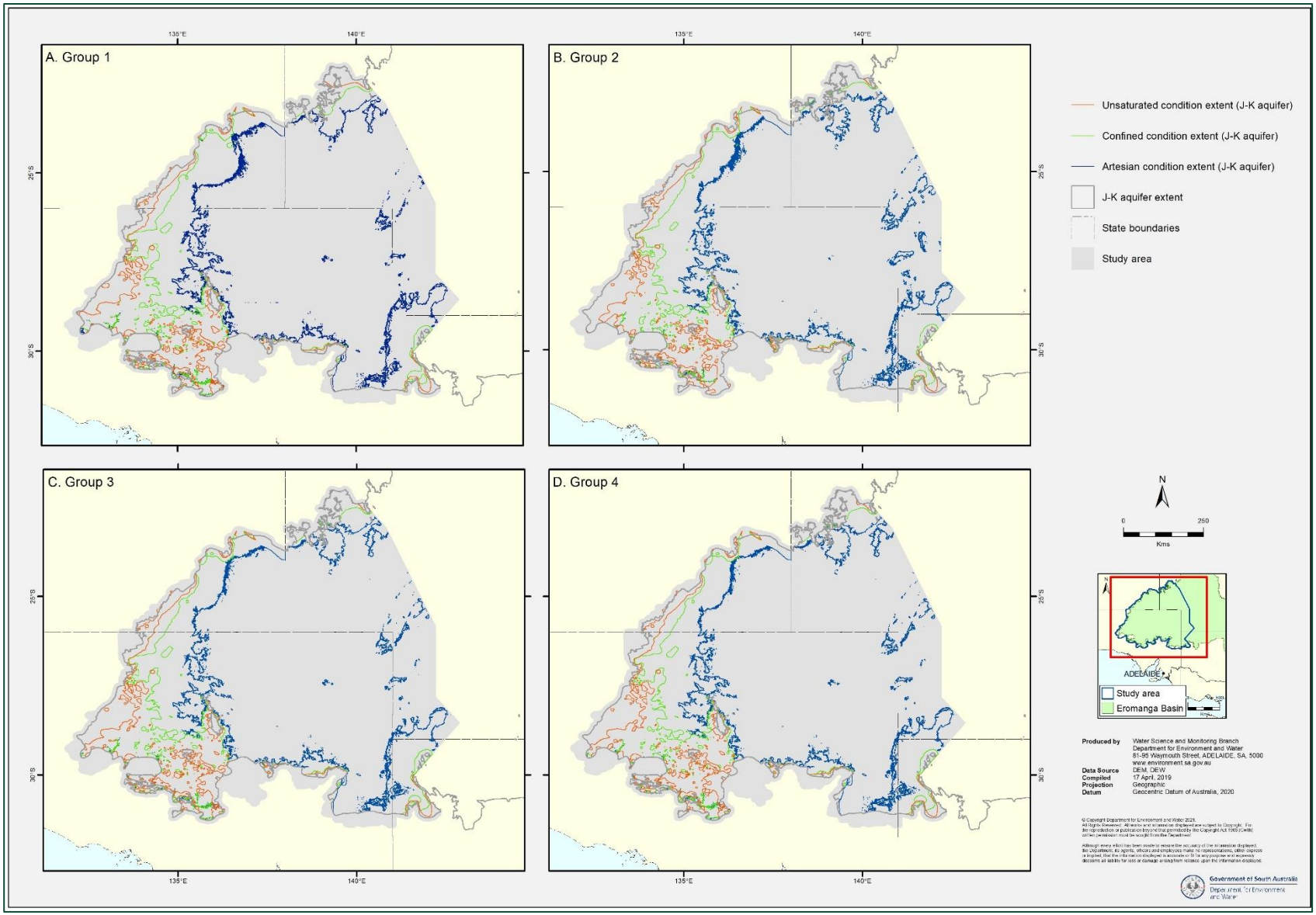

Figure 6.4: Extent of artesian, confined and unsaturated conditions in the J-K aquifer based on uncorrected potentiometric surface (environmental head)

Finally, the extent of unsaturated conditions in the J-K aquifer – defined as where the elevation of the uncorrected potentiometric surface has a lower elevation than the J Horizon – was estimated by subtracting the J- K aquifers potentiometric surfaces from the base J Horizon stratigraphic surface. Where the elevation of the J Horizon and the potentiometric surface are equal represents the boundary between unconfined and dry groundwater conditions (Figure 6 4). Near the western and south-western margins of the study area where there was limited or no data for the interpolation of the potentiometric surfaces and stratigraphic surfaces, the boundary between dry and unsaturated groundwater conditions can vary by up to 20 km.

6.5 Initial groundwater conditions for numerical modelling, J-K aquifer

For the purposes of choosing an initial condition for modelling, a representative surface from Group 3 was chosen (Figure 6.2C, Figure 6.5A). The reasons for this choice are as follows:

- Group 3 displays a groundwater flow pattern like what has been previously conceptually understood to occur (see for example, Ransley et al. 2015), with inflows from the north (NT), as well as north-east and east (Qld).
- Although Groups 1 and 4 broadly share this general inflow pattern from the NT and Qld, the gradient of flow is less steep than these other groups. Within the constraints of hydraulic conductivity values either derived from literature or core porosity work (Volume 3), Group 3 was considered representative of more conservative groundwater volume inflows than the other two groups. It is recognised that similar groundwater flow volumes might be achieved with Group 1, depending upon the hydraulic conductivity values used after calibration.
- Unlike what is typically seen in Group 1, Group 3 interpolations generally indicate inflow from interpreted recharge areas located north of Bedourie in south-west Qld, which also matches previously understood conceptualisations. In general, potentiometric surfaces in Group 3 appear to show no-flow on the eastern margin (northern NSW) as well as outflow along the southern margin of the Frome Embayment. As with other flow features described above, this more closely matches the primary conceptual hydrogeological model (CHM).
- Compared to Group 4, there are fewer anomalous or single-point derived contours, particularly in areas of sparse data (Figure 6.5A). We note in some other groups, particularly in the NT and the Frome Embayment, there are features that would be difficult to replicate in a model given the data available.
- The contour features associated with flow from the NT into SA appear more conservative in nature than Groups 1 and 4, which would easier to replicate using a model.

Group 2 is the 'primary alternative' to Group 3. Group 2 was selected because it is the group of surfaces that shows the least flow from the east and therefore differs the most from the primary conceptualisation (Figure 6.2B, Figure 6.5B). Group 2 shares some similarity with the density-corrected potentiometric surface interpretations developed by Sampson et al. (2013) and Rousseau-Gueutin et al. (2013) in that inflow appears to be predominantly sourced from the north and north-east, rather than the east. However, the more extensive area included in interpretation undertaken for this study compared to these other studies and the similarities to the interpretation undertaken by Ransley et al. (2015) suggest the use of potentiometric surface interpretations that show inflows from the east for primary analysis, in this study.

6.6 Potentiometric surfaces of the Hutton–Poolowanna Aquifer

Separate uncorrected and corrected potentiometric surfaces for the Hutton–Poolowanna aquifer (model Layer 5) were generated as these units were deemed to be generally isolated from younger J-K aquifer units by the regionally confining Birkhead Formation (Figure 6.6and B). The key features of the uncorrected potentiometric surface are inflows from the east via Queensland and a depression in the potentiometric surface (60 m AHD) centered on the western flank of the Cooper Basin (Figure 6.6A and B).

An areal average reference density of 953.76 kg/m^3 was calculated using the Hutton Sandstone and Poolowanna Formation dataset and used to derive a density-corrected potentiometric surface for the Hutton Sandstone and Poolowanna Formation Figure 6.6B). Key features of the corrected potentiometric surface include:

- Although a depression in the potentiometric surface is still evident along the western flank of the Cooper Basin, the main depression (30 m AHD) occurs to the east of the western flank.
- A hydraulic gradient at the SA-Qld border of between 4.1 x 10^{-4} and 7.4 x 10^{-4} is indicative of inflow.
- A 30 m AHD contour is directly adjacent to a 100 m AHD high in the potentiometric surface (Figure 6.6C). Here, correction of formation pressures at the petroleum wells, Paranta-1 and Rossco-1, to the reference density resulted in a reduction in pressure of approximately −31 m and −25 m, respectively. Whereas correction to the reference density at the neighboring petroleum well, Cadenza-1, resulted in an increase in pressure of approximately 24 m. The pressure of the Hutton Sandstone between 2,096 m and 2,167 m bgs has been measured in each of the three wells. However, what drives the correction differences in this instance is the measured temperature (and therefore water density). Cadenza-1 recorded a temperature of 98°C, compared to 127 to 130°C for the other two wells, and is considerably lower than a formation temperature predicted using the linear line of best fit of maximum groundwater temperature and screen interval (that is, 127°C). However, there is no documented reason for excluding the data point.
- Typically, the formation (water) pressure data is limited in extent to the Cooper Basin region in SA, and with only several data points located in Qld, extrapolation of potentiometric contours to the north of the Cooper Basin in SA needs to be treated with caution.

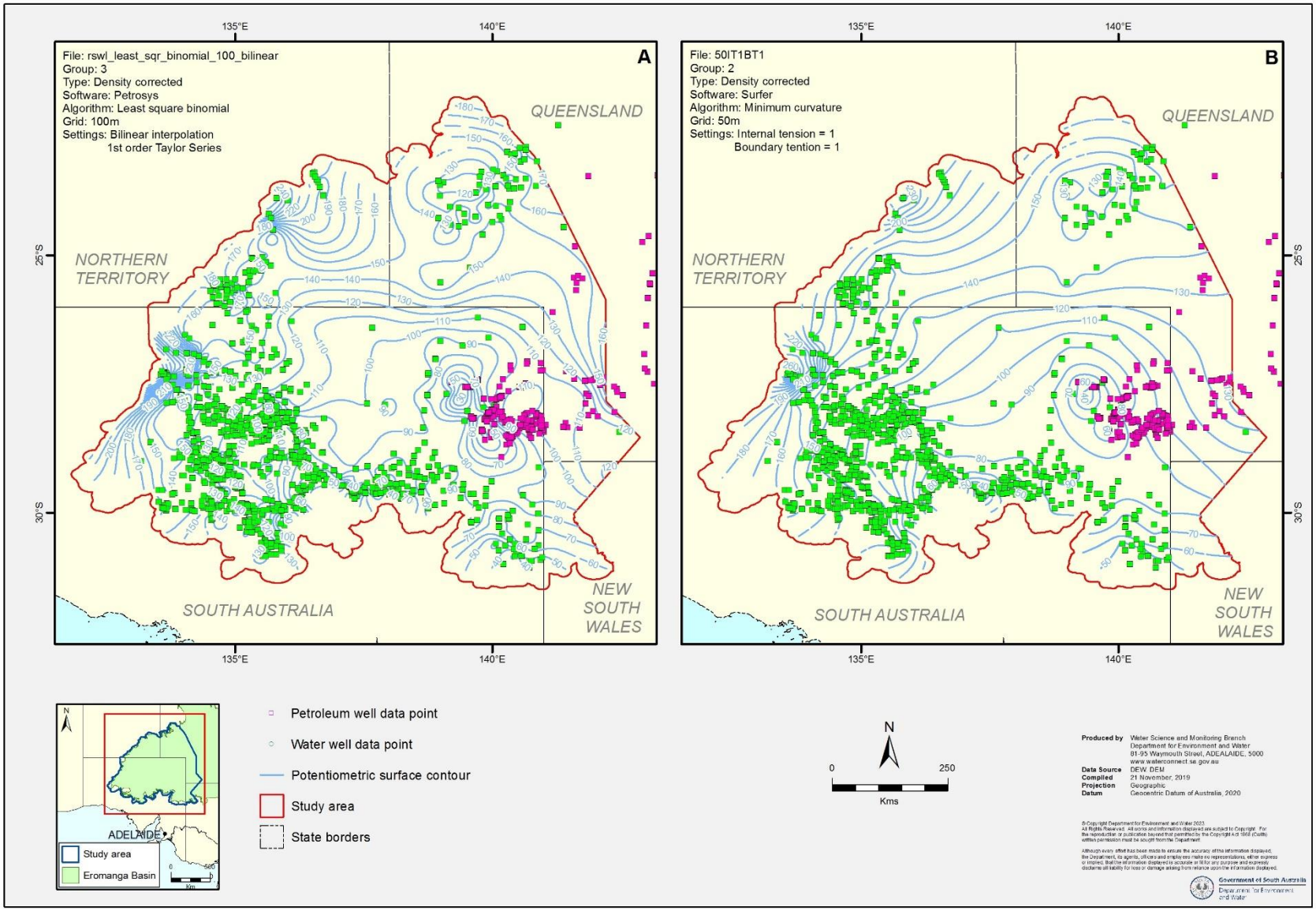

Figure 6.5: A) Density-corrected potentiometric surface for the J-K aquifer (Layer 1 and 3) B)'Primary alternative' density-corrected potentiometric surface

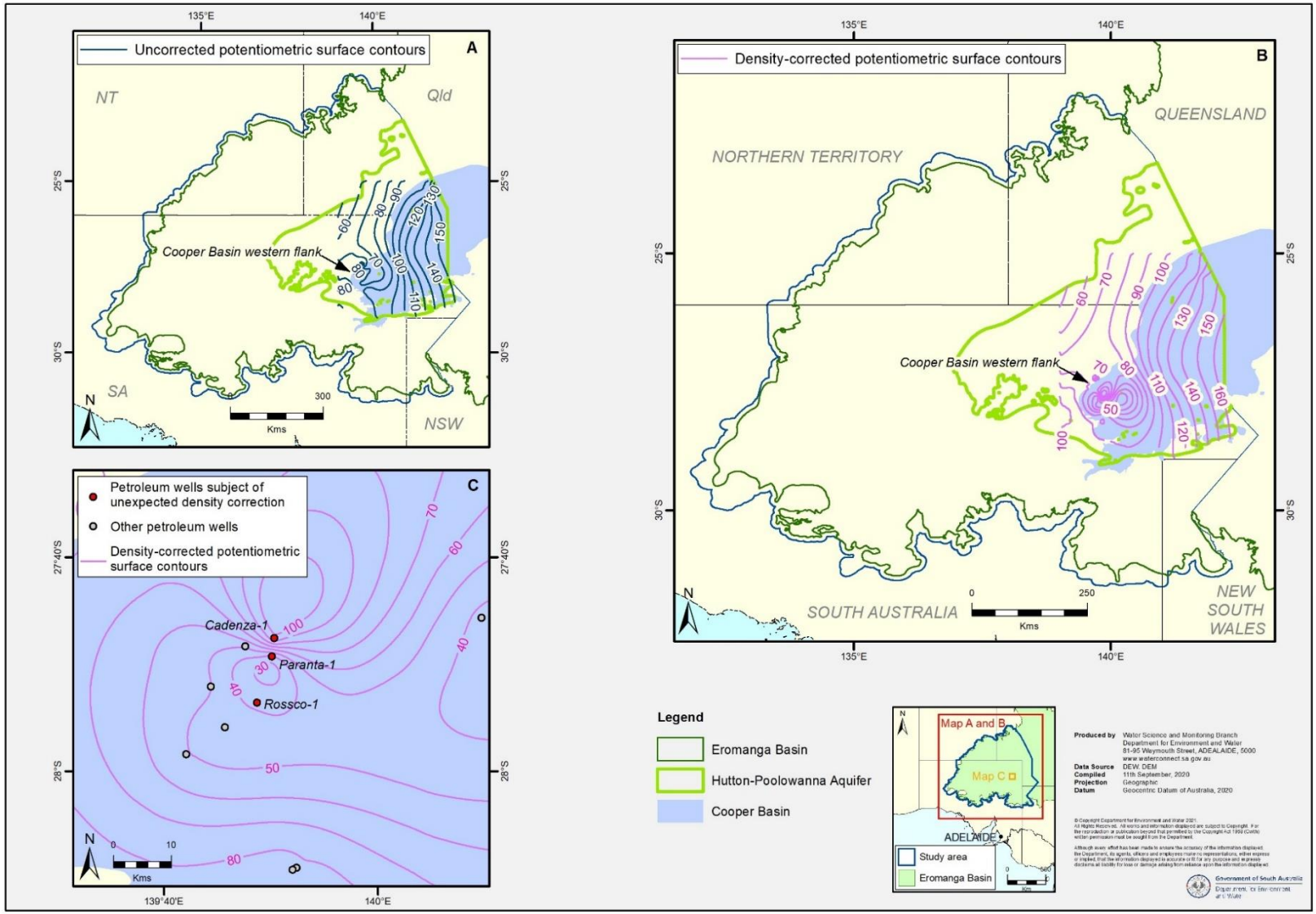

Figure 6.6 : A) Uncorrected and B) density-corrected potentiometric surface of the Hutton Sandstone and Poolowanna Formation. C) Density-corrected head contours near Cadenza-1 and Paranta-1

7 Driving force ratio

Where density variations exist, groundwater flow in a sedimentary aquifer may be affected by to two driving forces (Rousseau-Gueutin et al. 2013):

- the hydraulic head gradient caused by pressure and/or topographic differences
- buoyancy due to density differences and the slope of the aquifer.

A driving force ratio (DFR) (or mixed convection ratio) defines the significance of hydraulic factors compared to buoyancy along the slope of the aquifer. When the DFR is less than a threshold value of 0.5 then the main driving force for groundwater flow is gravity and groundwater flow rates and directions can be described accurately by the freshwater potentiometric surface (Rousseau-Gueutin et al. 2013). However, when the DFR is between 0.5 and 1, then the influence of buoyancy forces on groundwater flow is significant and the freshwater potentiometric surface may not accurately represent groundwater flow conditions. In these cases, it is important to use an areal average density to correct the potentiometric surface. Where the DFR is greater than a threshold value of 1, then free convection can occur, and the uncorrected potentiometric surface are considered unreliable in inferring gravity-driven groundwater flow rates and directions. According to Rousseau-Gueutin et al. (2013), a significant portion of the GAB in SA, particularly the depocentre areas associated with the Poolowanna Trough and the Cooper Basin, exhibit a DFR >0.5–1.0 and thus may be influenced by mixed convection processes and possibly free convection.

The DFR depends on the head gradient. A map of DFR therefore allows a first approximation of how accurately each potentiometric surface group represents groundwater flow conditions in the J-K aquifer. The DFR was mapped for the four representative potentiometric surface groupings described in Chapter 6.

7.1 Mapping the driving force ratio

The difference in density between the reference density (997.2 kg/m^3) and density at the measurement point (ρ_i) was estimated for each potentiometric surface raster cell using an estimate of ρ_i as described in Equation 1 (repeated below).

$$\boldsymbol{DFR} = \frac{\rho_i - \rho_f}{\rho_f} \frac{|\nabla E|}{|\nabla H|} \quad 9$$

Where ρ_i is the density at the measurement point, ρ_f is the freshwater density, ∇E is the aquifer slope and ∇H is the hydraulic gradient.

The slope of the aquifer (∇E) was calculated on the mid-point depth of the J-K aquifer (a combined Layers 1 and 3) using the GDAL 'Slope' tool in QGIS using the original structure surface files from Novak (2020) (Figure 7.1). The hydraulic gradient (∇H) for each density-corrected potentiometric surface was also calculated using the GDAL 'Slope' tool (Figure 7.2).

Figure 7.3 presents the DFR estimates for one example of each of the four groupings of derived potentiometric surfaces. The representative surface for each of the groupings are the same as those detailed in Section 5.4. In summary, the mapped DFR for each of the representative potentiometric surfaces returned the following results:

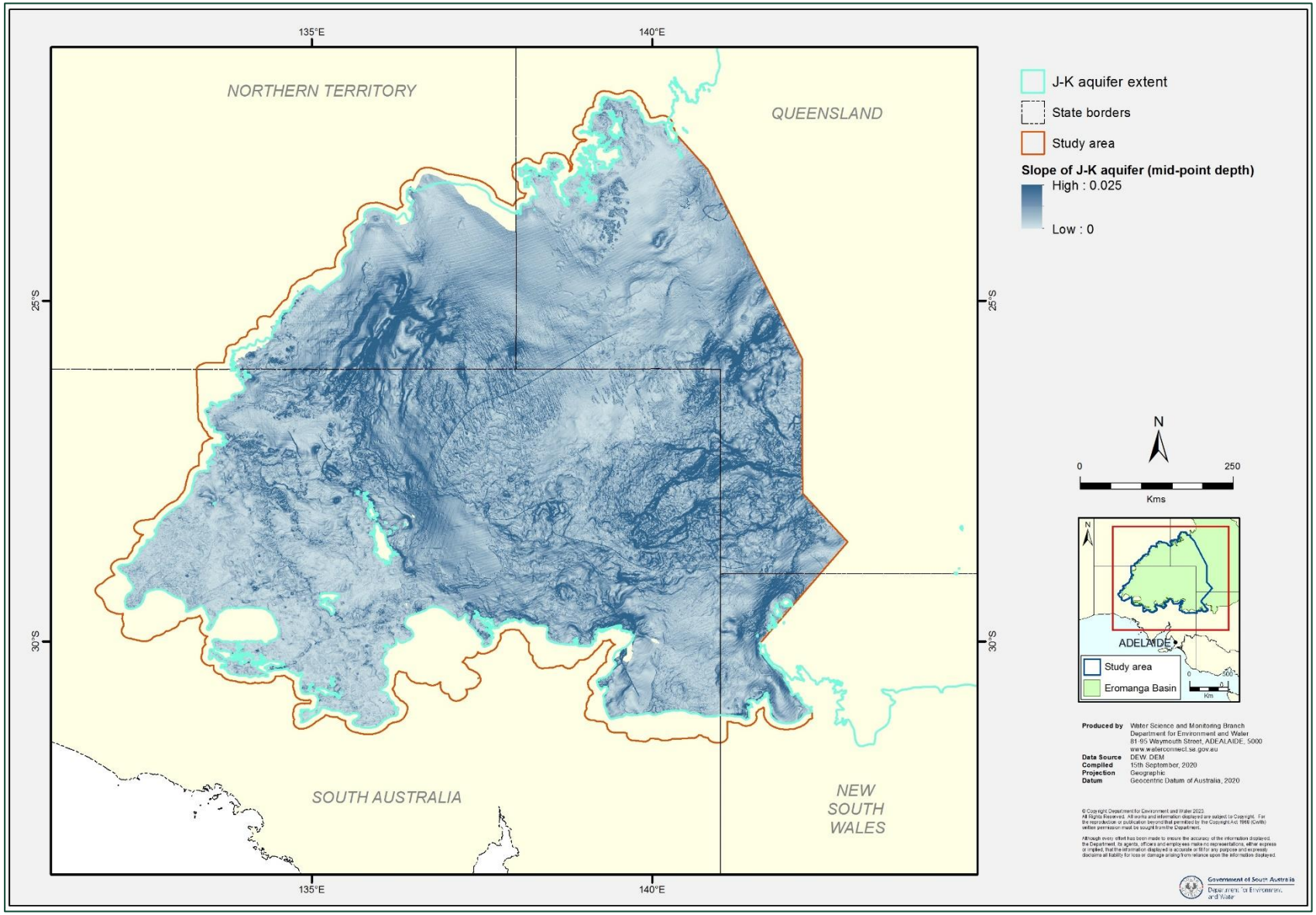

Figure 7.1: Slope of the Main Eromanga Aquifer Sequence (mid-point depth)

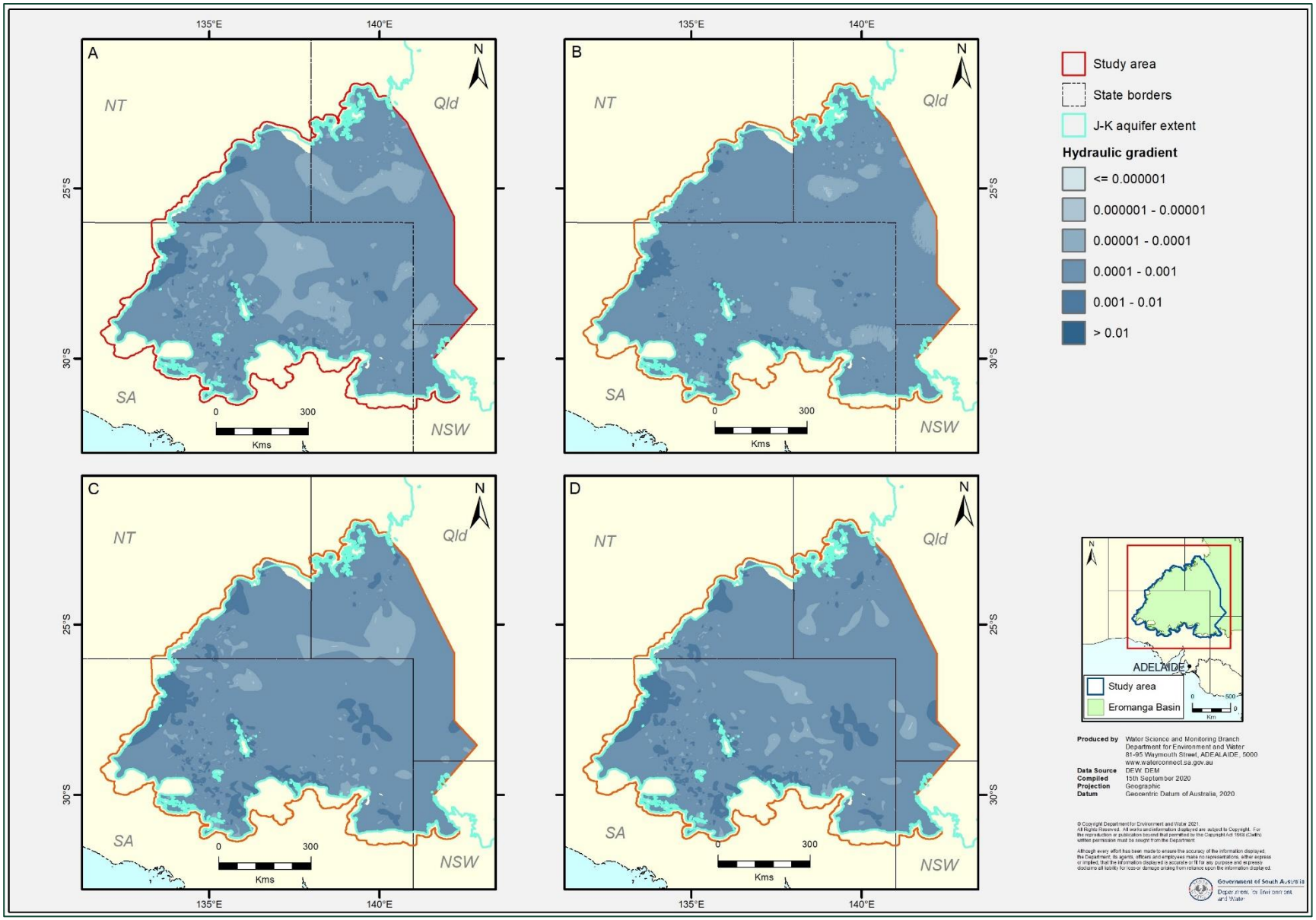

Figure 7.2: Hydraulic gradient of the J-K aquifer (Group 1, Panel A; Group 2, Panel B; Group 3, Panel C; Group 4, Panel D)

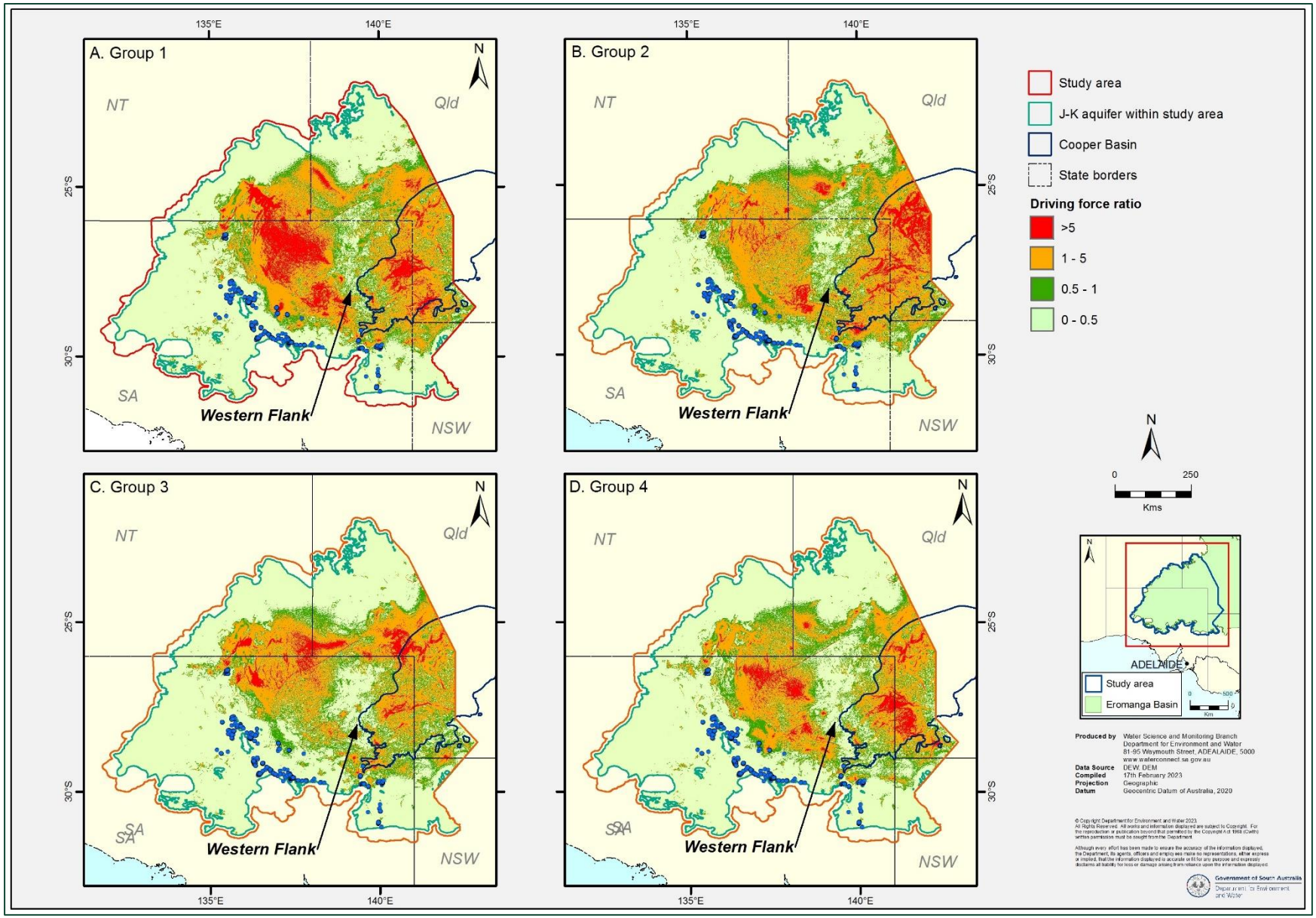

Figure 7.3: Driving force ratio (Group 1, Panel A; Group 2, Panel B; Group 3, Panel C; Group 4, Panel D)

Table 7.1: Summary of mapped DFR for each of the representative potentiometric surface

Group	DFR<0.5	DFR<1	DFR<5
1	≈50%	≈63%	≈92%
2	≈53%	≈67%	≈95%
3	≈59%	≈73. %	≈96%
4	≈60%	≈74%	≈96%

The Group 4 density-corrected potentiometric surface presents a marginally larger proportion of the study area where the DFR is less than 1 and less than 0.5 compared to the other three surfaces, while this difference between Groups 3 and 4 become insignificant for DFR >5. (Table 7.1; Figure 7.3).

In all cases, there are considerable areas in the central and eastern portions of the study area where the DFR >1. Bachu and Michael (2002) stated that for areas where the DFR is between 0.5 and 1 that errors in density correction are likely, which can be partly addressed by using an optimised reference density in hydraulic head calculation. For the study area in question, the size and complexity of the aquifers suggests that the optimal reference density will vary sub-regionally. Ideally, in regionally extensive sloping aquifers, local-scale potentiometric surface maps that are underpinned by appropriate reference elevations are preferable, as the choice of reference elevation may affect the inferred groundwater flow direction, even under hydrostatic conditions (Post et al. 2007).

Nearer to the location of the GAB springs, for all groups, but notably Group 3 and 4, density-corrected potentiometric surfaces are less prone to issues related to free convection, as the area of DFR <0.5 extends east of the Peake and Denison Inliers. While this analysis, as well as past analysis by Rousseau-Gueutin et al. (2013) indicates that the Eromanga Basin in SA is predominantly a forced convection (horizontal) flow system near these key management zone, this may also be reflective of the choice of reference density (Section 5.4.1). Therefore, the density-correction methodology adopted appears in accordance with the recommendation of Bachu and Michael (2002), who stated that:

> *There is no single or critical value of the DFR, below which the error in using hydraulic heads alone is negligible, and above which it is not acceptable anymore; rather, the decision regarding the error acceptability should and can be made on a case-by-case basis.*

DFR analysis confirms that error related to density correction is minimal near GAB springs, which are the most critical regions for groundwater management.

7.2 Implications for modelling and uncertainty

As described above, driving force ratio analysis suggests that groundwater flow in large portions of the J-K aquifer in the central and eastern portions of the study area may be subject to free convection because of high groundwater temperatures and aquifer configuration.

However, the interpretation of dominant free convection in regions predicted by DFR is still considered uncertain for the following unresolved reasons:

- Problematically, for this study, many areas where DFR >1, tend to coincide with regions of sparse data, such as the Poolowanna Trough and parts of the Cooper Basin region east of the Western Flank. (Figure 7.3). Further, DFR >5 emphasises the strong control slope has on the ratio calculation, particularly in the absence of well-derived data. Areas where DFR>5 coincide with identified structural complexity, such as folding and faulting mapped during structure surface development (Volume 2;, Novak 2020). By extension, the J-K aquifer within

the Cooper Basin region also contains known confining units and therefore zones of heterogeneous lithology, such as the Westbourne Formation and McKinley Member, which are not accounted for in this assessment. As detailed in Section 4, lithology has an important control on thermal conductance and in turn, thermal gradient and therefore assumptions using a linear thermal gradient model may be incorrect at certain scales. That being said, Irvine et al. (2015) identified that while aquifer vertical heterogeneity is an important consideration in the extensive Yarragadee Basin, Western Australia, the intervening low permeability layers (albeit quite thin) do not necessarily preclude free convection, even with relatively low thermal gradients (20 to 25°C/km).

- The impact of current extraction from the basin is also unknown, particularly in the Cooper Basin region, where large extractions associated with oil and gas production over a wide area may cause any convection cells to break down.

While the effects of temperature variations on the hydrodynamics of the GAB hydrogeological super-basin are the subject of ongoing research, for the purpose of this model, it is assumed that the Eromanga Basin in SA is predominantly a forced convection (horizontal) flow system. Whilst more work is needed to confirm the existence of free convection, the work required is substantial. Further and in simple terms, the assumption of forced convection flow system is justified due to the various intervening aquitards that disturb what could otherwise allow 3D mixed convection cells to develop due to the high thermal gradient. Across the Eromanga Basin, the Rayleigh number is largely less than the theoretical critical number ($4\pi^2$ for horizontal layers), and the mixed convection ratio is largely <1, given certain assumptions of the vertical hydraulic conductivity (K_v), thickness and geothermal gradient (Love et al. 2013a). Logic would suggest that applying a geothermal gradient of around 48°C/km as actually applies to the GAB, rather than the 100°C/km that was assumed for some areas for some investigations, would reduce the potential for free convection flow, but confirmation depends on the findings of ongoing research. Further details of modelling implications are presented in Section 9.3.

8 Review of pressure versus elevation data with respect to groundwater flow

The Cooper Basin region is an area where free convection may occur due to elevated heat flow, compounded by the presence of thermally insulating coal horizons. Further, the region is also the site of a significant oil and gas industry, with the resulting extractions potentially having an important influence on groundwater pressure. Finally, previous modelling and water-balance calculations have implied a significant proportion of inflow and outflow from the Main Eromanga Aquifer Sequence occurs via vertical leakage (see for example, Radke et al 2000; Welsh 2000; Welsh 2006).

To determine the significance of hydraulic gradients at differing spatial and temporal scales to model conceptualisation and subsequent depiction, we examined pressure data (expressed as formation head) versus screen elevation for all quality-checked drill test results from the Cooper Basin region as collected from the Petroleum industry.

Pressure versus depth profiles were generated to determine the distribution of formation pore pressures and used to infer vertical (upward or downward) or horizontal flow components within the Eromanga and Cooper basin region. The same formation-pressure database as compiled for potentiometric surface calculation was used in this analysis (Section 2.2), with data compiled from petroleum industry tests including DST, RFT, and FMT. For this exercise, pressure data was required to be described against a common height datum and so was converted to a Reduced Standing Water Level (RSWL) (m AHD) prior to analysis. The following scales and data-subsets were examined and compared to interpret the following:

- the entire data set from the Main Eromanga Aquifer Sequence for general spatial and temporal trends
- data from specific formations from within the Main Eromanga Aquifer Sequence to compare differences between aquifer and confining layers
- data from Individual wellfields to highlight the difference between local and regional gradient scales
- finally, data from the Main Eromanga Aquifer Sequence and the underlying Cooper Basin sediments to define the pressure relationship between the Main Eromanga Aquifer Sequence and the basement.

For the following section, we used freshwater head-corrected pressure data. As discussed earlier, the development of a potentiometric surface for use in modelling explored a range of assumptions with respect to how density correction may be applied to pressure data. Despite this analysis, the heterogeneous distribution of data points within the study area, and the complexity of the basin configuration and aquifer composition meant that a high degree of uncertainty remains with respect to determining either a single reference density, or multiple reference densities based on zones of similar hydrogeological characteristics with which to undertake density correction. By extension, the same uncertainties that impact derivation of a density-corrected potentiometric surface may also impact the following comparative review of pressure and elevation data in the Cooper Basin region. Therefore, the following section provides a relative comparison between pressure head readings with elevation via the use of a single density reference. This treatment is like that used to derive the density-corrected potentiometric surfaces described in the previous section and therefore is subject to similar limitations.

8.1 Petroleum well-derived pressure data

As described Chapter 4, Theory of density and flow, initial examination of the entire dataset shows, there is an overall proportional relationship between screen depth and formation pressure (Figure 8.1). This suggests that, from a regional standpoint, the formation pressure at a given screen elevation may be inferred. However, this relationship is more pronounced within the south-west corner of the Cooper Basin, with the relationship between these two variables less pronounced to the east.

Screen depth (m bgs) and formation pressure (in m head) are measured from the individual well head and therefore do not account for variations in land-surface elevation. For the interpretation of groundwater flow, such data requires correction to a common height datum to derive screen elevation and a reduced standing water level (RSWL) (m AHD). The migration direction of groundwater should become apparent when the density corrected RSWL is compared to the screen elevation. A proportional or inversely proportional relationship would indicate either downward or upward migration of groundwater, whereas if the screen elevation is independent of the corrected RSWL, lateral flow conditions are interpreted to predominate, or indeed the occurrence of localised flow cells within the larger dataset. When petroleum well-derived data from the Main Eromanga Aquifer Sequence is viewed in totality (Figure 8 2), a relationship between RSWL and screen elevation suggests a general downward vertical migration. Further, this downward gradient trend appears more pronounced within the south-western corner of the Cooper Basin. Specifically, RSWL data from the south-western corner is more likely to display a proportional relationship between pressure and elevation than elsewhere, with this relationship on average suggesting downward migration of groundwater.

This may be a function of areal drawdown caused by petroleum hydrocarbon production resulting in aquifer depressurisation or inherent hydrodynamics. In contrast, data from the eastern Cooper basin appears to display a more independent relationship between these two variables. However, we note that depressurisation because of petroleum hydrocarbon production is likely to be occurring in parts of the eastern Cooper Basin as well; this more independent relationship may be related to data density in this region compared to others, with fewer data points from which to interpret relationship trends.

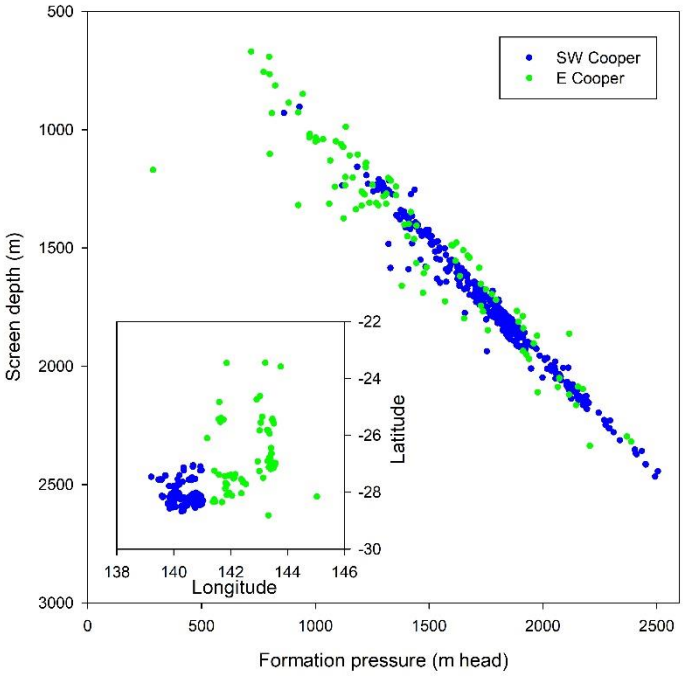

Figure 8.1: Formation pressure vs screen depth for petroleum wells in the Eromanga Basin units of the Cooper Basin region.

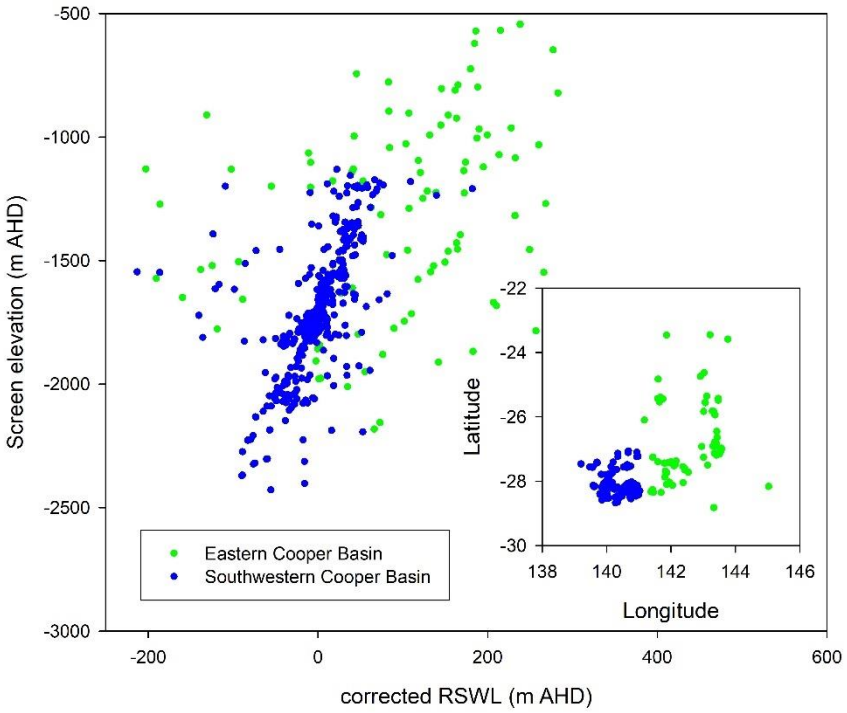

Figure 8.2: Density-corrected RSWL vs screen depth for petroleum wells in the Eromanga Basin units of the Cooper Basin

8.2 Aquifer and confining Units

To assess the likelihood of vertical migration, data from the aquifer and confining unit formations were isolated from one another and analysed separately. Further, analysing data from smaller scale subsets, either within sub-basinal areas, particular wellfields or even at the individual well scale can also provide insight.

Downward migration of groundwater within the Namur and Adori sandstone, which are major constituents of the J-K aquifer that make up Layer 3 in the model (Table 1.1), and the Hutton Sandstone, which is a major constituent of the Hutton-Poolowanna Aquifer or Layer 5, can be discerned within the south-western portion of the Cooper Basin (Figure 8 3 and Figure 8 4). However, there is a small gradient of about 0.1 for the Namur and Adori sandstones and about 0.2 for the Hutton Sandstone. Additionally, within an area further to the east, the Namur and Adori sandstones have a similar pressure versus elevation characteristic, with a gradient of about 0.2. Elsewhere, no definitive relationship was observable, potentially a consequence of insufficient data to define such a gradient, combined with variations in formation depth or indeed the predominance of lateral or localised flow conditions.

With respect to the confining units of the Murta (Layer 2), Westbourne, (minor component of Layer 3), Birkhead (Layer 4) and Poolowanna (component of Layer 5), a downward vertical migration is observed (Figure 8 5). The hydraulic gradient is relatively steep as may be expected for confining units, with a wide variation in RSWL with respect to given depth. Although a hydraulic gradient is observed, the proportional relationship this is based on is weak when compared to aquifer units. The coefficient of determination (r^2) value of linear trend-lines fitted through data from each confining unit varies from 0.04 (Birkhead Formation) to 0.5 (Murta Formation).

As before, such trends may be related to either depressurisation caused by petroleum hydrocarbon production resulting in aquifer depressurization or inherent hydrodynamics.

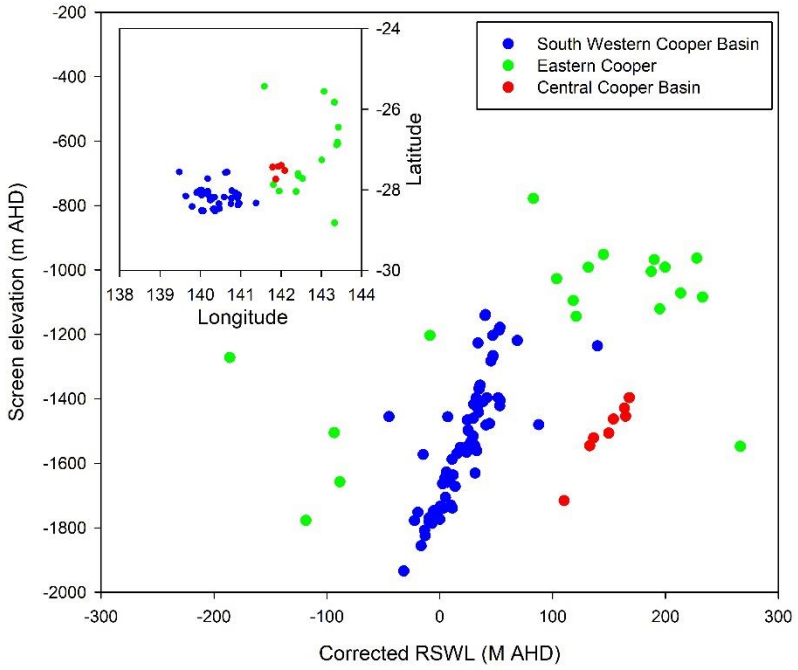

Figure 8.3: Namur and Adori Sandstone-derived RSWL measurements from Petroleum well derived test-work

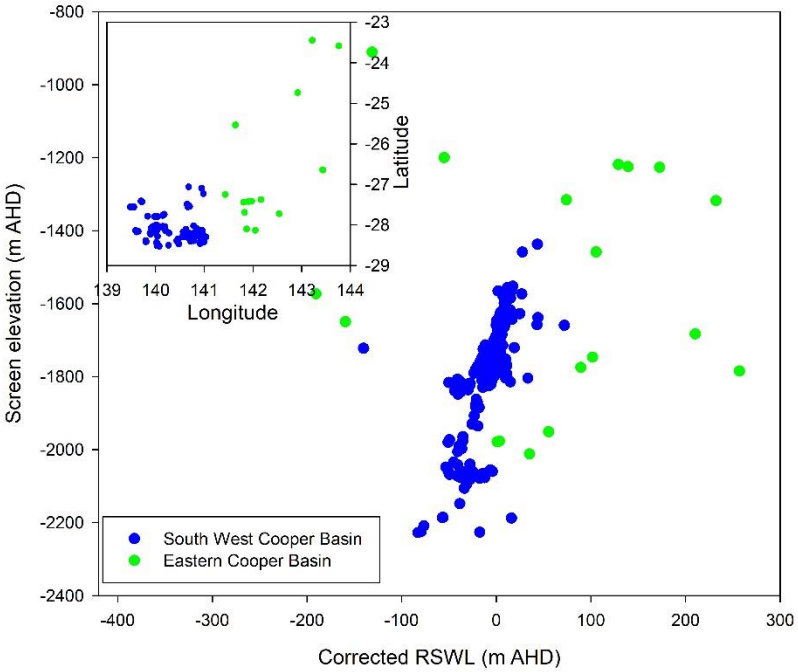

Figure 8.4: Hutton Sandstone-derived RSWL measurements from Petroleum well derived test work

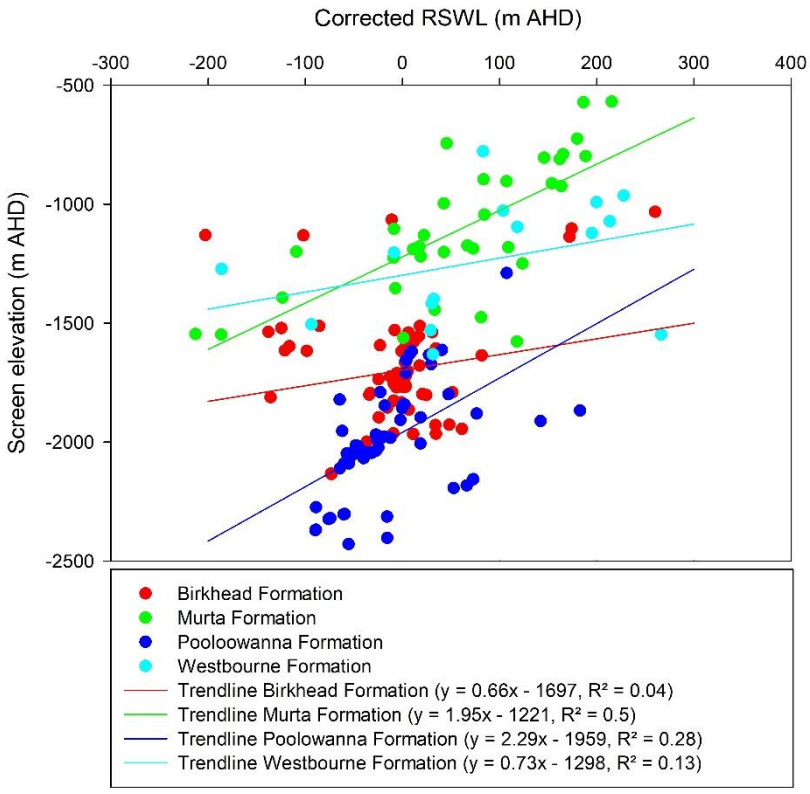

Figure 8.5: Birkhead, Murta, Poolowanna and Westbourne Formation-derived RSWL measurements from petroleum well derived test work

8.3 The wellfields scale

Many wells from the south-western corner of the Cooper Basin display a consistent trend between pressure and elevation through multiple formations, suggesting overall downward migration of groundwater. For example, wells within the Worrior Wellfield (Figure 8.6) display a reasonably consistent gradient of 0.1 and downward migration through pressure measurements from the Namur and Adori sandstones, through the Hutton Sandstone and into the Poolowanna Formation (Figure 8.7). This gradient is consistent with the regional gradient for the Namur, Adori, and Hutton sandstones for the south-western corner of the Cooper Basin.

Conversely, the gradient may change at a wellfield or even at a per-well scale. For example, within the Snatcher Wellfield (Figure 8.6), with pressures predominantly obtained from the Hutton Sandstone, a steeper gradient of 0.6 appears to exist between and within formations compared to the regional trend, although gradients are more in keeping with the regional trend if individual wells are examined (Figure 8.8). The wider Snatcher Wellfield trend may therefore reflect spatially localised or time-constrained drawdown within part of the wellfield. With respect to drawdown, we note that Snatcher 6 through to Snatcher 10 tests were undertaken in the latter half of 2013 and therefore lower corrected RSWLs may be a function of timing of drawdown impacts post completion of the wells Snatcher 1 though to Snatcher 5 (Figure 8.9).

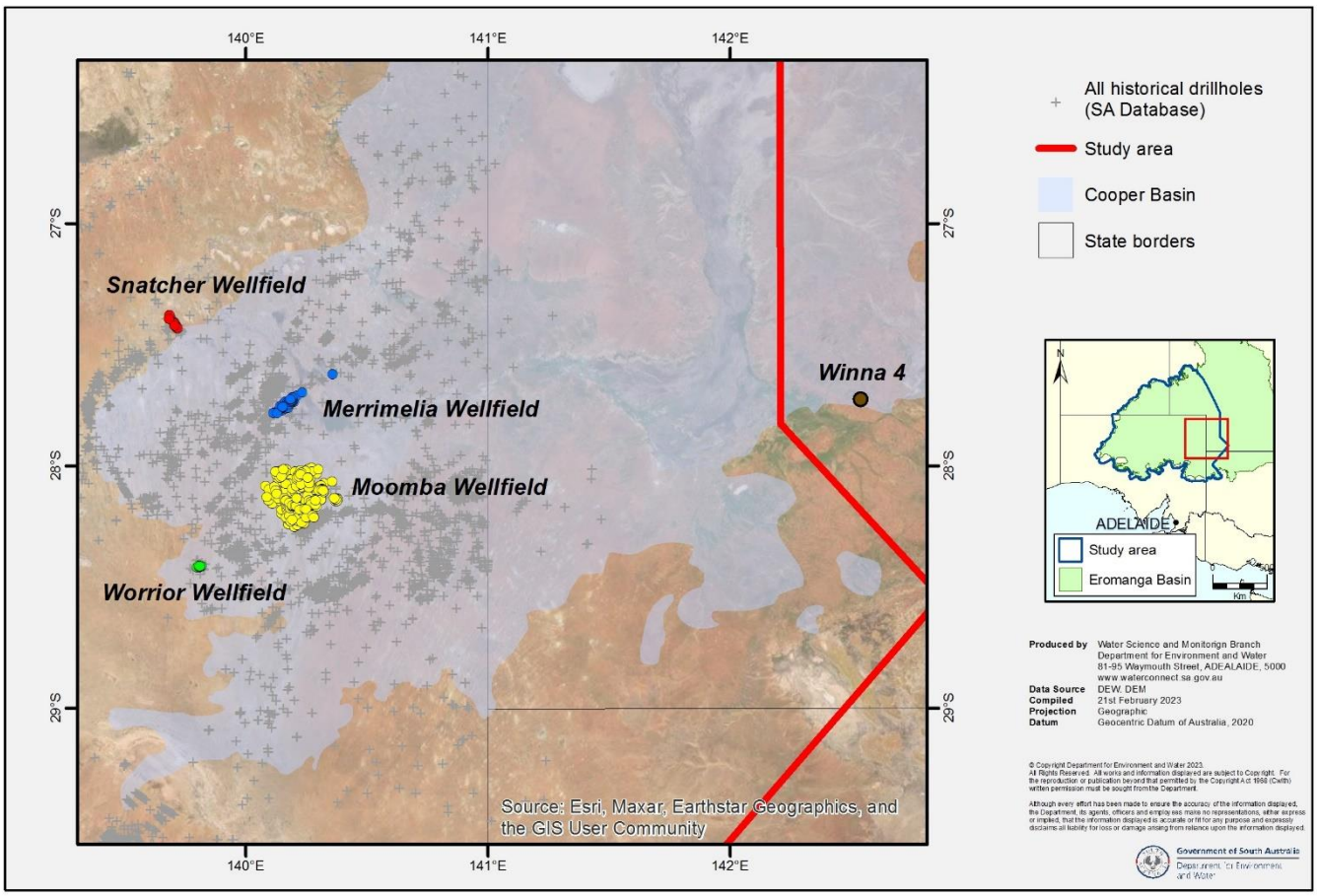

Figure 8.6: Location map for Worrior, Snatcher, Moomba, Merrimilia wellfields and Winna 4

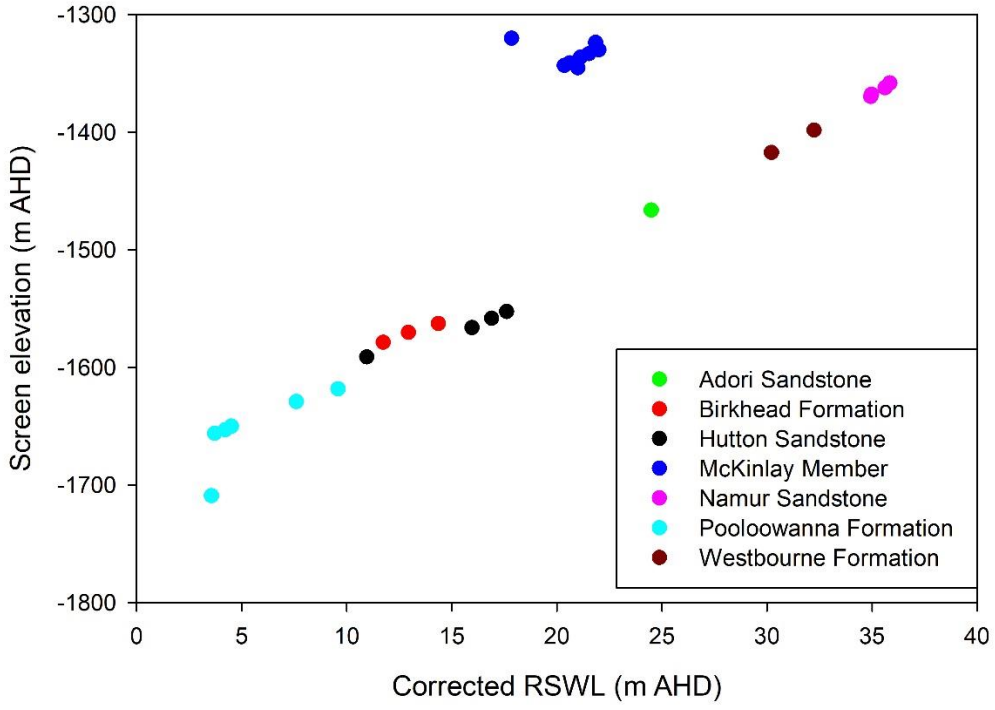

Figure 8.7: RSWL measurements from Worrior Wellfield

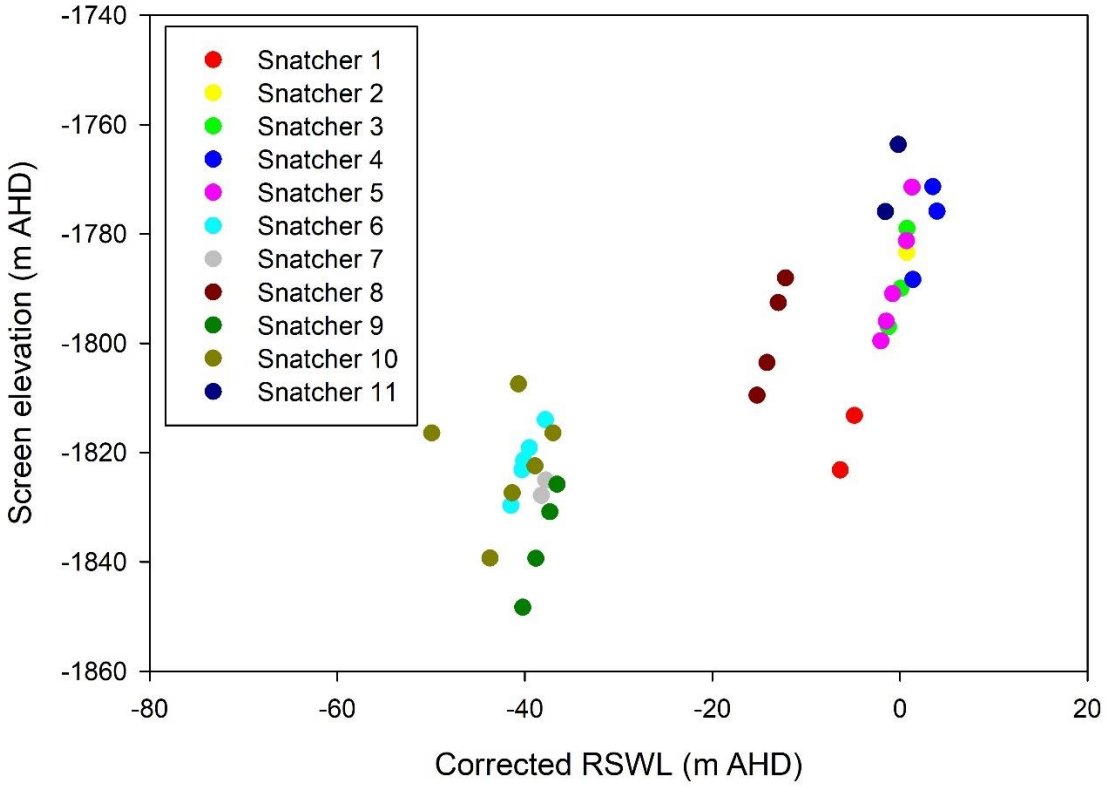

Figure 8.8: RSWL measurements from Snatcher Wellfield

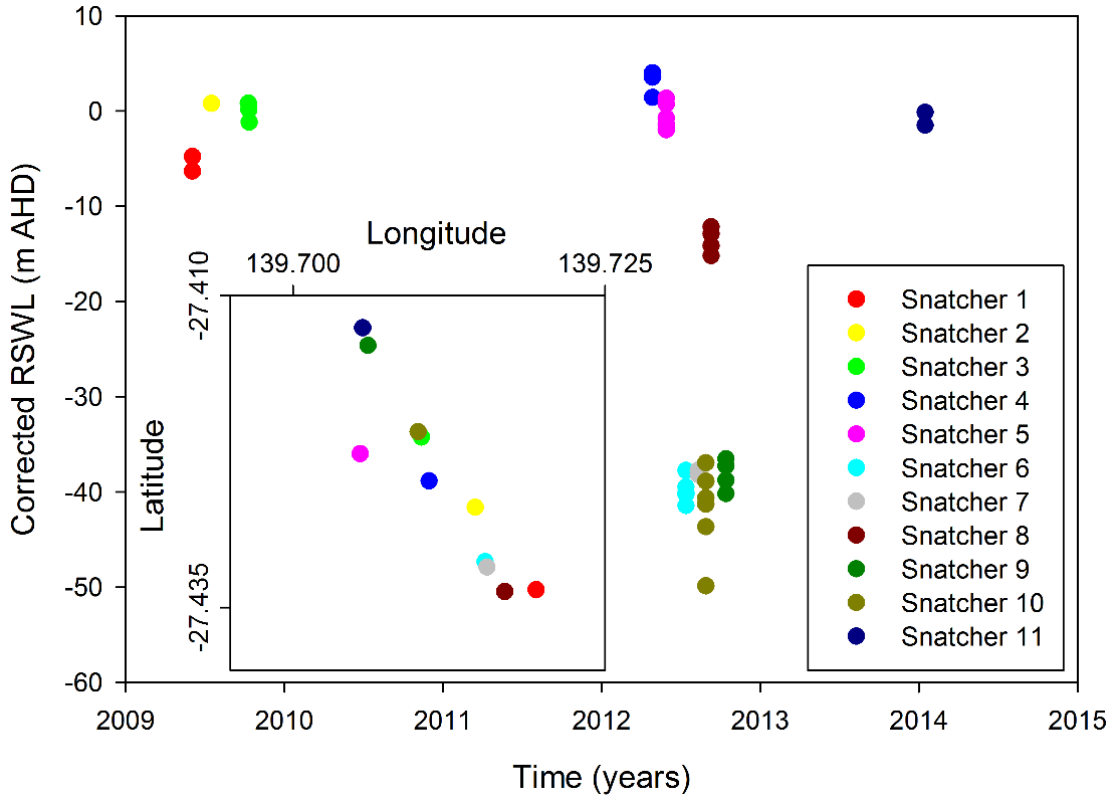

Figure 8.9: RSWL measurements from Snatcher Wellfield compared to time

A similar example to Snatcher can be found within the Merrimelia and Moomba Wellfields (Figure 8.6). Here, RSWL data appear to vary between 70 and 181 m over 3 depth ranges of approximately −1,570, −1,830 and −2,070 m AHD (Figure 8.10). Such steep gradients may reflect the influence of confining units associated with the Murta and Birkhead Formations, compartmentalisation within the Hutton Sandstone aquifer, McKinlay and Poolowanna Formations as well as the potential impacts of groundwater extraction.

With respect to well-scale variations in pressure, Winna 4 located within the Queensland portion of the Cooper Basin (Figure 8.6) provides a case in point (Figure 8 11). Pressure measurements were taken within the Murta Formation, and Namur and Adori Sandstones, Westbourne Formation and Hutton Sandstone. While RSWL measurements taken from the sandstone units appeared consistent and independent of depth, gradients were determinable within confining units or either side of a confining unit where aquifer measurements were available. From this data, there appears to be an upward gradient evident through the Murta Formation but downward gradients through the Westbourne and Birkhead Formations. We note that Winna-4 was originally drilled as an appraisal well targeting oil in the Murta Formation and therefore gradient trends may be related to petroleum hydrocarbon production.

Further, in a number of wells, the McKinlay Member displays notable differences in head when compared to the underlying Namur Sandstone. Although the gradient of change between pressure and depth are similar, there appears to be a consistently lower pressure. An example is provided from the Worrior Wellfield (Figure 8.7). During consultations, Beach Petroleum suggested this may be related to the lithological composition of the McKinlay Formation, with water within the upper-McKinlay Formation thought to be primarily contained within isolated sand lenses that are easily depleted.

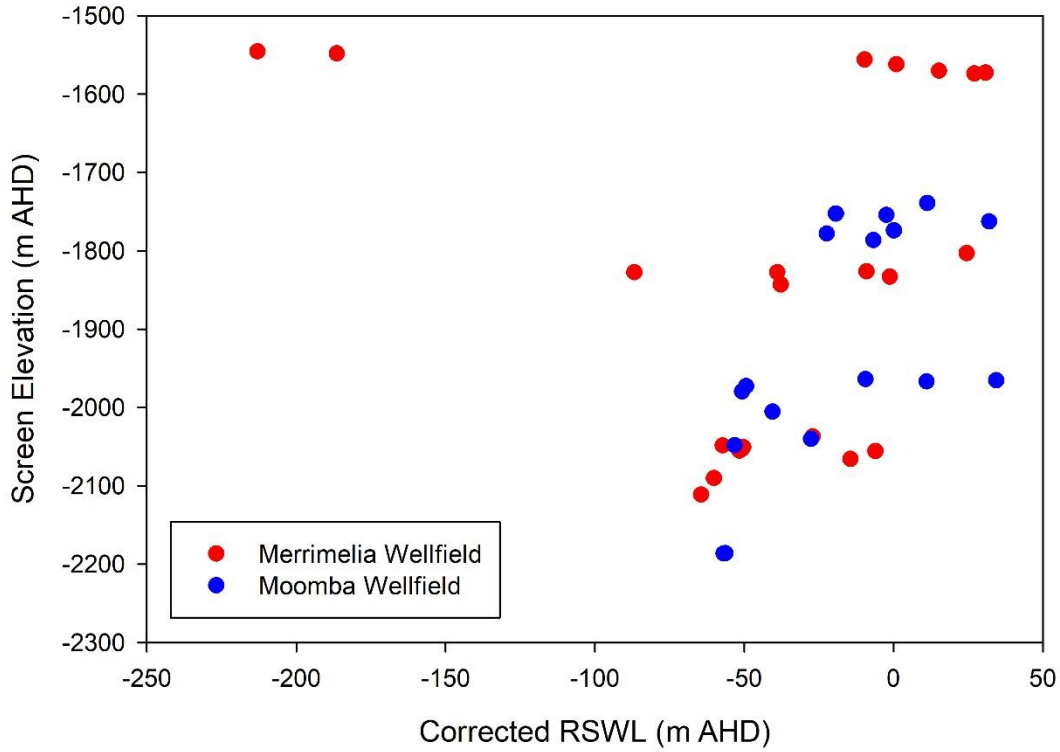

Figure 8.10: RSWL measurements from Merrimelia and Moomba wellfields

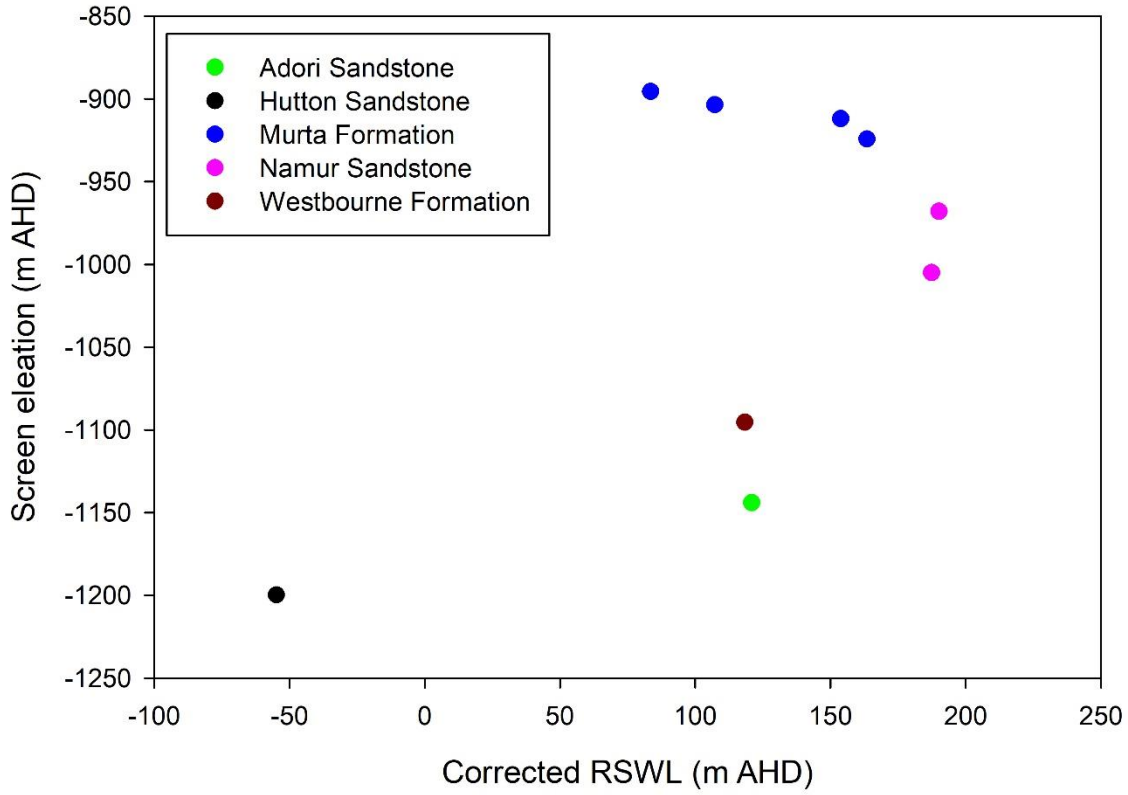

Figure 8.11: RSWL measurements from Winna 4

8.4 Comparison between the Cooper and Eromanga Basins

Finally, we made a broad comparison between pressure head measurements from the Cooper Basin with those from the Eromanga Basin to establish what the prevailing groundwater gradient might be between these two strata sequences. At a regional scale, there generally appears to be a continuation of the pressure to depth relationship established using Eromanga Basin measurements within the Cooper Basin (Figure 8.12). When corrected to a common datum, the bulk of Cooper and Eromanga measurements plot on a linear trend with a gradient of 0.15, like that observed for Hutton and Namur Sandstone aquifers. In addition to this general trend, the impact of petroleum-related groundwater extraction from the Cooper Basin is evident, with a notable number of measurements taken between 1980 and 2000 with lower-than-expected pressure heads. Notably, there are few concomitant results in the Eromanga Basin, although the few that exist require confirmation as to what may be causing this pressure decline considering the depressurisation evident in the Cooper Basin. With respect to conceptualisation, these data suggest the prevailing pressure condition is likely to be downward from the Eromanga to the Cooper Basin in both ambient and post-production circumstances, although the downward gradient evident is not particularly sharp.

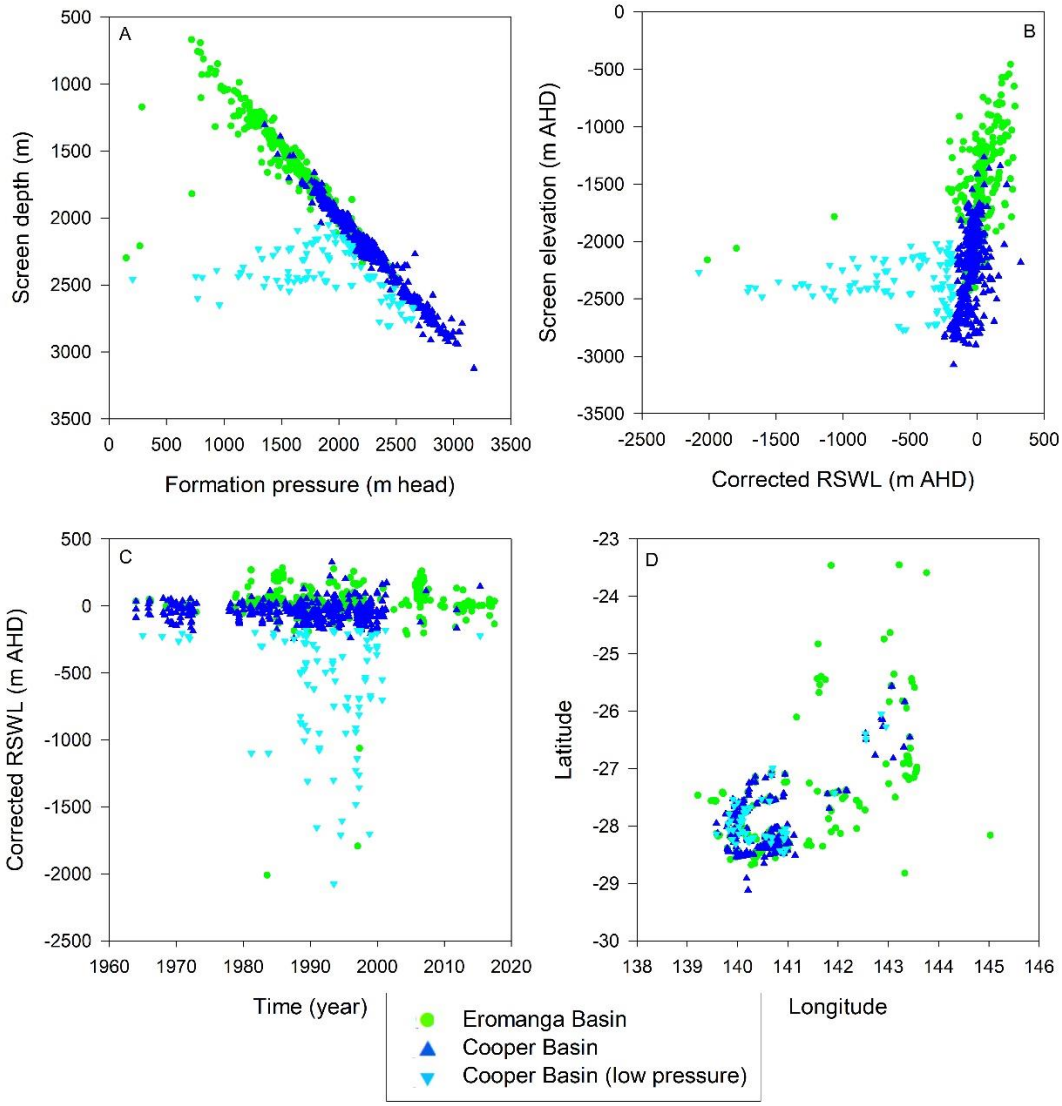

Figure 8.12: Comparison of pressure versus depth between Cooper and Eromanga Basin-derived measurements. A) Formation pressure (m head) versus screen depth (m), B) Corrected RSWL versus Screen elevation (m AHD), C) Corrected RSWL versus Time (years), D) Location of data points

8.5 Summary of pressure versus elevation data analysis

Overall, when RSWL measurements are compared to elevation, a predominantly downward gradient is observed. When considered against pressures found in the underlying Cooper Basin as well as other information, the predominant downward gradient, as well as the limited examples of upward gradient, may find causal explanation primarily in petroleum hydrocarbon extraction. Variations in trend related to either data availability or basin configuration appears evident. Further, variations in gradient are evident at a localised, wellfield scale. The general magnitude of the gradient appears reflective of the lithology of the formation from which measurement was taken, with sandstone formations displaying a lower gradient than finer-grained formations.

While the evidence for a vertical gradient may suggested vertical leakage, the predominant downward gradient in an area where artesian conditions exist indicate that at least in the Cooper Basin region, this leakage is predominantly outflow. Further, while evidence for vertical gradients may support the notion of free convection, the history of petroleum hydrocarbon extraction in the region makes using these pressure-to-elevation relationships difficult to ascribe in this case.

9 Data gaps and limitations

Through the process of data compilation, analysis and literature review, a number of critical data gaps were made apparent, both with respect to raw data as well as conceptual understanding. The following section provides a discussion of those data gaps considered important with respect to the development of a CHM and ultimately the numerical model construction.

9.1 Well distribution

Although J-K aquifer wells are numerous, they are not evenly distributed across the basin. For instance, within the central and eastern parts of the FNPWA, there is a relatively small number of wells supplying highly pressurised groundwater to multiple watering points. In contrast, near the margins of the GAB and particularly within the western J-K aquifer where sub-artesian and unconfined conditions prevail, there is a much larger number of wells, abstracting water either by pump or by using the much lower artesian pressures for single watering points. Further, there are large parts of the basin where there are no wells present, with the largest and most prominent area being between Kati Thanda-Lake Eyre and the Cooper Basin. This heterogeneity in well distribution creates uncertainty in all drilling-based geological and hydrogeological datasets and is an issue with no readily available solution.

This has rendered parts of the potentiometric surface reliant on very few data points in some areas. Unlike other data limitations there is currently little redress possible except that regular review of the potentiometric surface used for modelling should be undertaken to ensure it is up to date and uses all available information.

9.2 Data quality

Although a protocol for data validation that attempted to limit the use of poor-quality data being used in potentiometric surface generation was employed, there may be unresolved data quality issues impacting interpretation. These data quality issues include:

- lack of information on bore depth, completion depth, and formation in which a bore was completed
- lack of or inaccurate ground surface elevation data, or inaccurate spatial location of a bore
- inconsistent or poor pressure-head measurement methodology, including inadequate shut-in times, poorly calibrated instrumentation or undetected calibration 'drift' over time.

In some cases, data of limited verifiable quality was used because of data paucity. Such areas may be highlighted in future works as priority areas for monitoring assessment.

9.3 Temperature gradients and correcting water levels for density and non-isothermal flow

As discussed in Chapter 5, correction of aquifer pressure measurements to account for density assumes a linear temperature gradient between the screened interval and measurement point. Where aquifer pressure measurements are not accompanied by corresponding temperature measurements, the temperature gradient in the well cannot be ascertained. Where a bottom-hole temperature was not recorded for an individual well, the temperature was estimated using an approximate geothermal gradient for the GAB J-K aquifer across the study area derived from the available information. As the Cooper Basin region is a key area of the model, effort was made to collate formation temperature and pressure data from petroleum industry tests within the Eromanga Basin in SA and Qld and where unavailable, an estimate based on temperature gradient was made.

However, as described in Chapter 4, significant variations in thermal gradient (but not necessarily the flux) may occur between Mesozoic and Permo-Carboniferous units, driven by the insulator effects of significant coal measures found in the latter. Such variations are best described when a continuous temperature log for a given well is collected. Investigations by Energy Resources Division (Department for Energy and Mining) found that there are only 13 petroleum or geothermal wells in the Cooper and Eromanga basins that have continuous temperature logs. It appears that most or all of the petroleum-well data is production data from the Permian Patchawarra to Merrimelia zone, with no data recorded shallower than about 2,500 metres depth. The only wells that have data across the Eromanga interval are geothermal wells, and only 2 of the 7 known geothermal wells yielded data. However, these wells are all in the Nappamerri Trough area, which does not provide any regional insight. This identifies a data requirement of continuous temperature data from shut-in monitoring bores. Consequently, the lack of continuous temperature log data represents a data gap concerning variations in temperature gradient over the study area.

By extension, there is evidence to suggest that free convection may be occurring within deeper parts of the basin. This occurs where groundwater flow is governed by both the freshwater hydraulic head gradient and a buoyancy gradient (mixed convection). In those locations there are unanswered questions regarding the validity of Darcy's Law, the use of a potentiometric surface and the reliability of water balance and flow vector assessments. However, as detailed in Section 7, there are several uncertainties regarding the evidence for free convection:

- Much of the area indicated as being potentially subject to free convection is where data is sparse.
- The lithology of the aquifers is likely to be more heterogeneous than the assumptions used during interpretation.
- The impact of current extraction from the basin is unknown.

Undoubtedly, further work is still required to understand the impact on inferred groundwater-flow directions and rates when interpreting a regionally extensive potentiometric surface of the J-K aquifer.

In light of this uncertainty, it is worth remembering that a key principle in best practice modelling is the need for an optimum consideration on complexity (Barnett et al. 2012). In this case, there is limited time and budget to develop the model and run scenarios to investigate water management options. These constraints mean that isothermal modelling packages with relatively fast run times are required, rather than packages that use highly complex density- and temperature-coupled models that run much more slowly and ideally require more data.

Given these uncertainties and technical complexities, for the purposes of this model, free convection will be ignored and forced convection assumed across the study area. The adoption of gravity-driven (isothermal) flow assumptions may impose limitations in modelling interpretations similar to those when such assumptions are applied to the potentiometric surface. These limitations may be at least partly addressed through careful weighting of observations. For example, observations in central parts of the basin where the driving force ratios (DFR) suggest free convection could be assigned relatively low weights during the model calibration, given such observations are likely subject to substantial temperature-based density corrections and hence are likely to be subject to potentially significant measurement error. Assigning low weightings to this data would therefore recognise a) the inherent uncertainty in the readings and b) that a gravity-driven (isothermal) flow-based numerical model may not be able to match these observations. Longer term, this assumption will be revisited periodically as new data, scenarios and technology come to hand.

9.4 Sub regional groundwater flow systems

For this conceptual hydrogeological model, groundwater levels and pressures from the Cadna-owie Formation, Algebuckina Sandstone and lateral equivalents such as the Namur Sandstone and Adori Sandstone have been interpreted together, resulting in the using of a single potentiometric surface used to describe groundwater flow for the main J-K aquifer. Conceptually, this is considered acceptable because of the lateral stratigraphic continuity these units have across the study area.

However, at a sub-regional level, there may be lateral discontinuity caused by either structural deformation or lithological heterogeneity and consequently several discrete or semi-discrete groundwater flow systems may be present. To reveal the presence of such partitioned groundwater flow systems, applying a hydraulic stress to the aquifer and monitoring drawdown propagation in a monitoring well network is an excellent method (see for example, Bense and Person 2006) but this is easier to accomplish at smaller scales; at larger, more regional scales this may be difficult to accomplish. At larger scales, such groundwater flow systems may be indicated by differences in hydrochemistry, (see for example, Howe et al. 2008; Priestley et al. 2013); however, recent suggestions by Sandiford et al. (2020) concerning the influence of neotectonics in the region indicate that a limitation on hydrochemistry as a groundwater flow system mapping tool is that the deformation responsible for partitioning, or indeed, preferential flow, may be either ongoing or younger than the water molecules in the aquifer.

For the purposes of groundwater regulation and management, the concept that recharge areas in unconfined parts of a groundwater system are laterally connected to discharge areas in confined and artesian areas is useful to portray as it fosters a 'whole of groundwater system' approach to management. Further, in the absence of concrete evidence one way or the other, assuming lateral continuity across the basin is considered a conservative approach to take with respect to constructing a model for regulatory and management purposes. Finally, best practice modelling principles (Barnett et al. 2012) encouraged the development of an unbiased balance between model simplicity and complexity, noting that model predictions that integrate larger areas are often less uncertain because characterisation methods are well-suited to discern bulk properties.

Having said that, it is not unreasonable to describe this modelling approach as a traditional data-driven aquifer simulation methodology as distinct from an uncertainty-driven data assimilation and decision-support methodology (Doherty and Moore 2020; Middlemis and Peeters, 2019). Together, both approaches could cover a very extensive range of conceptualisation, parameterisation and simulation methods, consistent with best practice guiding principles to investigate uncertainty (Middlemis and Peeters, 2019).

10 Closing remarks, model assumptions and conclusions

A scientifically sound and density-corrected potentiometric surface is crucial to understanding and interpreting regional groundwater flow systems such as the Eromanga Basin where deep aquifer sequences involve high temperatures. Potentiometric surfaces were developed for the two main hydrostratigraphic unit or aquifer groupings within the Main Eromanga Aquifer Sequence.

The first and most extensive aquifer grouping is the Cadna-owie–Algebuckina–Adori–Namur Sandstone hydrostratigraphic unit (J-K aquifer), which describes groundwater flow in model Layer 1 (the Cadna–owie Formation) and Layer 3 (Namur–Algebuckina Sandstone aquifer). Although modelled as separate layers, for a large portion of the basin these two layers may be considered aquifers in high hydraulic communication with one another and therefore could be considered as a single aquifer unit. Collectively these units and layers are traditionally referred to in SA as the 'J-K aquifer'. Elsewhere, the Murta Formation confining unit (Layer 2) separates the Cadna-owie Formation from the underlying Namur Sandstone, and Kellett et al. (2012) have interpreted the Cadna-owie Formation as a leaky aquitard and therefore only pressure readings from the Namur–Algebuckina Sandstone Aquifer (Layer 3) have been used.

The other main aquifer grouping potentiometric surface interpreted was for the Hutton–Poolowanna hydrostratigraphic unit (Layer 5), which is laterally continuous with the J-K aquifer but is conceptually regarded sufficiently deep (hot) and hydraulically isolated by the overlying Birkhead Formation confining unit as to warrant separate treatment.

A total of 19 uncorrected and equivalent density-corrected potentiometric surfaces were generated. Key similarities between the potentiometric surfaces for the J-K aquifer include:

- a generally radial pattern, with inflows and recharge from the east, north, west and parts of the south, with flows toward discharge zones near the springs and along some of the southern margins
- steep hydraulic gradients along the west and north-western margins of the Eromanga Basin (for example, north and south of Marla)
- areas of inferred recharge from fractured rock aquifers along the southern area of the Peake and Denison Inliers and from the Northern Flinders Ranges
- a depression in the potentiometric surface occurs along the western flank of the Cooper Basin with drawdown due to co-produced extraction and pastoral water use
- a depression in the potentiometric surface adjacent to and north of Bedourie (Figure 1 1) due to drawdown
- areas of inferred discharge along the southern edge of the J-K aquifer south of Lake Frome, near Marree and to the south of Stuart Shelf and the Peake and Denison Inliers.

Based on observed similarities, the potentiometric surfaces could be grouped as:

- Group 1 infer groundwater inflow to SA from the NT, as well as via the northern and eastern border with Qld as shown by the steep hydraulic gradient along the eastern model boundary.
- Group 2 infer groundwater inflow into SA occurs from the NT and northern border with Qld. Groundwater inflow to SA along the eastern border with Qld is limited compared to other groupings.
- Group 3 infer groundwater inflow to SA occurs from the NT, as well as via the northern and eastern border with Qld. Groundwater flow from Qld along the eastern model boundary occurs along a lower hydraulic gradient compared to Group 1. Groundwater inflow to SA occurs along the border with NSW.

- Group 4 infer groundwater inflow to SA occurs from the NT, as well as via the northern and eastern border with Qld as shown by the steep hydraulic gradient along the eastern model boundary.

Density correction to all valid hydraulic head measurements from the J-K aquifer were undertaken using the areal mean reference density of 997.2 kg/m^3. This mean density was estimated for groundwater within the J-K aquifer that was coincident with the GAB springs. A reference density was used in preference to a freshwater density correction (999 kg/m^3) due to the potential for buoyancy forces acting on groundwater flow.

These potentiometric surfaces were used to describe the extent of artesian and non-artesian conditions, saturated and confined aquifer conditions, generally found within the J-K aquifer within the study area. Between the four groupings, in most areas there are only subtle differences (<100 m) between the extent of artesian, confined unsaturated and dry extents.

For the purposes of choosing an initial condition for modelling, a representative surface from Group 3 was chosen as this group displayed the best combination of conceptual correctness, a conservative approach and simplicity.

Group 2 is the 'primary alternative' to Group 3. Group 2 was selected because it is the group of surfaces that show the least flow from the east and therefore differ the most from the primary conceptualisation, in that it shows only limited inflows into SA from the eastern border with Qld, with most flow coming from the north.

DFR analysis suggests that between 40 and 50% of the study area may be influenced by mixed convection processes (and possibly free convection), predominantly in the deeper parts of the Eromanga Basin and encompassing the Cooper Basin region. Therefore, an isothermal assumption and potentiometric surfaces in such areas may be inaccurate. However, and most importantly, key management zones around artesian springs are not interpreted to be impacted by free convection and therefore the generated potentiometric surfaces are still considered useful for the purposes of this study.

Separate uncorrected and corrected potentiometric surfaces for the Hutton–Poolowanna aquifer were generated. Potentiometric surface contours for the Hutton–Poolowanna aquifer show a general inflow into the study area from the east (Figure 1C).

Pressure versus elevation data collected from petroleum wells in the Cooper Basin region generally indicate downward groundwater flow. The gradient is less steep in aquifer units than confining units, likely due to the hydraulic conductivity. Flow is also influenced by local basin configuration and pumping, which can lead to difficulty in interpreting a single gradient when data is corrected to a common height datum. The general downward migration may be naturally occurring; however, it may also be related to depressurisation caused by petroleum hydrocarbon production. The case for depressurisation is strengthened by data from the underlying Cooper Basin, which show greater downward flow when compared to results from the overlying Eromanga Basin strata.

A number of data gaps, limitations and uncertainties became apparent during the development of the potentiometric surfaces. In brief, these included 1) the heterogeneous distribution of wells, 2) unresolved or undetected data quality issues, 3) uncertainty with respect to the linear temperature gradient assumption used to correct for density effects, and 4) the impact undefined sub-regional groundwater flow systems may have on modelling and interpretation. However, despite such uncertainties, the approach adopted here to develop initial potentiometric surface inputs for a numerical model with regulatory and management purposes is considered a conservative approach. Further, the approach taken is also considered one that follows best-practice modelling principles (Barnett et al. 2012) by following development of an unbiased balance between model simplicity and complexity, noting that model predictions that integrate larger areas are often less uncertain because characterisation methods are well-suited to discern bulk properties.

11 Appendices

A. Exploration of gridding methodology used to develop the potentiometric surface

11.1 Comparison of initial gridding outputs from two software packages

Initial gridding was performed using the Minimum Curvature algorithm in *Surfer*™ (Golden Software) with Boundary Tension set to 1.0 to limit curvature of the potentiometric surface at the edge of the grid geometry. The grid geometry was set to Longitude (132.0E, 143.5E) and Latitude (31.5S, 22.0S) with a cell size set to approximate 100 m x 100 m. The final grid file was clipped to the extent of the J-K aquifer within the study area and contoured at intervals of 10 metres above Australian Height Datum (m AHD).

The rationale for using Minimum Curvature was to ensure consistency with the potentiometric surface generated by Sampson et al. (2013). Sampson et al. (2013) used Minimum Curvature in the *Petrosys*™ (Petrosys®) gridding package with estimation type 'slope' (1st order Taylor series polynomial) and 'bicubic' interpolation options selected. The 2019 dataset was subsequently gridded using *Petrosys*™ and the options applied by Sampson et al. (2013) to verify that any change in the interpreted potentiometric surface was a result of changes to hydraulic head data, not interpolation of the dataset. A comparison of grids generated by *Surfer*™ and *Petrosys*™, however, highlighted significant differences including:

- up to ±40 m difference in the interpolated surfaces in areas with no data
- greater than ±0.2 m difference in the interpolated artesian head calculated at approximately 75% of springs (important because spring flows can be dependent on quite small artesian aquifer pressures)
- greater than ±0.5 m difference in the interpolated artesian head calculated at approximately 25% of springs.

Inconsistencies between the two potentiometric surfaces generated using Minimum Curvature in *Surfer*™ and *Petrosys*™ established the need to develop a more rigorous procedure for generating the 2019 J-K aquifer potentiometric surface. Subsequently, additional gridding and contouring was undertaken using *Petrosys*™, *Surfer*™ and *ArcMap*™.

The 2019 dataset was then gridded and contoured using *Surfer's GridData_Comparison* script to provide a preliminary review and comparison of available methods (Figure 11.1). Several alternative gridding algorithms were tested and rejected including Natural Neighbour, Triangulation with Linear Interpolation, Radial Basis Function, Modified Shepard's Method and Nearest Neighbour.

11.2 Exploring different gridding algorithms

11.2.1 Surfer™

Minimum Curvature

Minimum Curvature generates smooth surfaces and is often used for groundwater applications. In producing a smoothed surface, not all data points are honoured exactly. Internal Tension and Boundary Tension options are used to control the amount of curvature between data points, which then dictate how effectively the surface honours the data. Both the Internal Tension and Boundary Tension have a range between zero and 1. When tension is set to zero, a modified biharmonic differential equation is solved; whereas when tension is set to 1, the Laplacian differential equation is solved. Higher tension values limit curvature between data, but the resulting surface does not necessarily honour the data points exactly. Lower tension values provide more exact honouring of data points, but the resulting surface may produce local extremes outside of the expected data range.

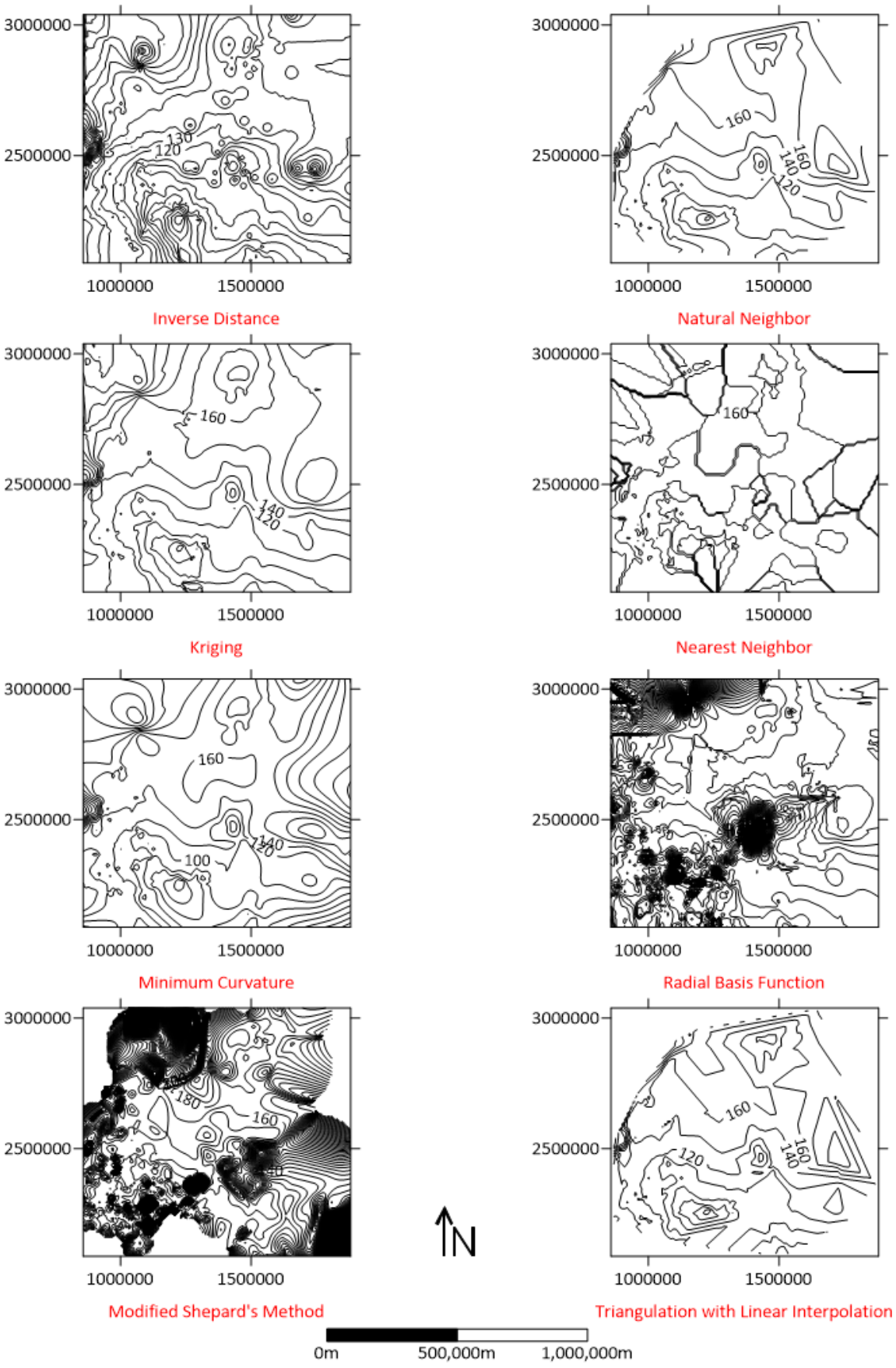

Figure 11.1: Comparison of typical gridding methods using *Surfer's 'GridData_Comparison'* script (Datum: GDA94 SA Lamberts; Contours at: 20 m AHD intervals)

A total of seven different Internal Tension (IT) and Boundary Tension (BT) combinations were tested. These included:

1. IT = 0, BT = 0
2. IT = 0, BT = 1
3. IT = 1, BT = 0
4. IT = 1, BT = 1
5. IT = 0.25, BT = 0.75
6. IT = 0.5, BT = 0.5
7. IT = 0.75, BT = 0.25

Default values for the maximum number of iterations (10,000) and relaxation factor (1) were used. The default maximum residual is calculated in *Surfer*™ by dividing the difference between the minimum and maximum data values by 1,000. In this case, the maximum residual was calculated to be 0.31. To enable grid convergence for the IT = 0, BT = 0 grids at 100 m x 100 m and 50 m x 50 m cell sizes, the maximum residual was increased to 0.62 and 0.93 respectively.

Kriging

Kriging is a geostatistical gridding method that can produce accurate grids of the data using an appropriate variogram model. Multiple theoretical variograms were fitted to the experimental variogram. For each theoretical variogram, two grids were generated with 1,000 m x 1,000 m cell sizes by setting the search criteria to a) 'no search', which uses all available data, and b) 16 sectors. The following theoretical variograms provided acceptable fits to at least part of the experimental variogram:

- Wave
- Rational Quadratic
- Gaussian
- Cubic.

Figure 11.2 illustrates the Wave, Rational Quadratic, Gaussian and Cubic theoretical variograms from the penultimate data set. Surfaces generated using the Wave, Rational Quadratic, Gaussian and Cubic theoretical variograms generated potentiometric contours that did not align with the current conceptual understanding of groundwater flow in the J-K aquifer in SA and were not used further (discussed later).

Although the following theoretical variograms provided fewer desirable fits to the experimental variogram, the potentiometric surfaces generated using these variograms did resemble components of the current conceptual understanding of groundwater flow in the J-K aquifer in SA:

- Spherical
- Exponential
- Linear.

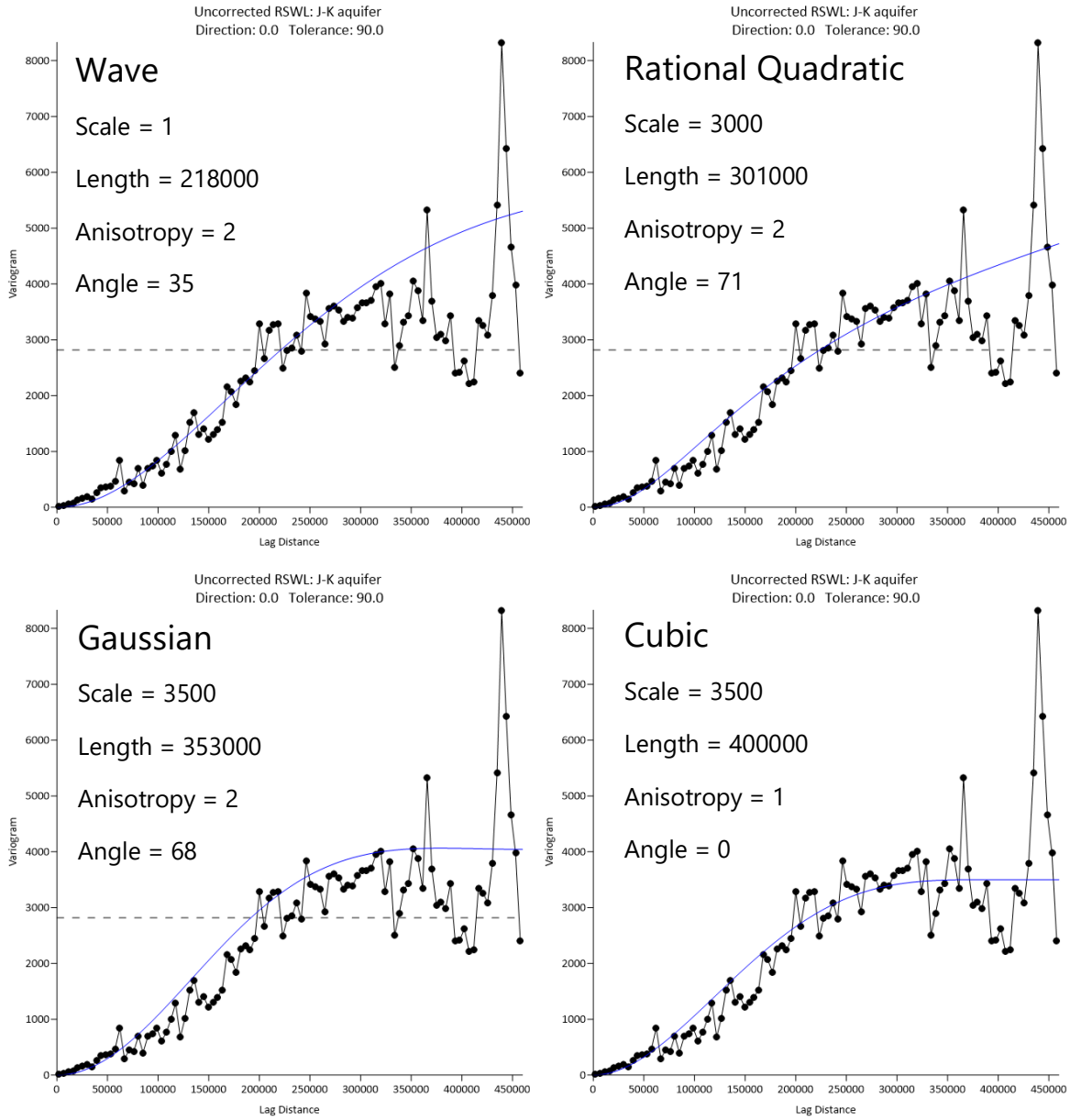

Figure 11.2: Initial *Surfer*™ variograms

Spherical, Exponential and Linear variograms generated from the final data set are provided in Figure 11.3. For brevity, the Spherical, Exponential and Linear variograms generated from the penultimate data set are not provided as these were updated as part of the final gridding and contouring sequence. The scale, length, anisotropy, angle and slope (Linear variogram only) are also shown for each theoretical variogram.

Limiting the search criteria (16 sectors) generated gridding artefacts and was not implemented for the smaller grid cell sizes.

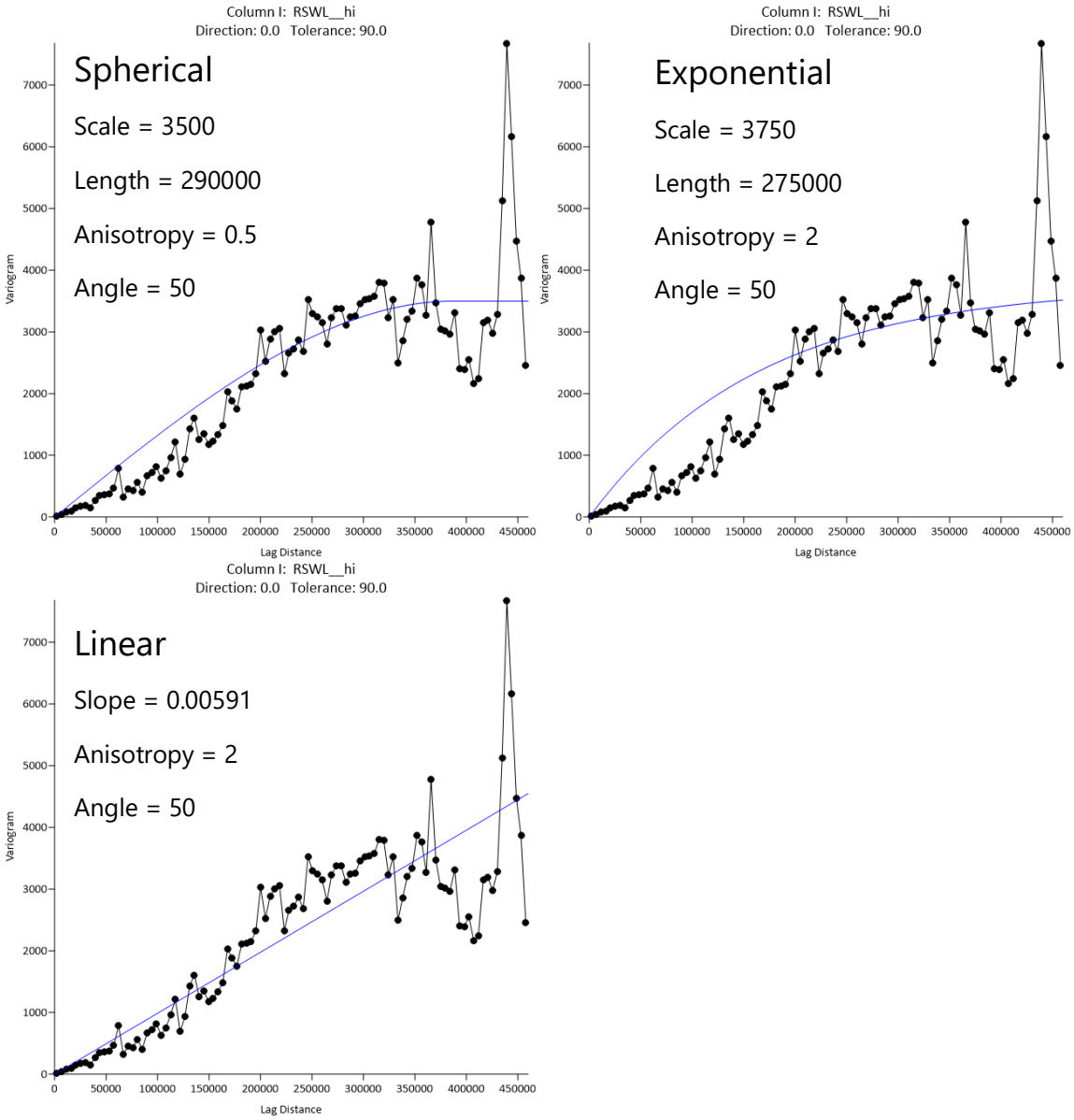

Figure 11.3: Final *Surfer*™ Variograms

Inverse Distance to a Power

The Inverse Distance to a Power algorithm weights data points so that the influence of neighbouring data points decreases with distance. Adjusting the weighting power specifies how quickly the influence weighting of data points at distance reduces such that higher weighting powers generate grid values closer to the value of the nearest data point (that is, honour the data points more closely).

Weighting powers of 2, 3 and 4 were generated at 1,000 m x 1,000 m cell size grids for two search criteria settings: a) 'no search' and b) 16 sectors.

11.2.2 Petrosys™

Minimum Curvature

Petrosys™ applies tension in the Minimum Curvature algorithm. This may more precisely honour data points, but the resulting surface can produce local extremes outside of the expected data range.

Petrosys™ uses two 'estimation' types to approximate integrals 1) slope and 2) slope + curvature, which use 1st order and 2nd order Taylor series polynomials, respectively. *Petrosys*™ also uses an Interpolation method to determine how intermediate values between known data points are calculated. The two options are bicubic and bilinear. Bicubic interpolation uses slope information to generate a smoother grid, while bilinear uses a linear relationship between data points. For larger cell sizes, the bilinear interpolation method may produce more angular surfaces; however, as cell size reduces, the difference diminishes between grids generated using bicubic and bilinear interpolation.

Minimum Curvature surfaces were generated for all combinations of estimation type and interpolation method from 10,000 m x 10,000 m to 100 m x 100 m cell sizes and repeated for the second gridding extent for 5,000 m x 5,000 m to 100 m x 100 m cell sizes.

Hybrid

The Hybrid method is typically used for datasets with highly fault-controlled surfaces owing to the use of first order Least Squares at the location of faults and Minimum Curvature elsewhere. As discussed previously, no faults were incorporated into the development of the 2019 potentiometric surfaces; however, Hybrid surfaces were generated for completeness. Only the slope (1st order Taylor series polynomial) estimation type was used.

Hybrid method surfaces were generated at 1,000 m x 1,000 m cell size grids for both the bicubic and bilinear interpolation methods.

Polynomial

Petrosys™ Polynomial method fits a 3rd order polynomial to the data points. Again, only the slope (1st order Taylor series polynomial) estimation type was used. One polynomial method surface was generated at 1,000 m x 1,000 m cell size using the bilinear interpolation method.

Least Squares

Two Least Squares methods are available in *Petrosys*™ 1) Least Squares Binomial and 2) Least Squares Plane. Least Squares Binomial fits an exponential function to the data points, whereas Least Squares Plane fits a plane through the data points. In both cases, the slope (1st order Taylor series polynomial) estimation type was used; and surfaces were generated at 1,000 m x 1,000 m cell size using the bilinear interpolation method.

Distance Weighted Average

The Distance Weighted Average method tends to smooth out local highs and/or lows. A weight is assigned to each value that is inversely proportional to the square of the distance of the data point to the grid cell; and all data points near a grid cell are used to estimate the grid cell value. The slope (1st order Taylor series polynomial) estimation type was used; and surfaces were generated at 1 ,000 m x 1,000 m cell size using both the bicubic and bilinear interpolation method.

11.2.3 ArcMap™

Spline

Spline is a two-dimensional Minimum Curvature algorithm with two interpolation options:
1) Regularised and 2) Tension. The Regularized option generates smooth surfaces but may produce local extremes outside of the expected data range – similar to zero internal and boundary tensions in *Surfer*™. The Tension option generates less-smooth surfaces with data constrained by the available data range – similar to internal and boundary tensions being applied in *Surfer*™. Surfaces were

generated at 100 m x 100 m cell size for both the Regularized and Tension options using the default Weight parameter.

Kriging

Based on the results of Kriging using *Surfer*™, only the Linear, Spherical and Exponential theoretical variograms were used to generate Kriging surfaces in *ArcMap*™. Variogram parameters applied in *Surfer*™ were also applied in *ArcMap*™. Surfaces were generated at 100 m x 100 m cell size for all 3 variograms.

Inverse Distance Weighting

Like the Distance Weighted Average method in *Petrosys*™ and Inverse Distance to a Power method in Surfer™, Inverse Distance Weighting interpolates cell values based on linearly weighted data points with weights a function of inverse distance. The default value of '2' was used for the Power parameter to generate a single surface at 100 m x 100 m cell size.

11.3 Penultimate sequence of gridding and contouring

One hundred and twenty eight (128) uncorrected potentiometric surfaces were generated in *Petrosys*™, *Surfer*™ and *ArcMap*™ exploring different gridding algorithms, options within each gridding algorithm, cell size and origin of the grid to determine:

1. the potentiometric surfaces that best reflect the current conceptual understanding of groundwater flow in the J-K aquifer in SA based on visual inspection of the potentiometric surfaces in comparison with previously published literature (Sampson et al. 2013; Smerdon et al. 2012; Ransley et al. 2015). This included:
    a. smooth potentiometric contours
    b. groundwater flow from the western margin of the study area in SA towards Oodnadatta and the transition and saturated groundwater discharge zone found near springs as described by Costelloe et al. (2012) located south of the Peake and Denison Inliers (Figure 3.1)
    c. a regional groundwater divide occurring in the central portion of the western GAB extending from the northern rivers in the NT to the Kati Thanda-Lake Eyre/Maree region (Figure 3.1)
    d. groundwater flow towards spring discharge features near the southern margin of the Eromanga Basin (Figure 3.1)
    e. a groundwater depression along the western flank of the Cooper Basin area (Figure 3.1)
    f. a groundwater depression in the northern portion of the mapped area in Qld (Figure 3.1)
2. gradients indicating groundwater flow from Qld and NSW into SA (Figure 3.1), giving:
    a. the potentiometric surfaces that best match the measured water level data, determined statistically as the percentage of back interpolated raster values within ±1 m and ±0.5 m of the measured hydraulic head value at each well (refer to next section)
    b. the potentiometric surfaces that represent artesian conditions at all mapped spring locations.

The first gridding extent was set to match hydrostratigraphic mapping of the top of the Cadna-owie formation or 'C Horizon', which is typically regarded as the top of the Main Eromanga Aquifer Sequence, as well as the nominal top of the J-K aquifer by DEM. Using a GDA 94 SA Lamberts co-ordinate system, the gridding extent had eastings of 675,000 mE and 1,905,000 mE and northings of 1,980,000 mN and 3,130,000 mN. A second mapping extent only covered the extent of well locations used in generating the 2019 potentiometric surfaces had eastings of 855,000 mE and 1,885,000 mE and northings of 2,085,000 mN and 3,040,000 mN.

A range of grid sizes including 10,000 m x 10,000 m, 5,000 m x 5,000 m, 2,000 m x 2,000 m, 1,000 m x 1,000 m, 500 m x 500 m, 250 m x 250 m, 100 m x 100 m and 50 m x 50 m were tested in order to compare gridding run times against the best match to measured water level and representation of artesian conditions at mapped spring locations.

Well coordinates and subsequent gridding was undertaken using the spatial reference system GDA94 SA Lamberts to ensure consistency with, and a gridding precision between, the potentiometric surfaces and the updated stratigraphic surfaces, the development of which is described in *Volume 2: Hydrogeological Framework*.

11.4 Back interpolation results

Back interpolation refers to a process of extracting the interpolated water elevation (or pressure head) value from each generated potentiometric surface at each input data point and spring location and comparing this to the measured value used to generate the potentiometric surface. This enables:

- assessment of how effectively each algorithm was at generating a surface that fits the well data
- assessment of the adequacy of each algorithm at estimating artesian conditions where GAB springs are known to have permanent flow.

For consistency, the back-interpolation procedure was undertaken in *ArcMap*™ for all grids using the 'Extract Multi Values to Points' spatial analyst tool with the 'bilinear interpolation of values at point locations' check box ticked to calculate the interpolated value at the data point rather than providing the raster cell value.

All 128 gridded surfaces were back interpolated against the well locations (841 wells). Fifty-five of the 128 gridded surfaces produced at least 90% of the extrapolated raster values within ±1 m of the measured hydraulic head value at each well (Appendix B, Table 11.1). The better performing algorithms, in terms of matching well data, were typically Minimum Curvature with no internal tension, and improvements to fitting the well data were achieved with decreasing grid cell size. Grids generated using Minimum Curvature also provided potentiometric surfaces that resembled the current conceptual understanding of groundwater flow. As an example, Figure 11.4A illustrates the expected features including the direction of groundwater flow, location of regional groundwater divides and groundwater depressions from a *Surfer*™ generated potentiometric surface using Minimum Curvature with no internal or boundary tension.

In all 128 cases, back interpolation at springs listed in the SA Geodata GAB spring project groups (5,129 springs, 27 March 2020), using an initial assumption that all GAB springs were not extinct, gave at least some values below the elevation of the spring indicating a poor match to artesian conditions at these spring locations. However, in 83 of the 128 gridded surfaces, there were less than 2% of the back interpolated values (at springs) below each spring elevation. Again, as with the fit-to-well data, improvements to fitting artesian conditions at spring locations were typically achieved with decreasing grid cell size. However, in contrast to the back interpolation of well locations, the Minimum Curvature grids with internal tension provided a lower number of locations with non-artesian conditions at known spring locations compared to Minimum Curvature grids with no internal tension.

Kriging and Inverse Distance Weight surfaces generated in *ArcMap*™ (at 100 m x 100 m cells) provided more than 95% of extrapolated raster values within ±1 m of the measured hydraulic head value at each well, and less than 2% of the gridded surface below each spring elevation. However, these algorithms depicted non-smooth, angular potentiometric contours that did not resemble the conceptual understanding of groundwater flow in the J-K aquifer in SA. Both of the *ArcMap*™ spline gridding options (tension and regularised) provided poor matches against the well-data (less than 86% within ±1 m of the measured hydraulic head value at each well) and poor representation of artesian conditions at spring locations (more than 13% of the gridded surface below each spring elevation).

Petrosys™ did not generate any grids using the Kriging algorithm that presented smooth potentiometric contours. In *Surfer*™ the theoretical variograms that best fit the well data included Wave, Rational Quadratic, Gaussian and Cubic. However, each of these produced local data extremes and anisotropic potentiometric contours that did not resemble the current conceptual understanding of groundwater flow conditions; and/or provided a poor fit to the well and spring data (1,000 m x 1,000 m cell size). As an example, Figure 11.4B and C illustrate potentiometric surfaces generated using the Rational Quadratic variogram in *Surfer*™, setting the search criteria to 16 sectors (Figure 11.4B) and setting the search criteria to 'no search', which uses all available data (Figure 11.4C). Limiting the search criteria (16 sectors) generated gridding artefacts, while both Rational Quadratic surfaces generated local data extremes and groundwater flow patterns that did not resemble the current conceptual understanding of groundwater flow direction, location of regional groundwater divides and groundwater depressions.

Grids generated using the Linear, Spherical and Exponential theoretical variograms in *Surfer*™ were less desirable in terms of fitting the experimental variogram, although they generated more realistic potentiometric contours (compared to the Wave, Rational Quadratic, Gaussian and Cubic Kriging surfaces) and back interpolation fitted to the well and spring data.

Gridding using Inverse Distance to Power was tested using the power of 2, 3 and 4 in *Surfer*™ at 1,000 m x 1,000 m cell size. Although generating the lowest percentage of spring locations where the gridded surface was below each spring elevation (0.5%, Inverse Distance to Power 2), all Inverse Distance to Power surfaces produced multiple bullseyes and groundwater divides that did not resemble the current conceptual understanding of groundwater flow in the J-K aquifer in SA. For example, Figure 11.4D illustrates a potentiometric surface generated using the Inverse Distance to a Power algorithm with the power set to 4.

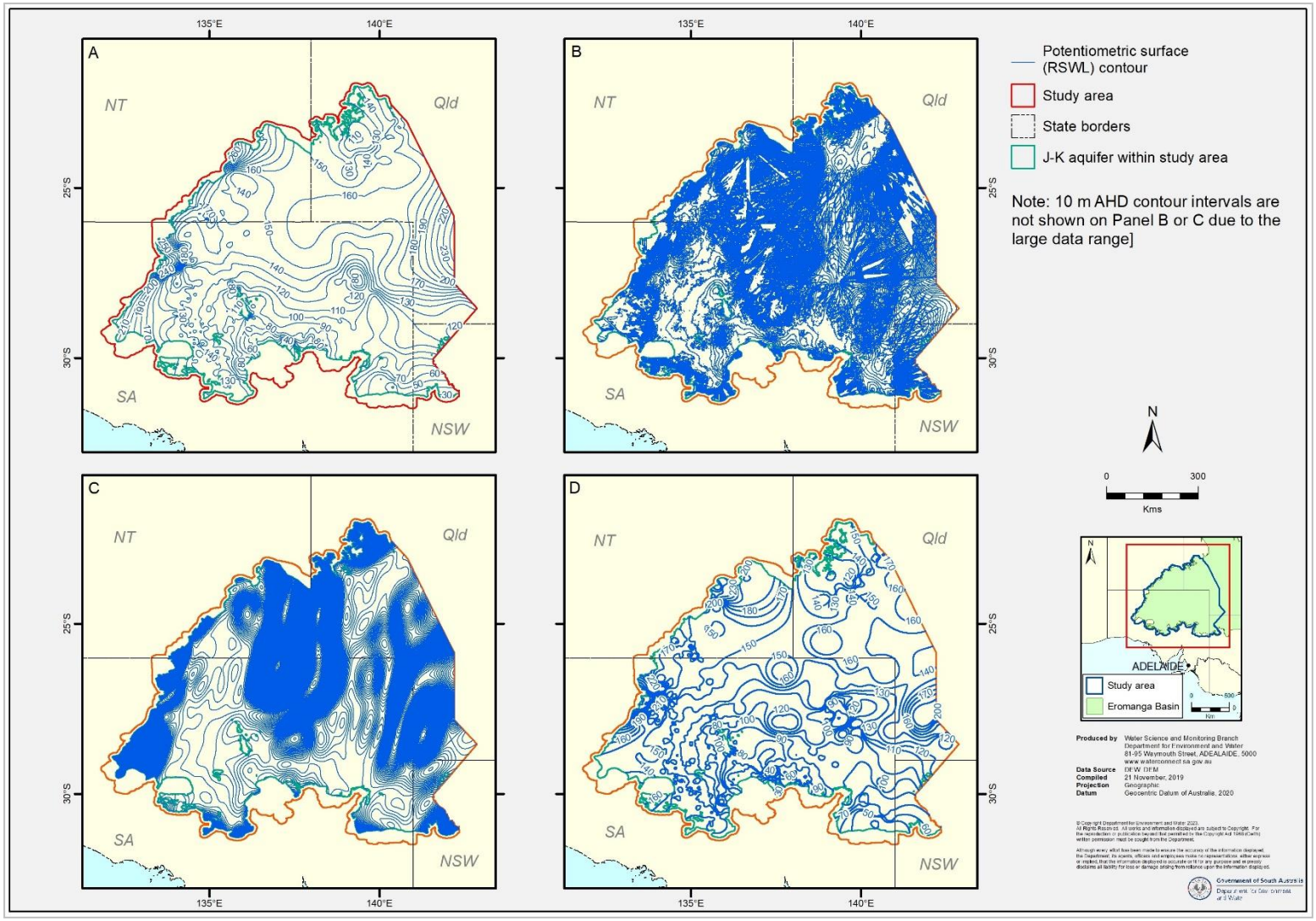

Figure 11.4: Example of an acceptable potentiometric surface (A) and those excluded from further analysis (B, C, D) [10 m AHD contour intervals are not shown on Panel B or C due to the large data range]

Petrosys™ was used to grid the data set within a second mapping extent only using variants of the Minimum Curvature algorithm. The second mapping extent covered the limits of the well locations only, thus a reduction in the grid size by 200 km (x direction) and 195 km (y direction). A comparison of back interpolation values between the two mapping extents was used to ascertain whether a change in the grid origin and extent would improve the match to the measured water level data and the representation of artesian conditions at all mapped spring locations. Equal or very similar back interpolation values were determined at well locations from the two mapping extents, while very small decreases in the number of spring locations with non-artesian conditions were noted for several, but not all surfaces generated using the second mapping extent. These results suggested that the origin and extent of the grid may influence the potentiometric surface, but it is not significant in terms of estimating artesian head at springs.

11.5 Final sequence of gridding, contouring and back interpolation

Validation of the penultimate potentiometric surfaces and the hydraulic head data used to derive the surfaces identified inconsistencies related to the use of DEM-derived ground elevation data to calculate water elevations in m AHD. Further, validation of results from the penultimate gridding sequence (specifically the 250 m x 250 m, 100 m x 100 m and 50 m x 50 m cell size grids) involved re-evaluation of adjacent wells with more than 0.5 m offset in hydraulic head value. This resulted in older or suspect records being removed and a reduction in the final dataset to 815 wells.

The final sequence of gridding and contouring was only implemented using *Surfer*™ and *Petrosys*™, as the gridding results from *ArcMap*™ were generally poor. One hundred and ten (110) surfaces were re-gridded.

11.5.1 Surfer™

Based on the results of the penultimate gridding sequence and back interpolation, gridding in *Surfer*™ was completed only on the smaller grid cell range (250 m x 250 m, 100 m x 100 m and 50 m x 50 m).

As per the penultimate stage of gridding, 7 Minimum Curvature surfaces were generated at each grid cell size based on the Internal Tension and Boundary Tension combinations detailed below. Likewise, 3 Kriging surfaces were generated at each grid cell size based on the theoretical variograms presented in Figure 11.3. Although surfaces generated by the Inverse Distance to a Power method showed unrealistic bullseyes, this method provided a low percentage of spring locations with the interpolated surface below the spring vent elevations. Therefore, one Inverse Distance to a Power method surface was generated using the power of 2 at a cell size of 100 m x 100 m.

11.5.2 Petrosys™

Since the *Petrosys*™ workflow was already established and automated, the final dataset was gridded using both grid origins and extents (Minimum Curvature variants only), and included cell sizes from 10,000 m x 10,000 m to 100 m x 100 m. No grids at 50 m x 50 m were generated using *Petrosys*™ due to the processing requirements and available computing power.

Minimum Curvature surfaces were generated for all combinations of estimation type (slope – 1st order Taylor series polynomial and slope + curvature – 2nd order Taylor series polynomial) and interpolation method (bicubic and bilinear) from 10,000 m x 10,000 m to 100 m x 100 m cell sizes and repeated for the second gridding extent for 5,000 m x 5,000 m to 100 m x 100 m cell sizes.

Hybrid surfaces were generated using both estimation types (slope – 1st order Taylor series polynomial and slope + curvature – 2nd order Taylor series polynomial) and interpolation methods (bicubic and bilinear). Hybrid method surfaces were generated at 1,000 m x 1,000 m, 250 m x 250 m and 100 m x 100 m grid cell sizes.

One polynomial surface was generated at 1,000 m x 1,000 m cell size using the bilinear interpolation method and slope (1st order Taylor series polynomial) estimation type; with a further 2 Polynomial surfaces generated at 250 m x 250 m cell size using both the bicubic and bilinear interpolation method and slope (1st order Taylor series polynomial) estimation type.

Least Squares Binomial, Least Squares Plane and Distance Weighted Average surfaces were generated at 1,000 m x 1,000 m, 250 m x 250 m and 100 m x 100 m grid cell sizes using the slope (1st order Taylor series polynomial) estimation type and bilinear interpolation method.

11.6 Selection of acceptable 2019 potentiometric surfaces

A second round of back interpolation was carried out on all the regenerated 110 gridded surfaces against the final well dataset (815 wells) (Appendix B, Table 11.2). Thirty-one (31) of the 110 gridded surfaces produced at least 98% of the back interpolated raster values within ±1m of the measured hydraulic head value at each well. Twenty-five (25) of the 110 gridded surfaces produced at least 97% of back interpolated raster values within ±0.5 m of the measured hydraulic head value at each well. Of these surfaces, 19 fulfilled both conditions and were therefore considered the most scientifically plausible. Of these 19, four groupings based on gross similarity in algorithm and gridding settings and ultimately similar potentiometric surface patterns could be made. For the purposes of analysis of flow condition, representatives of each group were employed. In summary, these groups are detailed below, with the key representative surface highlighted:

- Group 1. **Minimum Curvature, Internal Tension = 0, Boundary Tension = 0 (*Surfer*, 50 m grid)**

  Minimum Curvature, Internal Tension = 0, Boundary Tension = 1 (*Surfer*, 50 m grid)

- Group 2. **Minimum Curvature, Internal Tension =1, Boundary Tension = 1 (*Surfer*, 50 m grid)**

  Minimum Curvature, Internal Tension = 1, Boundary Tension = 0 (*Surfer*, 50 m grid)

- Group 3. Minimum Curvature, Internal Tension = 0.25, Boundary Tension = 0.75 (*Surfer*, 50 m grid)

  Minimum Curvature, Internal Tension = 0.5, Boundary Tension = 0.5 (*Surfer*, 50 m grid)

  Minimum Curvature, Internal Tension = 0.75, Boundary Tension = 0.25 (*Surfer*, 50 m grid)

  Least Square Plane, Bilinear interpolation, 1st order Taylor series (*Petrosys*, 100 m grid)

  Least Square Binomial, Bilinear interpolation, 1st order Taylor series (*Petrosys*, 100 m grid)

  Distance Weighted Average, Bilinear interpolation, 1st order Taylor series (*Petrosys*, 100 m grid)

  Distance Weighted Average, Bicubic interpolation, 1st order Taylor series (*Petrosys*, 100 m grid)

- Group 4. **Minimum Curvature, Bicubic interpolation, 1st order Taylor series (*Petrosys*, 100 m grid)**

  Minimum Curvature, Bicubic interpolation, 2nd order Taylor series (*Petrosys*, 100 m grid)

  Minimum Curvature, Bilinear interpolation, 1st order Taylor series (*Petrosys*, 100 m grid)

  Minimum Curvature, Bilinear interpolation, 2nd order Taylor series (*Petrosys*, 100 m grid)

  Hybrid, Bicubic interpolation, 1st order Taylor series (*Petrosys*, 100 m grid)

  Hybrid, Bicubic interpolation, 2nd order Taylor series (*Petrosys*, 100 m grid)

  Hybrid, Bilinear interpolation, 1st order Taylor series (*Petrosys*, 100 m grid)

  Hybrid, Bilinear interpolation, 2nd order Taylor series (*Petrosys*, 100 m grid)

Back interpolation of all 110 gridded surfaces was also performed against a listing of springs compiled as part of an Environmental Impact Statement (EIS) compilation which was being conducted BHP by the consultancy JBS&G Pty Ltd in April 2020 and then revised during this study. This included springs listed in the SA Geodata GAB spring project groups as well as springs identified by the EIS that were not listed in the SA Geodata GAB spring project groups, notably a new spring group at Billa Kalina South. Springs located in the Edith, Tarlton and Bitter spring groups were excluded from the final list of springs used for back interpolation as these springs are recognized as non-GAB springs (Wohling et al. 2013). Subsequently, springs from these three spring groups have been removed from the SA Geodata GAB spring project group. In total, final back interpolation was conducted on 5,163 spring vent locations. This included the 5,129 confirmed GAB springs currently in SA Geodata, as well as additional spring locations recorded and provided to DEW by BHP. Note that earlier phases of back interpolation were restricted to SA Geodata spring only. These additional spring locations will be added to SA Geodata at a future point in time.

As per previous back interpolation of potentiometric surfaces at spring locations, all 110 gridded surfaces presented spring locations with non-artesian conditions. However, at 95 of the 110 gridded surfaces, non-artesian conditions comprised 2% or less of spring locations. In general, back interpolation found:

- In most cases, the smaller cell size provided the best fit to artesian conditions at spring locations.
- Distance Weighted Average, Least Square Binomial and Least Square Plane methods in *Petrosys*™ provided better results (that is, a lower percentage of back interpolation results below the comparative spring elevation) compared to the Minimum Curvature and Hybrid methods as the Distance Weighted Average, Least Square Binomial and Least Square Plane methods tended to smooth or average out the interpolated hydraulic gradient.
- Bicubic interpolation in *Petrosys*™ provided better results (that is, a lower percentage of back interpolation results below the comparative spring elevation) than the bilinear interpolation for all the cell sizes.

Applying internal tension in *Surfer*™ provided better results (that is, a lower percentage of back interpolation results below the comparative spring elevation) compared to surfaces where no internal tension was applied as the internal tension tended to smooth or average out the interpolated hydraulic gradient.

B. Back Interpolation of potentiometric surfaces against well and spring datasets

Table 11.1: Back interpolation of penultimate potentiometric surfaces against well and spring datasets

(Note: 5129 total springs (SA Geodata only), cells are square).					Back interpolation to well data points Measured hydraulic head minus interpolated surface (m)						Back interp. to spring locations Spring elev. > ground elev.	
Gridding program	Gridding method	Gridding option	Grid Cell length m	Gridding extent	Min.	Max.	Range	Average	Std. Dev.	% within ± 1 m	COUNT	%
Surfer	Minimum Curvature	Internal tension = 0, Boundary tension = 0	50	1	−3.15	5.67	8.82	0.007	0.36	96.9%	119	2.3%
Surfer	Minimum Curvature	Internal tension = 0, Boundary tension = 1	50	1	−3.01	5.72	8.72	0.006	0.36	97.0%	119	2.3%
Surfer	Minimum Curvature	Internal tension = 1, Boundary tension = 0	50	1	−2.65	6.08	8.73	0.018	0.69	90.5%	46	0.9%
Surfer	Minimum Curvature	Internal tension = 1, Boundary tension = 1	50	1	−2.52	6.08	8.59	−0.008	0.63	91.1%	45	0.9%
Surfer	Minimum Curvature	Internal tension = 0.25, Boundary tension = 0.75	100	1	−6.59	9.54	16.13	0.003	0.56	95.6%	94	1.8%
Surfer	Minimum Curvature	Internal tension = 0.5, Boundary tension = 0.5	100	1	−6.56	9.81	16.37	0.001	0.58	95.4%	82	1.6%
Surfer	Minimum Curvature	Internal tension = 0.75, Boundary tension = 0.25	100	1	−6.34	10.18	16.53	−0.005	0.67	93.8%	62	1.2%
Surfer	Minimum Curvature	Internal tension = 0, Boundary tension = 0	100	1	−6.66	9.38	16.05	0.003	0.56	95.7%	120	2.3%
Surfer	Minimum Curvature	Internal tension = 0, Boundary tension = 1	100	1	−6.58	9.37	15.95	0.003	0.55	95.6%	112	2.2%
Surfer	Minimum Curvature	Internal tension = 1, Boundary tension = 0	100	1	−5.87	10.68	16.54	0.018	0.92	86.0%	53	1.0%
Surfer	Minimum Curvature	Internal tension = 1, Boundary tension = 1	100	1	−5.93	10.60	16.53	−0.011	0.89	86.6%	52	1.0%
Surfer	Kriging	Cubic variogram, no search	100	1	−11.14	19.88	31.02	0.000	1.41	88.0%	399	7.8%
Surfer	Kriging	Exponential variogram, no search	100	1	−3.79	9.05	12.84	0.007	0.51	96.1%	94	1.8%
Surfer	Kriging	Linear variogram, no search	100	1	−3.79	9.04	12.83	0.007	0.51	96.1%	94	1.8%
Surfer	Kriging	Spherical variogram, no search	100	1	−6.53	5.68	12.22	0.000	0.53	95.8%	138	2.7%
Surfer	Minimum Curvature	Internal tension = 0, Boundary tension = 0	250	1	−6.72	9.84	16.56	0.002	0.74	93.5%	157	3.1%
Surfer	Minimum Curvature	Internal tension = 0, Boundary tension = 1	250	1	−6.71	9.84	16.55	0.003	0.74	93.6%	143	2.8%
Surfer	Minimum Curvature	Internal tension = 1, Boundary tension = 0	250	1	−5.17	10.98	16.15	0.044	1.21	79.5%	41	0.8%
Surfer	Minimum Curvature	Internal tension = 1, Boundary tension = 1	250	1	−5.16	10.79	15.95	0.002	1.12	80.5%	39	0.8%
Surfer	Kriging	Cubic variogram, no search	250	1	−11.14	19.92	31.06	0.000	1.41	88.0%	399	7.8%

(Note: 5129 total springs (SA Geodata only), cells are square).					Back interpolation to well data points Measured hydraulic head minus interpolated surface (m)						Back interp. to spring locations Spring elev. > ground elev.	
Gridding program	Gridding method	Gridding option	Grid Cell length m	Gridding extent	Min.	Max.	Range	Average	Std. Dev.	% within ± 1 m	COUNT	%
Surfer	Kriging	Exponential variogram, no search	250	1	−6.14	7.50	13.64	−0.007	0.70	93.3%	94	1.8%
Surfer	Kriging	Linear variogram, no search	250	1	−6.15	7.49	13.64	−0.007	0.70	93.3%	94	1.8%
Surfer	Kriging	Spherical variogram, no search	250	1	−7.88	6.84	14.72	−0.011	0.76	93.1%	138	2.7%
Surfer	Minimum Curvature	Internal tension = 0, Boundary tension = 0	500	1	−10.48	9.90	20.38	−0.016	1.01	90.8%	154	3.0%
Surfer	Minimum Curvature	Internal tension = 0, Boundary tension = 1	500	1	−10.36	9.88	20.24	−0.019	1.00	91.0%	128	2.5%
Surfer	Minimum Curvature	Internal tension = 1, Boundary tension = 0	500	1	−9.77	10.45	20.22	0.015	1.45	71.0%	42	0.8%
Surfer	Minimum Curvature	Internal tension = 1, Boundary tension = 1	500	1	−9.77	10.43	20.20	−0.032	1.38	71.8%	44	0.9%
Surfer	Kriging	Cubic variogram, no search	500	1	−11.14	19.98	31.12	−0.001	1.41	88.0%	399	7.8%
Surfer	Kriging	Exponential variogram, no search	500	1	−9.30	8.07	17.38	−0.009	1.01	88.9%	94	1.8%
Surfer	Kriging	Linear variogram, no search	500	1	−9.30	8.07	17.38	−0.009	1.01	88.9%	94	1.8%
Surfer	Kriging	Spherical variogram, no search	500	1	−11.22	8.30	19.52	−0.011	1.07	89.7%	138	2.7%
Surfer	Minimum Curvature	Internal tension = 0, Boundary tension = 0	1000	1	−11.49	10.72	22.21	−0.030	1.30	85.6%	155	3.0%
Surfer	Minimum Curvature	Internal tension = 0, Boundary tension = 1	1000	1	−11.38	10.93	22.31	−0.033	1.30	85.7%	120	2.3%
Surfer	Minimum Curvature	Internal tension = 1, Boundary tension = 0	1000	1	−11.56	13.03	24.58	0.028	1.83	64.8%	57	1.1%
Surfer	Minimum Curvature	Internal tension = 1, Boundary tension = 1	1000	1	−11.55	13.02	24.58	−0.030	1.75	66.5%	57	1.1%
Surfer	Kriging	Cubic variogram, no search	1000	1	−11.14	20.08	31.22	0.001	1.41	87.8%	399	7.8%
Surfer	Kriging	Cubic variogram, 16 sector search	1000	1	−9.79	9.63	19.42	−0.021	0.97	91.7%	999	19.5%
Surfer	Kriging	Exponential variogram, no search	1000	1	−10.57	13.17	23.74	−0.018	1.29	82.6%	94	1.8%
Surfer	Kriging	Exponential variogram, 16 sector search	1000	1	−10.56	13.17	23.73	−0.019	1.29	82.5%	94	1.8%
Surfer	Kriging	Gaussian variogram, no search	1000	1	−48.98	51.86	100.84	0.000	8.47	16.6%	132	2.6%
Surfer	Kriging	Gaussian variogram, 16 sector search	1000	1	−21.17	26.43	47.60	0.000	5.13	25.3%	1163	22.7%
Surfer	Kriging	Rational Quadratic variogram, no search	1000	1	−17.06	22.25	39.31	−0.014	3.93	35.2%	133	2.6%
Surfer	Kriging	Rational Quadratic variogram, 16 sector search	1000	1	−29.99	26.09	56.08	−0.014	5.72	22.1%	340	6.6%
Surfer	Kriging	Linear variogram, no search	1000	1	−10.59	13.18	23.77	−0.018	1.29	82.6%	94	1.8%

(Note: 5129 total springs (SA Geodata only), cells are square).					Back interpolation to well data points Measured hydraulic head minus interpolated surface (m)						Back interp. to spring locations Spring elev. > ground elev.	
Gridding program	Gridding method	Gridding option	Grid Cell length m	Gridding extent	Min.	Max.	Range	Average	Std. Dev.	% within ± 1 m	COUNT	%
Surfer	Kriging	Linear variogram, 16 sector search	1000	1	−10.56	13.18	23.74	−0.019	1.29	82.5%	94	1.8%
Surfer	Kriging	Spherical variogram, no search	1000	1	−13.10	12.73	25.83	−0.034	1.41	82.4%	138	2.7%
Surfer	Kriging	Spherical variogram, 16 sector search	1000	1	−13.11	12.72	25.84	−0.034	1.41	82.4%	128	2.5%
Surfer	Kriging	Wave variogram, no search	1000	1	−33.18	30.75	63.93	0.000	6.56	21.2%	467	9.1%
Surfer	Kriging	Wave variogram, 16 sector search	1000	1	−20.57	23.25	43.82	0.045	4.60	29.0%	134	2.6%
Surfer	Inverse Distance to a Power	Power = 2	1000	1	−10.36	15.53	25.89	−0.038	1.34	84.1%	25	0.5%
Surfer	Inverse Distance to a Power	Power = 2	1000	1	−10.36	15.52	25.88	−0.037	1.32	85.5%	55	1.1%
Surfer	Inverse Distance to a Power	Power = 3	1000	1	−10.63	14.37	25.00	−0.044	1.25	88.3%	68	1.3%
Surfer	Inverse Distance to a Power	Power = 3	1000	1	−10.64	14.34	24.99	−0.044	1.25	88.3%	80	1.6%
Surfer	Inverse Distance to a Power	Power = 4	1000	1	−11.61	13.84	25.45	−0.044	1.23	89.3%	114	2.2%
Surfer	Inverse Distance to a Power	Power = 4	1000	1	−11.61	13.84	25.45	−0.044	1.23	89.3%	126	2.5%
Surfer	Minimum Curvature	Internal tension = 0, Boundary tension = 0	2000	1	−11.36	21.59	32.95	0.007	1.71	77.1%	139	2.7%
Surfer	Minimum Curvature	Internal tension = 0, Boundary tension = 1	2000	1	−11.34	21.58	32.92	−0.008	1.70	76.3%	127	2.5%
Surfer	Minimum Curvature	Internal tension = 1, Boundary tension = 0	2000	1	−11.46	21.37	32.83	0.015	2.26	56.8%	65	1.3%
Surfer	Minimum Curvature	Internal tension = 1, Boundary tension = 1	2000	1	−11.46	21.37	32.83	−0.045	2.19	58.1%	58	1.1%
Surfer	Minimum Curvature	Internal tension = 0, Boundary tension = 0	5000	1	−12.95	21.32	34.27	−0.011	2.56	55.9%	164	3.2%
Surfer	Minimum Curvature	Internal tension = 0, Boundary tension = 1	5000	1	−13.15	21.28	34.44	0.011	2.56	56.5%	145	2.8%
Surfer	Minimum Curvature	Internal tension = 1, Boundary tension = 0	5000	1	−13.40	19.27	32.67	0.211	3.24	43.6%	108	2.1%
Surfer	Minimum Curvature	Internal tension = 1, Boundary tension = 1	5000	1	−13.44	19.27	32.71	0.120	3.15	44.4%	108	2.1%
Petro−sys	Minimum Curvature	Bilinear interpolation, 1st order Taylor series	100	1	−7.90	3.79	11.69	−0.004	0.45	96.6%	102	2.0%
Petro−sys	Minimum Curvature	Bilinear interpolation, 2nd order Taylor series	100	1	−7.08	3.19	10.27	−0.003	0.41	96.8%	109	2.1%

(Note: 5129 total springs (SA Geodata only), cells are square).					Back interpolation to well data points Measured hydraulic head minus interpolated surface (m)						Back interp. to spring locations Spring elev. > ground elev.	
Gridding program	Gridding method	Gridding option	Grid Cell length m	Gridding extent	Min.	Max.	Range	Average	Std. Dev.	% within ± 1 m	COUNT	%
Petro-sys	Minimum Curvature	Bicubic interpolation, 1st order Taylor series	100	1	−7.51	3.56	11.07	−0.003	0.43	96.9%	99	1.9%
Petro-sys	Minimum Curvature	Bicubic interpolation, 2nd order Taylor series	100	1	−6.59	3.48	10.07	−0.002	0.39	96.8%	95	1.9%
Petro-sys	Minimum Curvature	Bicubic interpolation, 1st order Taylor series	100	2	−7.53	3.54	11.07	−0.003	0.43	96.9%	96	1.9%
Petro-sys	Minimum Curvature	Bilinear interpolation, 1st order Taylor series	100	2	−7.91	3.78	11.69	−0.004	0.45	96.6%	92	1.8%
Petro-sys	Minimum Curvature	Bicubic interpolation, 2nd order Taylor series	100	2	−6.68	3.56	10.24	−0.002	0.40	96.8%	95	1.9%
Petro-sys	Minimum Curvature	Bilinear interpolation, 2nd order Taylor series	100	2	−7.16	3.27	10.43	−0.004	0.41	96.8%	101	2.0%
Petro-sys	Minimum Curvature	Bilinear interpolation, 1st order Taylor series	250	1	−7.69	6.91	14.60	0.006	0.60	94.3%	95	1.9%
Petro-sys	Minimum Curvature	Bilinear interpolation, 2nd order Taylor series	250	1	−7.73	6.44	14.17	0.001	0.55	94.9%	104	2.0%
Petro-sys	Minimum Curvature	Bicubic interpolation, 1st order Taylor series	250	2	−7.21	7.06	14.27	0.010	0.56	94.5%	96	1.9%
Petro-sys	Minimum Curvature	Bilinear interpolation, 1st order Taylor series	250	2	−7.68	6.97	14.65	0.006	0.60	94.2%	100	1.9%
Petro-sys	Minimum Curvature	Bicubic interpolation, 2nd order Taylor series	250	2	−7.19	6.64	13.83	0.007	0.52	95.4%	99	1.9%
Petro-sys	Minimum Curvature	Bilinear interpolation, 2nd order Taylor series	250	2	−7.71	6.52	14.23	0.001	0.55	94.9%	98	1.9%
Petro-sys	Minimum Curvature	Bicubic interpolation, 1st order Taylor series	250	1	−7.20	7.02	14.22	0.010	0.56	94.5%	97	1.9%
Petro-sys	Minimum Curvature	Bicubic interpolation, 2nd order Taylor series	250	1	−7.18	6.60	13.78	0.007	0.52	95.5%	97	1.9%
Petro-sys	Minimum Curvature	Bilinear interpolation, 1st order Taylor series	500	1	−7.12	8.88	16.00	0.021	0.89	92.2%	94	1.8%
Petro-sys	Minimum Curvature	Bilinear interpolation, 2nd order Taylor series	500	1	−7.28	8.24	15.52	0.011	0.81	92.6%	104	2.0%
Petro-sys	Minimum Curvature	Bicubic interpolation, 1st order Taylor series	500	2	−6.73	9.13	15.86	0.022	0.84	92.7%	96	1.9%
Petro-sys	Minimum Curvature	Bilinear interpolation, 1st order Taylor series	500	2	−7.11	8.87	15.98	0.020	0.89	92.2%	99	1.9%
Petro-sys	Minimum Curvature	Bicubic interpolation, 2nd order Taylor series	500	2	−6.83	8.85	15.68	0.016	0.76	93.5%	99	1.9%
Petro-sys	Minimum Curvature	Bilinear interpolation, 2nd order Taylor series	500	2	−7.25	8.32	15.57	0.011	0.81	92.7%	97	1.9%
Petro-sys	Minimum Curvature	Bicubic interpolation, 1st order Taylor series	500	1	−6.72	9.08	15.80	0.022	0.83	92.7%	96	1.9%
Petro-sys	Minimum Curvature	Bicubic interpolation, 2nd order Taylor series	500	1	−6.82	8.80	15.62	0.016	0.76	93.5%	97	1.9%
Petro-sys	Polynomial	Bilinear interpolation, 1st order Taylor series	1000	1	−12.78	10.21	22.99	0.028	1.16	88.5%	101	2.0%
Petro-sys	Minimum Curvature	Bilinear interpolation, 1st order Taylor series	1000	1	−12.80	10.19	22.99	0.029	1.16	88.3%	94	1.8%

(Note: 5129 total springs (SA Geodata only), cells are square).					Back interpolation to well data points Measured hydraulic head minus interpolated surface (m)						Back interp. to spring locations Spring elev. > ground elev.	
Gridding program	Gridding method	Gridding option	Grid Cell length m	Gridding extent	Min.	Max.	Range	Average	Std. Dev.	% within ± 1 m	COUNT	%
Petro–sys	Minimum Curvature	Bilinear interpolation, 2nd order Taylor series	1000	1	−11.62	10.16	21.78	0.019	1.08	90.0%	104	2.0%
Petro–sys	Minimum Curvature	Bicubic interpolation, 1st order Taylor series	1000	1	−12.35	10.01	22.36	0.029	1.11	90.0%	97	1.9%
Petro–sys	Minimum Curvature	Bicubic interpolation, 2nd order Taylor series	1000	1	−11.11	9.94	21.05	0.023	1.04	91.3%	97	1.9%
Petro–sys	Minimum Curvature	Bicubic interpolation, 1st order Taylor series	1000	2	−12.26	10.08	22.34	0.029	1.11	90.1%	95	1.9%
Petro–sys	Minimum Curvature	Bilinear interpolation, 1st order Taylor series	1000	2	−12.77	10.26	23.03	0.029	1.16	88.3%	100	1.9%
Petro–sys	Minimum Curvature	Bicubic interpolation, 2nd order Taylor series	1000	2	−11.02	9.92	20.94	0.021	1.03	91.6%	100	1.9%
Petro–sys	Minimum Curvature	Bilinear interpolation, 2nd order Taylor series	1000	2	−11.46	10.13	21.59	0.017	1.07	90.6%	95	1.9%
Petro–sys	Least Square Plane	Bilinear interpolation, 1st order Taylor series	1000	1	−13.84	10.49	24.33	0.043	1.37	77.8%	67	1.3%
Petro–sys	Least Square Binomial	Bilinear interpolation, 1st order Taylor series	1000	1	−12.78	10.21	22.99	0.028	1.16	88.5%	101	2.0%
Petro–sys	Hybrid	Bicubic interpolation, 1st order Taylor series	1000	1	−12.33	10.01	22.34	0.029	1.11	90.0%	102	2.0%
Petro–sys	Hybrid	Bilinear interpolation, 1st order Taylor series	1000	1	−12.78	10.21	22.99	0.028	1.16	88.5%	101	2.0%
Petro–sys	Distance Weighted Average	Bicubic interpolation, 1st order Taylor series	1000	1	−12.37	10.26	22.63	0.046	1.24	88.8%	88	1.7%
Petro–sys	Distance Weighted Average	Bilinear interpolation, 1st order Taylor series	1000	1	−13.36	10.35	23.71	0.038	1.22	88.3%	90	1.8%
Petro–sys	Minimum Curvature	Bilinear interpolation, 1st order Taylor series	2000	1	−22.02	10.27	32.29	0.028	1.58	80.9%	95	1.9%
Petro–sys	Minimum Curvature	Bilinear interpolation, 2nd order Taylor series	2000	1	−21.55	10.27	31.82	0.011	1.48	85.5%	102	2.0%
Petro–sys	Minimum Curvature	Bicubic interpolation, 1st order Taylor series	2000	2	−16.98	20.01	36.99	0.072	1.63	84.4%	98	1.9%
Petro–sys	Minimum Curvature	Bilinear interpolation, 1st order Taylor series	2000	2	−17.04	16.29	33.33	0.065	1.58	80.6%	99	1.9%
Petro–sys	Minimum Curvature	Bicubic interpolation, 2nd order Taylor series	2000	2	−15.62	18.65	34.27	0.051	1.52	87.0%	94	1.8%
Petro–sys	Minimum Curvature	Bilinear interpolation, 2nd order Taylor series	2000	2	−15.87	14.54	30.41	0.037	1.43	84.7%	92	1.8%
Petro–sys	Minimum Curvature	Bicubic interpolation, 1st order Taylor series	2000	1	−21.67	10.13	31.80	0.015	1.51	84.9%	98	1.9%
Petro–sys	Minimum Curvature	Bicubic interpolation, 2nd order Taylor series	2000	1	−20.88	10.11	30.99	0.002	1.43	88.3%	95	1.9%
Petro–sys	Minimum Curvature	Bilinear interpolation, 1st order Taylor series	5000	1	−21.97	11.80	33.77	0.010	2.26	63.7%	83	1.6%
Petro–sys	Minimum Curvature	Bilinear interpolation, 2nd order Taylor series	5000	1	−22.50	10.84	33.34	−0.007	1.99	71.7%	110	2.1%

(Note: 5129 total springs (SA Geodata only), cells are square).					Back interpolation to well data points Measured hydraulic head minus interpolated surface (m)						Back interp. to spring locations Spring elev. > ground elev.	
Gridding program	Gridding method	Gridding option	Grid Cell length m	Gridding extent	Min.	Max.	Range	Average	Std. Dev.	% within ± 1 m	COUNT	%
Petro–sys	Minimum Curvature	Bicubic interpolation, 1st order Taylor series	5000	2	−22.98	11.21	34.19	−0.018	2.03	72.1%	98	1.9%
Petro–sys	Minimum Curvature	Bilinear interpolation, 1st order Taylor series	5000	2	−22.08	11.92	34.00	0.017	2.26	63.6%	101	2.0%
Petro–sys	Minimum Curvature	Bicubic interpolation, 2nd order Taylor series	5000	2	−23.15	10.72	33.87	−0.041	1.85	76.5%	99	1.9%
Petro–sys	Minimum Curvature	Bilinear interpolation, 2nd order Taylor series	5000	2	−22.68	10.87	33.55	−0.002	2.00	71.1%	88	1.7%
Petro–sys	Minimum Curvature	Bicubic interpolation, 1st order Taylor series	5000	1	−23.02	11.14	34.16	−0.019	2.03	72.2%	94	1.8%
Petro–sys	Minimum Curvature	Bicubic interpolation, 2nd order Taylor series	5000	1	−23.20	10.71	33.91	−0.039	1.84	76.7%	115	2.2%
Petro–sys	Minimum Curvature	Bilinear interpolation, 1st order Taylor series	10000	1	−22.82	15.13	37.95	0.110	3.56	39.4%	34	0.7%
Petro–sys	Minimum Curvature	Bilinear interpolation, 2nd order Taylor series	10000	1	−20.44	13.12	33.56	0.092	2.97	48.8%	39	0.8%
Petro–sys	Minimum Curvature	Bicubic interpolation, 1st order Taylor series	10000	1	−20.38	13.28	33.66	0.027	3.01	49.3%	37	0.7%
Petro–sys	Minimum Curvature	Bicubic interpolation, 2nd order Taylor series	10000	1	−22.27	11.32	33.59	−0.037	2.59	60.4%	78	1.5%
Arc Map	Spline	Regularized	100	1	−10.03	20.68	30.71	0.000	1.40	86.0%	850	16.6%
Arc Map	Spline	Tension	100	1	−66.60	38.28	104.87	−0.001	4.06	83.7%	700	13.6%
Arc Map	Kriging	Exponential	100	1	−3.62	6.98	10.60	0.004	0.47	95.4%	88	1.7%
Arc Map	Kriging	Linear	100	1	−3.62	6.98	10.59	0.004	0.47	95.4%	88	1.7%
Arc Map	Kriging	Spherical	100	1	−3.62	6.98	10.59	0.004	0.47	95.4%	88	1.7%
Arc Map	Inverse Distance Weighting	Power = 2	100	1	−5.13	8.54	13.67	0.001	0.50	95.4%	91	1.8%

Table 11.2: Back interpolation of final potentiometric surfaces against well and spring datasets

Note: 5 163 total springs. Cells are square.					Back interpolation to well data points Measured hydraulic head minus interpolated surface (m)									Back interp. to spring locations Spring elev. > ground elev.	
Gridding program	Gridding method	Gridding option	Grid cell length m	Gridding extent	Min.	Max.	Range	Average	Std. Dev.	COUNT within ±1 m	Percent within ±1 m	COUNT within ±0.5 m	Percent within ±0.5 m	COUNT	Percent
Surfer	Minimum Curvature	Internal tension = 0.25, Boundary tension = 0.75	50	1	−1.10	1.11	2.21	0.00	0.11	813	99.8%	806	98.9%	83	1.6%
Surfer	Minimum Curvature	Internal tension = 0.5, Boundary tension = 0.5	50	1	−1.12	1.25	2.37	0.00	0.15	812	99.6%	803	98.5%	71	1.4%
Surfer	Minimum Curvature	Internal tension = 0.75, Boundary tension = 0.25	50	1	−1.21	2.31	3.52	−0.01	0.28	804	98.7%	754	92.5%	50	1.0%
Surfer	Minimum Curvature	Internal tension = 0, Boundary tension = 0	50	1	−1.10	1.11	2.21	0.00	0.12	813	99.8%	806	98.9%	111	2.2%
Surfer	Minimum Curvature	Internal tension = 0, Boundary tension = 1	50	1	−1.10	1.11	2.21	0.00	0.11	813	99.8%	806	98.9%	109	2.1%
Surfer	Minimum Curvature	Internal tension = 1, Boundary tension = 0	50	1	−2.54	5.26	7.79	0.02	0.60	759	93.1%	633	77.7%	39	0.8%
Surfer	Minimum Curvature	Internal tension = 1, Boundary tension = 1	50	1	−2.41	3.34	5.75	−0.01	0.53	766	94.0%	649	79.6%	39	0.8%
Surfer	Kriging	Exponential variogram	50	1	−1.41	1.37	2.78	0.00	0.13	811	99.5%	806	98.9%	94	1.8%
Surfer	Kriging	Linear variogram	50	1	−1.41	1.37	2.78	0.00	0.13	811	99.5%	806	98.9%	94	1.8%
Surfer	Kriging	Spherical variogram	50	1	−1.35	1.60	2.95	0.00	0.14	810	99.4%	801	98.3%	108	2.1%

Note: 5 163 total springs. Cells are square.					Back interpolation to well data points Measured hydraulic head minus interpolated surface (m)									Back interp. to spring locations Spring elev. > ground elev.	
Gridding program	Gridding method	Gridding option	Grid cell length m	Gridding extent	Min.	Max.	Range	Average	Std. Dev.	COUNT within ±1 m	Percent within ±1 m	COUNT within ±0.5 m	Percent within ±0.5 m	COUNT	Percent
Surfer	Minimum Curvature	Internal tension = 0.25, Boundary tension = 0.75	100	1	−2.20	3.40	5.60	0.00	0.23	805	98.8%	797	97.8%	85	1.7%
Surfer	Minimum Curvature	Internal tension = 0.5, Boundary tension = 0.5	100	1	−2.20	3.75	5.95	0.00	0.27	804	98.7%	791	97.1%	75	1.5%
Surfer	Minimum Curvature	Internal tension = 0.75, Boundary tension = 0.25	100	1	−2.36	4.33	6.69	−0.01	0.41	791	97.1%	725	89.0%	57	1.1%
Surfer	Minimum Curvature	Internal tension = 0, Boundary tension = 0	100	1	−2.08	3.40	5.48	0.00	0.23	805	98.8%	796	97.7%	112	2.2%
Surfer	Minimum Curvature	Internal tension = 0, Boundary tension = 1	100	1	−2.14	3.27	5.41	0.00	0.22	805	98.8%	796	97.7%	105	2.0%
Surfer	Minimum Curvature	Internal tension = 1, Boundary tension = 0	100	1	−4.53	5.37	9.90	0.01	0.76	724	88.8%	577	70.8%	41	0.8%
Surfer	Minimum Curvature	Internal tension = 1, Boundary tension = 1	100	1	−4.48	5.35	9.82	−0.02	0.71	730	89.6%	586	71.9%	40	0.8%
Surfer	Kriging	Exponential variogram	100	1	−2.11	3.06	5.16	0.00	0.23	807	99.0%	789	96.8%	94	1.8%
Surfer	Kriging	Linear variogram	100	1	−2.11	3.06	5.16	0.00	0.23	807	99.0%	789	96.8%	94	1.8%
Surfer	Kriging	Spherical variogram	100	1	−2.19	3.19	5.38	0.00	0.25	803	98.5%	790	96.9%	108	2.1%

Note: 5 163 total springs. Cells are square.					Back interpolation to well data points Measured hydraulic head minus interpolated surface (m)									Back interp. to spring locations Spring elev. > ground elev.	
Gridding program	Gridding method	Gridding option	Grid cell length m	Gridding extent	Min.	Max.	Range	Average	Std. Dev.	COUNT within ±1 m	Percent within ±1 m	COUNT within ±0.5 m	Percent within ±0.5 m	COUNT	Percent
Surfer	Inverse Distance to a Power	Power = 2	100	1	−3.96	4.07	8.03	0.00	0.31	769	98.3%	753	96.3%	33	0.7%
Surfer	Minimum Curvature	Internal tension = 0.25, Boundary tension = 0.75	250	1	−4.85	4.92	9.77	0.00	0.48	796	97.7%	766	94.0%	84	1.6%
Surfer	Minimum Curvature	Internal tension = 0.5, Boundary tension = 0.5	250	1	−4.91	5.24	10.15	0.00	0.52	794	97.4%	741	90.9%	76	1.5%
Surfer	Minimum Curvature	Internal tension = 0.75, Boundary tension = 0.25	250	1	−5.01	6.01	11.02	0.00	0.66	764	93.7%	654	80.2%	55	1.1%
Surfer	Minimum Curvature	Internal tension = 0, Boundary tension = 0	250	1	−4.80	4.67	9.47	0.00	0.48	795	97.5%	769	94.4%	108	2.1%
Surfer	Minimum Curvature	Internal tension = 0, Boundary tension = 1	250	1	−4.82	4.66	9.48	0.00	0.47	796	97.7%	770	94.5%	110	2.1%
Surfer	Minimum Curvature	Internal tension = 1, Boundary tension = 0	250	1	−5.18	10.71	15.89	0.04	1.08	677	83.1%	500	61.3%	35	0.7%
Surfer	Minimum Curvature	Internal tension = 1, Boundary tension = 1	250	1	−5.17	7.14	12.31	0.00	0.97	682	83.7%	510	62.6%	34	0.7%
Surfer	Kriging	Exponential variogram	250	1	−4.42	5.71	10.13	0.01	0.49	791	97.1%	743	91.2%	94	1.8%
Surfer	Kriging	Linear variogram	250	1	−4.42	5.71	10.13	0.01	0.49	791	97.1%	743	91.2%	94	1.8%

Note: 5 163 total springs. Cells are square.					Back interpolation to well data points Measured hydraulic head minus interpolated surface (m)									Back interp. to spring locations Spring elev. > ground elev.	
Gridding program	Gridding method	Gridding option	Grid cell length m	Gridding extent	Min.	Max.	Range	Average	Std. Dev.	COUNT within ±1 m	Percent within ±1 m	COUNT within ±0.5 m	Percent within ±0.5 m	COUNT	Percent
Surfer	Kriging	Spherical variogram	250	1	−5.45	6.57	12.03	0.01	0.53	792	97.2%	750	92.0%	108	2.1%
Petrosys	Minimum Curvature	Bilinear interpolation, 1st order Taylor series	100	1	−1.96	1.82	3.78	0.00	0.21	805	98.8%	792	97.2%	94	1.8%
Petrosys	Minimum Curvature	Bilinear interpolation, 2nd order Taylor series	100	1	−1.49	1.30	2.79	0.00	0.16	809	99.3%	797	97.8%	94	1.8%
Petrosys	Minimum Curvature	Bicubic interpolation, 1st order Taylor series	100	2	−1.31	1.46	2.77	0.00	0.16	809	99.3%	796	97.7%	81	1.6%
Petrosys	Minimum Curvature	Bilinear interpolation, 1st order Taylor series	100	2	−1.98	1.86	3.84	0.00	0.21	802	98.8%	790	97.3%	81	1.6%
Petrosys	Minimum Curvature	Bicubic interpolation, 2nd order Taylor series	100	2	−1.00	1.07	2.07	0.00	0.12	812	99.6%	801	98.3%	89	1.7%
Petrosys	Minimum Curvature	Bilinear interpolation, 2nd order Taylor series	100	2	−1.46	1.55	3.01	0.00	0.16	804	99.0%	795	97.9%	83	1.6%
Petrosys	Minimum Curvature	Bicubic interpolation, 1st order Taylor series	100	1	−1.30	1.22	2.52	0.00	0.16	808	99.1%	794	97.4%	93	1.8%
Petrosys	Minimum Curvature	Bicubic interpolation, 2nd order Taylor series	100	1	−1.00	1.07	2.07	0.00	0.12	813	99.8%	801	98.3%	93	1.8%
Petrosys	Least Square Plane	Bilinear interpolation, 1st order Taylor series	100	1	−4.34	5.74	10.08	−0.02	0.65	737	90.4%	604	74.1%	67	1.3%

Note: 5 163 total springs. Cells are square.					Back interpolation to well data points Measured hydraulic head minus interpolated surface (m)									Back interp. to spring locations Spring elev. > ground elev.	
Gridding program	Gridding method	Gridding option	Grid cell length m	Gridding extent	Min.	Max.	Range	Average	Std. Dev.	COUNT within ±1 m	Percent within ±1 m	COUNT within ±0.5 m	Percent within ±0.5 m	COUNT	Percent
Petrosys	Least Square Binomial	Bilinear interpolation, 1st order Taylor series	100	1	−2.00	1.88	3.88	0.00	0.21	805	98.8%	792	97.2%	97	1.9%
Petrosys	Hybrid	Bilinear interpolation, 1st order Taylor series	100	1	−2.00	1.88	3.88	0.00	0.21	805	98.8%	792	97.2%	97	1.9%
Petrosys	Hybrid	Bicubic interpolation, 2nd order Taylor series	100	1	−1.00	1.07	2.07	0.00	0.12	813	99.8%	801	98.3%	95	1.9%
Petrosys	Hybrid	Bilinear interpolation, 2nd order Taylor series	100	1	−1.53	1.32	2.84	0.00	0.16	809	99.3%	797	97.8%	95	1.9%
Petrosys	Hybrid	Bicubic interpolation, 1st order Taylor series	100	1	−1.34	1.22	2.56	0.00	0.16	808	99.1%	794	97.4%	97	1.9%
Petrosys	Distance Weighted Average	Bicubic interpolation, 1st order Taylor series	100	1	−1.80	1.88	3.68	0.00	0.18	808	99.1%	794	97.4%	83	1.6%
Petrosys	Distance Weighted Average	Bilinear interpolation, 1st order Taylor series	100	1	−2.33	2.24	4.57	0.00	0.26	804	98.7%	781	95.8%	85	1.7%
Petrosys	Polynomial	Bicubic interpolation, 1st order Taylor series	250	1	−5.23	4.45	9.69	0.00	0.41	792	97.2%	771	94.6%	101	2.0%
Petrosys	Polynomial	Bilinear interpolation, 1st order Taylor series	250	1	−6.01	5.26	11.27	0.00	0.49	786	96.4%	758	93.0%	98	1.9%

Note: 5 163 total springs. Cells are square.					Back interpolation to well data points Measured hydraulic head minus interpolated surface (m)									Back interp. to spring locations Spring elev. > ground elev.	
Gridding program	Gridding method	Gridding option	Grid cell length m	Gridding extent	Min.	Max.	Range	Average	Std. Dev.	COUNT within ±1 m	Percent within ±1 m	COUNT within ±0.5 m	Percent within ±0.5 m	COUNT	Percent
Petrosys	Polynomial	Bicubic interpolation, 2nd order Taylor series	250	1	−2.79	3.95	6.73	0.00	0.31	794	97.4%	777	95.3%	98	1.9%
Petrosys	Polynomial	Bilinear interpolation, 2nd order Taylor series	250	1	−3.69	5.17	8.86	0.01	0.40	789	96.8%	771	94.6%	104	2.0%
Petrosys	Minimum Curvature	Bicubic interpolation, 1st order Taylor series	250	2	−5.17	4.52	9.69	0.00	0.41	792	97.2%	770	94.5%	97	1.9%
Petrosys	Minimum Curvature	Bilinear interpolation, 1st order Taylor series	250	2	−5.90	5.35	11.25	0.00	0.49	783	96.4%	756	93.1%	96	1.9%
Petrosys	Minimum Curvature	Bicubic interpolation, 2nd order Taylor series	250	2	−2.76	4.01	6.76	0.00	0.31	794	97.4%	776	95.2%	121	2.4%
Petrosys	Minimum Curvature	Bilinear interpolation, 2nd order Taylor series	250	2	−3.62	5.21	8.83	0.01	0.40	786	96.8%	768	94.6%	109	2.1%
Petrosys	Minimum Curvature	Bilinear interpolation, 1st order Taylor series	250	1	−5.90	5.35	11.25	0.00	0.49	786	96.4%	758	93.0%	93	1.8%
Petrosys	Minimum Curvature	Bilinear interpolation, 2nd order Taylor series	250	1	−3.63	5.28	8.92	0.01	0.40	789	96.8%	771	94.6%	102	2.0%
Petrosys	Minimum Curvature	Bicubic interpolation, 1st order Taylor series	250	1	−5.17	4.53	9.70	0.00	0.41	792	97.2%	772	94.7%	96	1.9%
Petrosys	Minimum Curvature	Bicubic interpolation, 2nd order Taylor series	250	1	−2.78	4.04	6.82	0.00	0.31	794	97.4%	777	95.3%	92	1.8%

Note: 5 163 total springs. Cells are square.					Back interpolation to well data points Measured hydraulic head minus interpolated surface (m)									Back interp. to spring locations Spring elev. > ground elev.	
Gridding program	Gridding method	Gridding option	Grid cell length m	Gridding extent	Min.	Max.	Range	Average	Std. Dev.	COUNT within ±1 m	Percent within ±1 m	COUNT within ±0.5 m	Percent within ±0.5 m	COUNT	Percent
Petrosys	Least Square Binomial	Bilinear interpolation, 1st order Taylor series	250	1	−6.01	5.26	11.27	0.00	0.49	786	96.4%	759	93.1%	98	1.9%
Petrosys	Hybrid	Bicubic interpolation, 1st order Taylor series	250	1	−5.23	4.45	9.69	0.00	0.41	792	97.2%	771	94.6%	101	2.0%
Petrosys	Hybrid	Bilinear interpolation, 1st order Taylor series	250	1	−6.01	5.26	11.27	0.00	0.49	786	96.4%	758	93.0%	98	1.9%
Petrosys	Hybrid	Bicubic interpolation, 2nd order Taylor series	250	1	−2.79	3.95	6.73	0.00	0.31	794	97.4%	777	95.3%	100	1.9%
Petrosys	Hybrid	Bilinear interpolation, 2nd order Taylor series	250	1	−6.01	5.26	11.27	0.00	0.49	786	96.4%	758	93.0%	98	1.9%
Petrosys	Distance Weighted Average	Bicubic interpolation, 1st order Taylor series	250	1	−6.57	6.74	13.31	−0.01	0.49	792	97.2%	764	93.7%	71	1.4%
Petrosys	Distance Weighted Average	Bilinear interpolation, 1st order Taylor series	250	1	−6.79	8.25	15.03	−0.01	0.59	784	96.2%	722	88.6%	71	1.4%
Petrosys	Minimum Curvature	Bicubic interpolation, 1st order Taylor series	500	2	−8.83	10.17	18.99	0.00	0.75	778	95.5%	732	89.8%	97	1.9%
Petrosys	Minimum Curvature	Bilinear interpolation, 1st order Taylor series	500	2	−8.58	12.57	21.14	0.00	0.85	761	93.7%	710	87.4%	96	1.9%

Note: 5 163 total springs. Cells are square.					Back interpolation to well data points Measured hydraulic head minus interpolated surface (m)									Back interp. to spring locations Spring elev. > ground elev.	
Gridding program	Gridding method	Gridding option	Grid cell length m	Gridding extent	Min.	Max.	Range	Average	Std. Dev.	COUNT within ±1 m	Percent within ±1 m	COUNT within ±0.5 m	Percent within ±0.5 m	COUNT	Percent
Petrosys	Minimum Curvature	Bicubic interpolation, 2nd order Taylor series	500	2	−7.41	9.24	16.65	0.01	0.65	781	95.8%	751	92.1%	121	2.4%
Petrosys	Minimum Curvature	Bilinear interpolation, 2nd order Taylor series	500	2	−7.50	11.47	18.97	0.01	0.76	772	95.1%	734	90.4%	109	2.1%
Petrosys	Minimum Curvature	Bilinear interpolation, 1st order Taylor series	500	1	−8.59	12.49	21.08	0.00	0.85	767	94.1%	716	87.9%	92	1.8%
Petrosys	Minimum Curvature	Bilinear interpolation, 2nd order Taylor series	500	1	−7.48	11.49	18.98	0.01	0.77	777	95.3%	740	90.8%	102	2.0%
Petrosys	Minimum Curvature	Bicubic interpolation, 1st order Taylor series	500	1	−8.83	10.13	18.97	0.00	0.75	778	95.5%	735	90.2%	95	1.9%
Petrosys	Minimum Curvature	Bicubic interpolation, 2nd order Taylor series	500	1	−7.44	9.31	16.75	0.01	0.66	782	96.0%	751	92.1%	92	1.8%
Petrosys	Polynomial	Bilinear interpolation, 1st order Taylor series	1000	1	−8.32	19.86	28.18	−0.01	1.24	712	87.4%	617	75.7%	99	1.9%
Petrosys	Minimum Curvature	Bilinear interpolation, 1st order Taylor series	1000	1	−8.52	19.82	28.34	−0.01	1.24	713	87.5%	615	75.5%	93	1.8%
Petrosys	Minimum Curvature	Bilinear interpolation, 2nd order Taylor series	1000	1	−7.77	20.27	28.04	0.00	1.17	735	90.2%	658	80.7%	102	2.0%
Petrosys	Minimum Curvature	Bicubic interpolation, 1st order Taylor series	1000	2	−9.32	18.45	27.77	−0.01	1.16	733	89.9%	658	80.7%	97	1.9%

Note: 5 163 total springs. Cells are square.					Back interpolation to well data points Measured hydraulic head minus interpolated surface (m)									Back interp. to spring locations Spring elev. > ground elev.	
Gridding program	Gridding method	Gridding option	Grid cell length m	Gridding extent	Min.	Max.	Range	Average	Std. Dev.	COUNT within ±1 m	Percent within ±1 m	COUNT within ±0.5 m	Percent within ±0.5 m	COUNT	Percent
Petrosys	Minimum Curvature	Bilinear interpolation, 1st order Taylor series	1000	2	−8.65	19.80	28.44	−0.01	1.25	708	87.2%	609	75.0%	96	1.9%
Petrosys	Minimum Curvature	Bicubic interpolation, 2nd order Taylor series	1000	2	−7.94	18.56	26.50	0.00	1.08	750	92.0%	699	85.8%	121	2.4%
Petrosys	Minimum Curvature	Bilinear interpolation, 2nd order Taylor series	1000	2	−7.67	20.53	28.21	0.01	1.17	732	90.1%	657	80.9%	109	2.1%
Petrosys	Minimum Curvature	Bicubic interpolation, 1st order Taylor series	1000	1	−9.33	18.43	27.75	−0.01	1.16	736	90.3%	658	80.7%	96	1.9%
Petrosys	Minimum Curvature	Bicubic interpolation, 2nd order Taylor series	1000	1	−8.59	18.78	27.38	0.00	1.09	758	93.0%	704	86.4%	92	1.8%
Petrosys	Least Square Plane	Bilinear interpolation, 1st order Taylor series	1000	1	−10.50	19.28	29.78	−0.06	1.88	494	60.8%	297	36.6%	60	1.2%
Petrosys	Least Square Binomial	Bilinear interpolation, 1st order Taylor series	1000	1	−8.32	19.86	28.18	−0.01	1.25	709	87.3%	614	75.6%	99	1.9%
Petrosys	Hybrid	Bicubic interpolation, 2nd order Taylor series	1000	1	−8.40	18.76	27.16	0.00	1.09	758	93.0%	702	86.1%	98	1.9%
Petrosys	Hybrid	Bilinear interpolation, 1st order Taylor series	1000	1	−8.32	19.86	28.18	−0.01	1.24	711	87.2%	615	75.5%	99	1.9%
Petrosys	Hybrid	Bicubic interpolation, 1st order Taylor series	1000	1	−9.14	18.43	27.57	−0.01	1.16	736	90.3%	656	80.5%	102	2.0%

Note: 5 163 total springs. Cells are square.					Back interpolation to well data points Measured hydraulic head minus interpolated surface (m)									Back interp. to spring locations Spring elev. > ground elev.	
Gridding program	Gridding method	Gridding option	Grid cell length m	Gridding extent	Min.	Max.	Range	Average	Std. Dev.	COUNT within ±1 m	Percent within ±1 m	COUNT within ±0.5 m	Percent within ±0.5 m	COUNT	Percent
Petrosys	Distance Weighted Average	Bicubic interpolation, 1st order Taylor series	1000	1	−11.62	17.02	28.64	−0.02	1.22	726	89.1%	647	79.4%	71	1.4%
Petrosys	Distance Weighted Average	Bilinear interpolation, 1st order Taylor series	1000	1	−10.88	18.31	29.19	−0.02	1.34	675	82.8%	559	68.6%	72	1.4%
Petrosys	Minimum Curvature	Bicubic interpolation, 1st order Taylor series	2000	2	−11.62	19.48	31.11	−0.03	1.50	643	78.9%	525	64.4%	97	1.9%
Petrosys	Minimum Curvature	Bilinear interpolation, 1st order Taylor series	2000	2	−10.39	20.55	30.93	−0.04	1.64	604	74.4%	454	55.9%	95	1.9%
Petrosys	Minimum Curvature	Bicubic interpolation, 2nd order Taylor series	2000	2	−9.53	21.71	31.23	0.01	1.36	692	84.9%	599	73.5%	117	2.3%
Petrosys	Minimum Curvature	Bilinear interpolation, 2nd order Taylor series	2000	2	−8.29	22.84	31.13	0.01	1.49	641	78.9%	534	65.8%	103	2.0%
Petrosys	Minimum Curvature	Bilinear interpolation, 1st order Taylor series	2000	1	−8.02	22.52	30.55	−0.02	1.63	611	75.0%	459	56.3%	93	1.8%
Petrosys	Minimum Curvature	Bilinear interpolation, 2nd order Taylor series	2000	1	−8.11	22.61	30.71	0.00	1.49	647	79.4%	534	65.5%	95	1.9%
Petrosys	Minimum Curvature	Bicubic interpolation, 1st order Taylor series	2000	1	−8.26	22.42	30.68	−0.01	1.50	656	80.5%	541	66.4%	95	1.9%

Note: 5 163 total springs. Cells are square.					Back interpolation to well data points Measured hydraulic head minus interpolated surface (m)									Back interp. to spring locations Spring elev. > ground elev.	
Gridding program	Gridding method	Gridding option	Grid cell length m	Gridding extent	Min.	Max.	Range	Average	Std. Dev.	COUNT within ±1 m	Percent within ±1 m	COUNT within ±0.5 m	Percent within ±0.5 m	COUNT	Percent
Petrosys	Minimum Curvature	Bicubic interpolation, 2nd order Taylor series	2000	1	−8.76	22.19	30.95	0.01	1.37	689	84.5%	610	74.8%	90	1.8%
Petrosys	Minimum Curvature	Bicubic interpolation, 1st order Taylor series	5000	2	−11.84	21.27	33.11	−0.12	2.42	457	56.3%	311	38.3%	89	1.7%
Petrosys	Minimum Curvature	Bilinear interpolation, 1st order Taylor series	5000	2	−12.74	20.47	33.21	−0.18	2.78	390	48.2%	234	28.9%	78	1.5%
Petrosys	Minimum Curvature	Bicubic interpolation, 2nd order Taylor series	5000	2	−9.62	22.06	31.68	−0.09	2.12	511	62.9%	375	46.2%	97	1.9%
Petrosys	Minimum Curvature	Bilinear interpolation, 2nd order Taylor series	5000	2	−10.19	22.07	32.26	−0.14	2.44	437	54.0%	285	35.2%	87	1.7%
Petrosys	Minimum Curvature	Bilinear interpolation, 1st order Taylor series	5000	1	−12.66	20.13	32.79	−0.16	2.76	394	48.3%	240	29.4%	79	1.5%
Petrosys	Minimum Curvature	Bilinear interpolation, 2nd order Taylor series	5000	1	−10.22	21.61	31.83	−0.11	2.43	450	55.2%	290	35.6%	96	1.9%
Petrosys	Minimum Curvature	Bicubic interpolation, 1st order Taylor series	5000	1	−11.77	21.06	32.83	−0.11	2.41	459	56.3%	297	36.4%	91	1.8%
Petrosys	Minimum Curvature	Bicubic interpolation, 2nd order Taylor series	5000	1	−9.73	22.08	31.81	−0.08	2.12	529	64.9%	387	47.5%	98	1.9%
Petrosys	Minimum Curvature	Bilinear interpolation, 1st order Taylor series	10000	1	−18.37	23.23	41.60	−0.17	4.66	260	31.9%	137	16.8%	34	0.7%

Note: 5 163 total springs. Cells are square.					Back interpolation to well data points Measured hydraulic head minus interpolated surface (m)									Back interp. to spring locations Spring elev. > ground elev.	
Gridding program	**Gridding method**	**Gridding option**	**Grid cell length m**	**Gridding extent**	**Min.**	**Max.**	**Range**	**Average**	**Std. Dev.**	**COUNT within ±1 m**	**Percent within ±1 m**	**COUNT within ±0.5 m**	**Percent within ±0.5 m**	**COUNT**	**Percent**
Petrosys	Minimum Curvature	Bilinear interpolation, 2nd order Taylor series	10000	1	−16.89	19.03	35.92	−0.24	3.94	303	37.2%	170	20.9%	39	0.8%
Petrosys	Minimum Curvature	Bicubic interpolation, 1st order Taylor series	10000	1	−15.44	19.12	34.56	−0.07	3.95	308	37.8%	164	20.1%	37	0.7%
Petrosys	Minimum Curvature	Bicubic interpolation, 2nd order Taylor series	10000	1	−13.28	20.68	33.96	−0.12	3.37	361	44.3%	222	27.2%	78	1.5%

C. EC to TDS conversion

Table 11.3: EC to TDS conversion table

EC (µS/cm)	TDS (mg/L)	Conversion factor	EC (µS/cm)	TDS (mg/L)	Conversion factor
100	55	0.55	5100	2852	0.559215686
200	110	0.55	5200	2909	0.559423077
300	165	0.55	5300	2966	0.559622642
400	220	0.55	5400	3023	0.559814815
500	275	0.55	5500	3080	0.56
600	330	0.55	5600	3137	0.560178571
700	385	0.55	5700	3195	0.560526316
800	440	0.55	5800	3252	0.560689655
900	495	0.55	5900	3309	0.560847458
1000	550	0.55	6000	3367	0.561166667
1100	605	0.55	6100	3424	0.561311475
1200	661	0.550833333	6200	3482	0.561612903
1300	716	0.550769231	6300	3539	0.561746032
1400	772	0.551428571	6400	3597	0.56203125
1500	827	0.551333333	6500	3654	0.562153846
1600	882	0.55125	6600	3712	0.562424242
1700	938	0.551764706	6700	3770	0.562686567
1800	994	0.552222222	6800	3827	0.562794118
1900	1049	0.552105263	6900	3885	0.563043478
2000	1105	0.5525	7000	3943	0.563285714
2100	1160	0.552380952	7100	4001	0.563521127
2200	1216	0.552727273	7200	4059	0.56375
2300	1272	0.553043478	7300	4117	0.563972603
2400	1328	0.553333333	7400	4175	0.564189189
2500	1384	0.5536	7500	4233	0.5644
2600	1440	0.553846154	7600	4291	0.564605263
2700	1496	0.554074074	7700	4349	0.564805195
2800	1552	0.554285714	7800	4407	0.565
2900	1608	0.554482759	7900	4465	0.565189873
3000	1664	0.554666667	8000	4524	0.5655
3100	1720	0.55483871	8100	4582	0.565679012
3200	1776	0.555	8200	4640	0.565853659
3300	1832	0.555151515	8300	4699	0.566144578
3400	1889	0.555588235	8400	4757	0.566309524
3500	1945	0.555714286	8500	4816	0.566588235
3600	2001	0.555833333	8600	4874	0.566744186
3700	2058	0.556216216	8700	4933	0.567011494
3800	2114	0.556315789	8800	4991	0.567159091
3900	2171	0.556666667	8900	5050	0.56741573
4000	2227	0.55675	9000	5109	0.567666667
4100	2284	0.557073171	9100	5167	0.567802198
4200	2340	0.557142857	9200	5226	0.568043478
4300	2397	0.55744186	9300	5285	0.56827957
4400	2454	0.557727273	9400	5344	0.568510638
4500	2510	0.557777778	9500	5403	0.568736842
4600	2567	0.558043478	9600	5462	0.568958333
4700	2624	0.558297872	9700	5521	0.569175258
4800	2681	0.558541667	9800	5580	0.569387755
4900	2738	0.55877551	9900	5639	0.56959596

EC (µS/cm)	TDS (mg/L)	Conversion factor	EC (µS/cm)	TDS (mg/L)	Conversion factor
5000	2795	0.559	10000	5698	0.5698
10500	5994	0.570857143	35500	22134	0.623492958
11000	6291	0.571909091	36000	22483	0.624527778
11500	6590	0.573043478	36500	22833	0.625561644
12000	6889	0.574083333	37000	23183	0.626567568
12500	7190	0.5752	37500	23535	0.6276
13000	7491	0.576230769	38000	23888	0.628631579
13500	7794	0.577333333	38500	24241	0.629636364
14000	8098	0.578428571	39000	24596	0.630666667
14500	8402	0.579448276	39500	24952	0.631696203
15000	8708	0.580533333	40000	25308	0.6327
15500	9015	0.581612903	40500	25666	0.633728395
16000	9323	0.5826875	41000	26024	0.634731707
16500	9632	0.583757576	41500	26384	0.635759036
17000	9942	0.584823529	42000	26744	0.636761905
17500	10253	0.585885714	42500	27106	0.637788235
18000	10565	0.586944444	43000	27468	0.638790698
18500	10878	0.588	43500	27831	0.639793103
19000	11192	0.589052632	44000	28196	0.640818182
19500	11507	0.590102564	44500	28561	0.641820225
20000	11824	0.5912	45000	28927	0.642822222
20500	12141	0.592243902	45500	29295	0.643846154
21000	12459	0.593285714	46000	29663	0.644847826
21500	12788	0.594790698	46500	30032	0.645849462
22000	13099	0.595409091	47000	30402	0.646851064
22500	13420	0.596444444	47500	30773	0.647852632
23000	13743	0.597521739	48000	31145	0.648854167
23500	14066	0.598553191	48500	31518	0.64985567
24000	14391	0.599625	49000	31892	0.650857143
24500	14716	0.600653061	49500	32267	0.651858586
25000	15043	0.60172	50000	32643	0.65286
25500	15370	0.602745098	50500	33019	0.653841584
26000	15699	0.603807692	51000	33397	0.654843137
26500	16029	0.604867925	51500	33776	0.65584466
27000	16359	0.605888889	52000	34155	0.656826923
27500	16691	0.606945455	52500	34536	0.657828571
28000	17024	0.608	53000	34917	0.658811321
28500	17357	0.609017544	53500	35300	0.659813084
29000	17692	0.610068966	54000	35683	0.660796296
29500	18028	0.611118644	54500	36067	0.661779817
30000	18364	0.612133333	80000	56000	0.7
30500	18702	0.613180328	100000	80000	0.8
31000	19041	0.614225806	140000	119000	0.85
31500	19381	0.615269841			
32000	19721	0.61628125			
32500	20063	0.617323077			
33000	20406	0.618363636			
33500	20750	0.619402985			
34000	21094	0.620411765			
34500	21440	0.621449275			
35000	21787	0.622485714			

D. Exploration of density corrections applied to the uncorrected potentiometric surface grids

An alternative density correction process was tested by applying the density correction to each cell of the uncorrected potentiometric surface grids as opposed to the individual well observations. Equations 1, 3, 4, and 6 were applied using the Raster Calculator in QGIS. A multi-step process for each potentiometric surface included:

- calculating the density of groundwater in the J-K aquifer as a function of temperature (Equation 3). This required:
    a. converting individual raster cells from units of m AHD to MPa
    b. calculating a representative aquifer temperature for every raster cell (Equation 6) which assumed a linear temperature gradient between the ground surface and mid-point depth of the J-K aquifer, consistent with the assumptions described in Section 5.2 for assigning bottom-hole temperatures. The choice of the mid-point depth of the J-K aquifer was preferred over the top or base of the aquifer to be uniform with the position that hydraulic heads are inferred in numerical model cells. The mid-point depth of the J-K aquifer reaches a depth of approximately 2,300 m in the Poolowanna Trough (Figure 11.5A). An obvious, sharp elevation change within the Poolowanna Trough aligns with the edge of the Birkhead Formation. The resulting groundwater temperature distribution also replicates the sharp step-change along the edge of the Birkhead Formation (Figure 11.5A).
- calculating the density of groundwater in the J-K aquifer as a function of temperature and salinity (Equation 4); which required 'rasterizing' the Thiessen polygons of J-K aquifer salinity into 50 m and 100 m cell sizes in QGIS
- calculating the reference-density head (Equation 1), which applied the elevation of the mid-point of the J-K aquifer as the z_i.

Figure 11.5B demonstrates one of the resulting potentiometric surface grids (using the uncorrected potentiometric surface Minimum Curvature, internal tension, and boundary tension both equal to 0.5) as an example. The other 18 density-corrected potentiometric surface grids with variations on the gridding settings are not presented here. Abrupt changes in the hydraulic head are evident at the boundary of the Birkhead Formation and along numerous salinity polygons. Equipotentials generated from this, and some other density-corrected grids presented chaotic, non-smooth contours that do not resemble the current conceptual understanding of groundwater flow conditions.

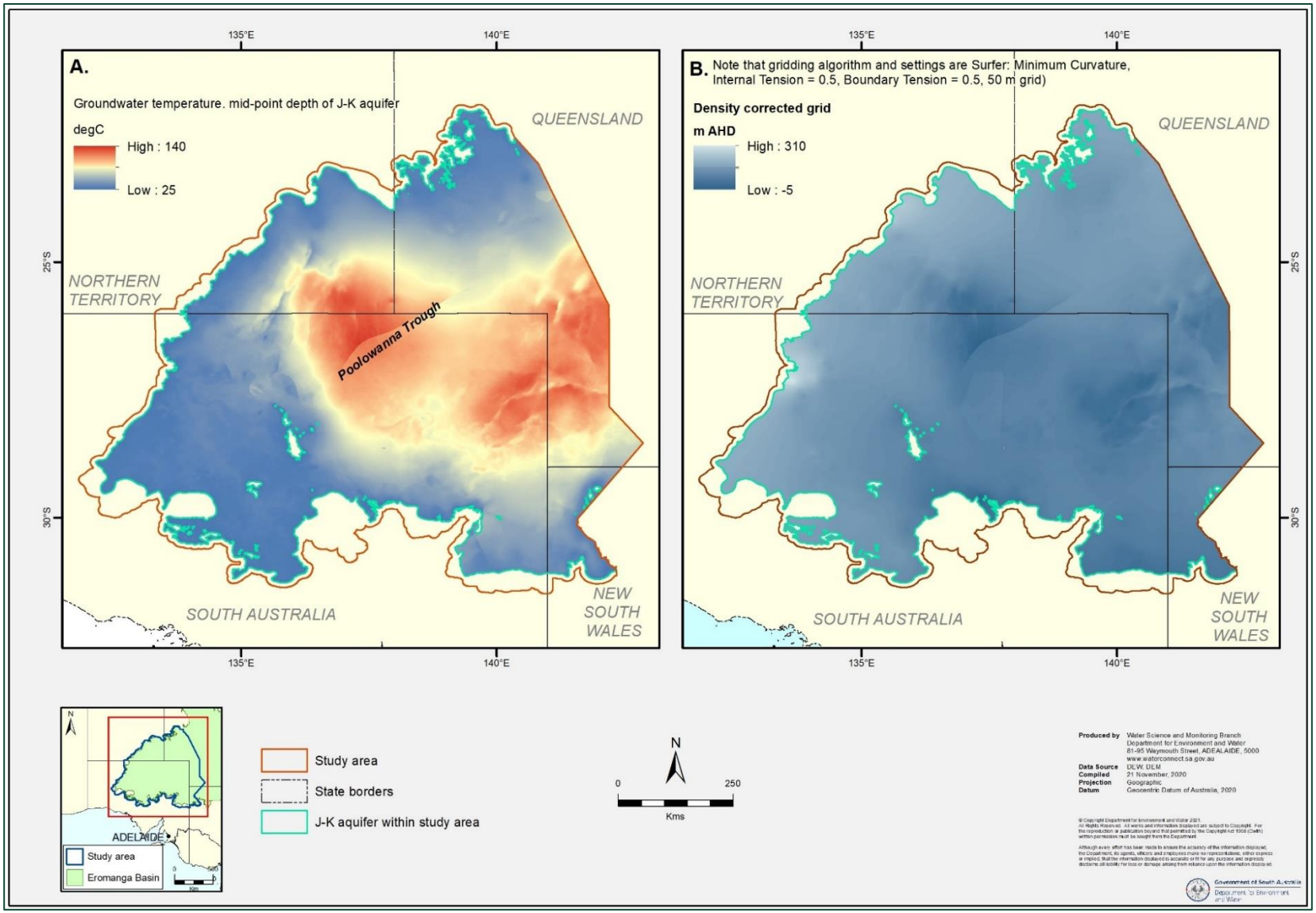

Figure 11.5: A) Groundwater temperature of the J-K aquifer (mid-point) and B) 2019 density-corrected potentiometric surface (grid method) of the J-K aquifer

E. 2019 Uncorrected Potentiometric Surface Contour Maps

Groupings are based off gross similarities in potentiometric surface characteristics. Chapter 6 provides descriptions of the groupings.

Figure .11.6: 2019 uncorrected potentiometric surfaces of the J-K aquifer (I)**, shown in Figure 11.6**

Group 1: Minimum Curvature, Internal Tension = 0, Boundary Tension = 0 (*Surfer*, 50 m grid)

Minimum Curvature, Internal Tension = 0, Boundary Tension = 1 (*Surfer*, 50 m grid)

Group 2: Minimum Curvature, Internal Tension =1, Boundary Tension = 1 (*Surfer*, 50 m grid)

Minimum Curvature, Internal Tension = 1, Boundary Tension = 0 (*Surfer*, 50 m grid)

Figure 11.7: 2019 uncorrected potentiometric surface of the J-K aquifer (II)**, shown in Figure 11.7**

Group 3: Minimum Curvature, Internal Tension = 0.25, Boundary Tension = 0.75 (*Surfer*, 50 m grid)

Minimum Curvature, Internal Tension = 0.5, Boundary Tension = 0.5 (*Surfer*, 50 m grid)

Minimum Curvature, Internal Tension = 0.75, Boundary Tension = 0.25 (*Surfer*, 50 m grid)

Least Square Plane, Bilinear interpolation, 1st order Taylor series (*Petrosys*, 100 m grid)

Figure 11.8: 2019 uncorrected potentiometric surface of the J-K aquifer (III)**, shown in Figure 11.8**

Group 3: Least Square Binomial. Bilinear interpolation, 1st order Taylor series (*Petrosys*, 100 m grid)

Distance Weighted Average, Bilinear interpolation, 1st order Taylor series (*Petrosys*, 100 m grid)

Distance Weighted Average, Bicubic interpolation, 1st order Taylor series (*Petrosys*, 100 m grid)

Figure 11.9: 2019 uncorrected potentiometric surface of the J-K aquifer (IV)**, shown in Figure 11.9**

Group 4: Minimum Curvature, Bicubic interpolation, 1st order Taylor series (*Petrosys*, 100 m grid)

Minimum Curvature, Bicubic interpolation, 2nd order Taylor series (*Petrosys*, 100 m grid)

Minimum Curvature, Bilinear interpolation, 1st order Taylor series (*Petrosys*, 100 m grid)

Minimum Curvature, Bilinear interpolation, 2nd order Taylor series (*Petrosys*, 100 m grid)

Figure 11.10: 2019 uncorrected potentiometric surface of the J-K aquifer (V)**, shown in Figure 11.10**

Group 4: Hybrid, Bicubic interpolation, 1st order Taylor series (*Petrosys*, 100 m grid)

Hybrid, Bicubic interpolation, 2nd order Taylor series (Petrosys, 100 m grid)

Hybrid, Bilinear interpolation, 1st order Taylor series (Petrosys, 100 m grid)

Hybrid, Bilinear interpolation, 2nd order Taylor series (Petrosys, 100 m grid)

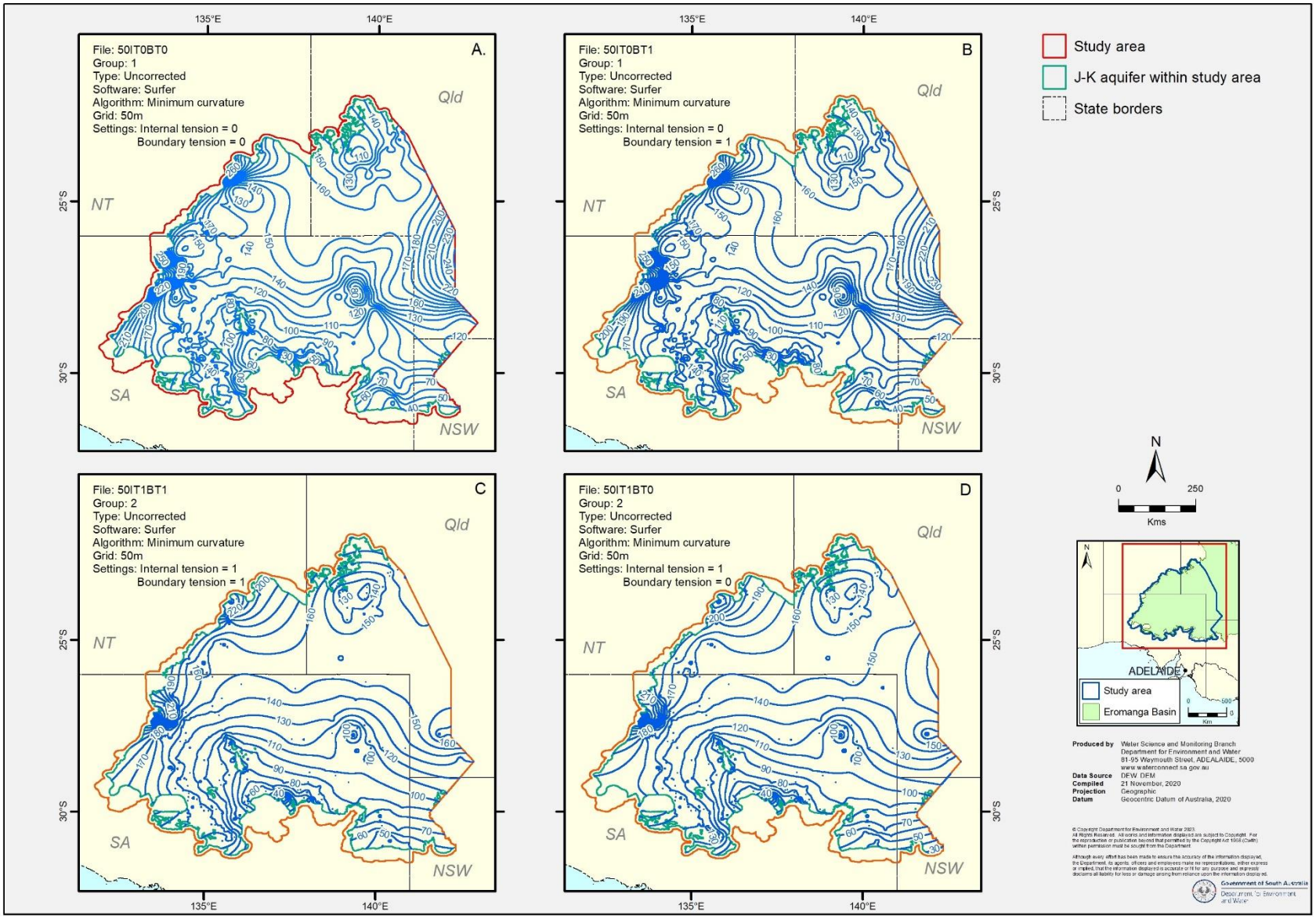

Figure .11.6: 2019 uncorrected potentiometric surfaces of the J-K aquifer (I)

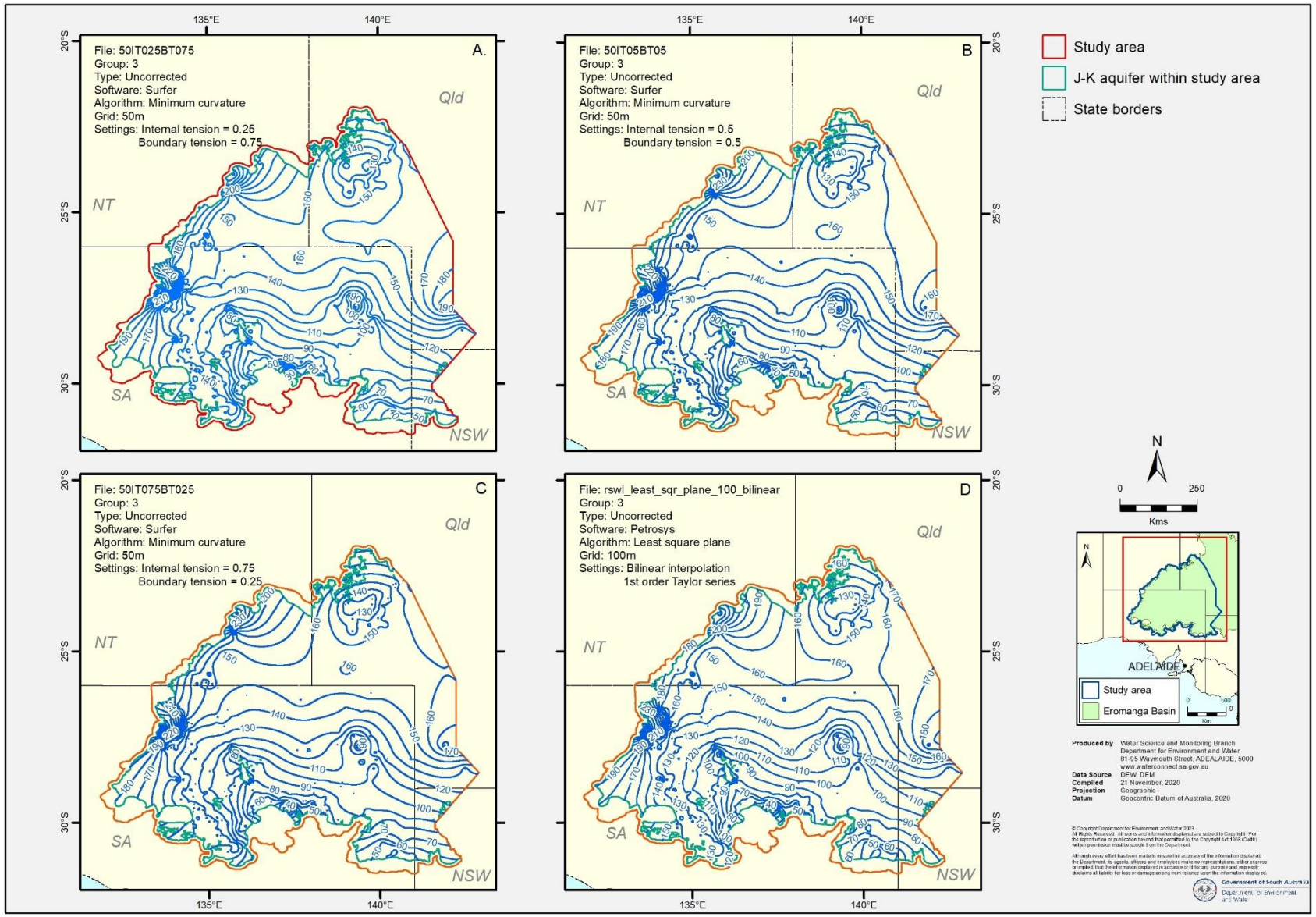

Figure 11.7: 2019 uncorrected potentiometric surface of the J-K aquifer (II)

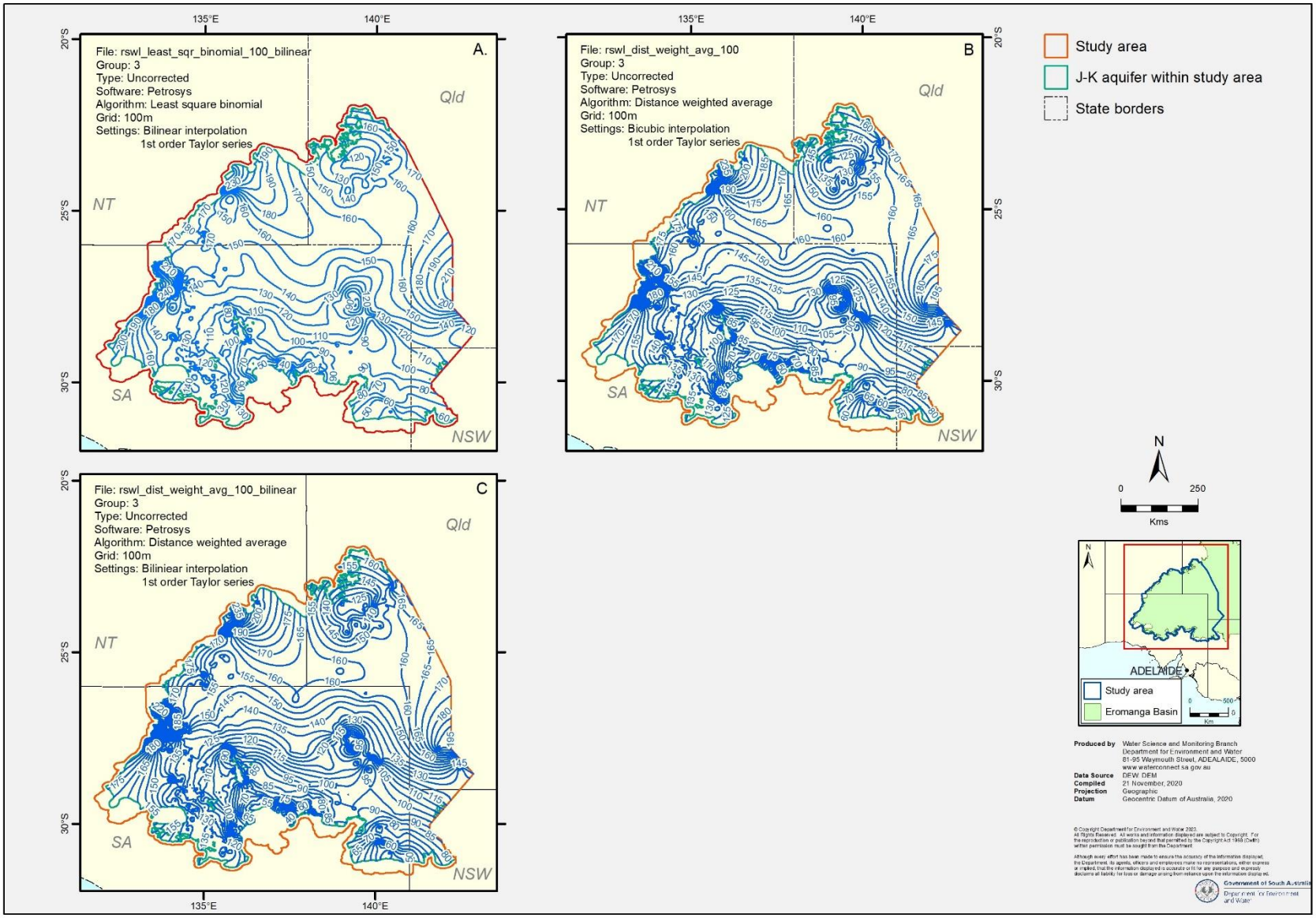

Figure 11.8: 2019 uncorrected potentiometric surface of the J-K aquifer (III)

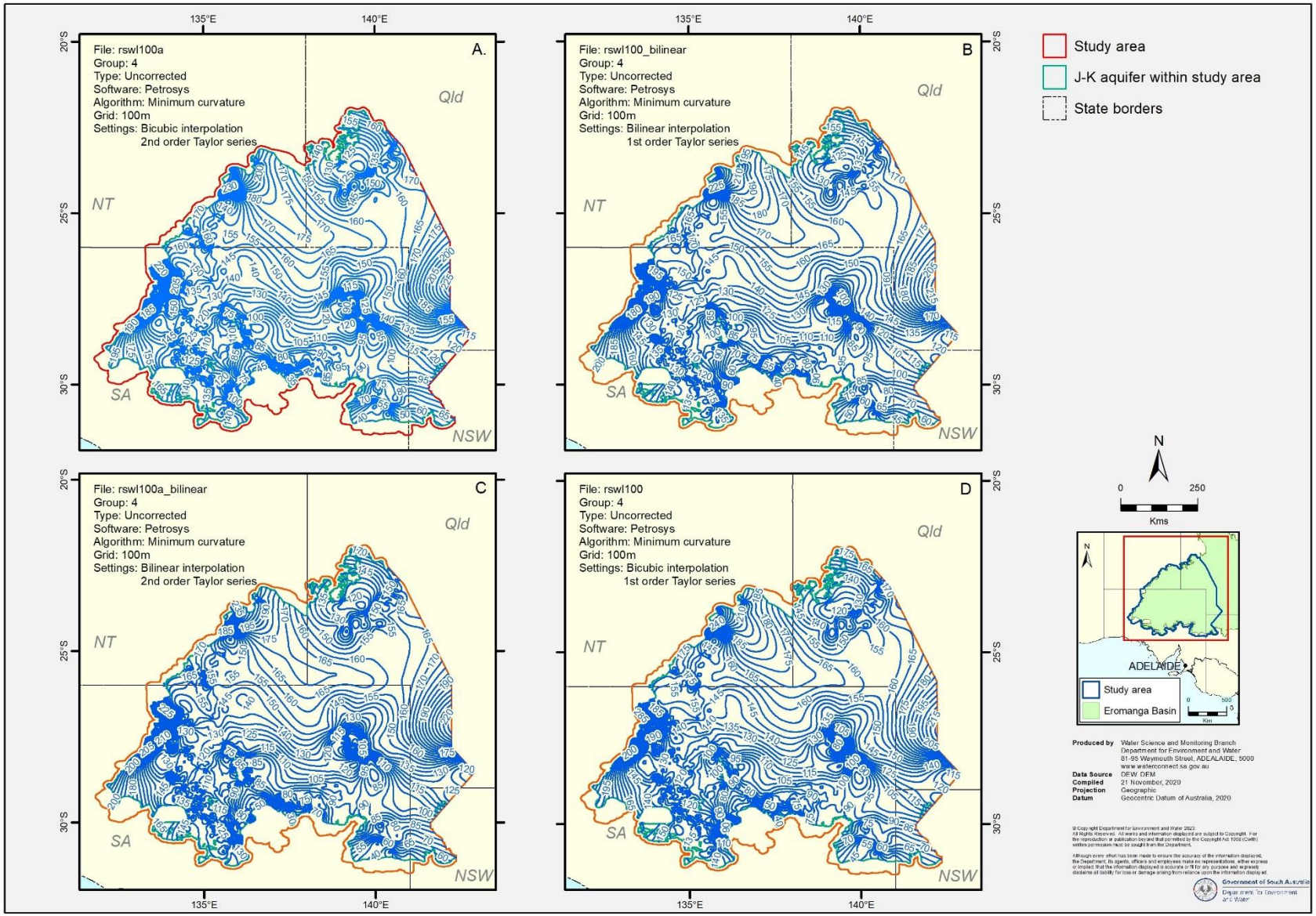

Figure 11.9: 2019 uncorrected potentiometric surface of the J-K aquifer (IV)

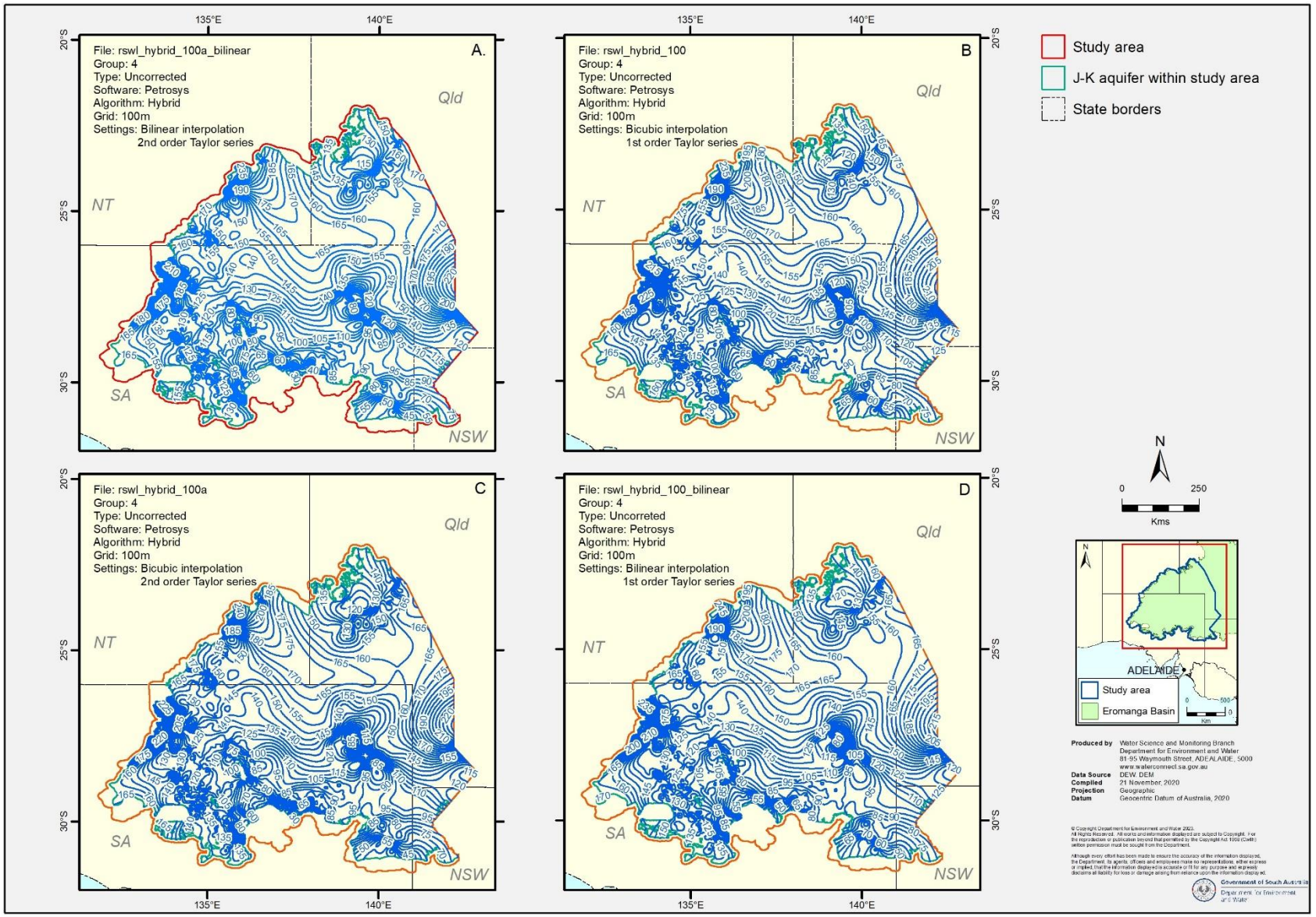

Figure 11.10: 2019 uncorrected potentiometric surface of the J-K aquifer (V)

F. 2019 Density-corrected Potentiometric Surface Contour Maps

Groupings are based off gross similarities in potentiometric surface characteristics. Chapter 6 provides descriptions of the groupings.

Figure 11.11: 2019 density-corrected potentiometric surface of the J-K aquifer (I)**, shown in Figure 11.11**

Group 1: Minimum Curvature, Internal Tension = 0, Boundary Tension = 0 (*Surfer*, 50 m grid)

Minimum Curvature, Internal Tension = 0, Boundary Tension = 1 (*Surfer*, 50 m grid)

Group 2: Minimum Curvature, Internal Tension =1, Boundary Tension = 1 (*Surfer*, 50 m grid)

Minimum Curvature, Internal Tension = 1, Boundary Tension = 0 (*Surfer*, 50 m grid)

Figure 11.12: 2019 density-corrected potentiometric surface of the J-K aquifer (II)**, shown in Figure 11.12**

Group 3: Minimum Curvature, Internal Tension = 0.25, Boundary Tension = 0.75 (*Surfer*, 50 m grid)

Minimum Curvature, Internal Tension = 0.5, Boundary Tension = 0.5 (*Surfer*, 50 m grid)

Minimum Curvature, Internal Tension = 0.75, Boundary Tension = 0.25 (*Surfer*, 50 m grid)

Least Square Plane, Bilinear interpolation, 1st order Taylor series (*Petrosys*, 100 m grid)

Figure 11.13: 2019 density-corrected potentiometric surface of the J-K aquifer (III)**, shown in Figure 11.13**

Group 3: Least Square Binomial. Bilinear interpolation, 1st order Taylor series (*Petrosys*, 100 m grid)

Distance Weighted Average, Bilinear interpolation, 1st order Taylor series (*Petrosys*, 100 m grid)

Distance Weighted Average, Bicubic interpolation, 1st order Taylor series (*Petrosys*, 100 m grid)

Figure 11.14: 2019 density-corrected potentiometric surface of the J-K aquifer (IV)**, shown in Figure 11.14**

Group 4: Minimum Curvature, Bicubic interpolation, 1st order Taylor series (*Petrosys*, 100 m grid)

Minimum Curvature, Bicubic interpolation, 2nd order Taylor series (*Petrosys*, 100 m grid)

Minimum Curvature, Bilinear interpolation, 1st order Taylor series (*Petrosys*, 100 m grid)

Minimum Curvature, Bilinear interpolation, 2nd order Taylor series (*Petrosys*, 100 m grid)

Figure 11.15: 2019 density-corrected potentiometric surface of the J-K aquifer (V)**, shown in Figure 11.15**

Group 4: Hybrid, Bicubic interpolation, 1st order Taylor series (*Petrosys*, 100 m grid)

Hybrid, Bicubic interpolation, 2nd order Taylor series (Petrosys, 100 m grid)

Hybrid, Bilinear interpolation, 1st order Taylor series (Petrosys, 100 m grid)

Hybrid, Bilinear interpolation, 2nd order Taylor series (Petrosys, 100 m grid)

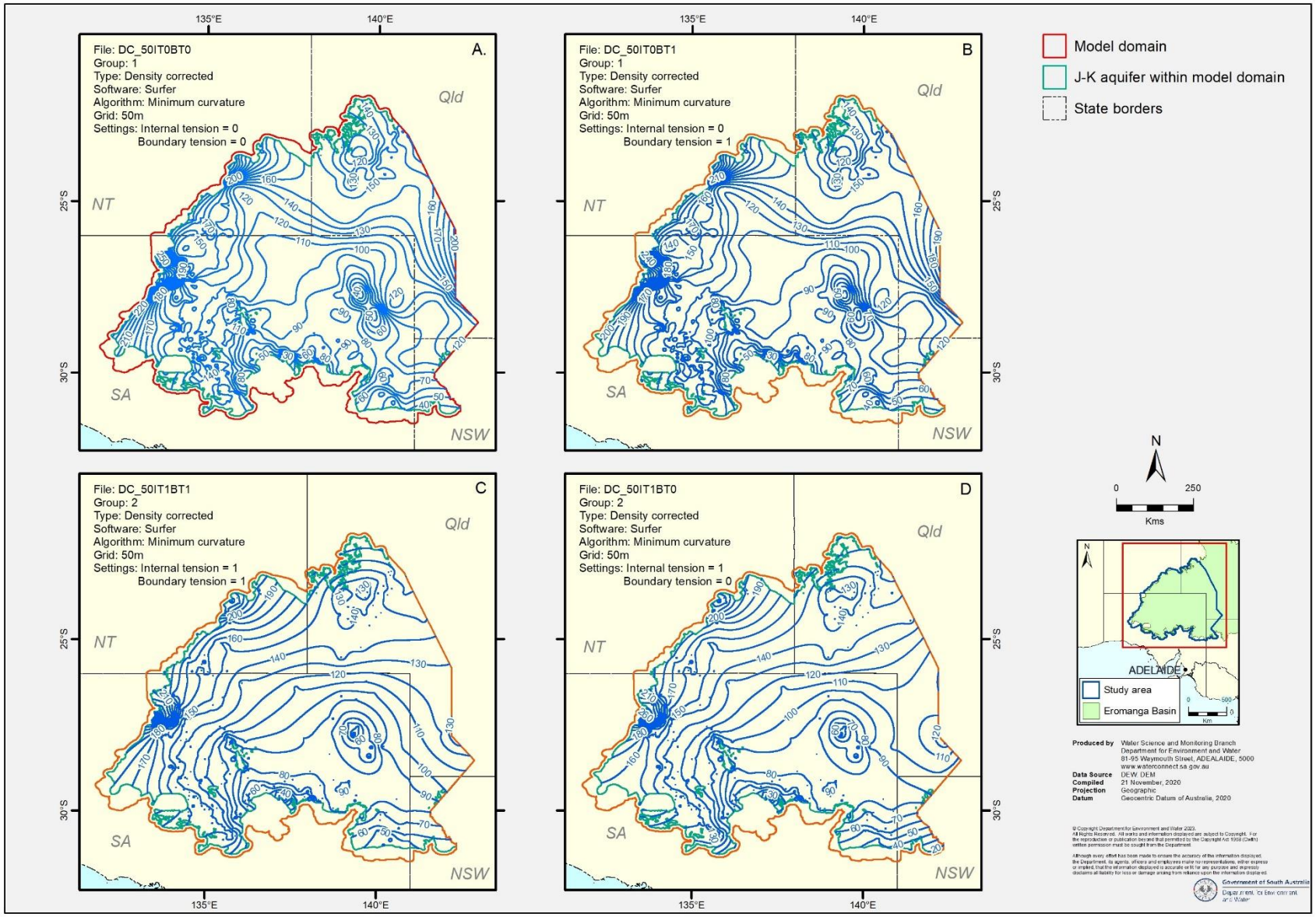

Figure 11.11: 2019 density-corrected potentiometric surface of the J-K aquifer (I)

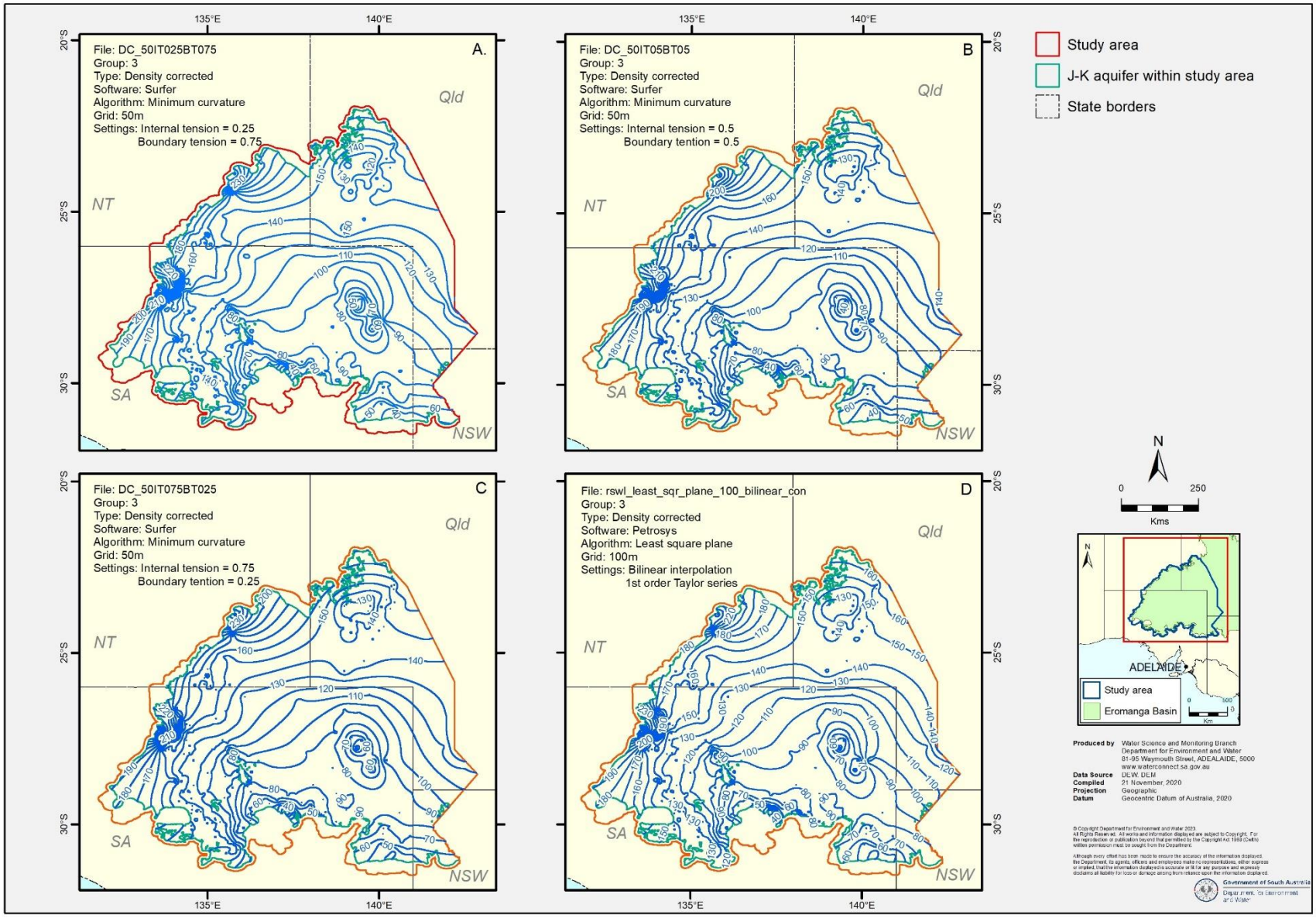

Figure 11.12: 2019 density-corrected potentiometric surface of the J-K aquifer (II)

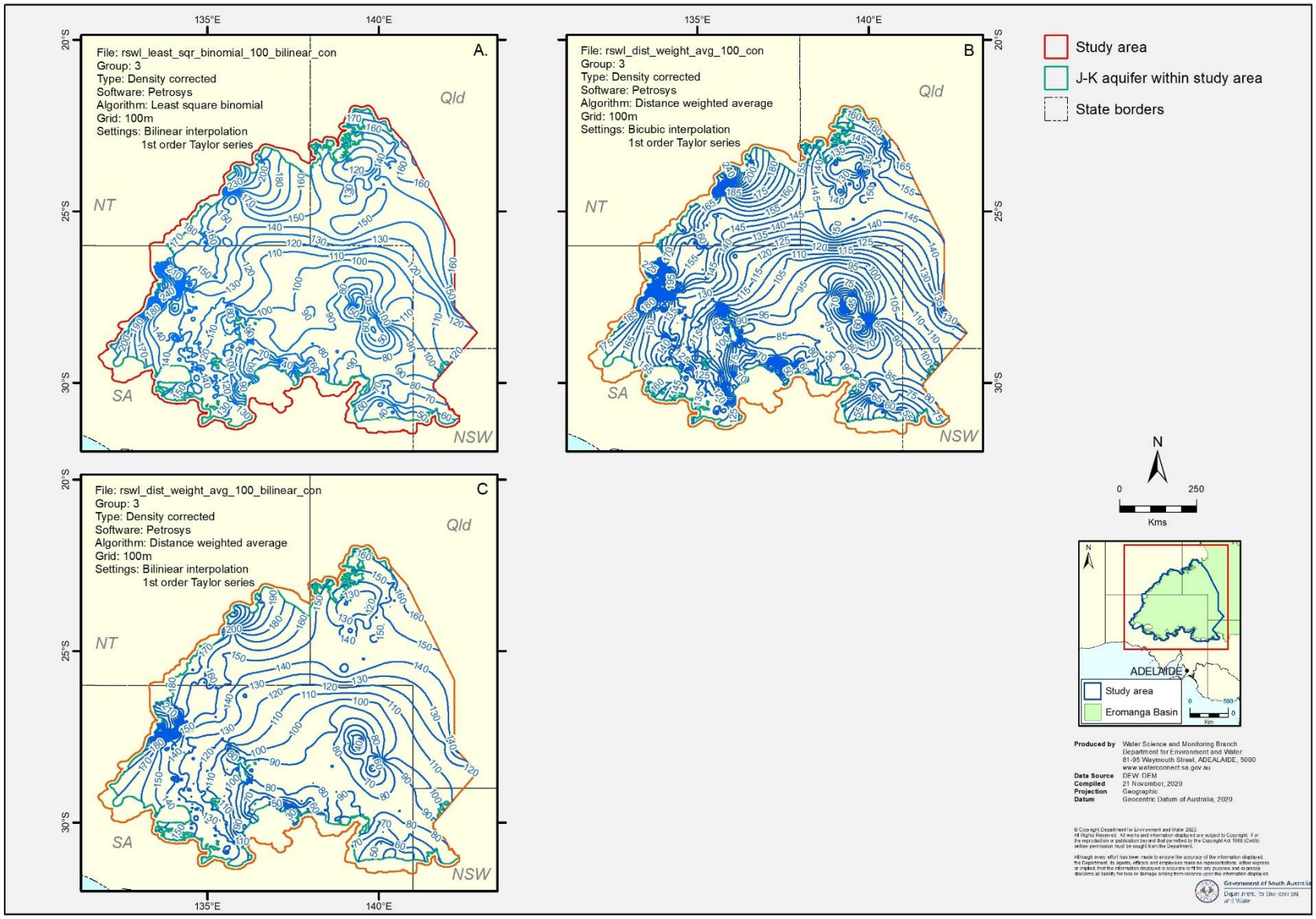

Figure 11.13: 2019 density-corrected potentiometric surface of the J-K aquifer (III)

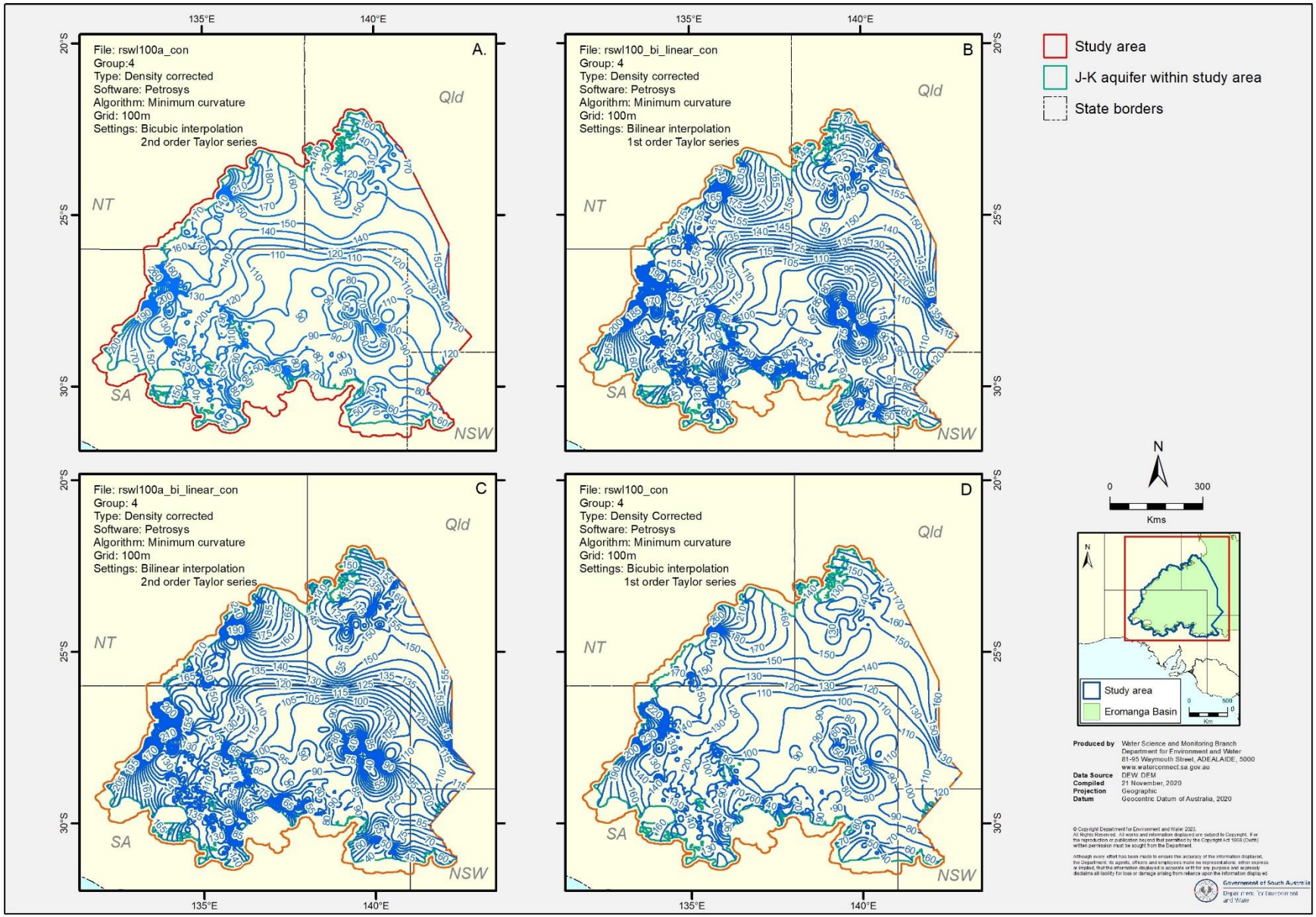

Figure 11.14: 2019 density-corrected potentiometric surface of the J-K aquifer (IV)

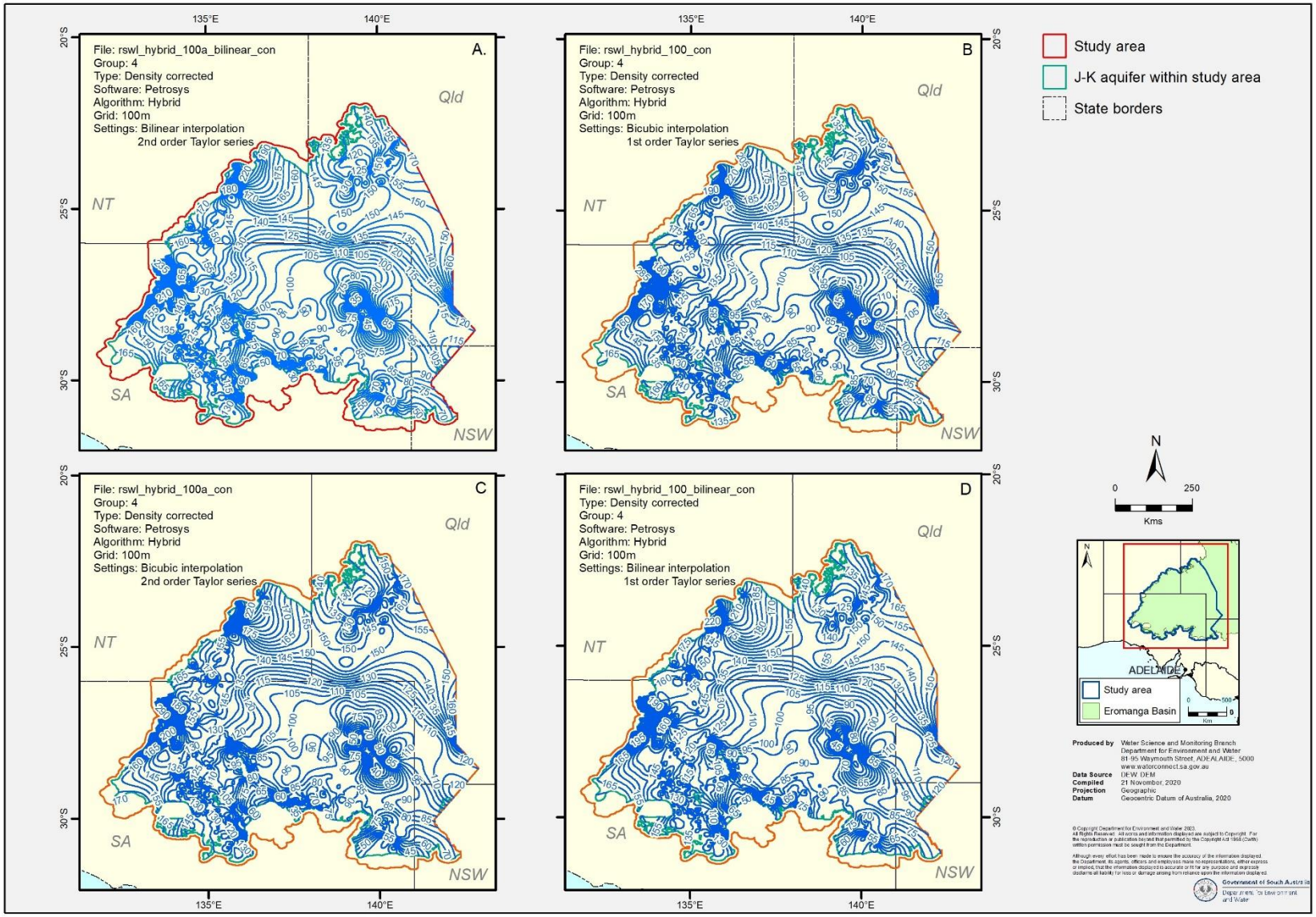

Figure 11.15: 2019 density-corrected potentiometric surface of the J-K aquifer (V)

12 Units of measurement

12.1 Units of measurement commonly used (SI and non-SI Australian legal)

Name of unit	Symbol	Definition in terms of other metric units	Quantity
day	d	24 h	time interval
gigalitre	GL	10^6 m^3	volume
gram	g	10^{-3} kg	mass
hectare	ha	10^4 m^2	area
hour	h	60 min	time interval
kilogram	kg	base unit	mass
kilolitre	kL	1 m^3	volume
kilometre	km	10^3 m	length
litre	L	10^{-3} m^3	volume
megalitre	ML	10^3 m^3	volume
metre	m	base unit	length
microgram	µg	10^{-6} g	mass
microlitre	µL	10^{-9} m^3	volume
milligram	mg	10^{-3} g	mass
millilitre	mL	10^{-6} m^3	volume
millimetre	mm	10^{-3} m	length
minute	min	60 s	time interval
second	s	base unit	time interval
tonne	t	1000 kg	mass
year	y	365 or 366 days	time interval

12.2 Shortened forms

bgs below ground surface

EC electrical conductivity (µS/cm)

13 Glossary

Act (the) — In this document, refers to the *Natural Resources Management (SA) Act 2004,* which supersedes the *Water Resources (SA) Act 1997*

Ambient — The background level of an environmental parameter (e.g. a measure of water quality such as salinity)

Ambient water monitoring — All forms of monitoring conducted beyond the immediate influence of a discharge pipe or injection well, and may include sampling of sediments and living resources

Ambient water quality — The overall quality of water when all the effects that may impact upon the water quality are taken into consideration

Aquiclude — In hydrologic terms, a formation that contains water but cannot transmit it rapidly enough to furnish a significant supply to a well or spring

Aquifer — An underground layer of rock or sediment that holds water and allows water to percolate through

Aquifer, confined — Aquifer in which the upper surface is impervious (see 'confining unit') and the water is held at greater than atmospheric pressure; water in a penetrating well will rise above the surface of the aquifer

Aquifer test — A hydrological test performed on a well, aimed to increase the understanding of the aquifer properties, including any interference between wells, and to more accurately estimate the sustainable use of the water resources available for development from the well

Aquifer, unconfined — Aquifer in which the upper surface has free connection to the ground surface and the water surface is at atmospheric pressure

Aquitard — A layer in the geological profile that separates two aquifers and restricts the flow between them

ArcGIS — Specialised GIS software for mapping and analysis developed by ESRI

Arid lands — In South Australia, arid lands are usually considered to be areas with an average annual rainfall of less than 250 mm and support pastoral activities instead of broadacre cropping

Artesian — An aquifer in which the water surface is bounded by an impervious rock formation; the water surface is at greater than atmospheric pressure, and hence rises in any well, which penetrates the overlying confining aquifer

Artificial recharge — The process of artificially diverting water from the surface to an aquifer; artificial recharge can reduce evaporation losses and increase aquifer yield; see also 'natural recharge', 'aquifer'

Basin — The area drained by a major river and its tributaries

BoM — Bureau of Meteorology, Australia

Bore — See 'well'

Buffer zone — A neutral area that separates and minimises interactions between zones whose management objectives are significantly different or in conflict (e.g. a vegetated riparian zone can act as a buffer to protect the water quality and streams from adjacent land uses)

^{14}C — Carbon-14 isotope (percent modern Carbon; pMC)

Catchment — That area of land determined by topographic features within which rainfall will contribute to runoff at a particular point

CFC — Chlorofluorocarbon; measured in parts per trillion (ppt)

Climate change — The balance of incoming and outgoing solar radiation which regulates our climate. Changes to the composition of the atmosphere, such as the addition of carbon dioxide through human activities, have the potential to alter the radiation balance and to effect changes to the climate. Scientists suggest that changes would include global warming, a rise in sea level and shifts in rainfall patterns.

CMB — Chloride mass balance

Cone of depression — An inverted cone-shaped space within an aquifer caused by a rate of groundwater extraction that exceeds the rate of recharge; continuing extraction of water can extend the area and may affect the viability of adjacent wells, due to declining water levels or water quality

Confining unit — A rock unit impervious to water, which forms the upper bound of a confined aquifer; a body of impermeable material adjacent to an aquifer; see also 'aquifer, confined'

CSG — coal seam gas

CSIRO — Commonwealth Scientific and Industrial Research Organisation

δD — Hydrogen isotope composition, measured in parts per thousand (**‰**)

Dams, off-stream dam — A dam, wall or other structure that is not constructed across a watercourse or drainage path and is designed to hold water diverted or pumped from a watercourse, a drainage path, an aquifer or from another source; may capture a limited volume of surface water from the catchment above the dam

Dams, on-stream dam — A dam, wall or other structure placed or constructed on, in or across a watercourse or drainage path for the purpose of holding and storing the natural flow of that watercourse or the surface water

Dams, turkey nest dam — An off-stream dam that does not capture any surface water from the catchment above the dam

DEW — Department for Environment and Water

DEWNR — Department of Environment, Water and Natural Resources (Government of South Australia)

DfW — former Department for Water (Government of South Australia)

dGPS — differential Global Positioning System

DO — Dissolved Oxygen

DOC — Dissolved Organic Carbon

Domestic purpose — The taking of water for ordinary household purposes; includes the watering of land in conjunction with a dwelling not exceeding 0.4 hectares

Dryland salinity — The process whereby salts stored below the surface of the ground are brought close to the surface by the rising watertable. The accumulation of salt degrades the upper soil profile, with impacts on agriculture, infrastructure and the environment.

DSS — Dissolved suspended solids

DWLBC — former Department of Water, Land and Biodiversity Conservation (Government of South Australia)

EC — Electrical conductivity; 1 EC unit = 1 micro-Siemen per centimetre (µS/cm) measured at 25°C; commonly used as a measure of water salinity as it is quicker and easier than measurement by TDS

Ecology — The study of the relationships between living organisms and their environment

Ecological processes — All biological. physical or chemical processes that maintain an ecosystem

Ecological values — The habitats, natural ecological processes and biodiversity of ecosystems

Ecosystem — Any system in which there is an interdependence upon, and interaction between, living organisms and their immediate physical, chemical and biological environment

Endemic — A plant or animal restricted to a certain locality or region

Environmental values — The uses of the environment that are recognised as being of value to the community. This concept is used in setting water quality objectives under the Environment Protection (Water Quality) Policy, which recognises five environmental values — protection of aquatic ecosystems, recreational water use and aesthetics, potable (drinking water) use, agricultural and aquaculture use, and industrial use. It is not the same as ecological values, which are about the elements and functions of ecosystems.

Ephemeral streams or wetlands — Those streams or wetlands that usually contain water only on an occasional basis after rainfall events. Many arid zone streams and wetlands are ephemeral.

Erosion — Natural breakdown and movement of soil and rock by water, wind or ice; the process may be accelerated by human activities

Evapotranspiration — The total loss of water as a result of transpiration from plants and evaporation from land, and surface water bodies

Fresh — A short duration, small volume pulse of streamflow generated by a rainfall event that temporarily, but noticeably, increases stream discharge above ambient levels

Fully-penetrating well — In theory this is a well-hole that is screened throughout the full thickness of the target aquifer; in practice, any screen that is open to at least the mid 80% of a confined aquifer is regarded as fully-penetrating.

GAB — Great Artesian Basin

GDE — Groundwater dependent ecosystem

Geological features — Include geological monuments, landscape amenity and the substrate of land systems and ecosystems

Geomorphic — Related to the physical properties of the rock, soil and water in and around a stream

Geomorphology — The scientific study of the landforms on the Earth's surface and of the processes that have fashioned them

GIS — Geographic Information System; computer software linking geographic data (for example land parcels) to textual data (soil type, land value, ownership). It allows for a range of features, from simple map production to complex data analysis

Groundwater — Water occurring naturally below ground level or water pumped, diverted and released into a well for storage underground; see also 'underground water'

Groundwater Data — Interactive map and search tool for viewing information about South Australia's wells with access to well details including, graphs showing water salinity and water level. It provides a variety of search methods, including filtering the results. [*waterconnect.sa.gov.au/Systems/GD/]*

Head (hydraulic) — Sum of datum level, elevation head and pressure head. The altitude to which water will rise in a properly constructed well. In unconfined aquifers it is the groundwater elevation, and in confined aquifers it is the potentiometric head.

Hydraulic conductivity (K) — A measure of the ease of flow through aquifer material: high K indicates low resistance, or high flow conditions; measured in metres per day

Hydrogeology — The study of groundwater, which includes its occurrence, recharge and discharge processes, and the properties of aquifers; see also 'hydrology'

Hydrography — The discipline related to the measurement and recording of parameters associated with the hydrological cycle, both historic and real time

Hydrology — The study of the characteristics, occurrence, movement and utilisation of water on and below the Earth's surface and within its atmosphere; see also 'hydrogeology'

Infrastructure — Artificial lakes; dams or reservoirs; embankments, walls, channels or other works; buildings or structures; or pipes, machinery or other equipment

Injection well — An artificial recharge well through which water is pumped or gravity-fed into the ground

Irrigation — Watering land by any means for the purpose of growing plants

Kati Thanda-Lake Eyre — Lake Eyre was co-named with the name used by the Arabana people in December 2012

Kati Thanda-Lake Eyre National Park — was proclaimed in November 2013 to recognise the significance of Lake Eyre to the Arabana people and co-name the lake Kati Thanda-Lake Eyre.

Lake — A natural lake, pond, lagoon, wetland or spring (whether modified or not) that includes part of a lake and a body of water declared by regulation to be a lake. A reference to a lake is a reference to either the bed, banks and shores of the lake or the water for the time being held by the bed, banks and shores of the lake, or both, depending on the context.

Land — Whether under water or not, and includes an interest in land and any building or structure fixed to the land

Licence — A licence to take water in accordance with the Act; see also 'water licence'

Licensee — A person who holds a water licence

LMWL — Local meteoric water line

m AHD — Defines elevation in metres (m) according to the Australian Height Datum (AHD)

MAR — Managed aquifer recharge (MAR) is a process where water is intentionally placed and stored in an aquifer for later human use, or to benefit the environment.

Metadata — Information that describes the content, quality, condition, and other characteristics of data, maintained by the Federal Geographic Data Committee

Model — A conceptual or mathematical means of understanding elements of the real world that allows for predictions of outcomes given certain conditions. Examples include estimating storm runoff, assessing the impacts of dams or predicting ecological response to environmental change

MODFLOW — A three-dimensional., finite difference code developed by the USGS to simulate groundwater flow

Molar (M) — A term describing the concentration of chemical solutions in moles per litre (mol/L)

Monitoring — (1) The repeated measurement of parameters to assess the current status and changes over time of the parameters measured (2) Periodic or continuous surveillance or testing to determine the level of compliance with statutory requirements and/or pollutant levels in various media or in humans, animals, and other living things

Natural recharge — The infiltration of water into an aquifer from the surface (rainfall, streamflow, irrigation etc). See also recharge area, artificial recharge

Natural resources — Soil, water resources, geological features and landscapes, native vegetation, native animals and other native organisms, ecosystems

NRM — Natural Resources Management; all activities that involve the use or development of natural resources and/or that impact on the state and condition of natural resources, whether positively or negatively

NWC — National Water Commission

$\delta^{18}O$ — Oxygen isotope composition, measured in parts per thousand (**‰**)

Observation well — A narrow well or piezometer whose sole function is to permit water level measurements

ORP — Oxidation Reduction Potential

Owner of land — In relation to land alienated from the Crown by grant in fee simple — the holder of the fee simple; in relation to dedicated land within the meaning of the *Crown Lands Act 1929* that has not been granted in fee simple but which is under the care, control and management of a Minister, body or other person — the Minister, body or other person; in relation to land held under Crown lease or licence — the lessee or licensee; in relation to land held under an agreement to purchase from the Crown — the person entitled to the benefit of the agreement; in relation to any other land — the Minister who is responsible for the care, control and management of the land or, if no Minister is responsible for the land, the Minister for Sustainability, Environment and Conservation.

Paleochannels — Ancient buried river channels in arid areas of the state. Aquifers in paleochannels can yield useful quantities of groundwater or be suitable for ASR

Percentile — A way of describing sets of data by ranking the dataset and establishing the value for each percentage of the total number of data records. The 90th percentile of the distribution is the value such that 90% of the observations fall at or below it.

Permeability — A measure of the ease with which water flows through an aquifer or aquitard, measured in m/d

Piezometer — A narrow tube, pipe or well; used for measuring moisture in soil, water levels in an aquifer, or pressure head in a tank, pipeline, etc.

PIRSA — Primary Industries and Regions South Australia (Government of South Australia)

Population — (1) For the purposes of natural resources planning, the set of individuals of the same species that occurs within the natural resource of interest. (2) An aggregate of interbreeding individuals of a biological species within a specified location

Porosity — The ratio of the volume of void spaces in a rock or sediment to the total volume of the rock or sediment (Middlemis, 2000).

Porosity, effective — The volume of the inter-connected void spaces through which water or other fluids can travel in a rock or sediment divided by the total volume of the rock or sediment.

Porosity, Primary — The porosity that represents the original pore openings when a rock or sediment formed (Middlemis, 2000).

Porosity, Secondary — The porosity that has been caused by fractures or weathering in a rock or sediment after it has been formed (Middlemis, 2000).

Potentiometric head — The potentiometric head or surface is the level to which water rises in a well due to water pressure in the aquifer, measured in metres (m); also known as piezometric surface

Prescribed water resource — A water resource declared by the Governor to be prescribed under the Act, and includes underground water to which access is obtained by prescribed wells. Prescription of a water resource requires that future management of the resource be regulated via a licensing system.

Prescribed well — A well declared to be a prescribed well under the Act

Production well — The pumped well in an aquifer test, as opposed to observation wells; a wide-hole well, fully developed and screened for water supply, drilled on the basis of previous exploration wells

PWA — Prescribed Wells Area

Recharge area — The area of land from which water from the surface (rainfall, streamflow, irrigation, etc.) infiltrates into an aquifer. See also artificial recharge, natural recharge

RSWL —Reduced Standing Water Level measured in meters AHD (Australian Height Datum). The elevation of the water level is calculated by subtracting the Depth to Water (DTW) from the reference elevation. A negative value indicates that the water level is below mean sea level.

SA Geodata — A collection of linked databases storing geological and hydrogeological data, which the public can access through the offices of PIRSA. Custodianship of data related to minerals and petroleum, and groundwater, is vested in PIRSA and DEW, respectively. DEW should be contacted for database extracts related to groundwater

Salinity — The concentration of dissolved salts in water or soil, expressed in terms of concentration (mg/L) or electrical conductivity (EC)

Screen (well completion) — the section of a well construction that allows groundwater to enter the well. In many instances, it is the section of the well where the casing is perforated to allow ingress of groundwater, although it may also refer to the section of a well that has no casing and is therefore "open".

SDE — South Australian government dataset containing all other spatially explicit data not housed by SA GEODATA, HYDSTRA, or BDBSA

Seasonal— Pertaining to a phenomena or event that occurs on a on a seasonal basis

Specific storage (S_s) — Specific storativity; the amount of stored water realised from a unit volume of aquifer per unit decline in head; measured in m^{-1}

Specific yield (S_y) — The volume ratio of water that drains by gravity to that of total volume of the porous medium. It is dimensionless

Stock use — The taking of water to provide drinking water for stock other than stock subject to intensive farming (as defined by the Act)

Storativity (S) — Storage coefficient; the volume of groundwater released or taken into storage per unit plan area of aquifer per unit change of head; it is the product of specific storage Ss and saturated aquifer thickness (dimensionless)

Surface water — (a) water flowing over land (except in a watercourse), (i) after having fallen as rain or hail or having precipitated in any another manner, (ii) or after rising to the surface naturally from underground; (b) water of the kind referred to in paragraph (a) that has been collected in a dam or reservoir

Sustainability — The ability of an ecosystem to maintain ecological processes and functions, biological diversity, and productivity over time

SWL — Standing Water Level (meters) recorded for the water well. This is the distance from the ground surface to the water surface. A negative value indicates that the water level is above ground level.

TDS — Total dissolved solids, measured in milligrams per litre (mg/L); a measure of water salinity

Tertiary aquifer — A term used to describe a water-bearing rock formation deposited in the Tertiary geological period (1–70 million years ago). Also known as the Paleogene to Neogene period.

Threatened species — Any species that is likely to become an endangered species within the foreseeable future throughout all or a significant portion of its range

Transmissivity (T) — A parameter indicating the ease of groundwater flow through a metre width of aquifer section (taken perpendicular to the direction of flow), measured in m^2/d

Tributary — A river or creek that flows into a larger river

Turbidity — The cloudiness or haziness of water (or other fluid) caused by individual particles that are too small to be seen without magnification, thus being much like smoke in air; measured in Nephelometric Turbidity Units (NTU)

Underground water (groundwater) — Water occurring naturally below ground level or water pumped, diverted or released into a well for storage underground

USGS — United States Geological Survey

Volumetric allocation — An allocation of water expressed on a water licence as a volume (e.g. kilolitres) to be used over a specified period of time, usually per water use year (as distinct from any other sort of allocation)

Water allocation — (1) In respect of a water licence means the quantity of water that the licensee is entitled to take and use pursuant to the licence. (2) In respect of water taken pursuant to an authorisation under s.11 means the maximum quantity of water that can be taken and used pursuant to the authorisation

WAP — Water Allocation Plan; a plan prepared by a water resources planning committee and adopted by the Minister in accordance with the Act

Water body — Includes watercourses, riparian zones, floodplains, wetlands, estuaries, lakes and groundwater aquifers

Water column — a section of water extending from the surface of a body of water to its bottom. In the sea or ocean, it is referred to as 'pelagic zone'

Watercourse — A river, creek or other natural watercourse (whether modified or not) and includes: a dam or reservoir that collects water flowing in a watercourse; a lake through which water flows; a channel (but not a channel declared by regulation to be excluded from this definition) into which the water of a watercourse has been diverted; and part of a watercourse

Water dependent ecosystems — Those parts of the environment, the species composition and natural ecological processes, that are determined by the permanent or temporary presence of flowing or standing water, above or below ground; the in-stream areas of rivers, riparian vegetation, springs, wetlands, floodplains, estuaries and lakes are all water dependent ecosystems

Water licence — A licence granted under the Act entitling the holder to take water from a prescribed watercourse, lake or well or to take surface water from a surface water prescribed area; this grants the licensee a right to take an allocation of water specified on the licence, which may also include conditions on the taking and use of that water; a water licence confers a property right on the holder of the licence and this right is separate from land title

Water plans — The State Water Plan, water allocation plans and local water management plans prepared under Part 7 of the Act

Water quality data — Chemical, biological, and physical measurements or observations of the characteristics of surface and groundwaters, atmospheric deposition, potable water, treated effluents, and wastewater, and of the immediate environment in which the water exists

Water quality information — Derived through analysis, interpretation, and presentation of water quality and ancillary data

Water quality monitoring — An integrated activity for evaluating the physical, chemical, and biological character of water in relation to human health, ecological conditions, and designated water uses

Water resource monitoring — An integrated activity for evaluating the physical., chemical., and biological character of water resources, including (1) surface waters, groundwaters, estuaries, and near-coastal waters; and (2) associated aquatic communities and physical habitats, which include wetlands

Water resource quality — (1) The condition of water or some water-related resource as measured by biological surveys, habitat-quality assessments, chemical-specific analyses of pollutants in water bodies, and toxicity tests. (2) The condition of water or some water-related resource as measured by habitat quality, energy dynamics, chemical quality, hydrological regime, and biotic factors

Well — (1) An opening in the ground excavated for the purpose of obtaining access to underground water. (2) An opening in the ground excavated for some other purpose but that gives access to underground water. (3) A natural opening in the ground that gives access to underground water

Wetlands — Defined by the Act as a swamp or marsh and includes any land that is seasonally inundated with water. This definition encompasses a number of concepts that are more specifically described in the definition used in the Ramsar Convention on Wetlands of International Importance. This describes wetlands as areas of permanent or periodic to intermittent inundation, whether natural or artificial., permanent or temporary, with water that is static or flowing, fresh, brackish or salt, including areas of marine water, the depth of which at low tides does not exceed six metres.

14 References

Adams J and Bachu S 2002, 'Equations of state for basin geofluids: Algorithm review and intercomparison for brines', *Geofluids*, 2:257–271, doi: 10.1046/j.1468-8123.2002.00041.x.

Ataie-Ashanti B, Simmons C and Irvine D 2018, 'Confusion About "Convection"!' *Ground Water*: 56(5). 683-687.

Bachu S and Michael K 2002, 'Flow of variable-density formation water in deep sloping aquifers: Minimizing the error in representation and analysis when using hydraulic-head distributions', *Journal of Hydrology,* 259(1):49–65, doi: 10.1016/S0022-1694(01)00585-6.

Barnett B, Townley LR, Post V, Evans RE, Hunt RJ, Peeters L, Richardson S, Werner AD, Knapton A and Boronkay A 2012, *Australian groundwater modelling guidelines*, Waterlines report, National Water Commission, Canberra, 203p.

Batzle M and Wang Z 1992, 'Seismic properties of pore fluids' *Geophysics*, 57(11):1396–1408.

Beardsmore G 2004, 'The influence of basement on surface heat flow in the Cooper Basin', *Exploration Geophysics,* 35:223–235.

Bekesi G, Tyler M and Waterhouse J 2013, 'Groundwater head in high temperature aquifers', *Quarterly Journal of Engineering Geology and Hydrogeology*, 46:87–94, doi: 10.1144/qjegh2012-035.

Bense VF and Person MA 2006, 'Faults as conduit - barrier systems to fluid flow in siliciclastic sedimentary aquifers', *Water Resources Research*, 42, W05421, doi: 10.1029/2005WR004480.

Bowyer DG 1991, *Recognition of Formation Waters from the Cooper and Eromanga Basins*. Proprietary Report, Santos Ltd.

Costelloe JF, Irvine EC, Western AW and Tyler M 2012, 'Identifying fluvial recharge and artesian upwards leakage contributions to arid zone shallow, unconfined groundwater', *Chemical Geology,* 326–327:189–200.

Doherty J and Moore C 2020, 'Decision Support Modeling: Data Assimilation, Uncertainty Quantification, and Strategic Abstraction', *Groundwater* (Issue Paper), 58(3):327–337, doi: 10.1111/gwat.12969.

Dubsky M and McPhail A 2001, *SA Cooper Basin Well Operations, Statement of Environmental Objectives (SEO): Water Pressure & Salinity Module,* Environmental Impact Research Report, SA Chamber of Mines & Energy, Adelaide.

Gallant JC, Dowling TI, Read AM, Wilson N, Tickle PK and Inskeep C 2011, *1 second SRTM-derived Digital Elevation Models User Guide*, Geoscience Australia, https://www.ga.gov.au/scientific-topics/national-location-information/digital-elevation-data , accessed 23rd May, 2023

Habermehl R and Pestov I 2002, 'Geothermal Resources of the Great Artesian Basin, Australia', *GHC Bulletin*, June.

Halihan T, Love A, Keppel M, Dailey MKM, Berens V and Wohling D 2020, 'Evidence for groundwater mixing at Freeling Spring Group, South Australia', *Hydrogeology Journal* 28:313–323

Holgate FL and Gerner EJ 2010, *OZTemp Well Temperature Data*, Geoscience Australia, Commonwealth of Australia, Canberra.

Horner DR 1951, 'Pressure Build-Up in Wells', Proceedings of the 3rd World Petroleum Congress, pp 25–43.

Hot Dry Rocks (HDR) 2011, 'Heat flow map of Australia', in RPS Aquaterra and Hot Dry Rocks (2012) *Geothermal Energy and Water Use*, Waterlines, National Water Commission, Canberra. http://archive.nwc.gov.au/library/waterlines/72, accessed 22nd November 2019.

Howe PJ, Baird DJ and Lyons DJ 2008, 'Hydrogeology of the South-East Portion of the Arckaringa Basin and South-West Portion of the Eromanga Basin, South Australia', in Lambert M, Daniell TM and Leonard M (eds) *Engineers Australia, Proceedings of Water Down Under 2008,* Modbury, South Australia, pp 573–585.

Irvine D, Sheldon H, Simmons C, Werner A and Griffiths C 2015, 'Investigating the influence of aquifer heterogeneity on the potential for thermal free convection in the Yarragadee Aquifer, Western Australia', *Hydrogeology,* 23:161–173.

Kellett JR, Radke BM, Ransley TR, Bell JG, Stewart GA 2012, 'Hydrogeological Framework', in Smerdon, BD and Ransley TR (eds) *Water resource assessment for the Central Eromanga region*. A report to the Australian Government from the CSIRO Great Artesian Basin Water Resource Assessment. CSIRO Water for a Healthy Country Flagship, Australia.

Keppel M, Wohling D, Jensen-Schmidt B and Sampson L 2015, *A hydrogeological characterisation of the Arckaringa Basin*, DEWNR Technical report 2015/03, Government of South Australia, Department of Environment, Water and Natural Resources, Adelaide.

Krieg GW, Alexander E and Rogers PA 1995, 'Eromanga Basin', in Drexel JF and Preiss W (eds) *The Geology of South Australia*. Geological Survey of South Australia, Adelaide, pp 101–105.

Love A, Wohling D, Fulton S, Rousseau-Gueutin P and De Ritter S (eds.) 2013a, *Allocating water and Maintaining Springs in the Great Artesian Basin, Volume II: Groundwater Recharge, Hydrodynamics and Hydrochemistry of the Western Great Artesian Basin*, National Water Commission, Canberra.

Love A, Shand P, Crossey L, Harrington GA, Rousseau-Gueutin P (eds.) 2013b, *Allocating Water and Maintaining Springs in the Great Artesian Basin, Groundwater: Volume III: Discharge of the Western Great Artesian Basin*, National Water Commission, Canberra.

McCutcheon SC, Martin JL and Barnwell TO 1993, 'Water quality', in Maidment DR (ed.) *Handbook of Hydrology*, McGraw-Hill, New York. pp11.1-11.69

Middlemis H, Walker G, Peeters L, Richardson S, Hayes P, Moore C 2019, 'Groundwater modelling uncertainty – implications for decision making. Summary report of the national groundwater modelling uncertainty workshop', 10 July 2017, Sydney, Australia, Flinders University, National Centre for Groundwater Research and Training, https://dspace.flinders.edu.au/xmlui/handle/2328/39111, accessed 19th November 2019

Office of Groundwater Impact Assessment (OGIA) 2016, *Hydrogeological Conceptualisation Report for the Surat Cumulative Management Area*, OGIA, Department of Natural Resources and Mines, Brisbane.

Pestov I 1998, 'Modelling Non-isothermal Flows in Porous Media: A Case Study Using an Example of the Great Artesian Basin, Australia', New Methods in Applied and Computational Mathematics (NEMACOM'98), Proceedings of the Centre for Mathematics and its Applications.

Pestov I 2000, 'Thermal Convection in the Great Artesian Basin, Australia', *Water Resources Management,* 14:391–403.

Post V, Kooi H and Simmons C 2007, 'Using Hydraulic Head Measurements in Variable-Density Ground Water Flow Analyses, *Groundwater*, 45(6):664–671,

Priestley S, Shand P, Love AJ, Crossey L and Karlstrom K 2013, 'Hydrochemistry', in Love AJ, Wohling D, Fulton S, Rousseau-Gueutin P and De Ritter S (eds) *Allocating water and maintaining springs in the Great Artesian Basin*

Volume II: Groundwater recharge, hydrodynamics and hydrochemistry of the Western Great Artesian Basin, National Water Commission, Canberra, pp 171–201.

Priestley SC, Shand P, Love AJ, Crossey LJ, Karlstrom KE, Keppel MN, Wohling DL and Rousseau-Gueutin P 2020, 'Hydrochemical variations of groundwater and spring discharge of the western Great Artesian Basin, Australia: implications for regional groundwater flow' *Hydrogeology Journal,* (28):263–278, doi: 10.1007/s10040-019-02071-3.

Queensland Government 2019a, *Petroleum and gas production and reserve statistics*, https://www.data.qld.gov.au/dataset/petroleum-gas-production-and-reserve-statistics, accessed 18 August 2019.

Queensland Government 2019b, *Queensland borehole series,* https://www.data.qld.gov.au/dataset/queensland-borehole-series, accessed 18 October 2019.

Radke BM, Ferguson J, Cresswell RG, Ransley TR and Habermehl MA 2000, *Hydrochemistry and implied hydrodynamics of the Cadna-owie - Hooray Aquifer Great Artesian Basin*, Bureau of Rural Sciences, Canberra.

Raffensperger P and Vlassopoulos D 1999, 'The potential for free and mixed convection in sedimentary basins', *Hydrogeology,* 7:505–520.

Ransley TR, Radke BM, Feitz AJ, Kellett JR, Owens R, Bell J, Stewart G and Carey H 2015, *Hydrogeological Atlas of the Great Artesian Basin*, Geoscience Australia, Canberra, doi: 10.11636/9781925124668.

Ransley TR and Smerdon BD (eds.) 2012, *Hydrostratigraphy, hydrogeology and system conceptualisation of the Great Artesian Basin*. A technical report to the Australian Government from the CSIRO Great Artesian Basin Water Resource Assessment. CSIRO Water for a Healthy Country Flagship, Australia. 324p.

Rousseau-Gueutin P, Simon S, Love A, Post V, Doublet C, Simmons C, Wohling D and Fulton S 2013, Groundwater flow and hydrodynamics, in Love A, Wohling D, Fulton S, Rousseau-Gueutin P and De Ritter S (eds) *Allocating water and Maintaining Springs in the Great Artesian Basin, Volume II: Groundwater Recharge, Hydrodynamics and Hydrochemistry of the Western Great Artesian Basin*, National Water Commission, Canberra. pp 121-170

Sampson L, Wohling D, Jensen-Schmidt B and Fulton S 2012, *South Australia and Northern Territory Great Artesian Basin (Eromanga) Hydrogeological Map – Part 1 & Part 2*, Government of South Australia, Department of Environment, Water and Natural Resources, Adelaide.

Sandiford M, Lawrie K and Brodie RS 2020, 'Hydrogeological implications of active tectonics in the Great Artesian Basin, Australia', *Hydrogeology Journal,* 28:57–73, doi: 10.1007/s10040-019-02046-4.

Simmons CT 2005, 'Variable density groundwater flow: From current challenges to future possibilities', *Hydrogeology Journal,* 13:116–119, doi: 10.1007/s10040-004-0408-3.

Smerdon BD, Welsh WD and Ransley TR (eds.) 2012, *Water resource assessment for the Western Eromanga region*. A report to the Australian Government from the CSIRO Great Artesian Basin Water Resource Assessment. CSIRO Water for a Healthy Country Flagship, Australia. 136p

Töth J 1963, 'A theoretical analysis of groundwater flow in small drainage basins', *Journal of Geophysical Research*, 68(16):4795–4812.

United States Geological Survey (USGS) 2019, Specific Conductance, Chapter 6.3 of Section A, National Field Manual for the Collection of Water-Quality Data, Book 9, Handbooks for Water-Resources Investigations Field Measurements.

Weatherill D, Simmons C, Voss C and Robinson N 2004,.'Testing density-dependent groundwater models: two-dimensional steady state unstable convection in infinite, finite and inclined porous layers', *Advances in Water Resources,* 27:547–562.

Welsh WD 2000, *GABFLOW: A steady state groundwater flow model of the Great Artesian Basin*, Bureau of Rural Sciences, Canberra.

Welsh WD 2006, *Great Artesian Basin transient groundwater model*, Bureau of Rural Sciences, Canberra.

Wohling D, Fulton S, Love AJ, Dailey M, Halihan T, Berens V, Purtschert R and Shand P 2013, 'Mountain System Recharge, in: Love, AJ, Wohling D, Fulton S, Rousseau-Gueutin P and De Ritter S (eds) *Allocating water and maintaining springs in the Great Artesian Basin Volume II: Groundwater recharge, hydrodynamics and hydrochemistry of the Western Great Artesian Basin*. National Water Commission, Canberra, pp 82–119.

Government
of South Australia

Department for
Environment and Water